Solid tumour growth: a comparison of mathematical models and computer simulations

Stott, Emma Louise

Award date:
1998

Awarding institution:
University of Bath

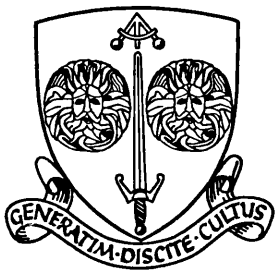

UNIVERSITY OF BATH

SCHOOL OF MATHEMATICAL SCIENCES

Solid Tumour Growth: A Comparison of Mathematical Models and Computer Simulations

submitted by

Emma Louise Stott

for the degree of

Ph.D.

of the University of Bath, 1998

ProQuest LLC
789 East Eisenhower Parkway
P.O. Box 1346
Ann Arbor, MI 48106-1346

Solid Tumour Growth: A Comparison of Mathematical Models and Computer Simulations.

submitted by

Emma L. Stott

for the degree of Ph.D.

of the

University of Bath

1998

Summary

In this thesis, we will present simulations of solid tumour growth. We gradually develop a biologically realistic simulation from an initially simplistic model. Continuum models are then presented in order to compare the two ways of modelling. Finally, we extend the simulation to model angiogenesis, the stage after avascular growth.

In the first chapter, the biological background of tumour growth and development is introduced and the link between tumour angiogenesis, tumour invasion and the dissemination of the disease is discussed. A review of selected mathematical models of avascular solid tumour growth and solid tumour deformation is included to give a brief history of the kind of models that this thesis will include. Some simulations of cell movements and processes are also discussed to give a slice of background for the simulations that will be presented.

Chapter 2 is a preliminary investigation into the general ideas behind simulating the growth of an avascular tumour on a lattice. The simulations that are presented do not reflect reality closely but pick out salient features that might be important in more realistic simulations. The first simulation, based on a 2-dimensional lattice, demonstrates cell sorting only, but the second includes cell proliferation. In the third, we consider the effects that the immune system might have on our growing tumour.

In Chapter 3, the idea of simulating avascular tumour growth on a lattice is carried further. We move to simulating on a 3-dimensional lattice, using an extension of the Potts model, the principle of which is energy minimisation. We include more realistic cell boundaries than in Chapter 2 and the simulation performs cell sorting and proliferation. We also allow for quiescence and death of cancer cells by introducing nutrient dependent growth. This simulation reflects well the known experimental data and growth curves of multicellular spheroids (MCS) grown *in vitro*.

In the fourth chapter, we present a continuum model of nutrient dependent tumour growth. In the model reviewed in Chapter 6, there is a travelling wave associated with the periphery of the tumour. This seems rather unrealistic from a biological point of view and so the main aim of this chapter is to develop a model in which the tumour volume eventually reaches a saturation level, and growth stops.

We then return to investigate Greenspan's continuum model of MCS growth, reviewed in the first chapter, in Chapter 5. We extend his model, including more realistic cell properties, such as nutrient dependent proliferation, and show that the new models fit the experimental growth curves better that the original simple one. These results are then compared to those obtained by our simulation in Chapter 3.

In Chapter 6, we review a paper written by Robert Gatenby and Edward Gawlinski which proposes acid production as a means of tumour invasion. In the paper, they show numerically that there are travelling waves associated with the tumour and healthy tissue boundary. We give an analytical proof of the existence of these waves. Then we compare their results of wave propagation speed with our simulation of acid-mediated invasion. The simulation is again based on a 3-D lattice and uses the Potts model.

Gatenby and Gawlinski's model is rather unrealistic, in that all tumour cells can grow logistically with the same rate, no matter where they are positioned within the tumour. We extend their model in Chapter 7, to include nutrient dependent growth. We extend the model further to include chemotaxis of the cancer cells up nutrient gradients. The simulation of Chapter 3 is developed to include diffusion (NB there was no diffusion in Ch.3) of nutrients to and acid from an MCS. Then the data gained from this is compared with that of the continuum models.

In Chapter 8 the biological background of angiogenesis and metastasis is introduced and then a simulation of capillary growth formation near a nodular tumour and also a simulation of the first stage of metastasis are presented.

Acknowledgements

I would like to thank the following people who have either contributed to this thesis, or just made my stay at Bath a happy one:

- Nick Britton, my supervisor, for his help and letting me babysit Rachel and Jenny;
- Mark Zajac for having the time and patience to answer any questions I had about the Potts model and for writing so many e-mails;
- Mark Chaplain for the many fruitful discussions and ideas;
- Sandy Anderson for his help and for letting me kip on his floor on my trips to Dundee.
- My office mates and friends:
    - Michelle Orme for the numerous tea sessions and reassurances in my early stages;
    - Abby Paine for being my sister and not throttling me when we lived together;
    - Rob Laister for loathing anything with fur and for many nights down the pub;
    - Elaine Crookes for going to pottery with me and not laughing at my works of art.
- Lastly, but most specially:

- My parents for all their love, help and support over the years and for not letting me leave school at 15;
- Steve, for all his help, mathematical and otherwise, listening patiently to me whinging about this thesis, introducing me to Herbert and, most of all, letting me be Mrs B.

Contents

1 Introduction and Brief Review of Mathematical Models of Tumour Growth. 1

1.1 Introduction. 1

1.2 Growth of Solid Tumours. 4

1.2.1 Early solid tumour growth. 4

1.2.2 Response of the Immune System to a Tumour. 5

1.2.3 Angiogenesis and Metastasis. 6

1.3 Mathematical Models of Avascular Tumour Growth. 8

1.4 Surface Geometry Coupled to Morphogen. 17

1.5 Simulations of Cell Movements and Processes. 17

1.5.1 Cellular Automata Models of Cell Movements. 17

1.5.2 Cell Sorting Models. 19

1.5.3 Other Simulations that use the Monte Carlo Method. 25

2 A Two-Dimensional Simulation of Cell Sorting, Proliferation and Effects of the Immune System. 31

2.1 Introduction. 31

2.2 Model with Sorting. 32

2.3 Model with Proliferation. 35

2.4 Effects of the Immune System. 35

2.5 Summary. 46

3 Simulations of Cell Sorting, Pattern Formation and Avascular Tumour Growth using the Potts Model. 47

3.1 Potts Models. 47

3.1.1 The Extended Potts Model 48

3.2 A Model of Avascular Tumour Growth. 50

3.2.1 Tumour growth. 50

3.2.2 Cell sorting 51

3.2.3 The Model. 52

3.3 Simulation of an Avascular Solid Tumour. 55
3.4 Simulation of an Avascular Carcinoma. 57
3.5 Discussion. 63

4 A Two Variable Continuum Model of avascular tumour growth 68
4.1 Description of Model. 68
4.2 Results. 72
4.3 Discussion. 73

5 Extension of Greenspan's Model of Solid Tumour Growth. 76
5.1 Assumptions. 76
5.2 Conservation of mass. 77
5.3 Model 1: Growth of a solid tumour with constant cell proliferation rate. . . . 79
5.4 Model 2: Growth of a solid tumour with nutrient dependent proliferation rate. 88
5.5 Model 3: Growth of a solid tumour with nutrient dependent proliferation rate and non-constant degradation. 98
5.6 Model 4: Growth of a solid tumour with non-constant nutrient consumption. . 103
5.7 Conclusion 113

6 Acid Mediation Hypothesis of Tumour Invasion 117
6.1 Introduction. 117
6.2 Travelling wave analysis. 119
6.2.1 Boundedness of solutions. 120
6.2.2 Ignoring diffusion of cancer cells. 122
6.3 Marginal Stability. 131
6.3.1 Introduction. 131
6.3.2 Determining the marginal stability point. 132
6.3.3 Solving for the marginally stable point. 134
6.4 Simulation of Acid Mediated Invasion. 135
6.5 Conclusions. 137

7 Extension of Gatenby and Gawlinski's model with Comparison to Simulation 141
7.1 Description of the model. 141
7.1.1 Fixed Points. 146
7.2 Solutions of the Model. 146
7.3 Discussion. 148
7.4 Simulation. 150
7.5 Results. 152
7.6 Conclusion. 155

8 Angiogenesis and Metastasis **156**

8.1 Angiogenesis. 156

8.1.1 The Process of Angiogenesis. 158

8.1.2 Angiogenesis Simulation. 160

8.1.3 Results. 161

8.1.4 Discussion. 161

8.2 Metastasis. 165

8.2.1 Metastasis Simulation. 166

8.2.2 Results. 167

8.2.3 Discussion. 168

8.3 Conclusions. 168

List of Figures

1-1 A cell colony consisting of three tiers - a top layer of proliferating cells in contact with the ambient medium; a middle layer of non-proliferating but viable cells and a base of necrotic debris. 14

1-2 Development of average cell shape during a proliferation cycle. 26

1-3 Simple diagram of an epithelial cell and two examples of possible interaction potentials. 28

1-4 Schematic flow chart of Drasdo's basic simulation algorithm. 29

2-1 Model with sorting: Configuration of sorting cells after (from left to right) 0 updates, 4000, 10,000, 20,000, 50,000 and 100,000 updates. Cancer cells are depicted by black pixels, normal cells by white. $1/T = 0.8$. 33

2-2 Schematic flow chart of basic algorithm for model with cell sorting and proliferation. 34

2-3 Model with proliferation and sorting: P(cancer cell proliferates) = 0.1, inverse temperature = 0.8, times are (from left to right) 1000 updates, 10,000, 50,000, 100,000, 500,000 and 1,000,000 updates. Again black pixel=cancer, white=normal. 36

2-4 Model with sorting and proliferation: Graph showing the variation of tumour growth rate with system temperature. T is the "temperature" of the system, t is the number of updates required for a tumour cell to reach annulus n, where the inner radius of annulus n has size, in cell diameters, n+initial radius of tumour. Increasing/decreasing the parameter k in (2.1) would give the same effects as shown here for increasing/decreasing T. 37

2-5 Immune model: Simulation results for a highly invasive tumour ($P = 0.8$, $q = 0.3$), times are (from left to right) 0 updates, 5000, 10,000, 15,000, 20,000 and 25,000 updates. $1/T = 0.8$. Key: black=tumour, dark grey=complexes, light grey=dead tumour cells, white=normal. 40

2-6 Simulation results for a highly invasive tumour, continued, times are (from left to right) 30,000, 35,000, 40,000, 50,000, 60,000 and 70,000 updates. 41

2-7 Immune model: Simulation results for an active immune system ($P = 0.4$, $Q = 0.3$), times are (from left to right) 3000 updates, 5000, 10,000, 15,000, 20,000 and 25,000 updates. $1/T = 0.8$. Key: black=tumour, dark grey=complexes, light grey=dead tumour cells, white=normal. 42

2-8 Simulation results for an active immune system, continued, times are 30,000, 35,000, 40,000, 50,000, 60,000 and 70,000 updates. 43

2-9 Immune model: Simulation results for a highly active immune system ($P = 0.2$, $Q = 0.4$), times are 3000 updates, 5000, 10,000, 15,000, 20,000 and 25,000 updates. Key: black=tumour, dark grey=complexes, light grey=dead tumour cells, white=normal. 44

2-10 Simulation results for a highly active immune system, continued, times are 30,000, 35,000, 40,000, 50,000, 60,000 and 70,000 updates. 45

3-1 Simple flow diagram of computer algorithm for Potts model with cell sorting and proliferation. 56

3-2 Cross sections of the initial configuration. Top: shows individual cancer cells only and normal cells as just solid white. Each colour represents a separate cell within the tumour. Bottom: shows only individual normal cells, with the tumour represented by the white mass in the centre. These two pictures are of the same configuration, but to show individual cells and for clarity of types, they are presented separately. 58

3-3 Cross section of rounded configuration, showing proliferating cancer cells only. Because this is a cross section, some cells may look slightly disjointed or very small, but the rest of the cell is in adjoining layers of the lattice and so it is more than likely that they are connected and not so small. 59

3-4 Cross sections of tumour. Top: only proliferating cancer cells shown individually. White=normal cells, solid blue=core of quiescent cells. Bottom: only normal cells and quiescent cancer cells shown individually. Solid blue = ring of cancer cells. Again, these two pictures are of the same configuration, but are displayed separately so as to show all cells individually, while keeping their type clear. . . 60

3-5 Cross sections of tumour. Top: only proliferating cancer and necrotic cells shown individually. Solid white surrounding tumour is normal tissue, while the solid white annulus is quiescent cancer cells. Bottom: normal and quiescent cells only. White central mass is the necrotic core, while the green ring is the proliferating cancer cells. 61

3-6 Graph showing the volume of the growing tumour vs. number of MCTS. 62

3-7 Graph of the growth of the three radii of the tumour vs. number of MCTS. Top curve: outer radius; middle curve:outer quiescent radius; bottom curve: necrotic radius. 62
3-8 Comparison of the growth of simulated outer tumour radius with Folkman and Hochberg's measurements for V-79 MCS. 63
3-9 Cross section of tumour showing a) substrate and tumour cells only and b) normal cells and substrate only. 64
3-10 Cross section of tumour showing a) substrate and tumour cells only and b) normal and quiescent cells only. 65
3-11 Cross section of tumour showing a) substrate, tumour cells and dead cells only and b) substrate, normal and quiescent cells only. 66
3-12 Graph of tumour volume vs. time. 67

4-1 Numerical solution of nutrient steady state (solid line) and plot of tumour steady state (dashed line), $\chi = 1.6 \times 10^{-3}$. 72
4-2 Numerical simulations of the model. 73
4-3 Comparison between numerical results and results of simulation in Chapter 3. . 74

5-1 Model 1: Graphs showing the second stage of development of a) the ratio of quiescent radius to outer radius; b) the dimensionless outer radius, with $M = 1/4$. 84
5-2 Model 1: Graphs showing the final stage of development of a) the ratio of necrotic radius to outer radius; b) the dimensionless outer radius, with $M = 1/4$. 86
5-3 Model 1: Graphs showing the steady state values a) x_∞ and b) η versus μ. . . 87
5-4 Model 1: Steady state values of the dimensionless outer radius of the tumour, η_∞, the dimensionless inner necrotic radius, $(\eta_o)_\infty$, and the thickness of the viable layer $\eta_\infty - (\eta_n)_\infty$ versus x_∞. 87
5-5 Model 1: Graphs to show the change in x and y with time. Again $M = 1/4$. . . 88
5-6 Model 1: Graph to show the growth and development of the dimensionless radius of the tumour. M=1/4, γ=0.1 and 0.2. Large dots separate the growth phases. 89
5-7 Graph to show the growth and development of the dimensionless radii of the tumour. $M = 1/4$, γ=0.1. 89
5-8 Model 2: Graphs showing the first stage of development of a) the dimensionless outer radius; b) the outer radius, with $M = 1/4$. 92
5-9 Model 2: Graphs showing the second stage of development of a) the ratio of quiescent radius to outer radius; b) the dimensionless outer radius, with $M = 1/4$. 94
5-10 Model 2:Graphs showing the last stage of development of a) the ratio of necrotic radius to outer radius; b) the dimensionless outer radius, with $M = 1/4$. 96
5-11 Model 2: Graphs showing the development of x and y with time, $M = 1/4$. . . 96

5-12 Model 2: Graph showing the development of α, the dimensionless outer radius with time, $M = 1/4$. 97
5-13 Model 2: Graph showing the growth of the dimensionless radii with time, $M = 1/4$, $\gamma = 0.1$. 97
5-14 Model 3: Graphs showing the first stage of development of the outer radius, with $s = 1, 2, 4, 5$ and $u(0) = 5$, as in simulations. 100
5-15 Model 3: Graphs showing the second stage of development of the outer radius and quiescent radius, with $s = 1$ (dash-dotted line), $s = 2$ (dotted line) and $s = 4$ (solid line). 102
5-16 Model 3: Graphs showing the final stage of development of the outer, quiescent and necrotic radii, with $s = 4$ and for two values of χ. 103
5-17 Model 3: Graph showing the total growth history of the three radii of the tumour with $s = 4$ and $\chi = 4$. 104
5-18 Model 3: Graph showing the total growth history of the three radii of the tumour with $s = 1$ and $\chi = 2$. 105
5-19 Graph showing the development of the three dimensionless radii for models 1 to 3. Model 1 is shown by a solid line, Model 2 by a dashed line and model 3 by a dotted line. The parameters chosen were $M = 1/4$, $\gamma = 0.1$ for model 1, $\gamma = 0.2$ for model 2 and for model 3, $\chi/s = 2.18$. 106
5-20 Graph showing the first two stages of development of the three dimensionless radii for models 1 to 3. Parameters are the same as in Figure (5-19). 106
5-21 Model 4: Graphs showing the second stage of development of a) the ratio of the quiescent radius to the outer radius; and b) the dimensionless outer radius, with $M = 1/4$. 110
5-22 Model 4: Graphs showing the last stage of development of a) the ratio of the quiescent radius to the outer radius; and b) the ratio of the necrotic radius to the outer radius; M=1/4. 112
5-23 Model 4: Graph showing the last stage of development of the radii, M=1/4, $\gamma = 0.1$. 112
5-24 Model 4: Graph showing the development of the necrotic, quiescent and outer radii, M=1/4, $\gamma = 0.1$. 113
5-25 Graphs showing the development of the outer radii of Greenspan's model (parameters $Q^2 = 0.4$, $\gamma = 0.2$), Chapter 3's simulation and Folkman and Hochberg's experimental results for V-79 spheroids. 115
5-26 Graphs showing the development of the outer radii for all four models with M=1/2, $\gamma = 0.5$ and $\chi/s = 3.08$. 116

6-1 Acid-mediated invasion. Tumour and live cells are shown individually, while the dead normal cells are shown as a solid white ring. 138
6-2 Comparison between simulation [a] and Gatenby's model [b]. 139

7-1 Graphs showing the development of the normal cell density, cancer cells density, dead cell density, acid concentration and nutrient concentration. 147
7-2 Graph of distance of tumour front from left hand boundary vs. time. 148
7-3 Simulation results. Key: white= healthy cells, light grey = quiescent, darker grey = dead healthy cells, dark grey = cancer cells. 153
7-4 Simulation results. Key: white= healthy cells, light grey = quiescent, darker grey = dead healthy cells, dark grey = cancer cells, black = necrotic core. . . . 153
7-5 Graph of average tumour radius versus time. 154
7-6 Comparison of radius graphs of continuum model (top) and simulation (bottom). 154

8-1 Initial configuration of the tumour (light grey) embedded in healthy tissue (white), with a blood vessel (dark grey) running down the side of the lattice. 162
8-2 Formation of a sprout. Key: light grey=tumour, white=healthy cells, dark grey=blood vessels. 162
8-3 Growth of capillaries towards tumour. Key: light grey=tumour, white=healthy cells, dark grey=blood vessels. 163
8-4 Formation of an anastomose. Key: light grey=tumour, white=healthy cells, dark grey=blood vessels. 164
8-5 Penetration of tumour by capillaries. Key: light grey=tumour, white=healthy cells, dark grey=blood vessels. 164
8-6 Formation of necrotic core and loosening of some cell bonds. Healthy cells, quiescent tumour and dead cells are not shown individually, but represented by solid blocks of white, grey and black, respectively. 167
8-7 Detail of cancer cell (black) loosening its bonds with its neighbours. Cancer cells are shown individually and quiescent cells are shown as a solid block of grey. . 168

Chapter 1

Introduction and Brief Review of Mathematical Models of Tumour Growth.

1.1 Introduction.

A tumour is an abnormal mass of tissue, the growth of which exceeds and is uncoordinated with that of the normal tissues [232]. Any cell in the body that is capable of division, has the potential to become malignant [190] and to proceed through various stages to eventually form a neoplasm or tumour. Neoplasia is the name used to describe a collection of diseases characterised by the uncontrolled, uncoordinated and excessive proliferation of cells.

Tumours usually start as a mild disorder of cell behaviour that may slowly develop into a full blown cancer. The progression from the earliest event to the clinically recognisable tumour can take many years and the formation of a tumour is the exception, not the rule, for transformed cells. Part of the reason for this long period is that the cells have to undergo a number of changes before they become hyperplastic and then truly cancerous [231]. Cancer cells require a particular developmental pathway. One of the requirements is to become immortal, *i.e.* the acquisition of the ability to undergo multiple divisions, sometimes with no limit [221]. To do so the cells must both ignore extracellular signals to halt cell division (both chemical and contact) and must also avoid the natural limit on the number of cell divisions caused by the exhaustion of telomeres.

Telomerase is an enzyme, usually produced only by the cells that make eggs and sperm, but also produced by many cancer cells [54]. Healthy cells are mortal because they contain a genetic clock. At the end of each chromosome is a chain of DNA made up of "beads" of

genetic material called telomeres. A young cell that has formed in the embryo has over 1000 telomeres on each chromosome tip. But every time it clones itself, between 10 and 20 of them are lost [54]. Eventually the chain becomes so short that the cell can no longer survive. It starts to accumulate damage and eventually dies. Telomerase in malignant cells can repair telomere chains damaged during cells division, allowing them to escape the aging process.

An example of the difference between healthy and cancer cell replication is an experiment performed with cells growing in a petri dish. Normal cells form a monolayer, growing until they reach the edges confluently, and then stop, whereas cancer cells carry on proliferating, lying across each other in a haphazard arrangement, no longer in a monolayer [232].

Partial understanding of the genetic mechanisms by which cancer cells escape from biochemical growth control, and mutate to cause the expression of oncogenes or the loss of anti-oncogenes, has been developed over the last decade [195]. Oncogenes cause excessive cell proliferation, while anti-oncogenes act to limit the division rate of normal cells. In either case, a mutated cell will have a proliferative advantage compared with its surrounding cells. These rapidly dividing mutant cells have undergone the first step in a series of genetic transformations which result in cancer.

Cells can die by two pathways, necrosis or apoptosis (from the Greek word meaning shedding of leaves in autumn [54]). Necrosis is the untimely death caused by damaging external factors such as poisons, excessive heat or lack of oxygen. The process is messy: membranes rupture and the contents of cells spill out uncontrollably. In addition, some of the cell's chemicals may have damaging effects on the surrounding tissue [54].

Apoptosis is an evolutionary conserved, innate process by which damaged or extraneous cells systematically inactivate, disassemble, and degrade their own structural and functional components to complete their own demise [127]. In normal tissue, apoptosis deletes unnecessary, damaged and potentially harmful cells to ensure structural and functional tissue homostasis. Apoptosis occurs in nearly every cell type throughout development and maturation.

Apoptosis proceeds in a much more orderly fashion than necrosis. A cell triggered to commit suicide first makes the enzymes it will need to destroy itself. Under the influence of suicide genes, the cell body then shrinks to a characteristic spherical shape, while the enzymes within repackage its contents, including genetic material, into digestible fragments that neighbouring cells can consume. Within a few hours the cell starts breaking up. Each fragment has chemical markers on its surface that attract phagocytic cells, the body's scavengers, which quickly remove all trace of it [54].

Many cancer cells have defects in one or more of the regulation of genes (e.g. P53) that control the apoptotic process. These defects render the tumour cells resistant to the induction of apoptosis by a wide variety of stimuli, including chemotherapeutic drugs and radiotherapy [127] and also add to the cells' apparent immortality.

A survival gene called *c-myc*, acts as a kind of switch for apoptosis. If the *c-myc* gene is turned on, it instructs the cell to proliferate; if it is not expressed, the cell kills itself. In almost all types of cancer, the *c-myc* gene appears in a mutated form that cannot be switched off [54].

c-myc is important in apoptosis, but it does not act in isolation. Other genes seem to impose checks and restraints on the way *c-myc* behaves. One such gene is *MTS1*, which acts as a "gatekeeper" for *c-myc*, preventing its activation and so promoting apoptosis. *MTS1* produces a protein that blocks the action of an enzyme in the pathway that allows messages from cell surface receptors to switch on *c-myc*. So *c-myc* stays switched off, and apoptosis can take place. In more than half of all human cancers, functional copies of *MTS1* are missing, leaving *c-myc* unchecked and the pathway to uncontrolled cell division open.

Tumours form two classes, benign and malignant. The critical distinction is their method of growth. Benign tumours grow by expansion, compressing or displacing surrounding normal tissue, and are usually encapsulated, but malignant tumours grow by local infiltration, destroying the tissue through which they invade. Benign tumours grow at their site of origin only, but malignant tumours may spread to distant sites, with cells detaching from the primary tumour and migrating to remote sites via the blood stream, in the lymphatics or across tissue spaces. This process is known as metastasis and the secondary tumours formed are metastases. The majority of deaths from cancer are due to the formation of metastases at sites remote from the primary tumour. Malignant tumours usually, though not necessarily, grow more rapidly than benign tumours. Once they reach a clinically detectable stage, malignant tumours generally show evidence of significant growth, with involvement of surrounding tissue, over weeks or months, whereas benign tumours often grow slowly over several years [232].

By virtue of their position, benign tumours may cause symptoms by compression of adjacent structures, like nerves or blood vessels, or in certain circumstances they may secrete hormones which contribute to the manifestation of disease. Thus, they are only life threatening if the growth is particularly large or near to essential organs. In contrast, malignant tumours always have the potential to cause death as a result of their aggressive growth behaviour. Malignant tumour cells tend to be "anaplastic" or less well differentiated than the normal cells of the tissue in which they arise. Benign tumours usually resemble normal tissue more closely [190].

The most common type of malignant tumours are carcinomas (cancer of the epithelia), which are solid tumours of the external and internal surfaces of tissues and organs. Lung cancer, prostate cancer, breast cancer and colorectal cancer account for over 50 % of all reported cancer in England and Wales [173]. In the majority of patients suffering from carcinomas, the disease has already spread (metastasised) before detection, resulting in multiple secondary tumours (metastases) which may occur in sites far removed from the primary cancer. Hence, the disease cannot be cured by treating the primary tumour alone. Metastases can be difficult to treat,

can cause a number of unpleasant symptoms and often prove to be fatal. The estimated annual death rate is 1 in 341 for men and 1 in 387 for women [174]. Thus, it is highly desirable to prevent metastases from developing and so it is important to investigate the mechanisms by which the tumour spreads prior to the formation of secondary tumours. Firstly, this requires understanding of the different stages of tumour growth, from the initial appearance of the neoplasm, right up to the point of metastases formation. Secondly, it requires identification of the different ways that tumour growth can be, at the very least, contained and ideally removed altogether.

1.2 Growth of Solid Tumours.

1.2.1 Early solid tumour growth.

The growth of most malignant and benign tumours takes place in two stages [143]. During the first stage, the tumour has no blood supply (avascular stage) and is usually 1-3mm in diameter. This is small enough to take in nutrients and expel waste products by diffusion alone. A few of the mathematical models describing this stage of growth are discussed in Section (1.3).

LaBarbera & Vogel [144] and Edelstein-Keshet [59] have both demonstrated the inadequacy of diffusion as a means of vital nutrient delivery. Fick's first law of diffusion results in the diffusive flux being given by

$$\mathbf{J} = D\nabla C,$$

where C= concentration of nutrient, D= diffusion coefficient [125, 144].

Consider a spherical tumour, of radius, r, volume $V = 4\pi r^3/3$ and surface area $S = 4\pi r^2$. Suppose that the tumour consumes the nutrient so that at $r = 0$, $C(0,t) = 0$, while its concentration at the tumour periphery is C_o (cf. [104]). Then the total amount of nutrient diffusing across the tumour surface per unit time will be approximately

$$J \approx DS\frac{C_o}{r} = 4\pi DC_o r, \text{ where we have taken } \frac{dC}{dr} \simeq \frac{C_o}{r},$$

i.e. the concentration difference per unit distance [59]. The rate at which the nutrient is consumed is proportional to the tumour's volume. If τ is the fixed constant representing the consumption rate of tumour cells per unit volume, then the rate at which nutrient is used is $4\pi r^3\tau/3$.

Thus,

$$\frac{\text{rate of supply}}{\text{rate used}} \simeq \frac{3DC_o}{\tau r^2}.$$

For the needs of the tumour to be met, the rate of supply of the nutrient must be greater than or equal to the rate at which it is used, *i.e.* the ratio must be greater than 1. Hence an approximate minimum requirement is

$$C_o = \frac{\tau r^2}{3D}$$

So, the external nutrient concentration must be, at the very least, proportional to the square of the tumour radius. If the tumour radius is large then this requirement is unrealistic. Hence, as the tumour grows, the nutrient concentration will decrease at the centre. The nutrient concentration also decreases towards the centre because of consumption. So, when the tumour is large enough, cells at the centre do not receive enough to remain alive and so die. These dead cells disintegrate into chemical compounds which are freely permeable through cell membranes. The mass or cell volume lost this way is replaced by cells pushed inward by the forces of adhesion and surface tension. Thus, when it reaches a critical size, the avascular tumour may become dormant and remain in a state of equilibrium [71, 111, 118]. Growth does not stop completely, but is 'balanced' by the death and disintegration of the dead cells. The tumour may remain in this dormant state for months or even years [180]. This period of dormancy ends when chemicals released by the tumour cause vascularization to occur. This process is called angiogenesis. If blood vessels do not supply the tumour with oxygen and nutrients, then the tumour either remains tiny or it dies.

1.2.2 Response of the Immune System to a Tumour.

If the immune system of the host recognises the the abnormality in the tumour, then the growth may be regulated by the immune response, which may be sufficient to eradicate the neoplasia completely.

The immune cells, B-lymphocytes (B-cell) and T-lymphocytes (T-cell) are the key players in the immune response of invertebrate animals [145]. Both B-cells and T-cells are created in bone marrow, but the T-cells develop further in the thymus gland. Both types of cells circulate in the blood stream and lymph system but are usually concentrated in the lymph nodes. These so-called lymphocytes can recognise certain free or cell surface antigens (molecules associated with foreign material e.g. virus, bacteria) or are produced by defective cells.

The appearance of antigen in the host triggers the response of the immune system to a neoplastic cell or a virus. The theory of B-cell response is called the Clonal Selection Theory. A specific receptor on the B-cell membrane will bind to the antigen in a manner analogous to a key fitting a lock [145]. The B-cells then produce clones which secrete antibodies. This is known as a *humoral* immune response, and the B-cells and their antibodies are collectively known as immunoglobulins. The antibodies bind to the antigens and mark them for destruction

by other immune cells such as macrophages or natural killer cells.

The response of T-cells to antigen is to reproduce clonally and then differentiate into several kinds of T-cell. T-cells do not produce antibodies and are only involved in these *cell-mediated* immune responses:

- **Cytotoxic T-cells** - these bind to antigen on the surface of an abnormal cell or virus and kill it by lysis (disrupting the membrane).
- **Suppressor T-cells** - these regulate the immune response by inhibiting excessive immune reactions.
- **Helper T-cells** - these bind to antigen on the surface of B-cells and release hormones which help the B-cells to divide.
- **Memory T-cells** - these are formed from cytotoxic T-cells which continue to circulate in the blood and lymph long after the immune reaction has taken place. They can rapidly respond to any other appearance of the same type of antigen. These are the key players in vaccinations - once the body has been exposed to a small amount of antigen, it can build up immunity to specific antigens.

MHC-encoded proteins (Major Histocompatibility Complex) mark every cell as 'foreign' or 'self'. These are encoded by genes in a specific region of the host DNA. There are millions of different MHC-encoding varieties, such that two unrelated individuals will be extremely unlikely to have the same MHC-encoded proteins. It is proposed that it is more difficult for the immune system to defend against tumour growth than viruses or bacteria, since the tumour cells and the adjacent normal cells will have the same or similar proteins [131]. Hence, the immune system may not recognise the developing tumour as being abnormal and so not respond sufficiently to curb subsequent growth. So-called *immunogenic* tumours induce a strong immune response. These tumours tend to be induced, for example, by a carcinogenic virus, rather than spontaneously occurring [184, 232].

1.2.3 Angiogenesis and Metastasis.

Folkman [14, 66, 68, 74, 75] has shown that cancer cells produce a distinct chemical factor, called Tumour Angiogenesis Factor (TAF), which stimulates the rapid formation of new capillaries. As the *in vivo* tumour approaches its diffusion limited size the local TAF concentration increases and induces neighbouring blood vessels to grow towards and into the colony. The malignancy becomes vascularized and perfusion then supplants simple diffusion as the dominant mechanism for the supply of nutrients and the removal of wastes. Once the tumour connects with the circulatory system all constraints imposed on it by diffusion are eliminated.

The growth of a vascularized tumour can be exponential and as well as providing a continuous supply of nutrients, the proximity of the blood vessels gives a route for cells to be released into the blood for metastasis. Blood flow within a tumour is often erratic and the endothelium is abnormal and liable to injury [21].

It is thought that tumour metastasis is a highly selective competition favouring the survival of a subpopulation of metastatic cells pre-existent within the heterogeneous population of the primary tumour [63]. This metastatic subpopulation dominates the primary tumour mass early in its growth. The cells in the subpopulation grow faster than the other tumour cells, adhere less to each other and become more metastatic the more they divide. They seem to have the ability to divide many more times than other tumour or normal cells. Most tumours consist of a large proportion of cells that are not capable of further division, typically in the range of 20-70%.

Tumour cells are thought to be more easily separated from a solid tumour mass than their counterpart normal cells from surrounding tissues [167, 221]. Also, adhesion between highly metastatic cells and other tumour cells is noticeably lower than that demonstrated by normal cells or benign tumour cells [207]. This implies that the organisation of tumour cells within the tumour itself may influence metastatic behaviour - if the subpopulation of metastatic cells are initially in the centre of the tumour, then they are less likely to be able to escape from the mass than those near the periphery.

Motility is a feature of almost all living cells, but usually is inhibited when close contact is made between similar cells, or between cells and a suitable substrate. Autocrine motility factor is released by transformed cells into their culture medium, and appears to stimulate their motility [167].

The arrest and metastasis formation of lymph-borne tumour cells at the regional lymph nodes and the arrest of malignant cells that enter the blood stream and form distant organ metastases are thought to be determined by anatomical and mechanical considerations [167]. It has been known for a long time that different types of cancer tend to form secondary tumours in certain organs and not in others [47]. The important tumour cell properties in the mechanical lodgement of circulating tumour cell clumps are their release into the lymph and blood systems and their abilities to undergo heterotypic and homotypic adhesion during their transport to distant sites. The most frequent distant organ site of blood-borne metastatic involvement is the lung.

To explain metastatic colonisation that cannot be due to mechanical lodgement and anatomical considerations, Paget [178, 179] proposed the 'seed and soil' hypothesis. This proposes that the micro-environment of each organ (the 'soil') influences the implantation, invasion and survival of particular tumour cells ('seed'). Tumour cells that form metastases are not invincible, and cannot grow just anywhere. It follows from Paget's hypothesis that both seed and soil

must have unique properties. For example, the cancer cell must be able to survive the journey through the blood stream, have the capacity for implantation on the 'chosen' organ and be able to survive and multiply to form a new colony once implantation has occurred. In addition the organ must be susceptible to implantation of the cells and be a suitable site for proliferation and vascularization to occur.

1.3 Mathematical Models of Avascular Tumour Growth.

The simplest experimental model of solid tumours are multicellular spheroids (MCS). These are three-dimensional, multicellular aggregates, which are grown in tissue culture (for a review see Durand [58]). MCS models are used to study the growth kinetics of small populations of cells and the re-growth kinetics of the population in response to cytotoxic treatments. MCS models have similar growth kinetics to tumour nodules and they develop microregions of quiescent cells in much the same way as solid tumours do. Furthermore, they have simple geometry and are easy to manipulate. However, it is difficult to compare MCS models directly with *in vivo* tumours, since they do not incorporate the influence of the host on the tumour's growth.

Experiments on the growth of nodular carcinomas by diffusion alone show that the pre-vascularized development of a tumour is regulated by the depletion of nutrients, the production of katabolites and the disintegration of necrotic cellular debris [210]. [A katabolite (or catabolite) is any product of catabolism, which is a metabolic process in which complex compounds are broken down into simpler substances]. When the tumour reaches its maximum avascular size (1–3mm), and enters a state of equilibrium, the tiny cell colony consists of three distinct concentric spherical shells [129, 130]. The outer shell is several layers thick and mitosis is prominent, the middle shell contains viable but non-proliferating cells and in the centre is a necrotic core [32].

This section reviews a few mathematical models which incorporate these ideas.

Probably the simplest and most schematic of one-dimensional prevascular tumour growth models is that of Glass [92]. The basic mechanism in this model is that of tissue size regulation via negative feedback from the tissue itself. There is evidence that control of cellular replication in some mammalian tissue is at least partially determined by such mechanisms [24, 175, 228]. The agents of negative feedback ("chalones") are tissue specific, mitotic inhibitors produced by the tissues, and it has been suggested that a breakdown in the normal functioning of the chalone mechanism may be responsible for limitless growth in at least some types of cancer [26, 27, 192]. Strong supporting evidence for this hypothesis comes from a study of the pattern of tumour growth [25].

Glass's model provides a limiting size for stable tissue growth, without describing the time evolution of the tissue prior to that limiting state. He solves the differential equation:

$$\frac{\partial C}{\partial t} = D\frac{\partial^2 C}{\partial x^2} - \lambda C + PS(x)$$

$C(x,t)$= chalone concentration, P= production rate of chalone, D= diffusion coefficient of C, λ= decay rate, and

$$S(x) = \begin{cases} 1 & \text{if } |x| \leq L/2 \\ 0 & \text{if } |x| > L/2 \end{cases}$$

for a slab of chalone-producing tissue of length L, centred at the origin, with the assumption that there is a switch mechanism acting on the mitotic rate, M, *i.e.* there is a critical value of chalone concentration, θ such that

$$M = \begin{cases} 0 & C \geq \theta \\ M_0 & C < \theta \end{cases}$$

Since the time scale for diffusion of chalone is small compared to a typical time scale for tissue growth, time dependence of C is dropped. By solving the new equation to find C, he then characterises the transition from stable to unstable growth by a dimensionless number, n, which is defined in terms of the parameters describing the system.

Shymko and Glass carried over these ideas in considerable detail in [198]. They also examine the stability of growth as a function of the values of the parameters describing the production, transport and decay of the chalone, and also as a function of the geometry of the growing tissue. Again, mitosis is assumed to switch on and off discontinuously as the concentration of inhibitor passes through the threshold value and they also assume that the initial geometry is maintained throughout growth.

Their conclusions are that stable tissue size is reached when mitosis becomes completely inhibited throughout the tissue. They find that the two consequences of including the effects of cell death in the formulation are

(i) stable limited growth may occur even in situations which were unstable without death and

(ii) a peripheral mitotic zone will exist even at the stable size.

When they changed the mitotic rate to a more realistic decreasing sigmoidal function of the concentration of growth inhibitory factors, they found that a transition zone appears between the inhibited and non-inhibited regions, and the width of this zone increases as the response

function becomes less steep. This results in a narrow outer mitotic zone in a tissue which would be at its stable size with no mitosis if the response function were discontinuous. They conclude that if the mitosis is never completely inhibited, some loss mechanism is required to achieve stability.

Adam [1] presents a one-dimensional model of tumour tissue growth in which the source of mitotic inhibitor is non-uniformly distributed within the tissue. He uses the schematic model of Glass [92] and examines the sensitivity of the results in this paper to non-uniform production of mitotic inhibitor (chalone) in the central tissue region. For this non-uniform production, he chose a continuous linearly decreasing function of distance from the centre of the tissue.

$$S(x) = \begin{cases} 1 - 2|x|/L & \text{if } |x| \leq L/2 \\ 0 & \text{if } |x| > L/2 \end{cases}$$

for a slab of chalone-producing tissue of length L, centred at the origin.

Chalone is produced at a rate P per unit length, diffuses with coefficient D and decays at a rate λ proportional to its concentration $C(x,t)$.

Since the time scale for diffusion of chalone is small compared to a typical time scale for tissue growth, time dependence of C is again dropped. As in Glass's model [92], the distribution of the chalone, $C(x)$, is used to determine the ultimate or limiting size of tissue and when limitless growth occurs.

The one-dimensional equation for the model is:

$$\frac{d^2C}{dx^2} - \alpha^2 C = \varpi(x)$$

where $\alpha = (\lambda/D)^{1/2}$, $\varpi(x) = -P\,S(x)/D$, with the mitotic rate, M, given again by:

$$M = \begin{cases} 0 & C \geq \theta \\ M_0 & C < \theta \end{cases}, \tag{1.1}$$

for a critical value of chalone concentration, θ.

This is then solved analytically to find $C(x)$. This function of chalone concentration is found to have a maximum at $x = 0$ followed by a minimum at $x_1 > L/2$. So, C(x) decreases monotonically from its value at $x = 0$ to its value at $x = L/2$ and similarly of $-L/2 \leq x < 0$.

He finds the values of $n = P/2\lambda\theta$ for which growth is stable (*i.e.* a limiting size of tissue exists). Overall, it is shown that for a schematic model of inhibitor-producing tissue embedded in an inhibitor free environment, significant modifications to the pattern of growth occur when compared with the results for uniform production of inhibitor, as obtained by Glass [92]. But, he concludes that to get any results that can be considered comparable to experimental data,

a three-dimensional model must be used.

He pursues this idea in a later paper [2], extending this simple one-dimensional model to two and three dimensions.

Then the equation governing the local concentration $C(r)$ of growth inhibitor (chalone) is assumed to be

$$\frac{\partial C}{\partial t} = D\nabla^2 C - \gamma C + \lambda S(r)$$

where λ is an inhibitor production rate, D is the diffusion coefficient and γ is the decay constant. The source term $S(r)$ is chosen to be a simple measure of non-uniform production of inhibitor within the tissue and is defined by

$$S(r) = \begin{cases} 1 - r/R & r \leq R \text{ (inside the tissue)} \\ 0 & r > R \text{ (outside).} \end{cases}$$

Again, diffusion of the chalone is assumed to be very rapid compared with the process of tissue growth, so he takes $\frac{\partial C}{\partial t} \equiv 0$ to compute the steady state distribution.

Thus the equation becomes

$$-D\nabla^2 C + \gamma C = \lambda S(r).$$

Also, as in [1], mitosis is assumed to be controlled by a discontinuous switch-like mechanism - described by (1.1).

Following Shymko and Glass's treatment [198], three basic geometric configurations are investigated:

a) A thin uniform cylindrical tube, of length 2R, centred at the origin. The concentration, $C(r)$ depends on axial distance r from the centre of the tube (one-dimensional model);

b) A thin cylindrical disc, where again $C = C(r)$, only $0 \leq r \leq R$ (two dimensions);

c) A sphere with $C = C(r)$, $0 \leq r \leq R$ (three dimensions);

with the additional assumption that initial geometry is conserved throughout growth.

Suitable boundary conditions are chosen and the differential equation solved analytically to find C(r) in the three cases. The concentration of growth inhibitor, C(r), is found, in all cases, to be a monotone decreasing function in [0,R].

For stable tissue growth, it is found that growth occurs initially throughout the tissue, but eventually a peripheral mitotic zone appears, which becomes increasingly narrow, finally disappearing when the stable size is reached.

The predictions of the nature and pattern of tissue growth in an environment for which

growth inhibitor is produced non-uniformly are compared with those when production is uniform [198]. It is seen that the limiting size reached in stable tissue growth may be greater for non-uniform production, but the prediction for growth pattern is the same in both models. Also, the effect that geometry can have on the growth patterns is the same for uniform and non-uniform production.

Adam takes this idea further again in [3], by setting up a model in which the source term for the inhibitor production rate is intermediate between being uniform throughout the tissue, as in [198] and highly non-uniform [1, 2], but otherwise arbitrary. He solves the equation

$$\frac{-D}{r^2}\frac{d}{dr}(r^2\frac{dC}{dr}) + \gamma_c C = S(r) \tag{1.2}$$

where

$$S(r) = \lambda - \frac{(\lambda - r)}{R}, \quad 0 \leq r \leq \lambda \tag{1.3}$$

subject to the conditions $DC'(R) + PC(R) = 0$ and $C(0) < \infty \; \forall R$.

He finds that the results for the uniform model [198] are recovered in the case with $r = \lambda$ and those from [2] with $r = 0$. So, the results for spheroids for which $0 < r < \lambda$ will be intermediate between these two extremes. The values of a, for which growth is stable and limited, are calculated and the width of the mitotic zone is observed as the tissue size increases.

He concludes that to make the model more realistic, a desirable feature to include would be to add central necrosis.

Chaplain and Britton [35] present another model for the production of growth inhibitory factor (GIF) within an MCS. Their main assumption is that GIF is produced by cells within the spheroid in some prescribed non-linear spatially dependent manner, as in [1]-[3]. The differential equation for the system is given by

$$\frac{\partial C}{\partial t} = D\nabla^2 C - \gamma C + \lambda S(r), \tag{1.4}$$

The source term chosen by Adam [1]-[3] is not smooth, that is, $S'(0) \neq 0$. So, Chaplain and Britton propose a smooth source term

$$S(r) = \begin{cases} 1 - r^2/R^2 & 0 \leq r \leq R \\ 0 & r > R \end{cases}$$

They use the fact that diffusion takes place over a much shorter time scale than that of spheroid growth. They consider spherical geometry and assume radial symmetry. Equation (1.4) and

boundary conditions then reduce to

$$\frac{d^2C}{dr^2} + \frac{2}{r}\frac{dC}{dr} - \kappa^2 C = -\frac{\lambda}{D}S(r),$$

$$\frac{dC}{dr} = 0, \quad r = 0, \qquad D\frac{dC}{dr} + PC = 0, \quad r = R,$$

where $\kappa^2 = \gamma/D$. They non-dimensionalise the system, solve the equation analytically and examine the steady state profile of the GIF in various spheroids of differing radii.

They find that their final GIF profile is comparable with the experimental data of Folkman and Hochberg [71].

Greenspan [103] bases his models on the fact that as the tumour expands, a critical size is reached when the central concentration of a vital nutrient falls below the level required to support cell life. Also, the production and diffusion of katabolites within the nodule further retards growth by restricting the number of cells that can subdivide. The phenomenological descriptions of the growth process are qualitatively the same for the one-dimensional and spherically symmetric growth problems. Greenspan's object is to study a one-dimensional model which includes all the phenomena, but whose mathematical solution is concise and simply described. So, for simplicity, he considers growth of a cell culture in a long tube with a very small cross-sectional area - see Figure (1-1).

His main assumptions for this one-dimensional model are:

(i) A cell dies when the local concentration of a vital nutrient, denoted by σ(z,t), falls below a critical level, σ_1 .

(ii) A chemical produced within the culture prevents cell mitosis without causing death when the local concentration denoted by $\beta(z,t)$, exceeds a critical level, β_1.

(iii) The concentrations σ(z,t), $\beta(z,t)$ are governed by simple diffusion equations (for which all diffusion coefficients and parameters are assumed to be constants). Moreover, since time variations are slow, the culture is essentially in a state of diffusive equilibrium at all times. The equations are then readily solved to obtain formulas for z_i(t) and z_g(t) in terms of the remaining unknown $z_o(t)$. Where $\sigma(z_i(t),t) = \sigma_1$ if $\sigma < \sigma_1$ somewhere; otherwise $z_i \equiv 0$, that is, z_i is the interface between the necrotic debris and the viable cells. $\beta(z_g(t),t) = \beta_1$ if $\beta > \beta_1$ somewhere in the region of viable cells; otherwise $z_g = \max(z_i(t),0)$, *i.e.* z_g is the interface between the viable and dividing cells - see Figure (1-1).

(iv) Necrotic debris disintegrates continually into simpler compounds that are freely perme-

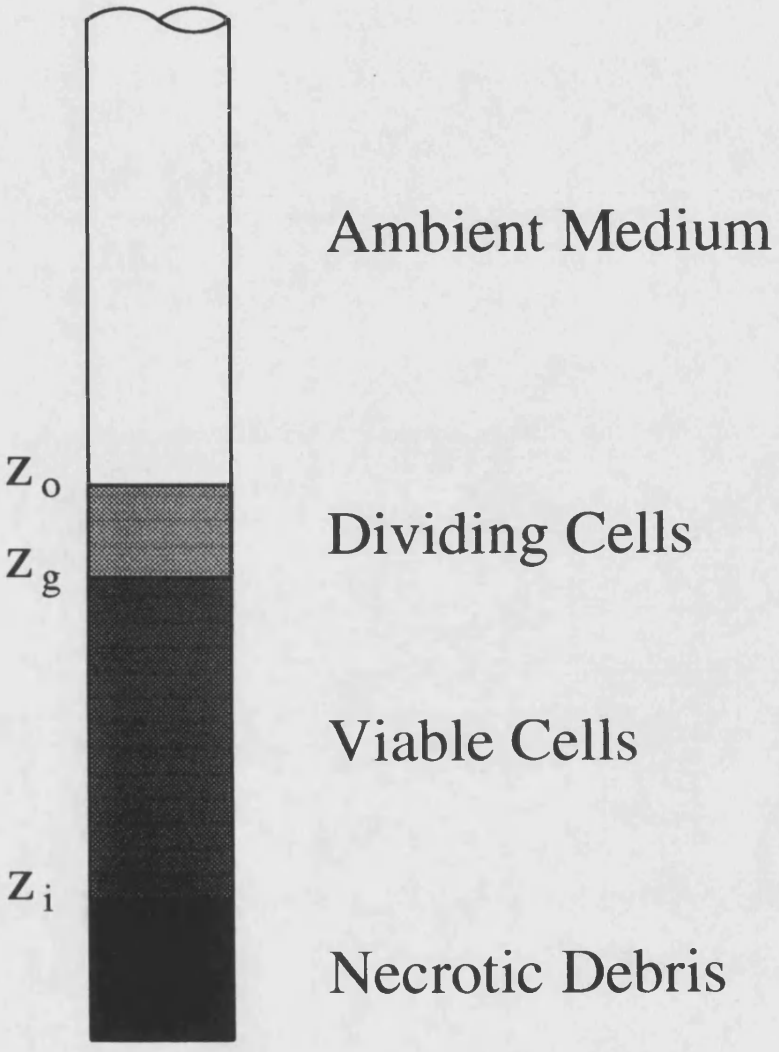

Figure 1-1: A cell colony consisting of three tiers - a top layer of proliferating cells in contact with the ambient medium; a middle layer of non-proliferating but viable cells and a base of necrotic debris.

able through the culture. The mass or cell volume lost this way in necrosis is replaced by cells pushed downward by the forces of cell adhesion and surface tension. The rate of loss of cell volume of dead material is taken to be proportional to the volume of dead material present at any time.

He concludes that if the necrotic material is the source of an effective chemical inhibitor then the growth of the cell population is in three distinct stages. In the first stage, all cells are alive and proliferating so that the growth rate is exponential. However, the concentration of the nutrient σ, which is maintained at a constant level σ_∞ in the ambient medium, decreases with distance from the interface z_o(t). At a time that depends on the consumption rate, C, of nutrient by live cells and its diffusivity k in the culture, cells at the bottom of the vial $z = 0$ are the first to die of nutrient deficiency. This occurs when the culture reaches the critical height

$$h_c = [2k(\sigma_\infty - \sigma_1)/C]^{1/2}.$$

Thereupon, the volume of necrotic debris begins to increase as does the concentration of chemical inhibitor β. However,the volume of live cells, $h_c\alpha$, remains constant forever after, although the proportions of dividing and non-dividing cells do vary. The third stage begins when sufficient chemical inhibitor has accumulated to affect the reproduction rate of the live cells at the necrotic boundary $z_i(t)$. The constant volume of live cells continues to "float" upwards on its necrotic base but the number of proliferating cells decreases as the inhibitor diffuses through the culture. The birth and death rates of cells are identical so that only the necrotic volume increases. The process approaches a steady state in which a small fraction of the viable cells in the segment $z_g \leq z \leq z_o$ reproduce to counterbalance exactly the volume lost in necrotic disintegration.

The description of growth is roughly similar when the chemical inhibitor is a waste product of metabolism.

In other papers [102, 104], Greenspan considers the growth of a spherical tumour, where spherical symmetry prevails at all time. Time, t, and radial distance, r, are the only independent variables. The other assumptions of the models are:

(i) Cancer cells die when the concentration of a vital nutrient, denoted $\sigma(r,t)$, falls below a critical level σ_l.

(ii) The vital nutrient (e.g. oxygen) is consumed by living cells only; the consumption rate may depend on nutrient concentration and cell proliferation as well as other factors.

(iii) A chemical is produced somewhere in the tumour which inhibits the mitosis of cancer cells without causing their death. Its concentration is denoted by $\beta(r,t)$, the critical level is β_l.

(iv) The carcinoma is in a state of diffusive equilibrium at all times.

He also includes a surface tension force proportional to the mean curvature κ to keep the tumour compact and a continuous mass. He assumes that as a new cell forms in the outer mitotic layer and expands to proper size it must push aside neighbouring cells of the culture. The forces of displacement are transmitted with attenuation cell to cell throughout the crowded population. The total pressure developed this way causes internal migration of cells and a drift of the entire colony as it builds in the direction of a richer nutrient supply. He adopts a "seepage" law of motion in which internal motion is proportional to the negative gradient of the pressure.

It is shown that under certain conditions the tendency of the colony to distort by either growth or elimination of material in the necrotic core overcomes the stabilising influence of the surface tension. The tumour development is then unstable, and may achieve a non-linear equilibrium, pinch apart, or even disintegrate depending on the dominant modes of instability and their development in time.

Burton [28] proposed a model, which is really the predecessor of Greenspan's models, in which only diffusion of oxygen (vital nutrient) is considered. He assumes that the supply of O_2 is confined to the periphery and that there is a critical level P_{O_2} in the tumour at which necrosis develops.

Landry *et al.* [142] derived a mathematical expression, based on biological observations and basic physical properties of 3D structures, relating growth rate of MCS to some easily measurable parameters. This growth equation predicts a linear expansion of the spheroid diameter with time and the calculated growth rate is claimed to be comparable to experimental data.

Calderón and Kwembe [29] discuss meanings and limitations of certain mathematical models, and give some new derivations of the existing models. They also present a theoretical justification for Gompertz's law of growth for tumours.

Laird [137, 140] and McCredie *et al.* [149], as well as many others cited in these references, have shown that the data for many solid tumours is fitted very well by the Gompertz Law of growth.

The model assumes a rate of growth for the tumour tissue given by [201]

$$\frac{dm}{dt} = k(\log \frac{A}{m})m \quad i.e. \quad m(t) = m_0 \exp(\log(\frac{m_0}{A})(1 - \exp(-kt))). \tag{1.5}$$

One shortcoming of using this law is that when the detection size or initial size is infinitesimally small, the Gompertzian curve is unobtainable.

A history of this model and its applications can be found in Chapter 3 of [4]. For an example of the direct use of the Gompertz law for modelling cancer, see [170].

1.4 Surface Geometry Coupled to Morphogen.

A *morphogen* is a substance responsible for some aspect of morphogenesis. Controversy surrounding their putative existence seems to be resolving in their favour [199, 214].

Cummings [40]-[44] has proposed a model for the morphogenetic movement of surfaces composed of cellular monolayers. The cells are presumed to be joined at their lateral surfaces. An otherwise unspecified substance called a "morphogen" is introduced which is the agent of change in the individual cell. The distribution of these cellular deformations are used to define a surface via equations given for the Gauss and Mean curvatures of the surface defined at each point. The Gauss curvature determines the metric of the surface "*g(u,v)*" in conformal coordinates *u,v*. A unique equation for the morphogen distribution over the surface is presented which has the property of size invariance, *i.e.* the model "regulates". The two resulting coupled equations for the metric and the morphogen can be solved self-consistently, once the individual cell deformation, as a function of morphogen level, is given. The surface geometry determines the morphogen distribution and the morphogen distribution in turn affects the surface geometry. He then extends the model to two morphogens and gives a formula for calculating with three or more.

He carries out numerical integration of the two coupled equations in the case of axial symmetry, and he concludes from this that individual cells deform by changing the ratio of their apical to basal areas as well as their heights. In [42], he presents a simple picture of gastrulation as an example of the formulation.

1.5 Simulations of Cell Movements and Processes.

1.5.1 Cellular Automata Models of Cell Movements.

A cellular automaton model consists of a simulation which is discrete in time, space and state. They are simple systems that mimic the physical laws, which are often numerically intractable, by a series of simple rules that are easy to compute quickly and in parallel.

Williams and Bjerknes [229] simulate the induction of a tumour in the basal layer of an epithelium using such a model. Their primary assumption is that tumour growth begins when a single abnormal cell divides faster than surrounding normal cells by a factor κ; the "carcinogenic advantage". Cells are placed on a hexagonal lattice and each cell has six nearest neighbours. Whenever a cell divides, one of its neighbours (chosen at random) is pushed out of

the basal layer. They found that the probability of regression (*i.e.* when the entire abnormal clone is pushed out of the basal layer) is $\frac{1}{\kappa}$, this was virtually the only mathematically rigorous result they obtained. They concluded from their model that the infiltrating patterns normally associated with cancer growth may be as much due to counter-invasion of the abnormal by the normal cells, as to invasion of the normal by abnormal cells.

Qi *et al.* [185], present a model describing the immune system surveillance against cancer. They consider a two-dimensional square lattice of $n \times n$ sites. Each site has four nearest neighbours and may accommodate either a normal cell, a cancerous cell, a complex or a dead cancer cell, where complexes are the product of the cytotoxic process. They assume that an effector (cytotoxic) cell is "hiding" in each compartment. At $t = 0$, only five cancer cells are set in the central part of the lattice and all the other sites are occupied by normal cells.
The rules of the system are:
(i) If the randomly chosen compartment (i, j) is occupied by an abnormal cell, it may proliferate with probability k_1' or may be bound by an effector cell hiding in the same site, to form a complex, with probability k_2. Because the proliferation rate k_1' *in vivo* decreases as the malignant tumour expands, they propose that it is reasonable to assume that $k_1' = k_1(1 - N_c/\phi)$, where N_c is the total number of cancer cells and ϕ is a constant. They introduce the concept of density, d of tumour cells to describe the effect of the mechanical pressure on cancer development and choose a critical density value, d_c. If the density is less than this value, the second daughter cell resulting from proliferation can only occupy one of the inside nearest (*i.e.* closest to the origin) neighbouring sites originally occupied by normal cells. The probability that one site will be invaded is the same as any other feasible site. If $d > d_c$, the second daughter cell may invade any one of the nearest neighbouring sites originally occupied by normal cells with equal probability for each neighbouring site.
(ii) If the compartment is occupied by a complex, it may dissolve with probability k_3. If it dissolves, the complex is replaced by a dead cancer cell and an effector cell E_0 hiding in the compartment.
(iii) If a dead cell occupies (i, j), it may escape or dissolve with probability k_4. If this does happen, the compartment will be occupied by a normal cell with a hiding effector cell. This operation, where a normal cell just "appears" in the middle of tumour tissue, is used to represent the infiltration of the normal tissue into the cancerous tissue.

They analyse their results and compare them with experimental data. The experimental results are systematically described invoking the Gompertz formula. They then obtain values for m_0, k and A in (1.5) using the method of least squares. The effects of k_1, k_2, k_3, k_4 on the Gompertz growth are investigated. It is found that N (maximum tumour size) and N_c (total number of cancer cells) increase with k_1. Increasing k_2 damps the growth of the tumour, since

the immune network plays a critical role in restraining a cancer. The smaller k_3 (or k_4), the slower the development of N_c. This is because the occupation of sites by complexes (or dead cells) prevents the cancer from proliferating. If k_3 (or k_4) is smaller, more complexes (or dead cells) stay inside the tumour. Thus, the smaller the value of k_3 (or k_4), the faster the development of N, that is, the faster the tumour grows, even though the number of proliferating cells isn't very high.

Ermentrout and Edelstein-Keshet [61], review a number of biologically motivated cellular automata that arise in models of excitable and oscillatory media, in developmental biology, in neurobiology and in population biology.

All simulations that run on computers are in fact cellular automata, since all computers operate at finite precision on numerical discretizations of the time and space domains.

1.5.2 Cell Sorting Models.

There have been many mathematical models developed to simulate cell movements within solid aggregates of biological cells. Cell sorting models are just one of the ways that have been used for this aim. In the rest of this section, I will try to summarise the experimental observations that have inspired these models, investigate the theory behind them, and also review a small selection of the models that I have encountered.

In a number of cell sorting experiments [10, 46, 88, 116, 168, 202, 203, 204, 218, 230], cells display a remarkable ability to migrate over distances much greater than one cell diameter in order to restore disrupted patterns or form new ones.

Probably the most fundamental facts concerning tissue reconstruction are the following four points:

(i) When the cells of different vertebrate embryonic tissues are dissociated and mixed, they are capable of establishing adhesions with one another and constructing common aggregates [116, 230].

(ii) Within such 'mixed' aggregates, containing cells from different tissues, the differing kinds of cells regroup, each with the others allied to it, to reconstruct the various tissues of origin [85, 206].

(iii) These tissues are reconstructed in definite positions; e.g. muscle is always built external to cartilage and the natural configuration of mesoderm, endoderm and ectoderm [115].

(iv) When the tissues employed are parts of a complex within the embryo, the geometry of the entire normal complex is reflected in the reestablished structures [205]

The natural configuration of mesoderm, endoderm and ectoderm from amphibian embryos can be recovered from excised tissues combined in the right proportions [115]. When mixed

together in suspension, neural and pigmented chicken embryo retina cells will precipitate to produce a disordered aggregate. The initially irregular aggregate rounds over time. Pigmented cells coalesce at the centre to form a sphere while neural cells organise to form an encompassing outer layer. Significantly, the outcome of sorting experiments is largely independent of the initial conditions [206]. An aggregate of neural cells rounds in isolation but spreads to engulf a pigmented cell aggregate if the two are placed in contact. Similarly, an intact fragment of chicken heart ventricle will envelope a chicken cartilage fragment. The coelenterate animal *Hydra vulgaris* [78, 193, 213] is basically a hollow cylinder with an extracellular matrix sandwiched between layers of endodermal and ectodermal cells. When dismantled at the cellular level, hydra display an amazing ability to recover their original state and when turned in-side-out they are able to re-invert themselves. These, and other observations, suggest an underlying mechanism for cellular pattern formation based on intrinsic cell properties rather than chemical gradients or the starting locations of cells in a tissue.

Experiments have demonstrated that differences in intercellular adhesivity determine the final state of cell sorting, the cell configuration approaching the global minimum of overall surface energy [205].

Preliminary Theory.

- **Steinberg's Differential Adhesion Hypothesis**

  Steinberg proposed the Differential Adhesion Hypothesis [99, 202, 203, 204] to explain cell sorting as a minimisation of contact energy at cell interfaces. Experiments [76, 115, 163] show that the strength of attachment between two cells which come into contact depends on the type of cells involved. The difference in adhesion energy results from the number and particular type of surface adhesion molecules present on the cell membrane. Classes of adhesion molecules include cadherins, N-CAM and many other varieties, some non-specifically adhesive, others, like N-CAM, extremely variable in sequence (and hence relative adhesivity) between cell types. Movement of a cell requires work against the adhesive forces of its neighbours under the constraint on cell volume imposed by membrane elasticity. Thus, affinity between neighbouring cells determines the energy of a cell aggregate. Energy is stored at interfaces between cells which have the potential to form stronger attachments with more amenable coupling partners. Cytoskeletal membrane fluctuations allow the cells in an aggregate to explore an abstract energy landscape randomly yet exhaustively. The local energy gradient drives cells. Dissipation inexorably leads to a configuration with absolute minimum energy. As jostling causes adhesion molecules to unbind and re-bind, strong bonds tend to replace weak bonds, making best use of the available binding energy and thereby maximising the work required to remove a cell from an aggregate. Differential adhesion is thought to play an important rôle in

processes such as cell recognition [29], gastrulation [148, 187], cell shaping [171], control of pattern formation [166] as well as cancer metastasis [211].

- **Monte Carlo Method**

  The Monte Carlo method obtains a single outcome for a function containing a probability value by selecting a pseudorandom number, comparing it to the probability value, and substituting 0 or 1 depending on whether the selected number exceeds the probability value. By repeating the simulation many times, a distribution of outcomes is obtained. Monte Carlo simulations are particularly useful in predicting outcomes where a simple set of initial conditions results in a large number of possible outcomes, from which it is too difficult or cumbersome to derive any analytical solutions. By performing repeated trials and observing the distribution of outcomes that evolve through time, one can predict the behaviour of complex systems.

  The name "Monte Carlo" arises from the random or "chance" character of the method and the famous casino in Monaco [134].

- **Ising Models**

  Models in which the degrees of freedom reside on a lattice and interact locally arise in several areas of condensed matter physics and field theory. The simplest of these is the Ising model, which can be taken as a crude description of a magnetic material [134].

  For example, using the magnetic language, the Ising model consists of a set of spin degrees of freedom interacting with each other and with an external magnetic field. Consider a model where the spin variables are located on the sites of an $N_x \times N_y$ square lattice. The spins can therefore be labelled S_{ij}, where i, j are the indices for the two spatial directions, or as S_α, where α is a generic site label. Each of these spin variables can either be "up" ($S_\alpha = +1$) or "down" ($S_\alpha = -1$). The Hamiltonian (sum of kinetic and potential energies) for the system is conventionally written as

$$H = -J \sum_{<\alpha,\beta>} S_\alpha S_\beta - B \sum_\alpha S_\alpha$$

  The notation $< \alpha, \beta >$ means that the sum is over nearest neighbour *pairs* of spins; these interact with a strength J. There are four nearest neighbours of any site (NSEW) not on the boundary. When J is positive, the energy is lower when a spin is in the same direction as its neighbours, while when J is negative, a spin will tend to be anti-aligned with its neighbours. The term involving B represents the interaction of the spins with an external magnetic field.

  Configurations of the system are specified by giving the values of all $N_x \times N_y \equiv N_s$ spin variables and the weighting (probability that it will be chosen) of any one of the 2^{N_s} spin

configurations, S, is

$$w(S) = \frac{e^{-H(S)}}{Z}$$

where the partition function is

$$Z(J,B) = \sum_S e^{-H(S)}.$$

A site is chosen at random, and a trial is performed to see if it is feasible to flip the spin of that site. If the change in Hamiltonian ΔH is negative, then the trial is accepted, if it is positive, it is accepted with probability $e^{-\Delta H - B}$.

An Ising model is the two-dimensional version of a *Potts Model.*

- **Metropolis Algorithm**

  One very general way to produce random variables with a given probability distribution of arbitrary form is the Metropolis algorithm [152]. As it requires only the ability to calculate the weight function for a given value of the integration variables, the algorithm has been applied widely in statistical mechanics problems, where the weight function of the canonical ensemble can be a very complicated function of the coordinates of the system and so cannot be sampled conveniently by other methods. However, it is not without its drawbacks.

  The algorithm can be implemented in one simple way. Suppose one wants to generate a set of points in a (possibly multi-dimensional) space of variables $\mathbf{X}$ distributed with a probability density $w(\mathbf{X})$. The Metropolis algorithm generates a sequence of points, $\mathbf{X_0}, \mathbf{X_1}, ...$, as those visited successively by a random walker moving through $\mathbf{X}$ space; as the walk becomes longer and longer, the points it connects approximate more closely the desired distribution.

  The rules by which the random walk proceeds through configuration space are as follows. Suppose the walker is at point $\mathbf{X_n}$ in the sequence. To generate $\mathbf{X_{n+1}}$, it makes a trial step to a new point $\mathbf{X_t}$. This new point can be chosen in any convenient manner, for example uniformly at random within a multidimensional cube of small side δ about $\mathbf{X_n}$. This trial step is then accepted or rejected according to the ratio

$$r = \frac{w(\mathbf{X_t})}{w(\mathbf{X_n})}$$

  If r is larger than one, then the step is accepted (*i.e.* $\mathbf{X_{n+1}} = \mathbf{X_t}$), while if r is less than one, the step is accepted with probability r. This latter is conveniently accomplished by comparing r with a random number η uniformly distributed in the interval [0,1] and ac-

cepting the step if $\eta < r$. If the trial step is rejected we put $\mathbf{X_{n+1}} = \mathbf{X_n}$. This generates $\mathbf{X_{n+1}}$, and we may then proceed to generate $\mathbf{X_{n+2}}$ by the same process, making another trial step. Any arbitrary point, $\mathbf{X_0}$ can be used as a starting point for the random walk.

Antonelli *et al.* [9] simulate cell-sorting in embryogenesis describable by Steinberg's differential adhesion mechanism, using the exchange model. The exchange principle allows the exchange of a given, randomly chosen, cell in an aggregate with one of its nearest neighbours depending on whether this decreases the free energy. Their model involves differential adhesion between cells on a hexagonal lattice, which exchange places so as to minimise the free energy of the system.

They successfully simulate transitivity, pattern reversal and engulfment by changing certain parameters of the model. Also, they tackle the problem of *duality* (where a simulation with 3 or more cell-types results in states whose interpretation is hampered by the presence of a form of figure-ground ambiguity).

Sulsky *et al.* [209] introduce Voronoi polygons (described in the following paragraph) as a suitable representation for a two-dimensional cell sheet. These polygons are defined in terms of a finite number of points making numerical simulations tractable, but also allowing cells to change neighbours and their shape in response to deforming forces without leaving gaps in the tissue. Using this geometry and Steinberg's adhesion hypothesis, they simulate rounding of uneven tissue and engulfment of two intact tissues, using the method described below.

To set up the initial configuration of cells, (Voronoi polygons), N markers are chosen at random within the two-dimensional domain. For biological applications it is convenient to refer to these markers as nuclei. A cell is then a region of space which consists of points closer to a given nucleus than to any other. Two cells are neighbours if they have an edge in common. Polygons constructed in this manner are also known as Meijering cells [89] or Dirichlet domains.

To each pair of cells, a characteristic surface tension, e_{ij} per unit length, is assigned, which means that the free energy of the aggregate can be written

$$V = \sum_{<i,j>} l_{ij} e_{ij}$$

where $< i, j >$ denotes a sum over pairs of cells and l_{ij} is the length of the edge between cell i and cell j. e_{ij} is assumed to be time independent, to avoid complication. The choice of cell geometry leads to a discrete problem of finding a path through the configuration space $C(\mathbf{x_i})$, of steepest descent along the surface $V(\mathbf{x_i}, e_{ij})$ with a given dissipation Φ. Also included are N

area constraints which express conservation of mass for cells with constant density,

$$\frac{dA_i}{dt} = 0$$

With the Voronoi polygons and these assumptions, they simulate the rounding up of tissue fragment, the engulfing of one tissue by another and the intermixing of two cell types.

Graner and Sawada [101] also use Dirichlet domains (Voronoi polygons) as a method to simulate biological cells. Free Dirichlet domains are similar to ordinary ones, with each cell denoted by a centre. The cell is the subset of the space which is nearer to its centre than any other, but with the additional constraint that the distance from the centre must be less than a specified quantity, R. If two centres are closer than 2R, their mediatrix plane is the contact surface between their cells. But, if two neighbouring centres are further apart than 2R, each cell has a free membrane, a spherical cap with radius R.

Free Dirichlet domains experience no singularity, not only during neighbour exchange, but also when a centre loses neighbours by drifting towards the edge of the cellular pattern. Instead of stretching and unrealistically elongating, the domain detaches from its neighbours and a portion of its membrane becomes free. If cell density is low and cells are not very adhesive, intercellular gaps can exist. So, this representation is suitable for loose aggregates or sub-confluent monolayers.

The energy of the configuration is the sum of the adhesion energy between neighbouring cells and the adhesion energy between free surfaces and the surrounding medium. (Adhesion energy is proportional to the length of the edge of contact). Each centre feels the local effect of the whole energy gradient, which acts on it as a force. This force moves the centre to minimise the total energy of the pattern along the steepest path of the energy landscape.

Using this representation of cells and the effect of a deterministic force based on the gradient of the cell-cell adhesion energy, they show that differential adhesion can be a general morphogenic mechanism.

The large-Q Potts model (Q is the number of different 'spins' in the model) is a combination of discrete and continuum methods. The model can simulate diffusive grain growth driven by surface energy, and can correctly simulate experimentally observed topological changes in cellular patterns in metals and soap froths [95]. (Grain growth is the increase in mean grain size which occurs upon annealing a polycrystalline aggregate after primary recrystalization is complete [110]). The Potts model can also be applied to biological systems such as the development of the slime mold, *Dictyostelium discoideum* [123, 194], and tumour growth [55, 56, 57].

Glazier *et al.* use this model for a starting point for their cell-sorting models. These will be discussed in Section (3.1).

1.5.3 Other Simulations that use the Monte Carlo Method.

Michelson [153] presents a Monte Carlo simulation of the dynamics of individual cell populations which express differential sensitivities to generic cytotoxic agents. The mathematical model which underlies the simulation system describes the population dynamics of two kinds of cells (sensitive and resistant) as a stochastic birth-death migration process while describing the transition probabilities as deterministic or phenomenological functions of an agent's (cytotoxic) concentration. The probability that a cell either dies or alters its phenotype in the presence of the agent, at a given level of activity, represents the intrinsic capacity of the "average" cell to respond to the biochemical/biophysical activities of the agent.

Drasdo *et al.* [55, 56, 57] describe the stochastic dynamics of tissues of cells with emphasis on epithelial cells and fibroblasts and fibrocytes of the connective tissue. They investigate pattern formation and growth characteristics of such cell populations in culture numerically, using Monte Carlo simulations for quasi-two-dimensional systems of cells.

All of their models are based on a simplified description of cell shapes. A course grained description is used, which takes into account the cell shapes only in a statistical sense. Attached to each cell is a region in space where most of the cell volume is located with overwhelming probability. The boundaries of these regions define shells around some geometrical surface which marks the average cell shape. Only short range cell interactions are considered.

They roughly distinguish between two age classes, the inter-phase and mitosis. During the inter-phase, the cell is steadily growing until it has doubled its mass, its organelles and DNA content. Then it enters mitosis where it deforms until the next cell division is completed, whereupon the daughter cells enter the inter-phase. See Figure (1-2).

A cell may migrate and rotate during its life.

Cell interaction is modelled by a potential, V, and a trial is accepted with probability $\propto \exp(-\Delta V)$ when $\Delta V > 0$ - this corresponds to the Metropolis algorithm [152]. Figure (1-3) shows a couple of examples of choices for this potential. a) is a square-well potential, where

$$V(i,j;\tau) = \begin{cases} \infty & \text{for } |\vec{r}_i - \vec{r}_j| \leq R_{ij}(\tau) \\ -\epsilon & \text{for } R_{ij}(\tau) \leq |\vec{r}_i - \vec{r}_j| \leq R_{ij}(\tau) + \delta \\ 0 & \text{otherwise} \end{cases}$$

and b) is a harmonic well, where

$$V(i,j;\tau) = \begin{cases} \infty & \text{for } |\vec{r}_i - \vec{r}_j| \leq R_{ij}(\tau) \\ -\epsilon \sin([|\vec{r}_i - \vec{r}_j| - R_{ij}]\pi/\delta) & \text{for } R_{ij}(\tau) \leq |\vec{r}_i - \vec{r}_j| \leq R_{ij}(\tau) + \delta \\ 0 & \text{otherwise} \end{cases}$$

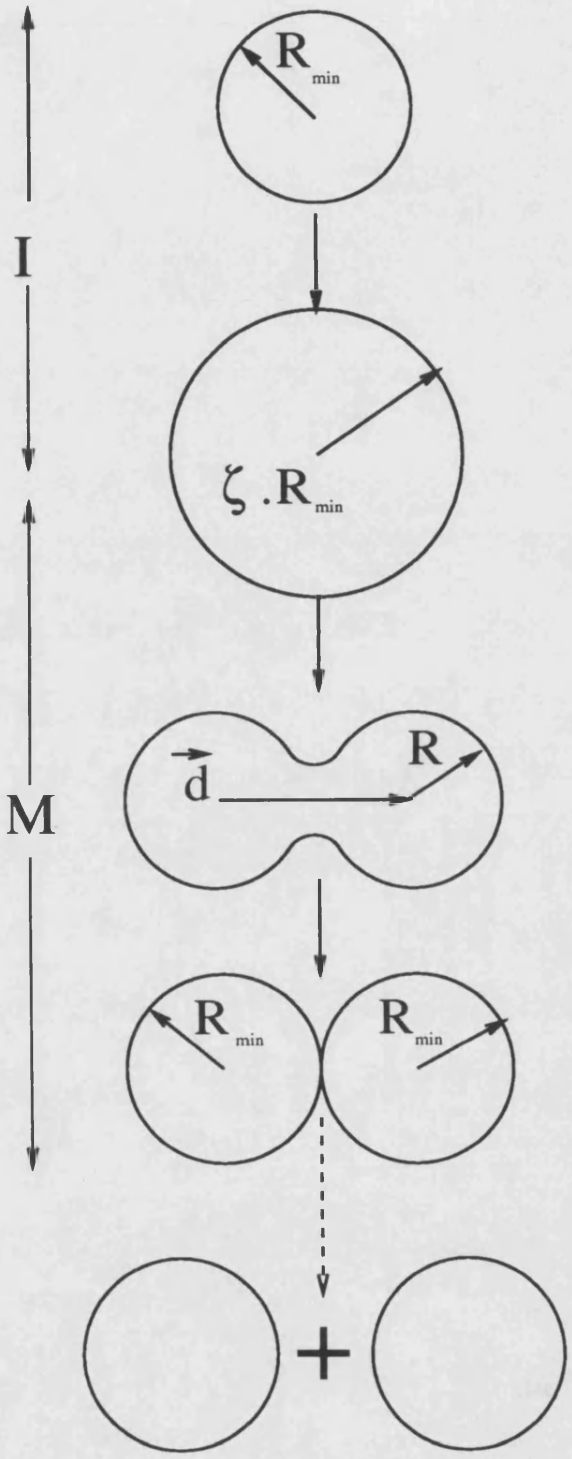

Figure 1-2: Development of average cell shape during a proliferation cycle.

The Monte Carlo method is used to simulate the stochastic dynamics, which are defined by the transition probabilities.

Their work is restricted to cell cultures as they can be regarded as quasi-two-dimensional structures and are more accessible to quantitative experimental methods.

The state S_i of a cell i is described by its position, its age class, and its shape. The cell position is given by the vector $\vec{r_i}$ of its centre of mass. For an I cell (cell in the inter-phase), the shape is characterised by its radius R_i, whereas for an M cell (cell undergoing mitosis), it is the vector $\vec{d_i}$, joining the centres of the corresponding dumbbell which fixes its shape.

During a single updating step, only one randomly chosen cell is considered as active and tries to perform one of the following actions α:
(i) $\alpha^I \in$ {migration, growth} for I cells,
(ii)$\alpha^M \in$ {migration, rotation, deformation} for M cells. See Figure (1-4) for the flow diagram of this algorithm.

A single migration trial consists of a shift $\vec{r_i} \rightarrow \vec{r_i}(1+\delta)$ of cell i in a random direction with a step length which is chosen at random from an interval $[0,\delta r_{max}]$. A rotation trial is defined similarly. During a growth step, the radius of an I cell is increased by a random amount $\delta R \in [0,\delta R_{max}]$, whereas during a deformation step, the length of $\vec{d}$ is increased and at the same time the dumbbell radius is decreased such that the volume of the cell is constant.

Whether a cell i actually performs its chosen trial or not depends on its interactions with other cells. If the trial decreases the cell interaction potential, then it will be performed, but if it increases it, then the trial is performed with probability proportional to exp(- change in potential).

This model "performs" wound healing of a skin cut and the spread of a sarcoma (cancer of the connective tissue) across an epithelial boundary, and results are given for these simulations. Drasdo it et al. then go on to discuss variations of this model, e.g. changing the mobility of the I and M cells, and give examples of cells in vivo that behave in the manner predicted.

Drasdo and Kree expand on the basic model in other later reports [55, 56].

Moore and Berman [161] propose that over generations polyclonal populations tend toward monoclonality (all remaining cells in population originate from one parent cell) when there is variation in the growth properties of the original cells in the initial population. Many tumours have a clonal phenotype. When all cells in a tumour have the same genetic characteristics, it is deduced that all cells in the tumour are descended from a single cell [62, 224]. They employ the Monte Carlo method to simulate the growth of cell clones with different probabilities of cell death.

They assume that tumours start off as populations of genetically distinct and independently dividing cells, each with a potential for unbounded growth with a constant cell cycle time per

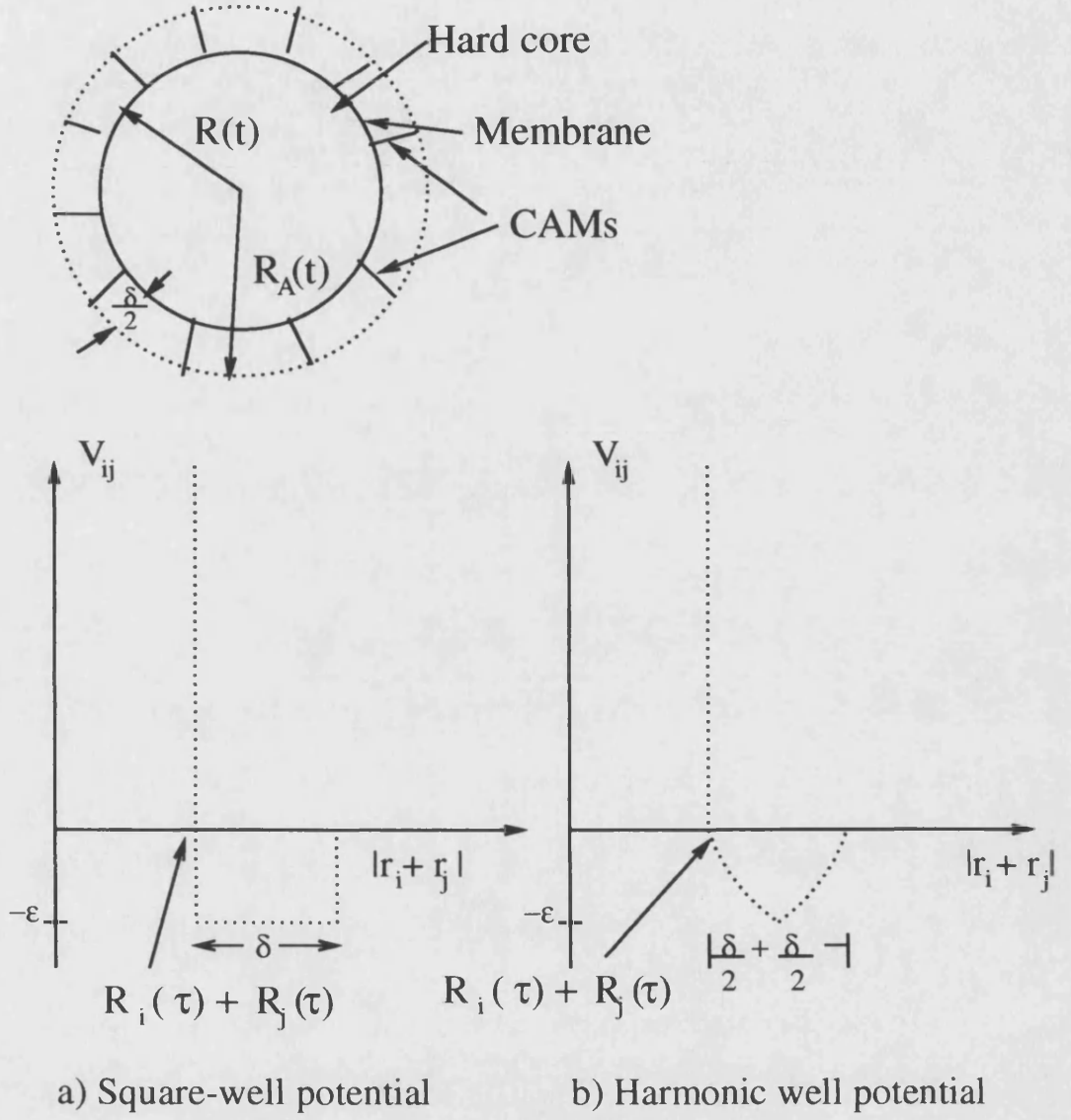

Figure 1-3: Simple diagram of an epithelial cell and two examples of possible interaction potentials.

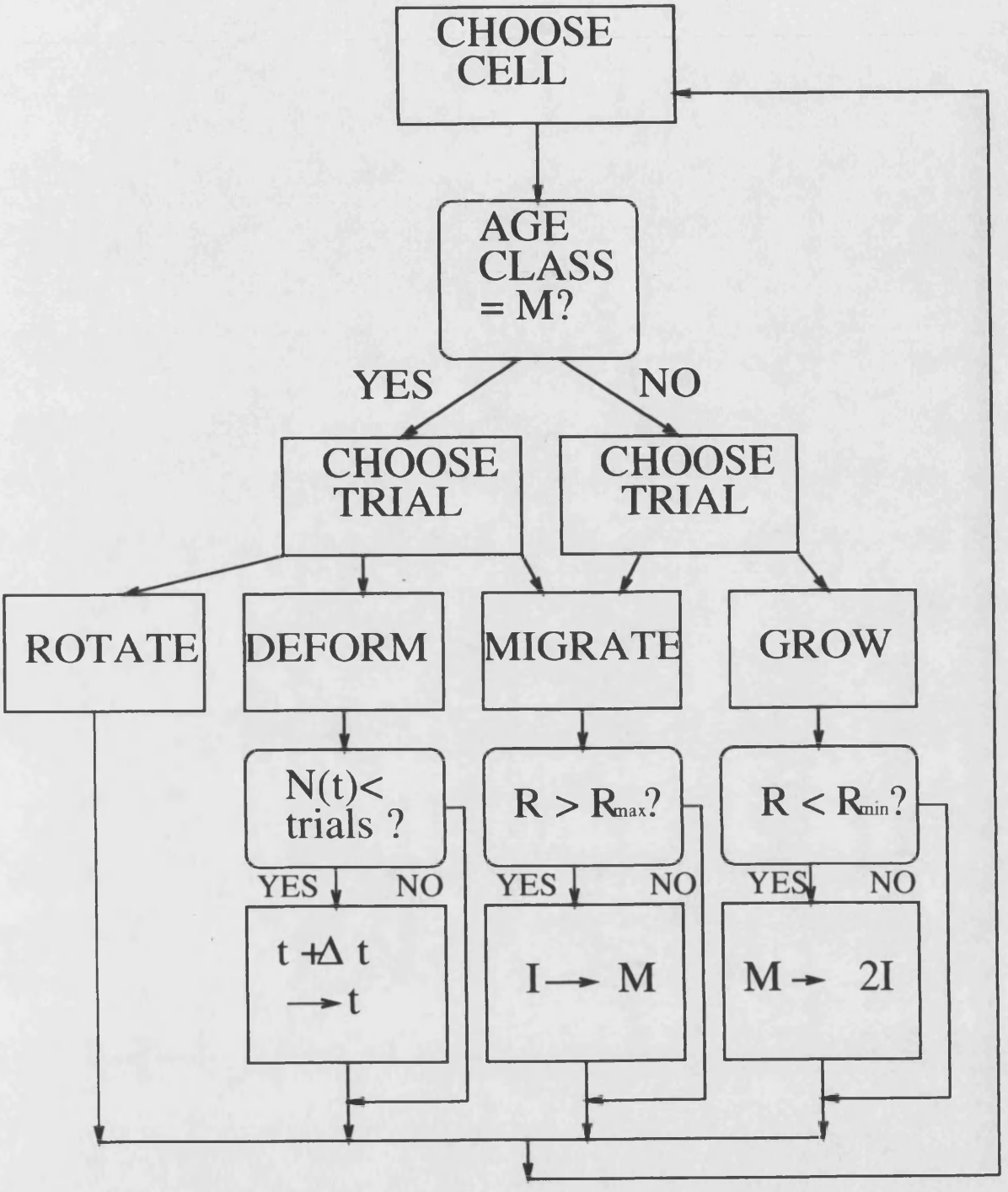

Figure 1-4: Schematic flow chart of Drasdo's basic simulation algorithm.

generation, t, and an inherited death probability, P which is constant.

Their results show that monoclonality can evolve either from minor differences in cell cycle time or in the probability of cell death in a polyclonal 'founder' population.

In a later paper [18], they show, again using Monte Carlo simulations, that small populations of cells with intrinsic cell loss rates, comparable to the cell loss rates observed clinically in human tumours, may regress spontaneously. Also that small variations in the intrinsic cell death probability near 0.5 result in large differences in the number of surviving cells calculated at the 100th generation. They assume that

(i) cancer therapy reduces the tumour burden but does not eliminate all tumour cells. They arbitrarily select 500 cells as the prototypic residual tumour burden;

(ii) residual tumour cells can all potentially give rise to clones of cells that divide until they reach a state where they no longer divide (necrotic and post-mitotic cells);

(iii) the likelihood of a cell entering a non-dividing state can be modelled probabilistically, since tumours as a whole seem to maintain characteristic population cell loss rates.

They compared their simulation results with a corresponding deterministic model. The deterministic model obtains an analytic solution for the number of cells produced by continuously growing populations. This model allows the existence of fractional cells and therefore cannot predict the extinction of clones. Also, the model produces only one answer for the behaviour of a population and does not give a range of possible results. When the simulations resulted in clones with large populations, the population as a whole behaved in a deterministic fashion (logarithmic growth) similar to those observed clinically. The findings provide a plausible explanation for the clinically observed failure of tumours to recur in instances where tumour burden remains following cancer therapy.

They also examine the hypothesis that early lesions operate under the identical growth kinetics of 'late' lesions (neoplasms), but that kinetic features favouring continuous growth in established lesions tend to favour extinction of lesions composed of small populations in [19]. They assume that each cell-cluster begins as a single cell that divides. At each new generation, each daughter cell may either divide or die. Death is determined by an inherited death probability, P, that is constant for the initial cell and all of its descendants. They use Monte Carlo methods again to simulate the growth of the cell populations.

The model demonstrates that small increments in the intrinsic cell loss probability in even the earliest progenitors of malignancy can strongly influence the subsequent development of neoplasia from initiated foci.

Chapter 2

A Two-Dimensional Simulation of Cell Sorting, Proliferation and Effects of the Immune System.

2.1 Introduction.

We started with a preliminary investigation into the general ideas behind simulating an avascular tumour on a lattice. The following models do not reflect reality closely, but pick out salient features that would be important in more realistic simulations later on.

Embryonic cells of two different types, when dissociated, randomly mixed, and reaggregated, can spontaneously sort to reestablish coherent homogeneous tissues [116]. Individual cells in aggregates move randomly in the absence of chemical gradient or adhesion gradients. Steinberg's Differential Adhesion Hypothesis (cf. Section 1.4.2) suggests that a mixture of two types of cells which adhere to one another with different strengths will rearrange themselves until free energy is reduced to a minimum. This is known as cell sorting. A potential energy can be attributed to a cellular pattern because adhesion energy is proportional to the contact area between two cells.

Adhesion energy of system + free energy = constant.

So, increasing the adhesion energy by breaking weak bonds and establishing strong bonds results in a direct decrease in free energy.

2.2 Model with Sorting.

The first model that we studied was very basic and involved sorting of two different types of cells - normal and cancer, but no proliferation. This is considered later in section 2.3.

Each cell was assigned a lattice site (i,j) on a square, two dimensional lattice, and the initial configuration was a roughly circular "tumour" (black cells) in the middle, surrounded by normal (white) cells.

As in the Ising model (cf. Section 1.5.2), the Hamiltonian or potential energy of the system is given by:

$$\mathcal{H} = \sum_{(i,j)(i',j')} (1 - \delta_{\tau(i,j)\tau(i',j')})$$

where (i,j) and (i',j') are neighbouring pixels, $\tau(i,j)$ is the type of cell at site (i,j) and δ_{ij} is the Krönicker delta, *i.e.*

$$\delta_{ij} = \begin{cases} 1 & \text{if } i = j \\ 0 & \text{if } i \neq j. \end{cases}$$

So, the free energy between two cells is 0 if they are the same type and 1 if they are different. The rules of the model were very simple:

(i) pick a cell at random;

(ii) pick one of its four neighbours at random;

(iii) if the two are the same colour/type, move on to choose another cell. If not, then the two cells swap places with Monte Carlo probability.

Monte Carlo probability is given by:

$$P(\tau(i,j) \to \tau(i',j')) = \begin{cases} \exp(-\Delta\mathcal{H}/kT) & \text{if } \Delta\mathcal{H} > 0 \\ 1 & \text{if } \Delta\mathcal{H} \leq 0 \end{cases} \tag{2.1}$$

where $\tau(i,j) = 0$ or 1 (cancer or normal cell, respectively). k is a constant and T is the temperature of the system, suitably chosen to allow optimum energy fluctuations. Throughout the rest of this chapter, we fix $k = 1$ and only allow the variable T to change its value. This is equivalent to merging the two constants, k and T, into one variable, so simplifying the choice of parameters.

For a fixed temperature, the simulation showed the spreading of the cancer cells and mixing of the two types of cell very well. Figure (2-1) shows the results of the simulation as time increases. In these pictures, it can be seen that individual cells, and also clumps of cancer cells, break away from the tumour mass. This is the beginnings of tumour metastasis.

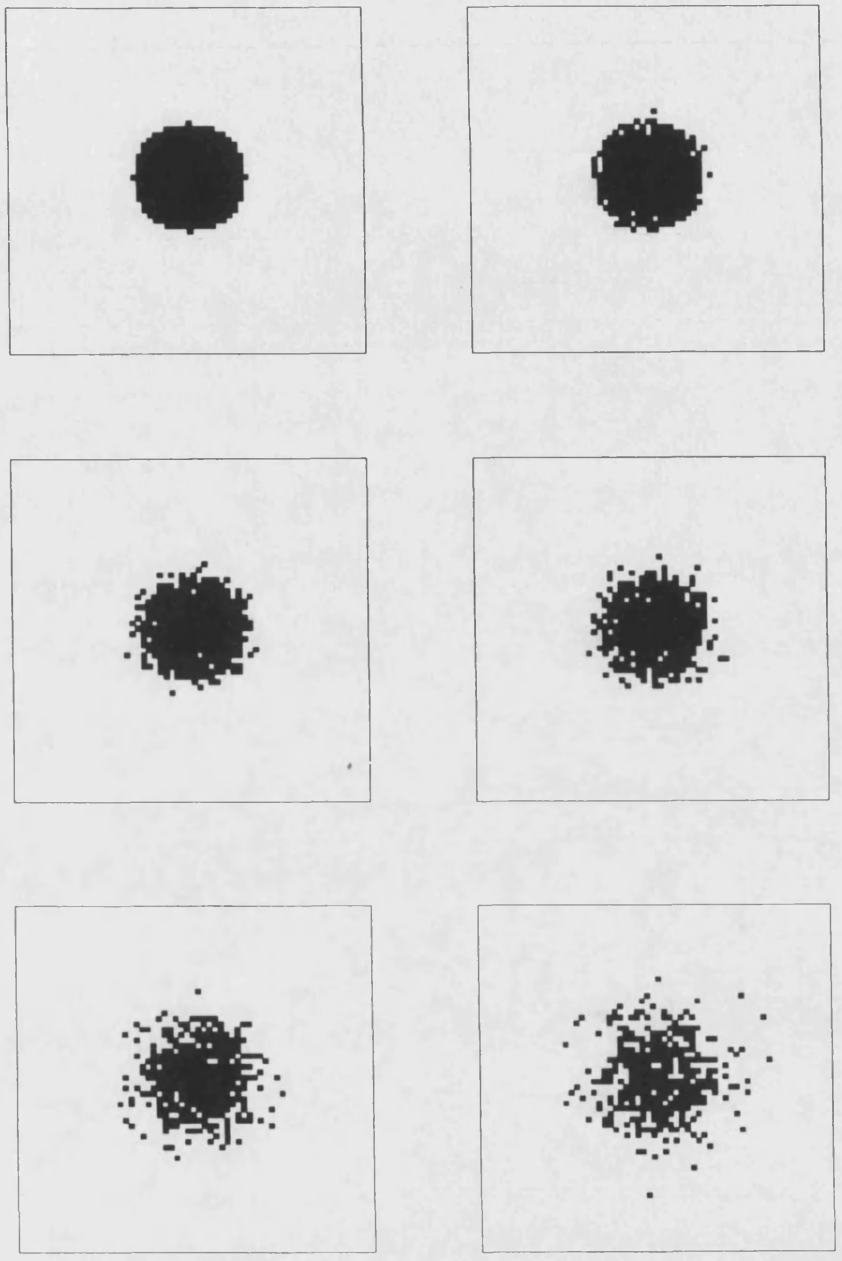

Figure 2-1: Model with sorting: Configuration of sorting cells after (from left to right) 0 updates, 4000, 10,000, 20,000, 50,000 and 100,000 updates. Cancer cells are depicted by black pixels, normal cells by white. $1/T = 0.8$.

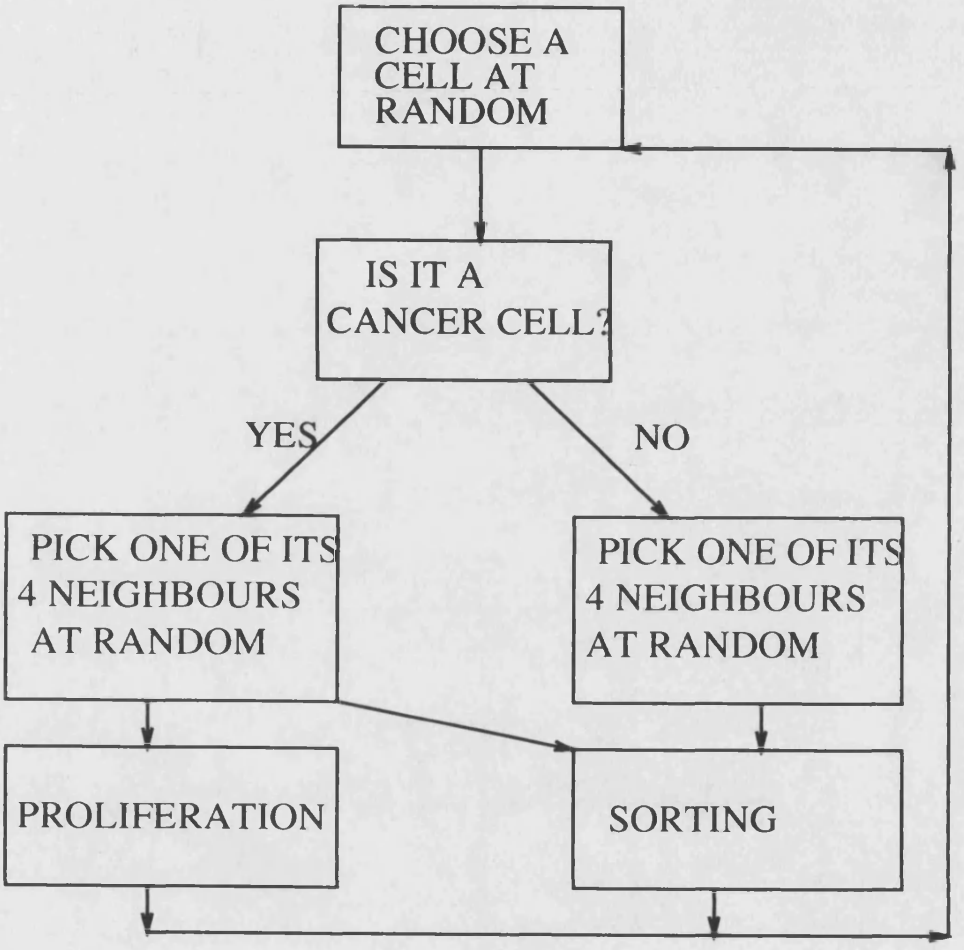

Figure 2-2: Schematic flow chart of basic algorithm for model with cell sorting and proliferation.

2.3 Model with Proliferation.

This model was then adapted to include proliferation. The flow chart for the algorithm is shown in Figure (2-2). If a cancer cell is chosen, then, it can either proliferate with a certain chosen probability, or it can swap places with one of its four neighbours, chosen at random with Monte Carlo probability. If it is a normal cell, it can only sort. We ignored proliferation of the normal cells because some cancer cells have a much higher proliferation rate [167] and also, it is more than likely that one of the two daughter cells will occupy a site that causes another normal cell to be "pushed" off the edge of the lattice, which does not change the configuration, but does waste computing time.

Sorting occurs as before, the Hamiltonian again being

$$\mathcal{H} = \sum_{(i,j)(i',j')} (1 - \delta_{\tau(i,j),\tau(i',j')})$$

If a cancer cell proliferates, then the randomly chosen neighbour and all consequent cells on that row/column are moved on one site, and the empty space left by the neighbour is filled with a cancer cell. Changing the probability of proliferation decides whether the tumour shows aggressive growth or just continuous steady growth. Some results are shown in Figure (2-3). Again, the tumour displays metastatic-like behaviour in allowing some cells to separate from the main body of the tumour.

The next step was to find the time taken for the tumour to spread across the lattice for different temperatures. Annuli concentric with the initial "circle" of cancer cells were set up and the times when a cancer cell first reached consecutive annuli were recorded. Four different seeds were used for generating the pseudorandom numbers required for the Monte Carlo method, and the average time was calculated from the data. The results are shown in Figure (2-4) for six different temperatures, the lattice size being 64×64, and the initial tumour radius 10 cell diameters.

2.4 Effects of the Immune System.

If the immune system of the host recognises the abnormality in the tumour, then the growth may be regulated by the immune response, which may be sufficient to eradicate the neoplasia completely.

The immune cells, B-lymphocytes (B-cell) and T-lymphocytes (T-cell) are the key players in the immune response of invertebrate animals [145]. Both B-cells and T-cells are created in bone marrow, but the T-cells develop further in the thymus gland. Both types of cells circulate in the blood stream and lymph system but are usually concentrated in the lymph nodes. These so-called lymphocytes can recognise certain free or cell surface antigens (molecules associated

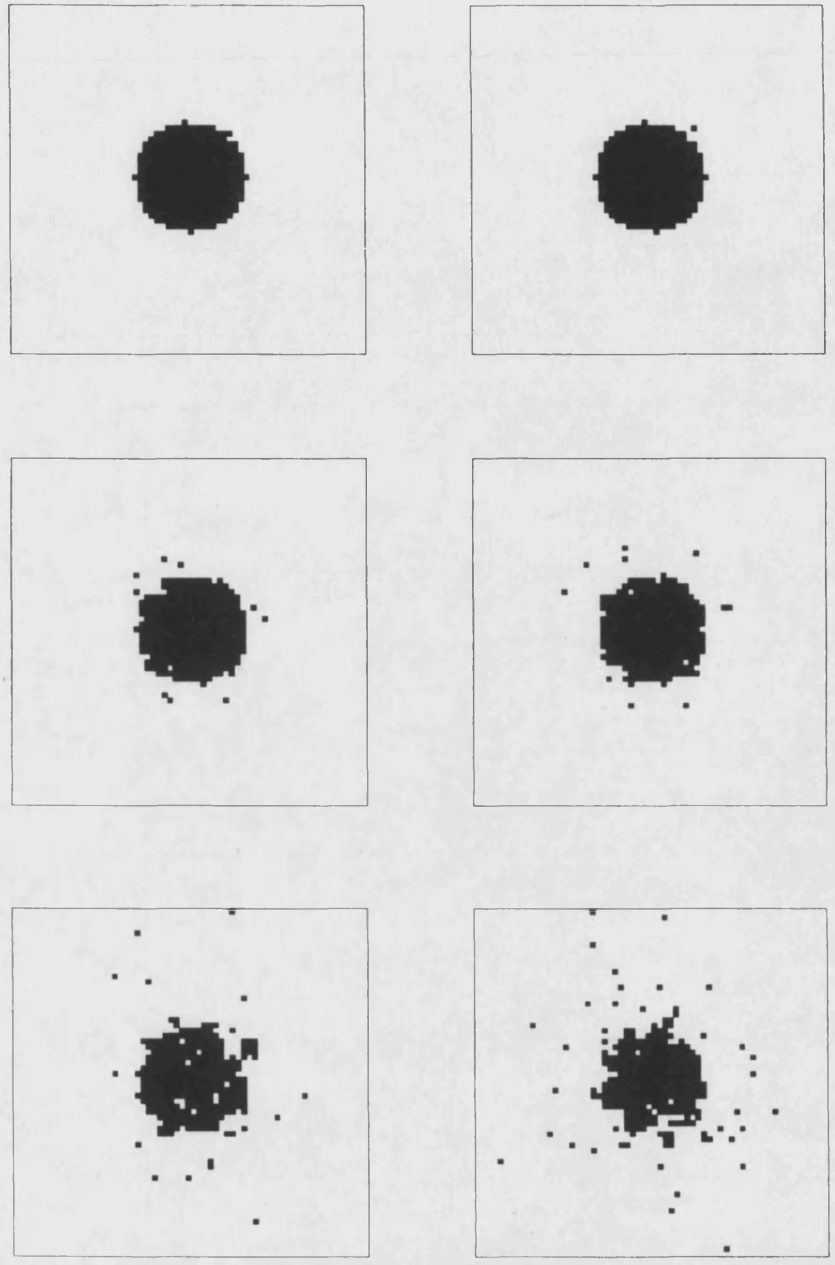

Figure 2-3: Model with proliferation and sorting: P(cancer cell proliferates) = 0.1, inverse temperature = 0.8, times are (from left to right) 1000 updates, 10,000, 50,000, 100,000, 500,000 and 1,000,000 updates. Again black pixel=cancer, white=normal.

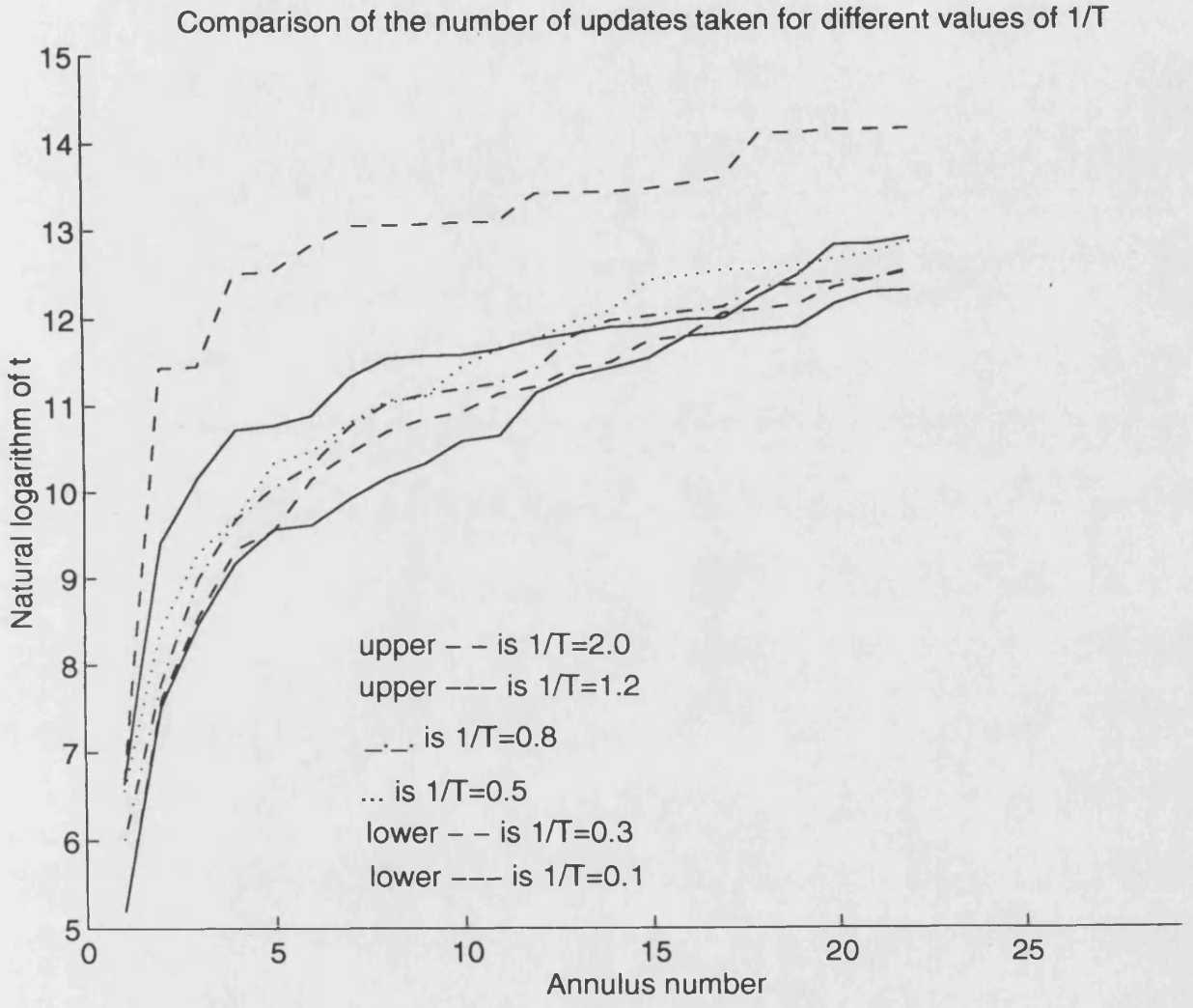

Figure 2-4: Model with sorting and proliferation: Graph showing the variation of tumour growth rate with system temperature. T is the "temperature" of the system, t is the number of updates required for a tumour cell to reach annulus n, where the inner radius of annulus n has size, in cell diameters, n+initial radius of tumour. Increasing/decreasing the parameter k in (2.1) would give the same effects as shown here for increasing/decreasing T.

with foreign material e.g. virus, bacteria) or are produced by defective cells.

The appearance of antigen in the host triggers the response of the immune system to a neoplastic cell or a virus. The response of the B-cells is called the Clonal Selection Theory. A specific receptor on the B-cell membrane will bind to the antigen in a manner analogous to a key fitting a lock [145]. The B-cells then produce clones which secrete antibodies. This is known as a *humoral* immune response, and the B-cells and their antibodies are collectively known as immunoglobulins. The antibodies bind to the antigens and mark them for destruction by other immune cells such as macrophages or natural killer cells.

The response of T-cells to antigen is to clonally reproduce and then differentiate into several kinds of T-cell. T-cells do not produce antibodies and are only involved in the cell-mediated immune responses described in Chapter 1.

Using some ideas of Qi *et al.* [185], discussed in Section (1.5.1) we developed the model further to incorporate some of the effects of the immune system on the tumour. Immune effector cells (T-cells and B-cells) attack tumour cells because they are recognised as being abnormal. These cells cytotoxically bind to the tumour cells to form complexes, which eventually dissolve into chemical compounds which diffuse through the tissue [119, 128, 186, 188, 191, 216, 217]. A realistic way of describing the rôle of the immune system in combating tumour populations in a simulation is to assume that in every lattice site, an effector cell is hiding, which can attack the tumour cell that it shares the site with, with a given probability. Then, when the complex has formed, it dies with another probability.

Necrotic debris disintegrates continually into simpler compounds that are freely permeable through the culture. The mass or volume lost this way in necrosis is replaced by cells pushed inward by the forces of cell adhesion and surface tension. So, when a cell dies and disintegrates, its volume is taken up by the cells surrounding it.

The algorithm for the simulation is:

(i) Pick a cell at random;

(ii) Pick one of its neighbours at random;

(iii) Choose between sorting or another process;

(iv) If sorting is chosen, then if the neighbour is a different type, it will swap with the original cell with Monte Carlo probability;

(v) Else: If the site contains a cancer cell, the cell will proliferate with probability P or will be bound by an effector cell to form a complex with probability 1-P.

(vi) If the site contains a complex, then the cells dies with probability Q

(vii) If the cell is dead and all its neighbours are dead, then that cell will disintegrate instantaneously and nearby cells will move up to fill its place.

The initial configuration was a small, roughly circular aggregate of cancer cells, surrounded by normal cells. Results are shown in Figure (2-5) to Figure (2-10). In these pictures, white represents normal cells, cancer cells are black, complexes are dark grey and dead cells are light grey. In comparison to Figure (2-1) and Figure (2-3), these pictures suggest that the presence of the immune system keeps the tumour more compact and does not allow the "breakaway" cells to move so far away from the central mass. From the figures, it can also be seen that the tumour grows more along the central axes than anywhere else. This is because of the symmetry of the lattice and also because we only allow the cells to interact with four neighbours. If the cells were allowed to have 8 neighbours (i.e. diagonal ones, as well as the 4 adjacent ones), then the characteristic growth of this particular model could be avoided.

Since, in our model, we have $P_i = 1 - P$, where P_i is the probability that a cancer cell will be attacked by an effector cell and P is the probability that a cancer cell will proliferate, it follows that if the tumour is invasive (P high), then the immune system will be weak.

If P is large and Q (probability that a cell dies) is small, then we have the case displayed in Figure (2-5) and Figure (2-6), where the tumour is highly invasive and spreads over the lattice very quickly. If P is not so large (level of proliferation not so high and immune system more active) and Q is still small, the tumour is less aggressive in its growth, but still takes up a lot of volume. If we then make Q larger, *i.e.* increase the death rate, then the tumour invades as aggressively, but the overall volume of the tumour is decreased, as in Figure (2-7) and Figure (2-8). If the proliferation rate is small and the immune system is active, then if the death rate is large, the tumour will regress very quickly (Figure (2-9) and Figure (2-10)), but if it is small, the tumour will still take a fair amount of volume up in the tissue space.

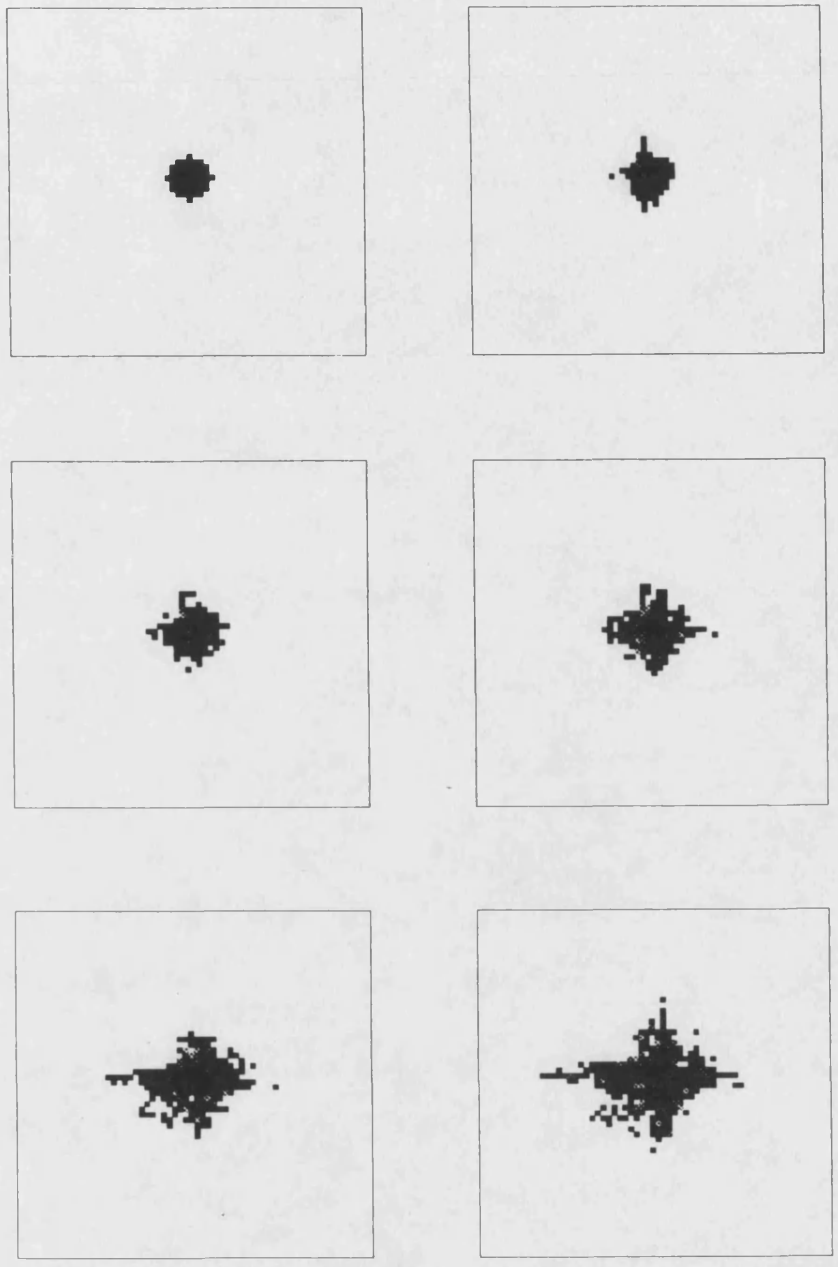

Figure 2-5: Immune model: Simulation results for a highly invasive tumour (P = 0.8, q = 0.3), times are (from left to right) 0 updates, 5000, 10,000, 15,000, 20,000 and 25,000 updates. $1/T$ = 0.8. Key: black=tumour, dark grey=complexes, light grey=dead tumour cells, white=normal.

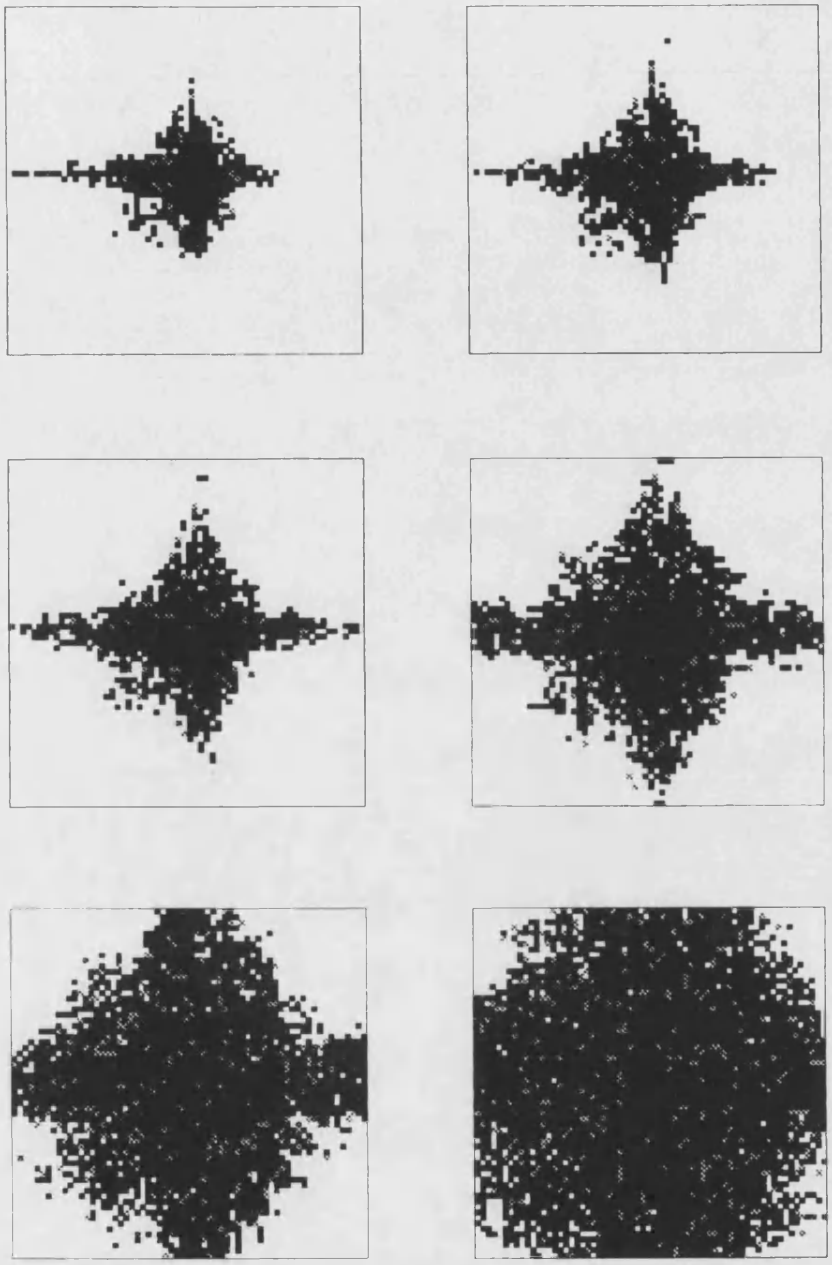

Figure 2-6: Simulation results for a highly invasive tumour, continued, times are (from left to right) 30,000, 35,000, 40,000, 50,000, 60,000 and 70,000 updates.

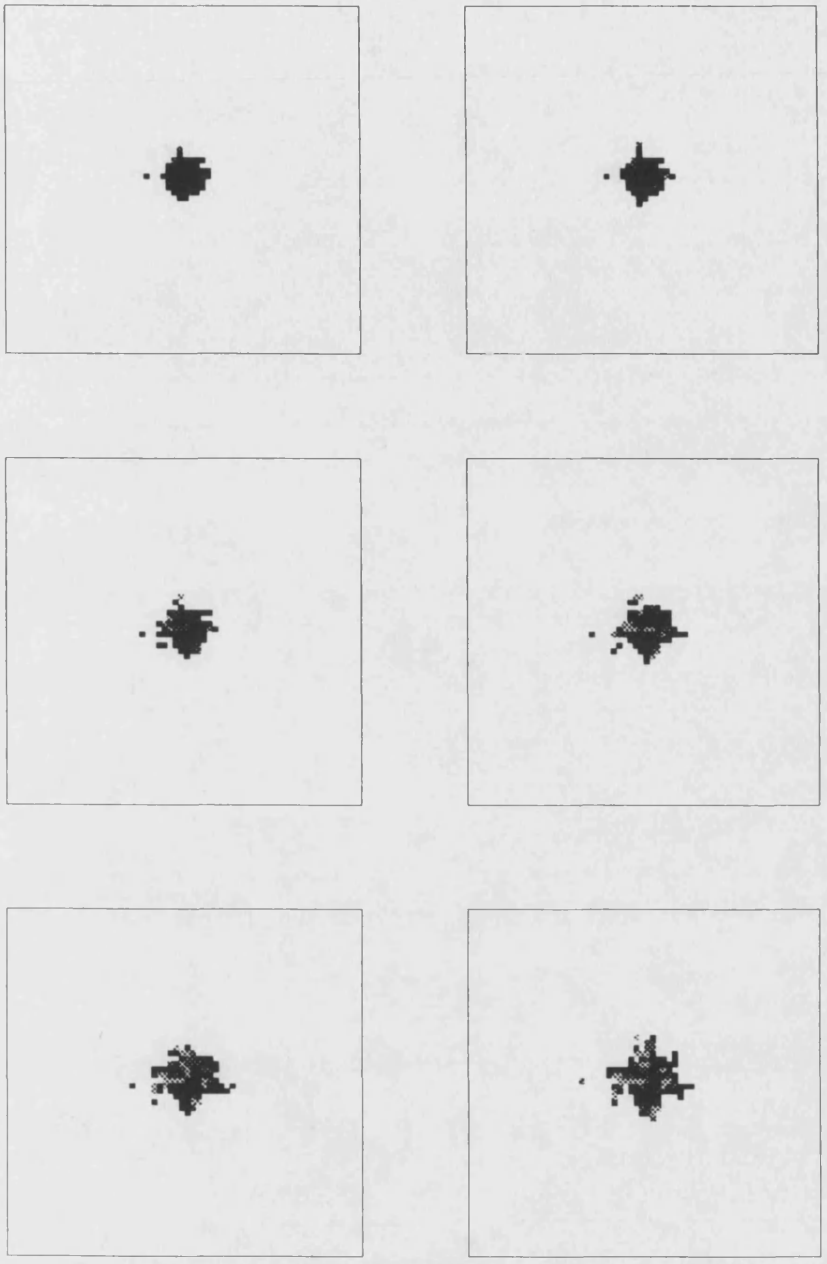

Figure 2-7: Immune model: Simulation results for an active immune system (P = 0.4, $Q = 0.3$), times are (from left to right) 3000 updates, 5000, 10,000, 15,000, 20,000 and 25,000 updates. $1/T = 0.8$. Key: black=tumour, dark grey=complexes, light grey=dead tumour cells, white=normal.

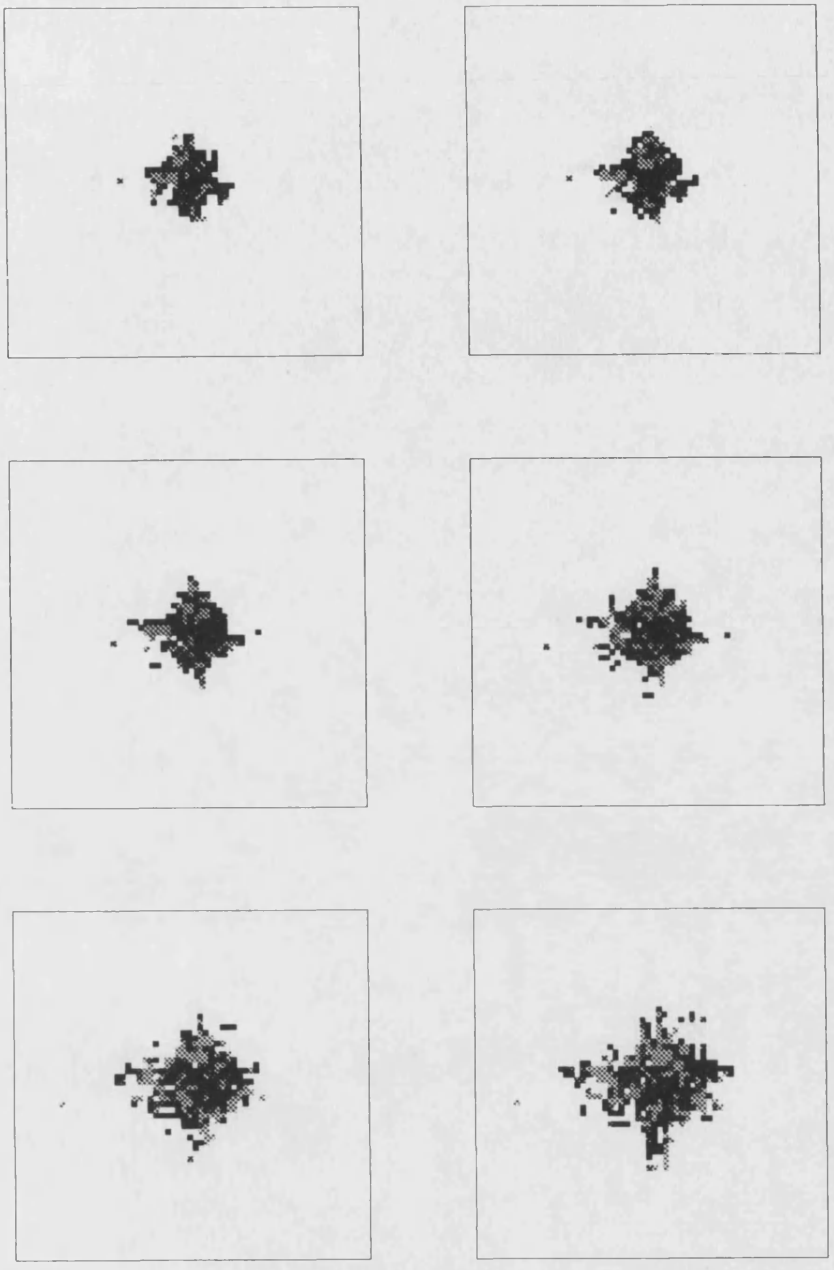

Figure 2-8: Simulation results for an active immune system, continued, times are 30,000, 35,000, 40,000, 50,000, 60,000 and 70,000 updates.

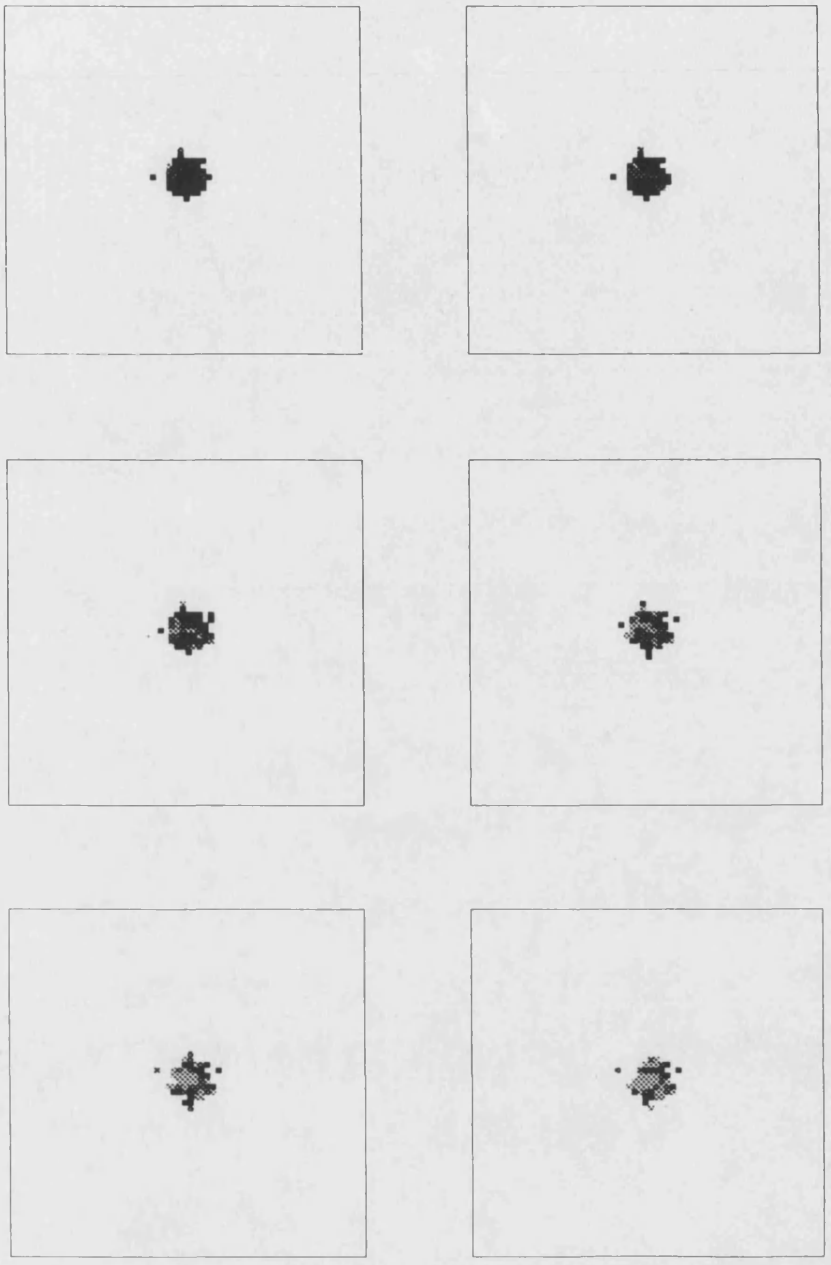

Figure 2-9: Immune model: Simulation results for a highly active immune system ($P = 0.2,\ Q = 0.4$), times are 3000 updates, 5000, 10,000, 15,000, 20,000 and 25,000 updates. Key: black=tumour, dark grey=complexes, light grey=dead tumour cells, white=normal.

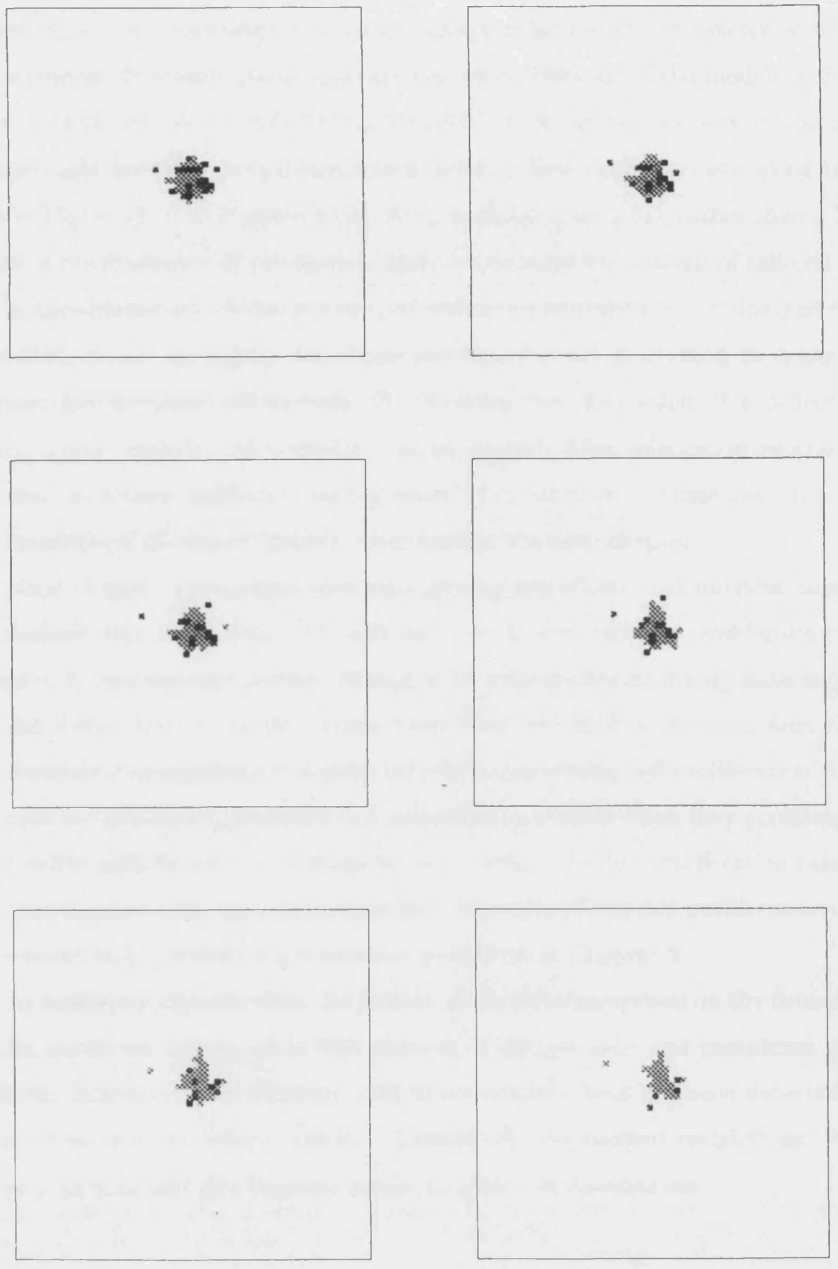

Figure 2-10: Simulation results for a highly active immune system, continued, times are 30,000, 35,000, 40,000, 50,000, 60,000 and 70,000 updates.

2.5 Summary.

The models presented in this chapter are schematic. Important factors in the systems regulating tissue growth and size (e.g. nutrient, chalones, cell density) have been ignored in an attempt to represent, in a simple simulation, factors that can lead to either cancerous growth of tumours, or regression. It is important to determine which features of the models will be preserved for more realistic simulations of growing tumours. As mentioned in Section 2.4, allowing the cells to have eight (or more) neighbours would prevent the excessive growth along the central axes as seen in Figure (2-5) to Figure (2-10). Also, simulating on a 3D, rather than a 2D lattice, would enhance the geometry of the tumour and also increase the realism of cell-cell interactions.

In the simulations of this chapter, all cells are constrained to occupy just one, square pixel. This leads to an unrealistic cell shape and also forces cell division to occur instantaneously, without any previous cell growth. By allowing cells to consist of a collection of connected pixels, a more realistic cell boundary can be formed. Also, cells can grow gradually, by gaining one pixel at a time, until they are big enough to split in two. These ideas are incorporated into the simulations of tumour growth, presented in the next chapter.

None of these simulations took into account the effects that nutrient concentration within the tumour has on growth. All cells had equal probability of proliferating and only died if attacked by the immune system. In fact, cells only proliferate if they have enough nutrient and can die if they have too little. Again, these ideas are dealt with in the next chapter.

Nutrient concentration is not the only factor governing cell proliferation. In many tumours, the cells are genetically unstable and mutations can occur when they proliferate. This can lead to daughter cells being more malignant, e.g. having a higher proliferation rate, or less adhesion to other tumour cells, than the parent cell. The idea of variable proliferation rate and adhesion is included in the metastasis simulation presented in Chapter 8.

In subsequent simulations, the actions of the immune system on the tumour will be ignored, as the model we have used in this chapter of effector cells and complexes is not particularly realistic. Henceforth, we consider solid tumours which have not been detected as foreign by the immune system and whose growth is limited only by nutrient restrictions. It would, however, be very easy to add this immune model to all of the simulations.

Chapter 3

Simulations of Cell Sorting, Pattern Formation and Avascular Tumour Growth using the Potts Model.

3.1 Potts Models.

A computer simulation can represent cells as one or more discrete units with rules to describe their interactions, emphasising supercellular processes. Continuum models are an alternative to solving the many body problem represented by cellular automaton patterns. Emphasising spatial and temporal variation of fields, these methods describe cellular patterns in terms of density functions which satisfy second order nonlinear differential equations for diffusion and wave propagation. They stress the interaction of each cell with the global environment, but, unlike simulation, cannot easily identify individual cells.

The large-Q Potts model, cf Section (1.5.2), (Q is the number of different 'spins' in the model) is a combination of discrete and continuum methods. This model can describe interactions between mechanisms for cellular pattern formation at all relevant length scales. It can simulate diffusive grain growth driven by surface energy [8], and can correctly simulate experimentally observed topological changes in cellular patterns in metals and soap froths [94, 227]. Grain growth is the increase in mean grain size which occurs upon annealing a polycrystalline aggregate after primary recrystalization is complete [110]. The Potts model can also be applied to biological systems such as the development of the slime mold, *Dictyostelium discoideum* [194], and tumour growth [55, 56, 57].

Graner and Glazier [100] use this model for a starting point for their cell sorting model. Cell-sorting occurs through the movement of cells rather than through cell growth. The Potts model simulates a pure material with a single surface energy, while cell sorting requires the presence of at least two different cell types. So, they simulate cell-sorting in two-dimensional aggregates using an extension of the two-dimensional Potts model which constrains cell size and allows for different surface energies between different cell (spin) types. For the Ising model, mismatched bonds between different cells (spins) have energy 1 and bonds between like spins have energy 0. The Hamiltonian is

$$\mathcal{H}_{\text{Ising}} = \sum_{\text{neighbours } (i,j)(i',j')} 1 - \delta_{\sigma(i,j)\sigma(i',j')},$$

where the neighbours may be of any desired range on either a square or hexagonal lattice. $\delta_{\sigma\sigma'}$ is the Krönicker δ. At each step, a site is selected at random and its spin is changed from σ to σ' with Monte Carlo probability, for a temperature $T > 0$,

$$P(\sigma(i,j) \to \sigma(i',j')) = \begin{cases} \exp(-\Delta\mathcal{H}/kT) & \text{if } \Delta\mathcal{H} > 0 \\ 1 & \text{if } \Delta\mathcal{H} \leq 0 \end{cases}$$

and for T=0,

$$P(\sigma(i,j) \to \sigma(i',j')) = \begin{cases} 0 & \text{if } \Delta\mathcal{H} > 0 \\ 0.5 & \text{if } \Delta\mathcal{H} = 0 \\ 1 & \text{if } \Delta\mathcal{H} < 0 \end{cases}$$

where $\Delta\mathcal{H}$ is the energy gain/loss produced by the change.

While the surface-energy driving mechanism is the same as for grain growth, biological cells have generally a fixed range of sizes. Thus the pattern cannot lose energy by coarsening, since cells cannot disappear. Instead, differences in contact energies between cells of different types (differential adhesion) cause cell motion which reduces the energy. To include these ideas, an elastic-area constraint is added to the Hamiltonian and a second "quantum" number τ, the cell type. The simulations, employ three cell types, "light", "medium" and "dark". The surface energy between two cells depends on the types of the cells. Each cell has a unique spin and consists of all lattice sites with that spin.

3.1.1 The Extended Potts Model

The Extended Potts Model [93, 95, 100] uses an array with as many as 200^3 elements to represent cellular patterns. The array is partitioned into domains. Clustered array elements sharing a common value delineate regions belonging to different cells, each labelled uniquely. A

second label, shared by all domains of the same type, distinguishes cells from different tissues. Cells have a type dependent volume constraint which models membrane elasticity so that no single cell can grow or shrink without bound. The array can include a border of neighbouring sites assigned to a domain of unlimited volume. This large domain represents a medium in which the cells exist. A homogeneous slab of sites inserted at the base of the array can be used to represent a substrate. With domains chosen sufficiently large, cells and tissues are free to deform almost arbitrarily as the array evolves.

The patterns formed by cells and tissues are characterised in terms of an abstract stored energy. Contributions to the energy include a sum over the coupling between neighbouring array elements together with a sum over contributions from the membrane elasticity of each cell:

$$\mathcal{H} = \sum_{\substack{\text{neighbour sites} \\ \sigma_{(i,j,k)} \neq \sigma_{(i',j',k')}}} J[\tau(\sigma_{(i,j,k)}), \tau(\sigma_{(i',j',k')})] + \sum_{\substack{\text{all domains} \\ \lambda_{\tau(\sigma)} \neq 0}} \lambda_{\tau(\sigma)}(v(\sigma) - V)^2 \ ,$$

where $\mathcal{H}$ is the total energy (the Hamiltonian), while domain σ of type τ includes $\sigma_{i,j,k}$ as a constituent array element. Coupling strengths are defined for every possible pair of domain types. The coupling matrix elements $J[\tau, \tau']$ give the energy stored in bonds between a site and its neighbours which are denoted by primes. The sum over neighbouring sites excludes neighbours within the same domain so that stored energy is localised at boundaries. For each cell, the volume under stress $v(\sigma)$ may differ from the common volume V for undeformed cells. The sum over domains excludes domains of unconstrained volume for which the elasticity λ_τ is set equal to zero. Cell elasticity imposes a global constraint on cell volume while cell couplings determine the work required to cause local membrane deformations.

The organisation of cells and tissues develops in a probabilistic manner under Monte Carlo dynamics. An array element is chosen at random and provisionally reassigned to a neighbouring domain. A change in energy results since a modified site couples differently with its neighbours and furthermore, volume is transferred between domains. The probability of accepting reassignments that change the total energy by ΔH is given by a Boltzmann factor:

$$P = \begin{cases} e^{-\Delta H/T_f} & \text{if} \quad \Delta H \geq 0 \\ 1 & \text{if} \quad \Delta H < 0 \end{cases} \ ,$$

where P is the probability of accepting an array modification and T_f is a parameter of the simulation which controls the amplitude of cell membrane fluctuations. A slight chance of accepting small energy gains allows cell patterns to escape from marginally stable states en route to a configuration of absolute minimum energy. Experiments and simulations [159, 160] have

shown that cells exhibit approximately Brownian motion and a roughly Maxwellian distribution of velocities consistent with statistical mechanical dynamics. Under repeated application of this algorithm, membrane curvature evolves realistically in response to gradual diffusion of domain boundaries within the array.

This model, with the area constraints and differential adhesivity, can simulate biological cell sorting, making detailed predictions about measurable properties of biological aggregates. Sorting shows a crossover between a rapid boundary-driven stage and a slower boundary-independent stage as observed in experiments using pigmented and neural epithelial cells from the eyes of seven day chick embryos [96, 158]. The rapid stage leads to a uniform light-cell-medium surface layer and partial bulk cell sorting and the slow stage leads to complete cell sorting. Chequer-board cell patterns, clumping, engulfment, partial sorting, cell dispersal and vacancy nucleation are also simulated.

3.2 A Model of Avascular Tumour Growth.

3.2.1 Tumour growth.

The growth of solid tumours in animals always involves some vascularization, but the earliest stages of development are regulated by the direct diffusion of nutrients and waste from and to surrounding tissue [143]. Experiments on the growth of nodular carcinomas *in vitro* [66, 118, 210], or those requiring techniques for the isolation of tumours *in vivo* [74, 215], show that the growth of a solid malignancy by diffusion alone leads asymptotically to a dormant but viable steady state. In this dormant state, the volume increase due to cell proliferation, is balanced by the degradation and volume loss in the necrotic core. For the simple model which we will develop, we will assume that the availability of a single, slow diffusing nutrient is the primary limit on tumour growth, and that other nutrients and the diffusion of waste are sufficiently rapid that they do not limit the growth rate.

When the tumour is tiny, every cell receives sufficient nutrient by diffusion and the growth rate of the population is exponential [83]. The consumption of nutrient by the cells means that the concentration of that nutrient must decrease towards the centre of the aggregate, as it is only supplied to the periphery.

As the tumour grows, supplying the nutrient to the central core by diffusion will become more and more difficult, so that the concentration there diminishes. Eventually, the concentration will fall below some critical level, at which cells become quiescent; alive, but no longer proliferating. If the nutrient level near these cells increases above the critical level, they reenter the proliferation cycle [80]. Many studies show that microenvironmental factors, such as O_2 and nutrient supply, as well as accumulation of metabolic wastes, greatly influence cell metabolism [107]. When quiescent cells appear, the growth of the tumour slows down to become linear

[38, 84], because part of the tumour volume is no longer involved in the production of new cells.

The tumour then grows until it reaches another critical size, where the nutrient concentration at the centre is not high enough to sustain life. At this stage, a necrotic core forms. This core contains cells in varying stages of disintegration. Dead cells break down into chemical compounds which are freely permeable through cell membranes. The mass or cell volume lost this way is replaced by cells pushed inward by the forces of adhesion and surface tension in the aggregate. Some cells, newly generated on the surface of the MCS gradually migrate toward the centre of the spheroid [151]. The growth rate decreases rapidly when the necrotic core forms because it becomes increasingly difficult to obtain nourishment and dispose of waste solely by diffusion. As the tumour continues to grow and develop, the outer shell of dividing cells becomes roughly constant in size - about 1-3 cells thick .

Eventually, the processes of necrotic disintegration, accumulation of mitotic wastes [222], mitotic inhibitory factors [79] and cell shedding [141] reduce the rate of growth so much that the overall volume of the sphere remains constant [71, 83, 118]. Although the tumour volume is in equilibrium, the cells in the outer shell still proliferate. But, the volume produced by this process is cancelled by the volume lost through necrotic disintegration and cell shedding.

The typical steady state configuration of an avascular tumour is a sphere, a few millimetres in diameter, which histological examination shows to consist of three distinct concentric annular shells [83, 129, 130]. In the thin, outermost shell, the cells are observed to grow and divide as they do in the exponential phase. In the adjoining shell, typically three times as thick as the proliferating layer, cells are quiescent and exhibit little or no proliferation [32]. The innermost core consists of necrotic debris [151]. The tumour may remain in this dormant state for months or even years [180].

3.2.2 Cell sorting

In a number of cell sorting experiments [10, 46, 88, 116, 168, 202, 203, 204, 218, 230], cells display a remarkable ability to migrate over distances much greater than one cell diameter in order to restore disrupted patterns or form new ones. The natural configuration of mesoderm, endoderm and ectoderm from amphibian embryos can be recovered from excised tissues combined in the right proportions [115]. When mixed together in suspension, neural and pigmented chicken embryo retina cells will precipitate to produce a disordered aggregate. The initially irregular aggregate rounds over time. Pigmented cells coalesce at the centre to form a sphere while neural cells organise to form an encompassing outer layer. Significantly, the outcome of sorting experiments is largely independent of the initial conditions [206]. An aggregate of neural cells rounds in isolation but spreads to engulf a pigmented cell aggregate if the two are placed in contact. Similarly, an intact fragment of chicken heart ventricle will envelope a chicken cartilage fragment. The coelenterate animal *Hydra vulgaris* [78, 193, 213] is basically a hollow

cylinder with an extracellular matrix sandwiched between layers of endodermal and ectodermal cells. When dismantled at the cellular level, hydra display an amazing ability to recover their original state and when turned in-side-out they are able to re-invert themselves. These, and other observations, suggest an underlying mechanism for cellular pattern formation based on intrinsic cell properties rather than chemical gradients or the starting locations of cells in a tissue.

Steinberg proposed the Differential Adhesion Hypothesis [99, 202, 203, 204] to explain cell sorting as a minimisation of contact energy at cell interfaces. Experiments [76, 115, 163] show that the strength of attachment between two cells which come into contact depends on the type of cells involved. The difference in adhesion energy results from the number and particular type of surface adhesion molecules present on the cell membrane. Classes of adhesion molecules include cadherins, N-CAM and many other varieties, some non-specifically adhesive, others, like N-CAM, extremely variable in sequence (and hence relative adhesivity) between cell types. Movement of a cell requires work against the adhesive forces of its neighbours under the constraint on cell volume imposed by membrane elasticity. Thus, affinity between neighbouring cells determines the energy of a cell aggregate. Energy is stored at interfaces between cells which have the potential to form stronger attachments with more amenable coupling partners. Cytoskeletal membrane fluctuations allow the cells in an aggregate to explore an abstract energy landscape randomly yet exhaustively. The local energy gradient drives cells. Dissipation inexorably leads to a configuration with absolute minimum energy. As jostling causes adhesion molecules to unbind and re-bind, strong bonds tend to replace weak bonds, making best use of the available binding energy and thereby maximising the work required to remove a cell from an aggregate. Differential adhesion is thought to play an important role in processes such as cell recognition [29], gastrulation [148, 187], cell shaping [171], control of pattern formation [166] as well as cancer metastasis [211].

As well as producing an inward pressure to maintain a compact solid mass, the surface tension caused by differential adhesion, causes individual cells and the tumour to round, as a sphere has the surface of minimum energy.

3.2.3 The Model.

We use an extension of the Potts model used by Glazier *et al.* [93, 95, 96, 100, 158] to simulate avascular tumour growth.

Tumour simulations based on the Extended Potts model include cells which grow and divide, cells which decay and cells which maintain relatively constant volume. Aside from mitosis, this is accomplished by considering necrotic, quiescent and proliferating cancer cells as distinct cell types, in addition to healthy cells, with growth rates and volume constraints for each type adjusted independently. While target volumes for healthy and quiescent cells remain

constant in time, target volumes are incremented for proliferating cells, to simulate growth and decremented for necrotic cell to simulate decay. By adjusting cell elasticities, which determine how easily cells shrink or grow, volume constraints for proliferating, quiescent and necrotic cells are made successively weaker. Accordingly, proliferating cells can grow at the expense of quiescent cells which, in turn, recoup their losses from decaying necrotic cells. The transfer of volume between domains is not meant to simulate the consumption of one cell by another. Quiescent cells, from the middle layer of the tumour, advance to fill a vacuum left behind when dissolved necrotic cell remnants diffuse away while proliferating cells, at the outer edge of the tumour, expand into space created when quiescent cells fall into the necrotic core.

We choose normal cells to have the strongest adhesive bonds with normal cells and cancer-normal bonds are the weakest, with cancer-cancer bonds in between, keeping the tumour compact from the resulting surface tension. This hierarchy of bonding strengths is consistent with biological evidence as tumour cells do adhere to themselves less strongly than their counterpart normal cells [167, 232]. Note that although growth and decay distinguish proliferating and necrotic cells from quiescent cells, all cancerous cells are taken to have the same binding properties. Tumour cells express fewer adhesion molecules than normal cells, especially N-CAMs and E-cadherins [155, 167, 207]. In fully transformed cancer cells the expression of cell adhesion molecules is often completely suppressed [132]. The progressive failure of adhesion during transformation results in progressive rounding of individual cells and loosening of cell-cell bonds in tumours. The intermediate value for normal-tumour cell binding is consistent with the assumption that normal and tumour cells were originally of the same type and hence express the same adhesion molecules only in different quantity. In this case the heterotypic adhesion is expected to be the geometric mean between the homotypic adhesivities.

Proliferating cancer cells grow in response to the demands of an increasing target volume with mitosis occurring whenever the ratio of surface area to volume for a cell drops below a threshold. This criterion for cell division reflects the fact that cell volume determines the demand for nutrients while cell surface area limits how much food can be absorbed. Since tumour cells grow and divide continuously without observing regulatory signals, the simplest assumption is that their growth rate is directly proportional to the supply of nutrients up to some saturating rate. Mombach *et al.* [156, 157] investigated mitosis in plants and showed that this assumption gave good quantitative agreement with experimentally observed cell distributions in plant epithelia. The cell is split at a plane through the centre of mass corresponding to a minimal cross section with all the array elements on one side of the cell assigned a previously unused index. After a split, each daughter cell starts with half the target volume of the parent cell so as not to be unduly stressed by a large deviation from the mandated size of the progenitor. Since, experimentally, mean tumour cell size is comparable to mean normal cell size, we apply mitosis at twice the typical cell size, which corresponds to a area/volume ratio of 0.6.

We do not include the growth of normal cells as increasing the volume of one normal cell would more than likely result in a decrease in volume of another normal cell and hence not affect the overall volume of normal tissue. Including the growth of normal cells would not affect the overall dynamics of the tumour's growth, as we assume that the tumour is more aggressive at keeping it's volume than the normal tissue is and so a normal cell would very seldom be allowed to take volume off a tumour cell.

Cells change type in response to a nutrient gradient within the tumour. We assume that the normal tissue is a homogeneous source of nutrient. The concentration of nutrient within the tumour is measured as a function of the distance of the centre of mass of a particular cell from the periphery of the tumour and the total volume of live (and hence nutrient consuming) cancer cells within the tumour. It has been shown that the volume of proliferating cells in the tumour remains roughly constant throughout the growth period [151] and so we require that

$$\text{volume of proliferating cells} = \frac{4}{3}\pi(R^3 - R_q^3) = A \ \text{ (constant)}$$

where R is the average tumour radius and R_q is the average outer radius of the quiescent shell. (A can be calculated from data of spherical tumours grown *in vitro* [71]). Now, the distance of the first quiescent cell from the edge of the tumour is $R - R_q$ and so we choose the critical distance to be D_q, where

$$D_q = R - R_q = \text{ integer part of } \left(\frac{3}{4\pi}\frac{A}{(R^2 + R_q^2)}\right)$$

The distance of the first dead cell from the periphery $D_d = 4D_q$. This approximation is close to the true diffusion determined concentration but is much simpler and computationally faster to implement.

The growth rate of proliferating cells is also linked to nutrient concentration [33]. The formula for the growth rate of the cells is given by:

$$\text{growth rate} = \begin{cases} 0 & \text{if } 0 \leq N \leq N_q \\ \frac{1}{2}(\frac{N}{N_q} - 1)^2 & \text{if } N_q \leq N \leq 3N_q \\ 2 & \text{otherwise.} \end{cases}$$

where N_q is proportional to $R - R_q$, while N is proportional to $R - d$, where d is the depth of a cell within the tumour. The depth of a cell is found by calculating the distance from the centre of mass of the cell to the outer edge of the tumour along each of the three orientations of the array (*i.e.* in the x, y and z directions) and then taking the minimum of these three. The increase in volume of the cancer cells is taken to be the integer part of growth rate.

The simulated decay of necrotic cells by reduction of target volume also depends upon

depth within the tumour. We assume that cells nearer the centre of the tumour will have been dead longer than those near quiescent cells and therefore will be more likely to have broken down into diffusible compounds and hence will lose volume more readily than those that have just died. So, we take the rate of reduction of volume to be proportional to the individual cell's distance from the edge of the necrotic core, up to some saturating rate. Necrotic cells in the outer layer of the core maintain constant volume while cells in the fourth layer from the edge and beyond lose two units of volume at each time step with a linear increase in the decay rate for intervening layers.

Modifications to the Extended Potts model for the purpose of modelling cancer can be summarised by considering changes to the functional dependence of target volumes, cell elasticities and cell types. Cell types and elasticities become a function of nutrient concentration, which varies spatially within the tumour:

$$\begin{aligned} \tau &\longrightarrow \tau(N)\,, \\ \lambda_\tau &\longrightarrow \lambda_\tau(N)\,, \end{aligned}$$

where τ is cell type and N is nutrient concentration. Through dependence on cell type, elasticities have an implicit dependence on nutrient concentration, in addition to an explicit dependence. Also, elasticities have an implicit dependence on position through the spatial variation in nutrient concentration within the aggregate. The target volumes become functions of time:

$$\begin{aligned} V_\tau &\longrightarrow V_\tau(\sigma,t)\,, \\ \tfrac{dV}{dt} &> 0 \quad \text{if} \quad \text{proliferating,} \\ \tfrac{dV}{dt} &= 0 \quad \text{if} \quad \text{normal, quiescent,} \\ \tfrac{dV}{dt} &< 0 \quad \text{if} \quad \text{necrotic,} \end{aligned}$$

where V_τ and λ_τ are target volume and elasticity respectively. Note that both target volume and cell elasticity depend on cell type as before. However, target volume may now vary for each cell σ since proliferating cells may be at different stages of the mitotic cycle. Despite these modifications, cell configurations are still characterised in terms of stored energy with the usual Monte Carlo dynamics driving rearrangement.

Evolution takes place on a 3D lattice. We show a flow diagram of the computer algorithm in Figure (3-1).

3.3 Simulation of an Avascular Solid Tumour.

We start off with a small homogeneous aggregate of tumour cells, embedded in normal tissue. All cells are initially set to be cuboids, to avoid packing problems, but the dynamics of the

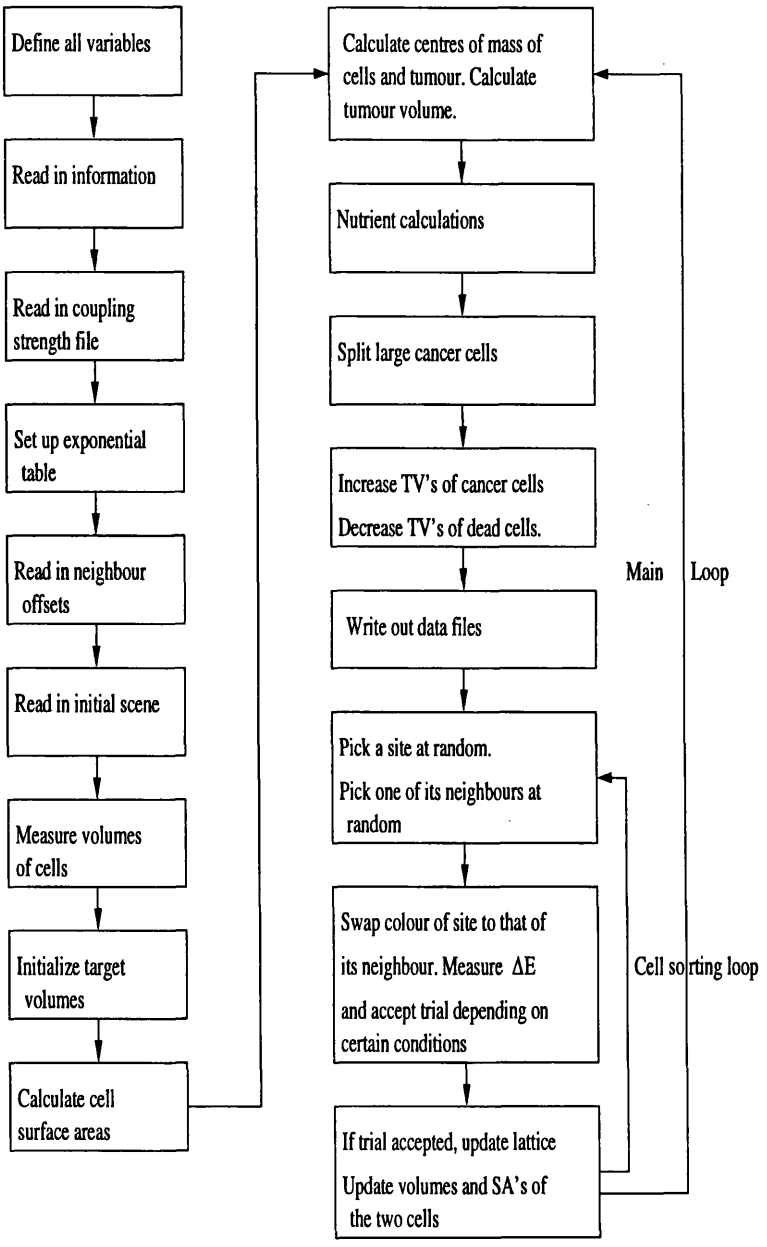

Figure 3-1: Simple flow diagram of computer algorithm for Potts model with cell sorting and proliferation.

model quickly allows them to round to a more natural shape.

The homogeneous source of nutrient models a multi-cell, spheroidal, avascular tumour. To keep the pictures simple, a cross section is taken in the X-Y plane, which slices the tumour in two. In the top picture of Figure (3-2), only cancer cells are shown individually and the normal cells are represented by a block of colour. In the bottom picture, only individual normal cells are shown, and this time, the tumour is a solid block of colour in the centre of the picture.

Figure (3-3) shows the tumour at a later time, when the surface tension has rounded both the cells and tumour.

As the tumour grows, the distance of the cells at the centre of the tumour from the periphery becomes large enough, that sufficient nutrient can no longer diffuse to them. Inadequately supplied cells become quiescent. Figure (3-4) shows the tumour with a quiescent core. Again, the picture shows cross sections through the tumour. If any of these quiescent cells manage to move nearer to the edge of the tumour, where the nutrient concentration is high enough to support mitosis, then these cells will start to proliferate again.

Later, the tumour becomes so big that the distance from the edge of the aggregate to the cells at the centre is too large for enough nutrient to diffuse to them and they die. A necrotic core then forms within the quiescent shell. The top picture of Figure (3-5) shows the proliferating cells and the position of the cells that have died. The bottom picture shows the normal and quiescent cells, with a solid block of colour in the centre to represent the necrotic core, and a ring of colour for the proliferating cells.

We measure the volume and the average radius of the tumour as it grows. Figure (3-6) shows the graph of volume versus simulation time. Initially, the growth is exponential, then at around time=700 MCTS, when quiescent cells first appear, the growth slows to linear. (MCTS=Monte Carlo Time Steps). At time=8600 MCTS, when the necrotic core forms, the growth slows down again and eventually levels off as the tumour reaches its diffusion limited steady state. This growth is consistent with the experimental evidence. Figure (3-7) is the graph of the average tumour radius versus simulation time. As can be seen, the width of the shell of quiescent cells is roughly three times as big as the width of the shell of proliferating cells, which is in good agreement with known histological data [151]. The top picture in Figure (3-8) shows the growth of the outer radius of the tumour and the bottom shows the graph obtained by Folkman and Hochberg in their experiments on the growth of MCS [71].

3.4 Simulation of an Avascular Carcinoma.

We use the same algorithm as above to simulate the growth of an avascular carcinoma. Carcinomas are solid tumours of epithelium, that is cells covering internal or external surfaces of the body, which have a supportive stroma of blood vessels and connective tissue. Carcinomas are

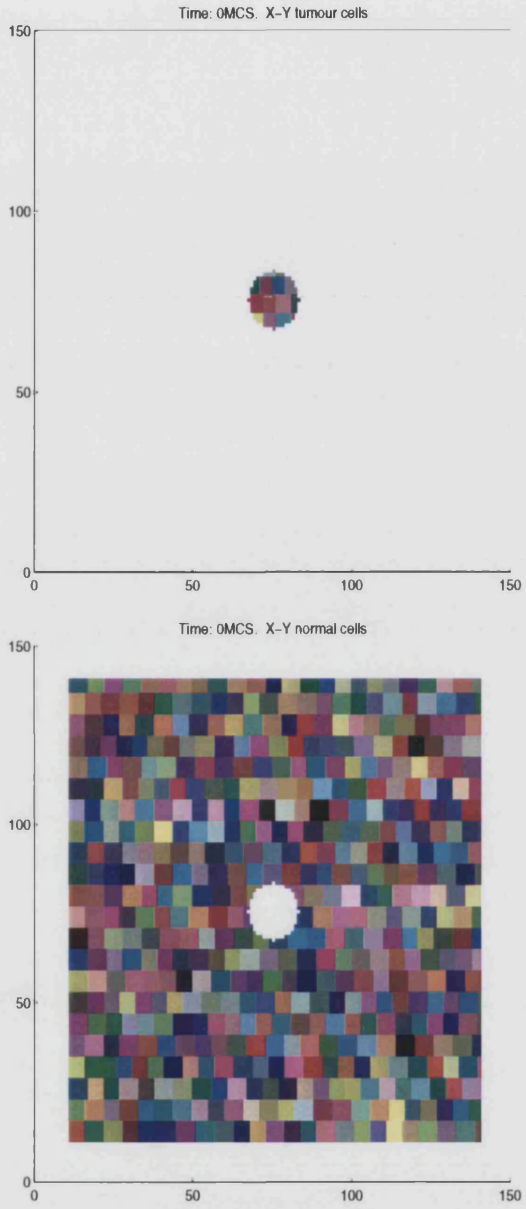

Figure 3-2: Cross sections of the initial configuration. Top: shows individual cancer cells only and normal cells as just solid white. Each colour represents a separate cell within the tumour. Bottom: shows only individual normal cells, with the tumour represented by the white mass in the centre. These two pictures are of the same configuration, but to show individual cells and for clarity of types, they are presented separately.

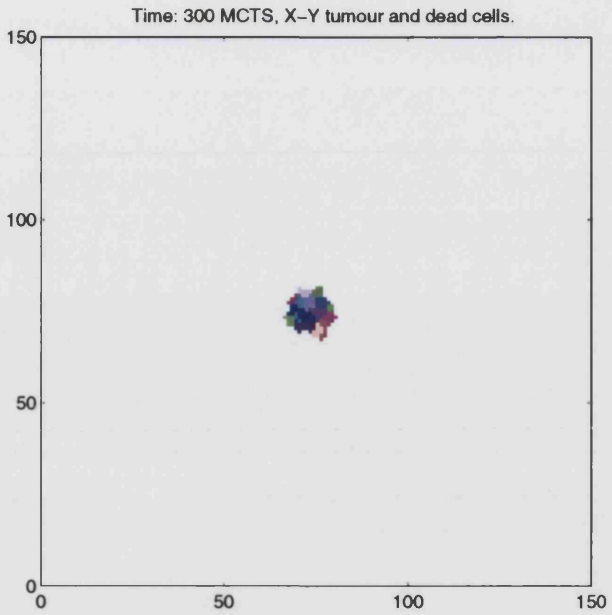

Figure 3-3: Cross section of rounded configuration, showing proliferating cancer cells only. Because this is a cross section, some cells may look slightly disjointed or very small, but the rest of the cell is in adjoining layers of the lattice and so it is more than likely that they are connected and not so small.

the most common type of human neoplasm, constituting about 96% of all malignant cancers [190]. Lung cancer, prostate cancer, breast cancer and colorectal cancer account for over 50% of all reported cancer in England and Wales [173]. Carcinomas are extremely aggressive in their growth. In the majority of patients who suffer from carcinomas, the disease has already metastasised before detection, resulting in multiple secondary tumours which may occur in sites far removed from the primary cancer. Hence the disease cannot be cured by treating the primary tumour alone. Wide-spread metastases can be difficult to treat, can cause a number of unpleasant symptoms and often prove to be fatal. (The estimated annual death rate is 1 in 341 for men and 1 in 387 for women [174]).

The initial configuration (Figure (3-9)) is a hemispherical tumour sat on an inert substrate (the skin). The tumour is surrounded by normal cells, which again, we take to be a homogeneous source of nutrient. The skin is also assumed to provide the carcinoma with a homogeneous source of nutrient. The concentration of nutrient at a point within the tumour is a function of the distance of that point, either from the skin or from the normal tissue surrounding it.

The tumour grows and spreads across the skin and, like the MCS, a quiescent shell forms (Figure (3-10)) and then, within this, a necrotic core (Figure (3-11)). Figure (3-12) shows the graph of tumour volume versus simulation time. As before, the volume increases as expected from experimental observations.

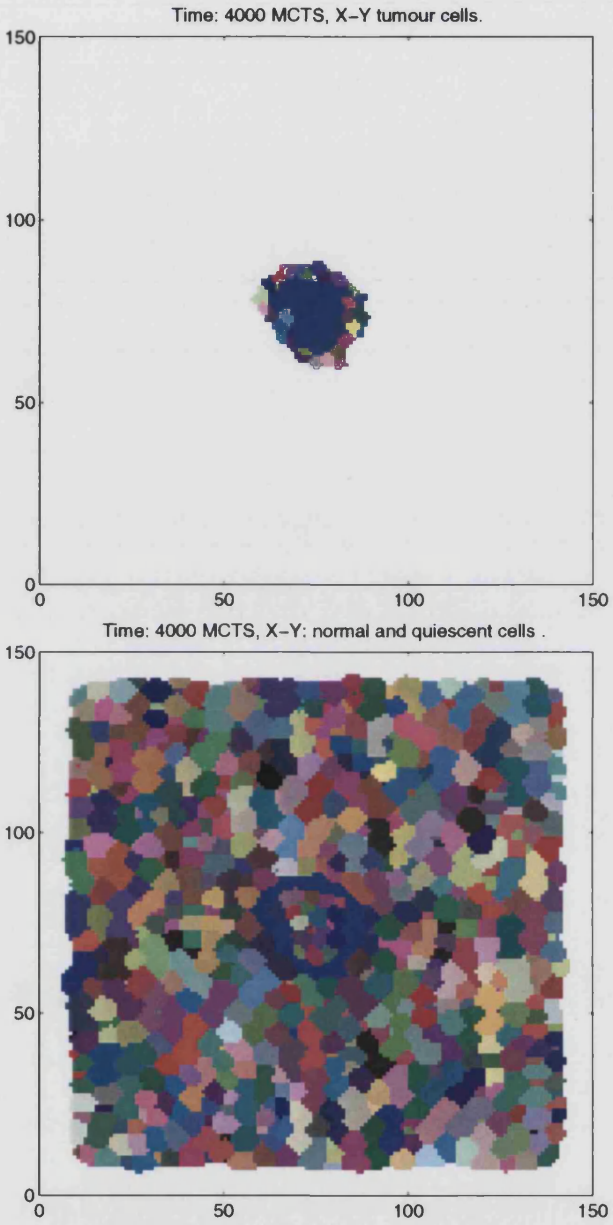

Figure 3-4: Cross sections of tumour. Top: only proliferating cancer cells shown individually. White=normal cells, solid blue=core of quiescent cells. Bottom: only normal cells and quiescent cancer cells shown individually. Solid blue = ring of cancer cells. Again, these two pictures are of the same configuration, but are displayed separately so as to show all cells individually, while keeping their type clear.

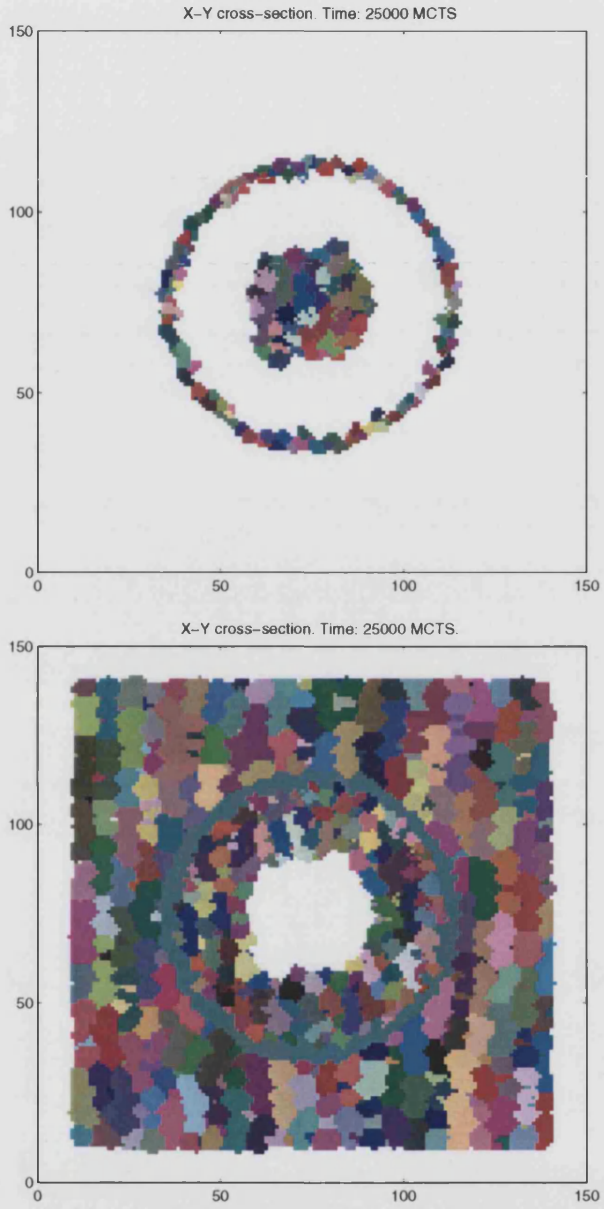

Figure 3-5: Cross sections of tumour. Top: only proliferating cancer and necrotic cells shown individually. Solid white surrounding tumour is normal tissue, while the solid white annulus is quiescent cancer cells. Bottom: normal and quiescent cells only. White central mass is the necrotic core, while the green ring is the proliferating cancer cells.

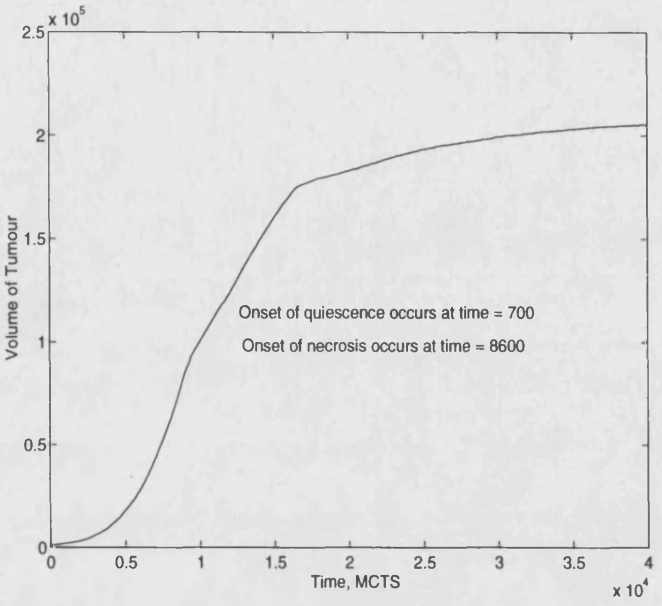

Figure 3-6: Graph showing the volume of the growing tumour vs. number of MCTS.

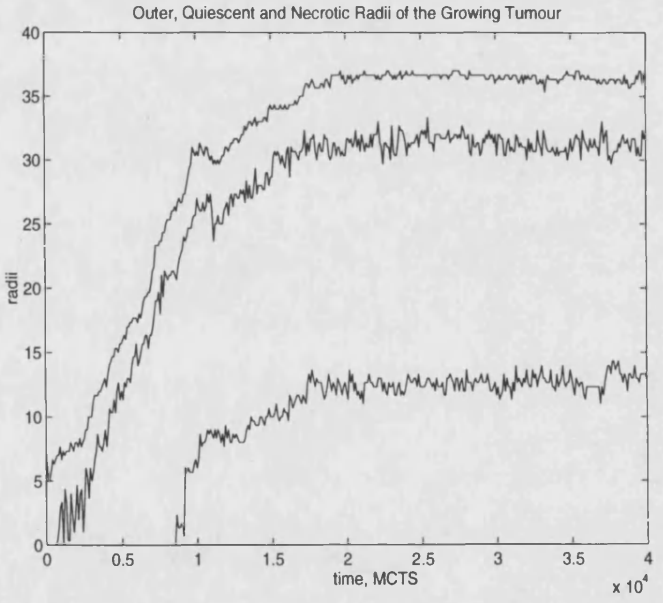

Figure 3-7: Graph of the growth of the three radii of the tumour vs. number of MCTS. Top curve: outer radius; middle curve:outer quiescent radius; bottom curve: necrotic radius.

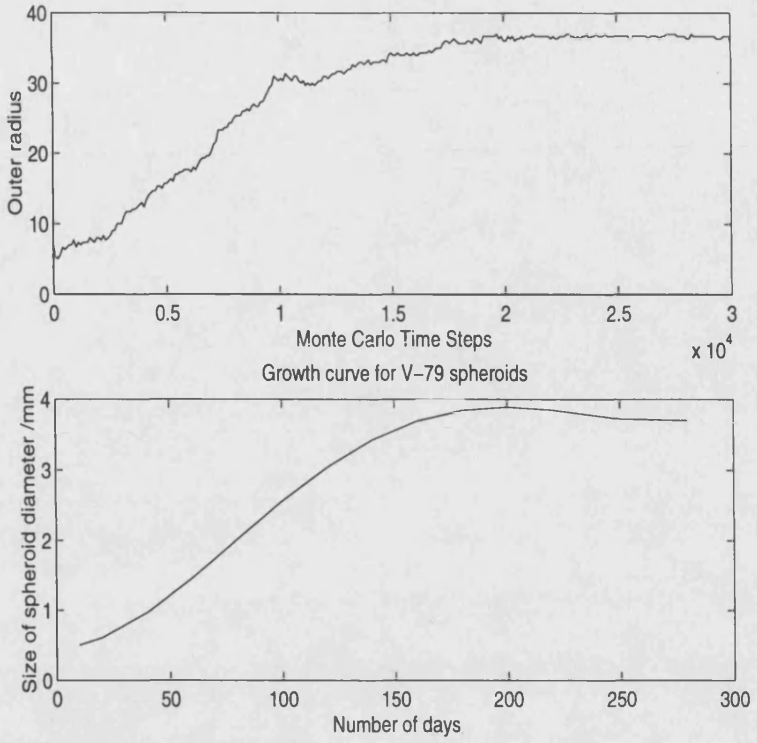

Figure 3-8: Comparison of the growth of simulated outer tumour radius with Folkman and Hochberg's measurements for V-79 MCS.

3.5 Discussion.

The Potts Model has proven to be a very useful tool in simulating cell movements. It includes features often neglected in the simplest models of tumour growth, such as cell-cell adhesion. However, we have made many simplifications. Our model of the adhesive properties of cells was as simple as possible. We concentrated on the essential features of the growth of a solid avascular tumour *in vivo*. But, we neglected the fact that normal tissue surrounding a tumour is not homogeneous, and nutrient would diffuse from nearby blood vessels and not be supplied to the periphery by a homogeneous source. We neglected orientation dependent mechanical and adhesive properties of cells.

Despite these assumptions, our model simulates avascular tumour growth well, reproducing experimental results for the increase of tumour volume.

Also, all of our cancer cells are equally aggressive in their growth and all have the same adhesivity. In a real tumour, some cells will be further down the malignant development pathway than others, so they will vary in their growth rate and adhesivity throughout the tumour. When a tumour cell divides, its daughters do not always have the same properties as the parent [167, 232]. For example, daughter cells may be more aggressive in their growth and also adhere less to other cancer cells, thus being more likely to break away from the tumour

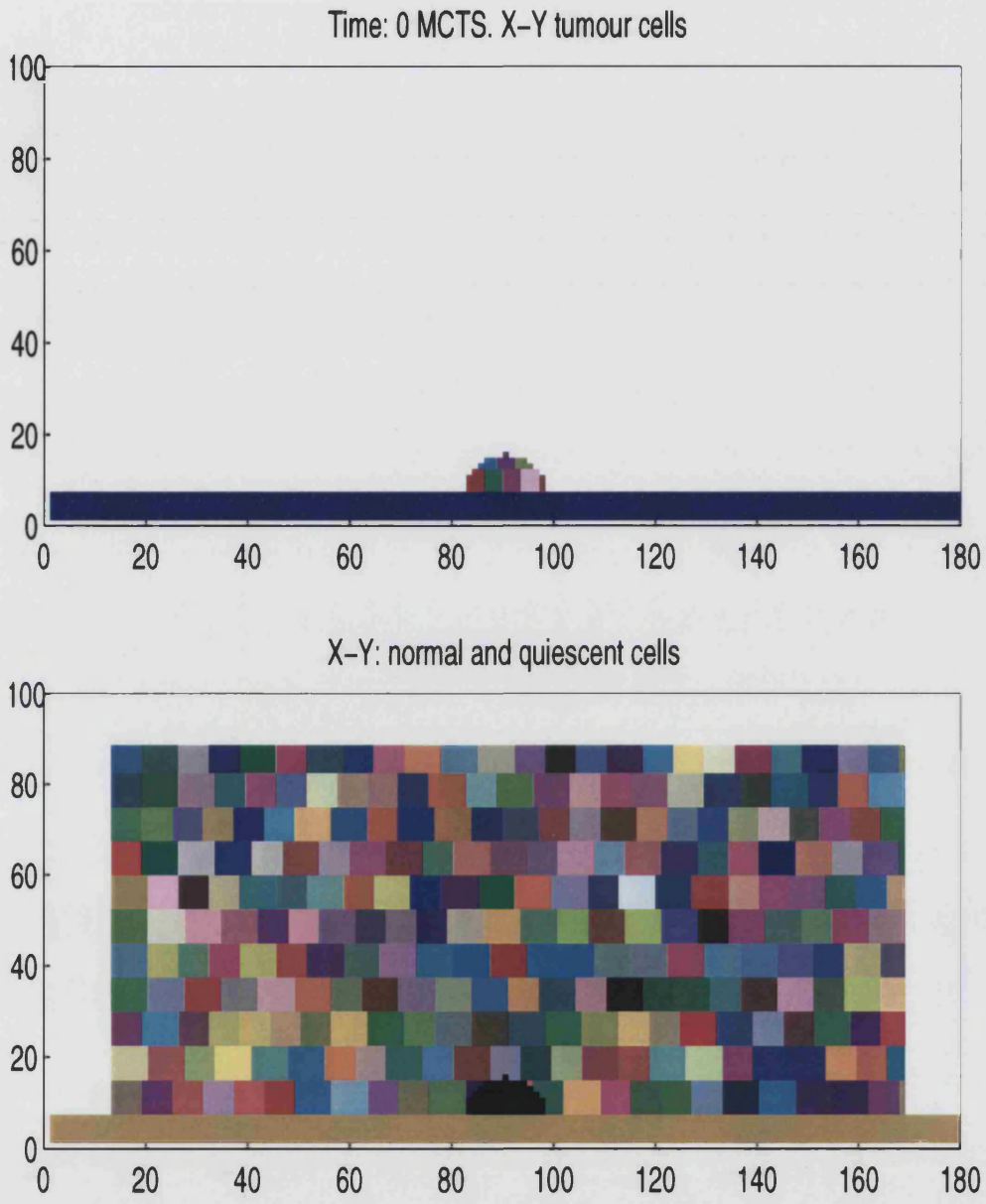

Figure 3-9: Cross section of tumour showing a) substrate and tumour cells only and b) normal cells and substrate only.

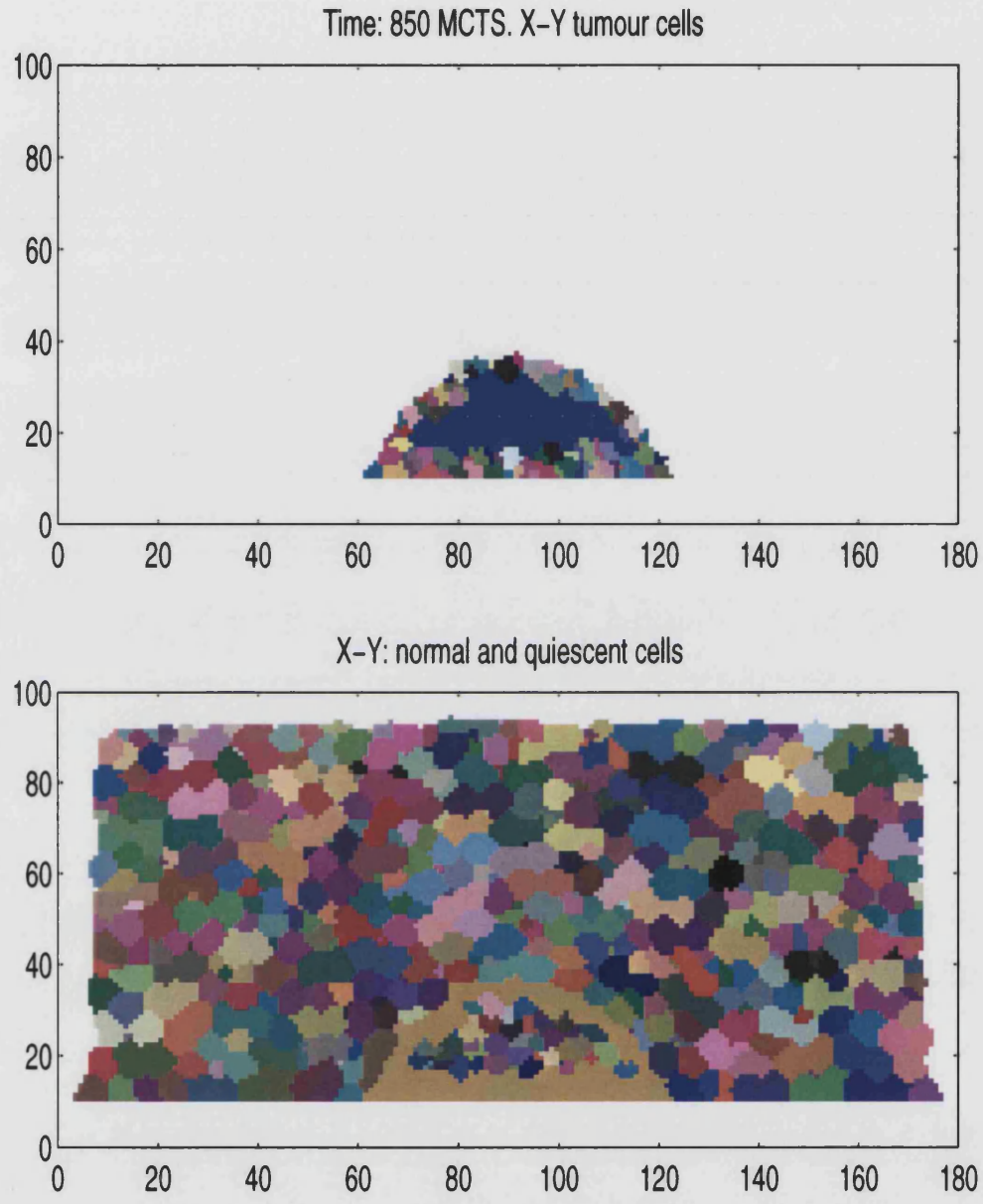

Figure 3-10: Cross section of tumour showing a) substrate and tumour cells only and b) normal and quiescent cells only.

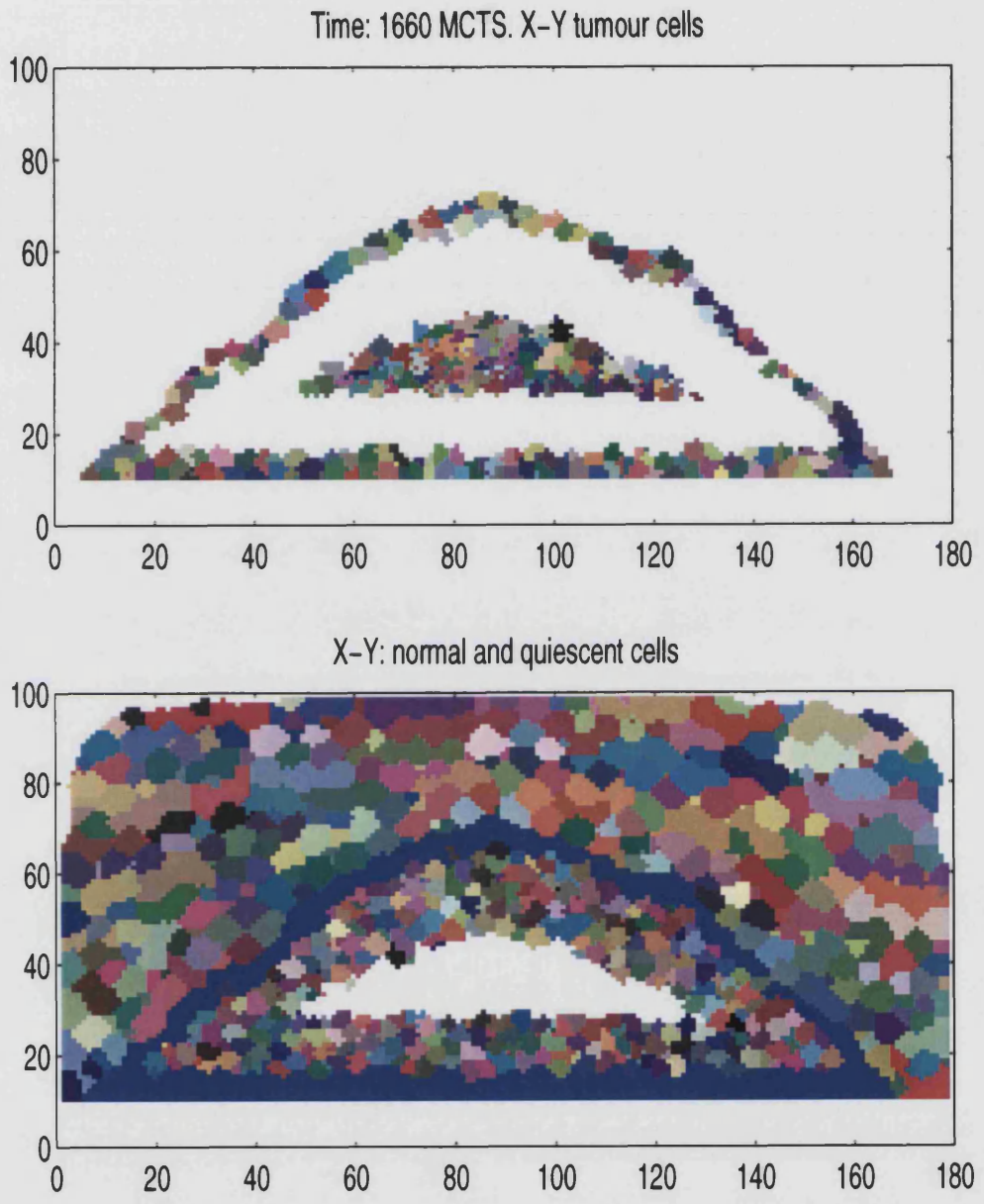

Figure 3-11: Cross section of tumour showing a) substrate, tumour cells and dead cells only and b) substrate, normal and quiescent cells only.

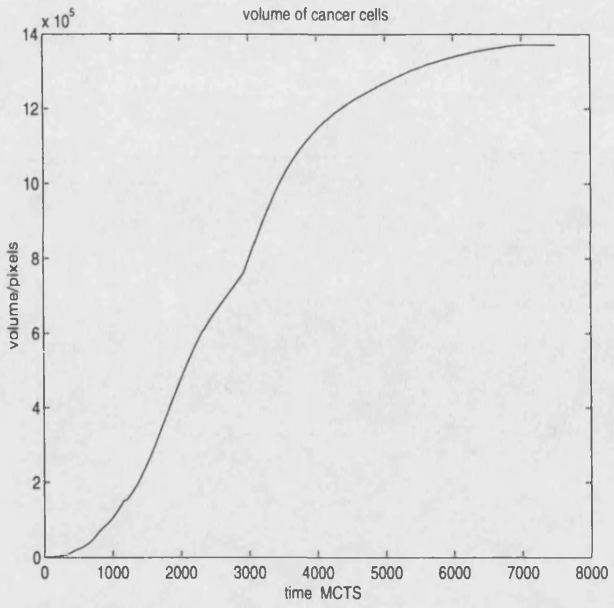

Figure 3-12: Graph of tumour volume vs. time.

mass into the normal tissue. Our model is developed to include metastasis by allowing the daughter cells to have randomly fluctuating growth rates and adhesivities with respect to the values of their parent cell, according to a probability matrix. The simulation of the evolution of a true metastatic, though avascular cancer is presented in Chapter 8.

Normal tissue is also not homogeneous - it contains extracellular matrix, fibrin, collagen, blood vessels etc..., so normal tissue is not a homogeneous source of nutrient. We have developed the model to include nutrient diffusing into the tumour from surrounding normal tissue in Chapter 7.

When a tumour reaches its diffusive equilibrium, it can no longer increase in size, unless it gets its own blood supply. It does this by releasing a chemical called Tumour Angiogenesis Factor into the surrounding tissue [232], which causes nearby blood vessels to form sprouts, which grow into new capillaries. These eventually penetrate the tumour mass and subsequent growth is exponential [14, 66, 71, 74, 180]. Our model has been extended to include these features in Chapter 8.

Chapter 4

A Two Variable Continuum Model of avascular tumour growth

In this chapter, we present a simplistic continuum model of nutrient-dependent solid tumour growth, using as few variables as possible to describe the system.

4.1 Description of Model.

The model is a system of two coupled reaction diffusion equations which determine the spatial distribution and temporal evolution of the two fields: $N(x,t)$, the density of cancer cells and $G(x,t)$, the concentration of an essential nutrient. The units of N are cells/cm^3 and those of G are expressed as a molarity (M). x and t are the position in space (in cm) and time (s) respectively.

The equations describing the system are:

$$\begin{aligned} \frac{\partial N}{\partial t} &= rN\left(1-\frac{N}{K}\right) + D_1\frac{\partial}{\partial x}\left[\tilde{\mathrm{D}}(G)\frac{\partial N}{\partial x}\right] + C\frac{\partial N}{\partial x} \\ \frac{\partial G}{\partial t} &= s(kG_c - G)\left(1-\frac{N}{K}\right) - dGN + D_2\frac{\partial^2 G}{\partial x^2} \end{aligned} \tag{4.1}$$

We assume that the cancer cells grow logistically, with rate r and carrying capacity K. This is equivalent to the assumption that cells will try to fill all available space. We allow cancer cells to diffuse with a nutrient-dependent diffusion coefficient. We also assume that when, at a certain point, the nutrient concentration, G, falls below some critical level G_c, the cancer cells there are dead and therefore will not diffuse at all. If $G \geq G_c$ then the cells will diffuse with a

coefficient that increases with G up to a saturation level. *i.e.* we take

$$\tilde{D}(G) = \begin{cases} 0 & \text{if } 0 \leq G \leq G_c \\ (G/G_c - 1)^2 & \text{if } G_c \leq G \leq 2G_c \\ 1 & \text{if } 2G_c \leq G. \end{cases}$$

This particular function is chosen because it is the simplest continuously differentiable function that satisfies the requirements. It would be slightly unrealistic from a biological point of view to choose a non smooth function.

Experiments performed by Dorie *et al.* [52, 53] on Multicell Spheroids (MCS), demonstrate that, on the whole, live labelled cells and inert microspheres undergo a slow migration towards the centre of the spheroid. The expected cell motion would involve active migration up the nutrient gradient rather than the observed migration down the nutrient gradient towards the spheroid centre where the nutrient concentration is low and the concentration of cell toxins and breakdown products is high.

McElwain and Pettet [151] propose that this inward motion of cells is a passive motion, driven by pressure gradients inside the MCS. These pressure gradients are thought to be generated by the high rate of proliferation near the periphery of the spheroid.

The last term, $C\frac{\partial N}{\partial x}$, in the top formula of (4.1) causes the cells to move towards a higher density of cells and thus takes this "inward flow" into account.

The tumour is assumed to be avascular, so nutrient is only provided by the network of blood vessels in the healthy tissue surrounding the tumour. To keep the model simple, an equation describing the dynamics of the healthy tissue is not included. Instead, we assume that it will occupy all space not taken up by tumour cells, up to the carrying capacity limit, K. Thus, the nutrient is produced at a rate proportional to $1 - N/K$. However, it would be biologically unrealistic for nutrient concentration to be able to increase indefinitely (*i.e.* be unbounded above) and so we also make the rate of production proportional to $1 - G/kG_c$, where $k > 1$ is a constant. It is also assumed that the essential nutrient (e.g. glucose, oxygen) is consumed at a rate proportional to the density of cancer cells and diffuses chemically.

The value of the parameters of this model can be found in Table 4.1.

The following transformation of variables renders (4.1) dimensionless:

$$N' = \frac{N}{K}, \quad t' = rt, \quad G' = \frac{G}{G_c}, \quad x' = \sqrt{\frac{r}{D_2}}x.$$

Using the transformations, the dimensionless form of the system becomes, on dropping the

Parameter	Estimate	References
r	1×10^{-6}/s	[219]
K	5×10^{7} cm^3	[86]
D_1	2×10^{-10}cm^2/s	[45]
C	$O(10^{-9}) - O(10^{-10})$cm/s	
s	3.6×10^{-4}/s	[22]
d	7.2×10^{-12} cm^3/s	[22]
D_2	3.9×10^{-7}cm^2/s	[31, 198]
G_c	7.9×10^{7} M	[22]

Table 4.1: Parameter values.

primes for convenience,

$$\begin{aligned} \frac{\partial N}{\partial t} &= N(1-N) + \Delta_1 \frac{\partial}{\partial x}\left[D(G)\frac{\partial N}{\partial x}\right] + \chi \frac{\partial N}{\partial x} \\ \frac{\partial G}{\partial t} &= \rho(k-G)(1-N) - \delta G N + \frac{\partial^2 G}{\partial x^2} \end{aligned} \tag{4.2}$$

where

$$\Delta_1 = \frac{D_1}{D_2},\ \chi = \frac{C}{\sqrt{rD_2}},\ \rho = \frac{s}{r},\ \delta = \frac{dK}{r} \text{ and } D(G) = \begin{cases} 0 & 0 \le G \le 1 \\ (G^2-1) & 1 \le G \le 2 \\ 1 & 2 \le G \end{cases}$$

The fixed points of this system are the solutions of

$$N(1-N) = 0 \quad \text{and} \quad \rho(k-G)(1-N) - \delta G N = 0$$

i.e. (0,k) and (1,0).

The eigenvalues of the linearisation of the model at $(1,0)$ are $\lambda = -1, -\delta$, and at $(0,k)$ they are $\lambda = 1, -\rho$. So, $(1,0)$ is stable to small perturbations in N or G and the point $(0,k)$ is unstable. Small perturbations from $(0,k)$, in N or G would grow until the system evolved toward $(1,0)$.

Let $y_1 = -N,\ y_2 = G,\ \mathbf{y} = (y_1, y_2)^T$. Then

$$\begin{aligned}\frac{\partial y_1}{\partial t} &= f_1(\mathbf{y}) + \Delta_1 \frac{\partial}{\partial x}\left[D(y_2)\frac{\partial y_1}{\partial x}\right] + \chi\frac{\partial y_1}{\partial x} \quad \text{where} \quad f_1(\mathbf{y}) = y_1(1+y_1)\\ \frac{\partial y_2}{\partial t} &= f_2(\mathbf{y}) + \frac{\partial^2 y_2}{\partial x^2} \quad \text{where} \quad f_2(\mathbf{y}) = \rho(k-y_2)(1+y_1) + \delta y_1 y_2.\end{aligned}$$

Then $\frac{\partial f_1}{\partial y_2} = 0,\ \frac{\partial f_2}{\partial y_1} = \rho(k-y_2) + \delta y_2$. In order for this system to be a quasi-monotone non-decreasing system, we need $0 \le y_2 \le k$, which is what we are trying to prove, but the comparison theorems (Theorem 5.3, p.242 [223]) allow for this and so we can still apply them here. See Chapter 6, section 6.2.1 for details.

Since $\mathbf{y}_1^* = (-1, 0)$ and $\mathbf{y}_2^* = (0, k)$ are solutions of the problem, $\mathbf{y}_1^*$ may be considered as a sub-solution and $\mathbf{y}_2^*$ a super-solution.
So if $\mathbf{y}_1^* \le \mathbf{y}(x,0) \le \mathbf{y}_2^*$ then $\mathbf{y}_1^* \le \mathbf{y}(x,t) \le \mathbf{y}_2^*,\ \forall t \ge 0$. *i.e.* $-1 \le y_1 \le 0$ and $0 \le y_2 \le G_1$ $\Rightarrow 0 \le N \le 1,\ 0 \le G \le k$. Thus we have a bounded system.

The steady states of the system are solutions of $\frac{\partial N}{\partial t} = 0$ and $\frac{\partial G}{\partial t} = 0$ *i.e.*

$$\begin{aligned}0 &= N^*(1-N^*) + \Delta_1 \frac{d}{dx}\left[D(G^*)\frac{dN^*}{dx}\right] + \chi\frac{dN^*}{dx}\\ \text{and} \quad 0 &= \rho(k-G^*)(1-N^*) - \delta G^* N^* + \frac{d^2G^*}{dx^2}\end{aligned}$$

Now, $\Delta_1 = 5.1 \times 10^{-4} \ll 1$. So the top equation can be approximated by

$$\frac{dN^*}{dx} = -\frac{1}{\chi}N^*(1-N^*)$$

This can be solved analytically to give

$$N^*(x) = \frac{1}{1+ae^{x/\chi}} \quad \text{where } a \text{ is an arbitrary constant. We choose } a = 1$$

without loss of generality, by fixing the origin appropriately and so that $N^* \in [0,1]$. Note that $N^* \to 0$ as $x \to \infty$ and $N^* \to 1$ as $x \to -\infty$ and also, $\frac{dN^*}{dx} \to 0$ as $x \to \pm\infty$.
Substituting this into the bottom equation gives:

$$\frac{d^2G^*}{dx^2} = \frac{k\rho}{1+e^{-x/\chi}} - G^*\left(\frac{\rho}{1+e^{-x/\chi}} - \frac{\delta}{1+e^{x/\chi}}\right)$$

This is a linear equation with analytic coefficients and hence there exists a solution which has a power series representation [Theorem 5.11, [37]]. We used the Matlab routine ODE23 to solve this equation numerically, taking the value of k to be 2. Figure (4-1) shows the results.

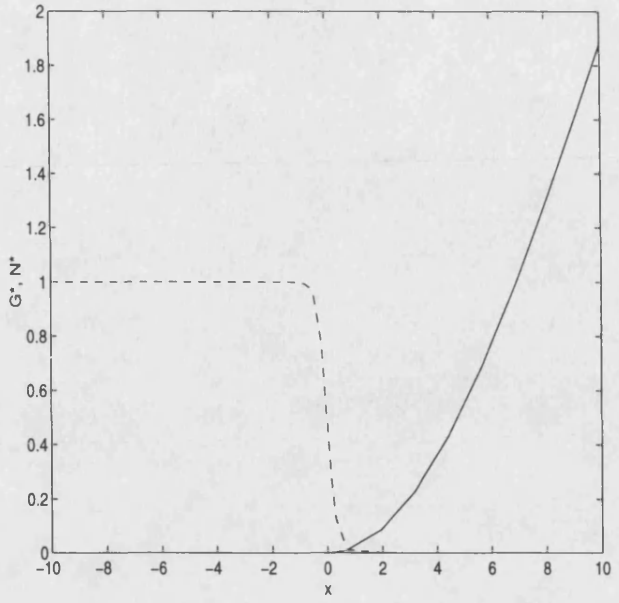

Figure 4-1: Numerical solution of nutrient steady state (solid line) and plot of tumour steady state (dashed line), $\chi = 1.6 \times 10^{-3}$.

Increasing (decreasing) χ decreases (increases) the steepness of the line joining $N^* = 1$ to $N^* = 0$.

4.2 Results.

We used the NAG routine D03PCF to solve the full system of equations numerically, with suitable boundary conditions. The dimensionless system size was taken to be 20, *i.e.* $-10 \leq x \leq 10$ and the value of k to be 2. The results are shown in Figure (4-2).

By assuming that the distance of the tumour periphery from the left hand boundary ($x+10$ in our numerical simulation) describes the length of the radius of a spherically symmetric tumour, we can calculate the volume of such a tumour and hence compare our numerical results to those of the simulation in Chapter 3. The two graphs are shown in Figure (4-3). The two graphs are quite comparable in shape, apart from the initial exponential growth in the simulation. Both have stages of linear growth which eventually saturates to some value of volume.

We can calculate the speed of growth of the tumour radii in the linear phase of growth from the graphs. We calculate the speed of growth of the radius in the linear phase of growth in the continuum model to be $17.76 \approx 0.09$ mm/day, which is comparable to the experimental growth rates obtained by Folkman and Hochberg [71].

If, instead of one spatial dimension, we had considered spherically symmetric tumour in three dimensions, the results would be very similar, but the speed of growth in the linear phase

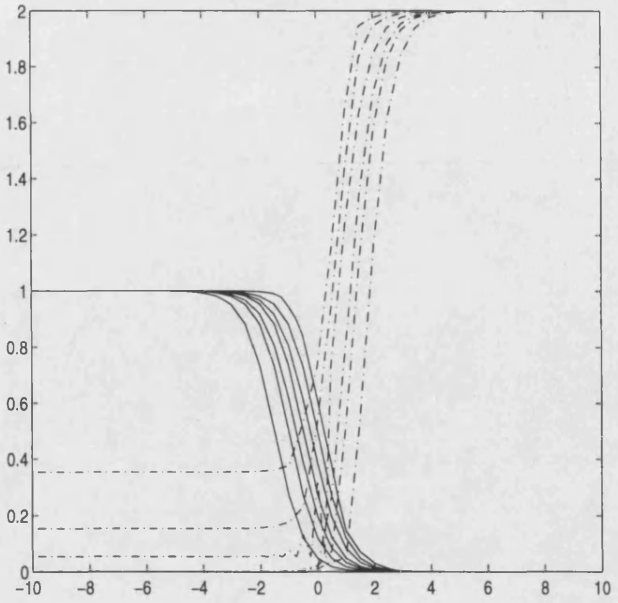

Figure 4-2: Numerical simulations of the model.

would have been slower.

4.3 Discussion.

This 2-variable continuum model is a very simple representation of nutrient dependent tumour growth. It assumes that the tumour is homogeneous, and that the only difference between dead and live tumour cells is that the dead cells don't diffuse through space. There is no distinction made between proliferating and quiescent tumour cells and it is assumed that all three "types" of tumour cell absorb nutrient at the same rate. The model also ignores the effect of the presence of healthy normal cells which usually surround the tumour *in vivo* and compete for available space. Despite these many simplifications, this system of equations reproduces the growth curve of an *in vitro* multicellular spheroid well, with similar results to the simulation in Chapter 3, for the increase of tumour volume. It would be unlikely to be able to reproduce the initial exponential growth of a multicellular spheroid with a continuum model where the dynamics depend on cell densities. This is because the dynamics are localised and therefore growth does not depend on the total number of cancer cells , only those that are present at a given spatial point.

The model in this chapter uses 2 PDE's to describe the development of cancer cell density and nutrient concentration with time. Quiescent and dead cells are not considered. If quiescence and death were to be added to the model, the shells would overlap slightly and not be distinct. Also, the growth and formation of the shells would be a continuous process. In the following

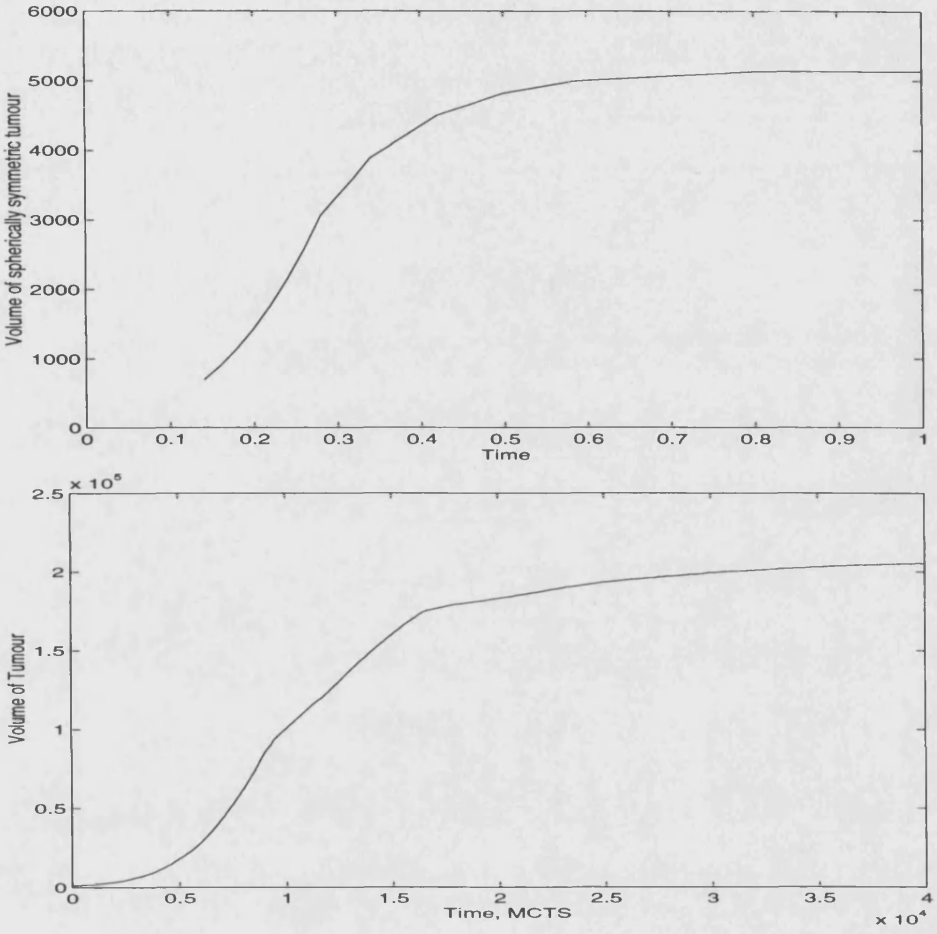

Figure 4-3: Comparison between numerical results and results of simulation in Chapter 3.

chapter (Chapter 5), we extend Greenspan's model of MCS growth. In these models, the tumour is divided into distinct compartments of proliferating, quiescent, and necrotic cells, and growth takes place in three distinct phases. It is assumed that all growth is spherically symmetric and that nutrient is in diffusive equilibrium, and thus the growth of the outer radius and the two inner radii of the tumour can be described using ODE's.

Chapter 5

Extension of Greenspan's Model of Solid Tumour Growth.

5.1 Assumptions.

The simplest experimental model of solid tumours are multicellular spheroids (MCS). These are three-dimensional, multicellular aggregates, which are grown in tissue culture (for a review see Durand [58]). MCS models are used to study the growth kinetics of small populations of cells and the re-growth kinetics of the population in response to cytotoxic treatments. MCS models have similar growth kinetics to tumour nodules and they develop micro-regions of quiescent cells in much the same way as solid tumours do. Furthermore, they have simple geometry and are easy to manipulate. However, it is difficult to compare MCS models directly with *in vivo* tumours, since they do not incorporate the influence of the host on the tumour growth.

Thomlinson and Gray [215], Burton [28] and Greenspan [102, 103, 104] have discussed simple mathematical models of multicell spheroids provided with nutrients by diffusion alone. The basic assumptions of these studies are:

(i) The solid tumour is assumed to be a multicell spheroid, *i.e.* complete spherical symmetry prevails throughout growth. The only independent variables are time, t, and radial distance, r.

(ii) Cancer cells die when the concentration of a crucial nutrient, denoted by $\sigma(r,t)$, falls below a critical level, σ_n.

(iii) The vital nutrient is consumed by living cells only: The consumption rate may depend on nutrient concentration and cell proliferation as well as other factors.

Greenspan [102] also assumes that

(iv) There is an adhesion or surface tension among living cells [210], which in a spherical geometry produces an inward pressure that maintains a compact solid mass.

(v) Necrotic cellular debris continually disintegrates into simpler chemical compounds that are freely permeable through cell membranes. The mass or cell volume lost this way is replaced by cells pushed downward by the forces of adhesion and surface tension.

These assumptions ensure that cell proliferation can continue when the tumour is in its steady state, where its volume remains constant. In this equilibrium, cells produced in the proliferating layer flow inward exactly compensating for the loss of cell volume in the necrotic core.

Experiments show that the MCS contains an inner layer of living, viable cells with a low mitotic index ([7, 16, 151]). Greenspan takes this facet of tumour growth into account by introducing a mitotic inhibitor into the model. However, the existence of this type of chemical has not been proved and so here, we assume that quiescence only occurs when cells do not have enough nutrient to divide i.e. we assume that

(vi) Cancer cells become quiescent (*i.e.* no longer proliferate), when the concentration of the crucial nutrient, σ(r,t), falls below a critical level, σ_q.

The time scale for diffusion of nutrient is small compared to a typical time scale for tissue growth. So, we also assume

(vii) The tumour is in a state of diffusive equilibrium at all times.

5.2 Conservation of mass.

We think of the tumour as a "fluid" that consists of incompressible cells held together by adhesive forces. Proliferation behaves like a source of incompressible fluid, while necrosis acts like a sink and the fluid domain or tumour size varies in extent to accommodate any imbalance in net production.

Following Greenspan [102] again, we incorporate the following approximations into the mathematical model:

a) All living tumour cells are identical and each is to be considered an incompressible structure of constant volume.

b) Cell division occurs "instantaneously" relative to the growth time of the tumour, and each daughter cell occupies the same volume as any other cell of the population.

c) The proliferation rate of cell volume by mitosis is described by a source distribution $S(\sigma)$ which is a function only of the local nutrient concentration. This function describes the rate at which cell volume is produced by mitosis per unit volume of living cells.

d) The necrotic core "loses" cell volume at a rate that at any time is proportional to the core volume. Moreover, this loss occurs at a uniform rate throughout the region of necrosis. The proportionality constant is denoted by 3λ. (The 3 is just for convenience later on).

The conservation of mass with distributed sources and sinks is equivalent to the conservation of volume. So, the conservation law is as follows:

$$A = B + C - D - E \tag{5.1}$$

with

A = total volume of living cells at any time t;

B = initial volume of living cells at time $t = 0$;

C = total volume of cells produced in time $t \geq 0$;

D = total volume of necrotic debris in the MCS at time t;

E = total volume lost from the necrotic core in time $t \geq 0$;

Let $R_o(t)$ be the outer radius of the nodule at any time t. $R_o(0)$ is then the initial radius of the tumour.

Let $R_q(t)$ be the radius at which cell proliferation ceases because the concentration of nutrient in the domain of living cells falls below the critical level σ_q. Since quiescence occurs when the nutrient level σ falls below the critical value σ_q, $R_q(t)$ is defined by the relationship

$$\sigma(R_q(t), t) = \sigma_q.$$

If $\sigma > \sigma_q$ everywhere, then $R_q(t) \equiv 0$.

Let $R_n(t)$ be the radius of the necrotic core. By definition

$$\sigma(R_n(t), t) = \sigma_n.$$

If $\sigma > \sigma_n$ everywhere, then $R_n(t) \equiv 0$.

Because dead cells obviously can't proliferate, we must have $\sigma_n \leq \sigma_q$, in other words, $R_n(t) \leq R_q(t)$ at all times.

The mathematical forms of the various terms in (5.1) are then as follows:

$$
\begin{aligned}
A &= \tfrac{4\pi}{3}(R_o^3(t) - R_n^3(t)) ; \\
B &= \tfrac{4\pi}{3}R_o^3(0) ; \\
C &= 4\pi \int_0^t dt \int_{R_q(t)}^{R_o(t)} S(\sigma) r^2 dr ; \\
D &= \tfrac{4\pi}{3}R_n^3(t) ; \\
E &= \tfrac{4\pi}{3} \int_0^t 3\lambda R_n^3(t) dt .
\end{aligned}
$$

Putting these into (5.1) gives the conservation of volume equation which governs the growth of the tumour:

$$R_o^3(t) = R_o^3(0) + 3\int_0^t dt \int_{R_q(t)}^{R_o(t)} S(\sigma) r^2 dr - \int_0^t 3\lambda R_n^3(t) dt.$$

Taking the derivative with respect to t gives a more useful form of this equation:

$$R_o^2 \frac{dR_o}{dt} = \int_{R_q(t)}^{R_o(t)} S(\sigma) r^2 dr - \lambda R_n^3. \tag{5.2}$$

5.3 Model 1: Growth of a solid tumour with constant cell proliferation rate.

In the first model, the rate of cell proliferation per unit volume in the growth region is assumed to be constant. Again, following Greenspan [102], we use the following simple approximations:

(i) The diffusivity, k, of the nutrient, σ, is uniformly constant throughout the tumour and the adjacent medium.

(ii) The nutrient is consumed at a constant rate per unit volume, a, by the living cells. So, we are assuming that quiescent and proliferating cells consume nutrient at the same rate.

(iii) The rate of cell proliferation per unit volume in the growth region is a constant, s. In terms of the step function,

$$H(x) = \begin{cases} 1 & x \geq 0; \\ 0 & x < 0, \end{cases}$$

the source distribution for new cells (or new volume) due to mitosis is approximated by

$$S(\sigma) = sH(\sigma - \sigma_q). \tag{5.3}$$

(iv) The composition of the ambient medium is held fixed throughout any experiment. The concentration of nutrient at the outer surface of the tumour is σ_∞.

With the source term given as in (5.3), the mass conservation law (5.2) can be written as

$$R_o^2 \frac{dR_o}{dt} = \frac{s}{3}[R_o^3 - R_q^3] - \lambda R_n^3. \tag{5.4}$$

The assumption of diffusive equilibrium implies that the equation for the concentration of σ is

$$\frac{1}{r^2}\frac{d}{dr}\left(r^2 \frac{d\sigma}{dr}(r)\right) = \frac{a}{k} H(r - R_n(t))H(R_o(t) - r). \tag{5.5}$$

The boundary conditions require σ and $\frac{\partial \sigma}{\partial r}$ to be continuous across every interface and in particular $\sigma = \sigma_\infty$ at $r = R_o(t)$; all functions are bounded at the origin. By definition, $R_q(t)$ and $R_n(t)$ satisfy

$$\sigma(R_q) = \sigma_q$$
$$\sigma(R_n) = \sigma_n$$

if solutions exist, otherwise, $R_q \equiv 0$, $R_n \equiv 0$.

Since time derivatives have been neglected in the diffusion equation, the only initial condition required is the value of $R_o(0)$. The initial size of the tumour is always assumed to be small so that $R_q(0) = 0$, $R_n(0) = 0$.

The general solution to (5.5) is:

$$\sigma(r) = \begin{cases} \dfrac{-b}{r} + c & \text{if } r \le R_n \\ \dfrac{a}{6k} r^2 - \dfrac{d}{r} + e & \text{if } R_n < r \le R_o, \end{cases}$$

where b, c, d and e are arbitrary constants. Using the facts that σ is bounded at $r = 0$, $\sigma(R_n(t)) = \sigma_n$, $\sigma(R_o(t)) = \sigma_\infty$ and $\frac{d\sigma}{dr}$ is continuous at $r = R_n$, this gives

$$\sigma(r) = \begin{cases} \sigma_n & \text{if } r \le R_n \\ \sigma_\infty - \dfrac{a}{6k}(R_o^2 - r^2) + \dfrac{aR_n^3}{3k}\left(\dfrac{1}{r} - \dfrac{1}{R_o}\right) & \text{if } R_n < r \le R_o. \end{cases} \tag{5.6}$$

Continuity of σ at $r = R_n$ gives the relation

$$\sigma_\infty - \sigma_n = \frac{a}{3k}\left(\frac{1}{2}(R_o^2 - R_n^2) - R_n^3\left(\frac{1}{R_n} - \frac{1}{R_o}\right)\right). \tag{5.7}$$

The value of the outer radius at which central necrosis first occurs is (putting $R_n = 0$ and solving for R_o)

$$R_c = \left[\frac{6k}{a}(\sigma_\infty - \sigma_n)\right]^{1/2}. \tag{5.8}$$

5.3. MODEL 1: GROWTH OF A SOLID TUMOUR WITH CONSTANT CELL PROLIFERATION RATE.

Growth retardation of live cells occurs when $R_q > 0$; the precise condition obtained from (5.6) is

$$\sigma_\infty - \sigma_q = \frac{a}{6k}(R_o^2 - R_q^2) - \frac{aR_n^3}{3k}\left(\frac{1}{R_q} - \frac{1}{R_o}\right). \tag{5.9}$$

The value of the outer radius at which quiescence first occurs is (putting $R_q = 0$ and $R_n = 0$ and solving for R_o)

$$R_1 = \left[\frac{6k}{a}(\sigma_\infty - \sigma_q)\right]^{1/2}.$$

Following Burton [28] and Greenspan [102], we make the problem dimensionless and the new variables are introduced

$$\eta = \frac{R_o(t)}{R_c}, \quad \eta_q = \frac{R_q(t)}{R_c}, \quad \eta_n = \frac{R_n(t)}{R_c}.$$

In this notation, the initial radius of the colony is $\eta(0) = R_o(0)/R_c$, the development of the necrotic core begins when $\eta = 1$ and continues for all $\eta > 1$.

The dimensionalization is completed by replacing time t by

$$\tau = st, \quad \frac{d}{dt} = s\frac{d}{d\tau}.$$

The dimensionless versions of (5.4), (5.7) and (5.9) are then:

$$\eta^2\frac{d\eta}{d\tau} = \frac{1}{3}[\eta^3 - \eta_q^3] - \frac{\lambda}{s}\eta_n^3;$$

$$\frac{6k(\sigma_\infty - \sigma_n)}{aR_c^2} = \eta^2 - \eta_n^2 - 2\eta_n^2(1 - \frac{\eta_n}{\eta}), \quad \eta \geq 1 \text{ only};$$

$$\frac{6k(\sigma_\infty - \sigma_q)}{aR_c^2} = \eta^2 - \eta_q^2 - 2\eta_n^3(\frac{1}{\eta_q} - \frac{1}{\eta}), \quad \eta \geq \eta_q \geq 1 \text{ only}.$$

Substituting for R_c from (5.8) and putting $\gamma = \frac{\lambda}{s}$, $M^2 = \frac{\sigma_\infty - \sigma_q}{\sigma_\infty - \sigma_n}$, these equations simplify to:

$$\eta^2\frac{d\eta}{d\tau} = \frac{1}{3}[\eta^3 - \eta_q^3] - \gamma\eta_n^3;$$

$$1 = \eta^2 - \eta_n^2 - 2\eta_n^3\left(\frac{1}{\eta_n} - \frac{1}{\eta}\right), \quad \eta \geq 1 \text{ only};$$

$$M^2 = \eta^2 - \eta_q^2 - 2\eta_n^3\left(\frac{1}{\eta_q} - \frac{1}{\eta}\right), \quad \eta \geq R_1/R_c \text{ only.}$$

M and γ are both dimensionless parameters.

The variables

$$x = \frac{\eta_n}{\eta}, \quad y = \frac{\eta_q}{\eta}$$

facilitate the mathematical operations and allow the various stages of tumour development to be described concisely.

Phase I: A period of exponential growth of the tumour until the onset of quiescence.

- *Range of variables:*

$$\eta(0) \leq \eta(\tau) \leq R_1/R_c = M.$$

- *Constraints:*

$$\eta_q \equiv 0, \ \eta_n \equiv 0.$$

- *Growth equation:*

$$3\frac{d\eta}{dt} = \eta.$$

- *Method:* Explicit integration.
- *Solution:*

$$\eta(\tau) = \eta(0)e^{\tau/3}, \quad \eta_q = \eta_n \equiv 0.$$

- *Time period:*

$$0 \leq \tau \leq \tau_1 = 3\ln\left(\frac{M}{\eta(0)}\right).$$

- *Discussion:* The tumour grows exponentially until the first cell at the centre of the sphere becomes quiescent.

Phase II: Period of retarded growth, during which the tumour consists of an outer mantle of dividing cells and an inner viable quiescent core.

- *Range of variables:*

$$R_1/R_c = M \leq \eta \leq 1, \quad 0 \leq y \leq (1-M^2)^{1/2}.$$

- *Constraints:*

$$x \equiv 0, \quad M \leq 1, \quad M^2 = \eta^2 - \eta_q^2.$$

- *Growth equation:*

$$\eta^2 \frac{d\eta}{d\tau} = \frac{1}{3}[\eta^3 - \eta_q^3].$$

- *Method:* Change of variable to y and exact integration to obtain y as an implicit function of time.
- *Formulation:* As $M^2 = \eta^2 - \eta_q^2$, this implies that $\frac{d\eta_q}{d\tau} = \frac{\eta}{\eta_q}\frac{d\eta}{d\tau}$.

  So,

$$\frac{dy}{d\tau} = \frac{d}{d\tau}\left(\frac{\eta_q}{\eta}\right) = \frac{1}{\eta_q}(1-y^2)\frac{d\eta}{d\tau}$$

  i.e.

$$\frac{dy}{d\tau} = \frac{1}{3y}(1-y^2)(1-y^3)$$

  with $y = 0$ at $\tau = \tau_1$, and $\eta = M(1-y^2)^{-1/2}$.

- *Solution:*

$$\frac{1}{2}\ln[(1-y^3)(1-y^2)^{-3/2}] + \frac{y}{2(1-y)}$$

$$-\frac{1}{\sqrt{3}}\left[tan^{-1}\left(\frac{2y+1}{\sqrt{3}}\right) - tan^{-1}\left(\frac{1}{\sqrt{3}}\right)\right] = \tau - \tau_1.$$

- *Time period:* This phase ends at time τ_2, when $y = (1-M^2)^{1/2}$. For small M, $\tau_2 - \tau_1 \sim \frac{1}{M^2}$.
- *Discussion:* For $M < 1$, the effect of the nutrient deficiency is to change the initial exponential growth rate to one that is approximately linear in time. This phase begins

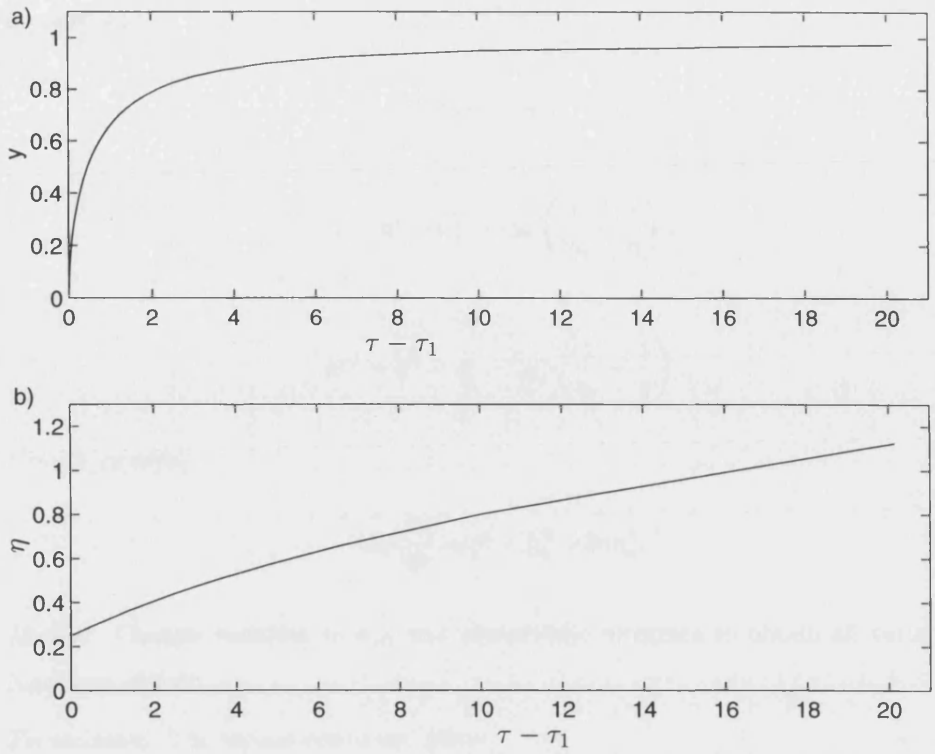

Figure 5-1: Model 1: Graphs showing the second stage of development of a) the ratio of quiescent radius to outer radius; b) the dimensionless outer radius, with $M = 1/4$.

at $\tau = \tau_1$ and $\eta = M$ and ends when $\eta = 1$, $\tau = \tau_2$, with the death of the first cell from even greater nutrient deficiency. Typical growth curves are shown in Figure (5-1).

The thickness of the layer of proliferating cells, measured by $1 - y$, decreases very rapidly and can be described as "thin" after only one or two time steps. The duration of phase II approaches zero as M approaches 1, *i.e.*, as the critical level of nutrient required for quiescence approaches the critical level required for death. If $M \geq 1$, there is no quiescence, as the critical level of nutrient required for death is higher than that required for quiescence. In this situation, the exponential phase ends with the onset of necrosis which marks the next and final stage of development.

Phase III: A period of retarded growth due to inhibition of mitosis and the death of cells which begins when $\sigma = \sigma_n$ at the centre of the tumour and lasts until the steady state is achieved (*i.e.* indefinitely).

- *Range of variables:*

$$1 \leq \eta \leq \eta_\infty, \quad (1 - M^2)^{1/2} \leq y \leq y_\infty, \quad 0 \leq x \leq x_\infty.$$

- *Constraints:*

$$\eta \geq \eta_q \geq \eta_n \geq 0,$$

$$1 = \eta^2 - \eta_n^2 - 2\eta_n^3\left(\frac{1}{\eta_n} - \frac{1}{\eta}\right),$$

$$M^2 = \eta^2 - \eta_q^2 - 2\eta_n^3\left(\frac{1}{\eta_q} - \frac{1}{\eta}\right).$$

- *Growth equation:*

$$3\eta^2\frac{d\eta}{d\tau} = \eta^3 - \eta_q^3 - 3\gamma\eta_n^3.$$

- *Method:* Change variables to x, y and numerically integrate to obtain all variables as functions of time.

- *Formulation:* The second constraint gives

$$\frac{1}{\eta} = (1-x)(2x+1)^{1/2}$$

and so

$$\frac{1}{\eta^2}\frac{d\eta}{d\tau} = 3x(2x+1)^{-1/2}\frac{dx}{d\tau}$$

i.e.

$$\frac{9x}{(2x+1)(1-x)}\frac{dx}{d\tau} = 1 - y^3 - 3\gamma x^3. \tag{5.10}$$

The third constraint gives

$$M^2(x-1)^2(2x+1) = 1 - y^2 - 2x^3(1/y - 1) \tag{5.11}$$

with $x = 0$ and $y = (1-M^2)^{1/2}$ at $\tau = \tau_2$.

- *Solution:* The numerical integration proceeds forwards in time until the solution curves asymptote to their steady state values x_∞, y_∞, which are solutions of (5.10),(5.11) with $dx/d\tau = 0$. Figure (5-2) shows the graphs.

  Putting $dx/d\tau = 0$ in (5.10), gives,

$$y = (1 - 3\gamma x^3)^{1/3}.$$

5.3. MODEL 1: GROWTH OF A SOLID TUMOUR WITH CONSTANT CELL PROLIFERATION RATE.

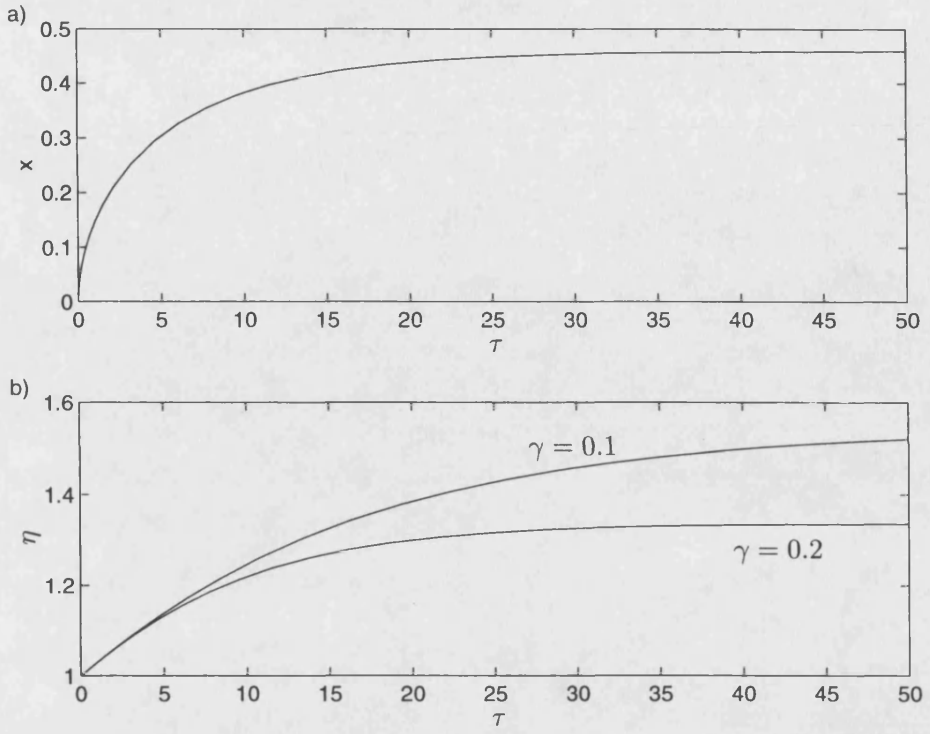

Figure 5-2: Model 1: Graphs showing the final stage of development of a) the ratio of necrotic radius to outer radius; b) the dimensionless outer radius, with $M = 1/4$.

Substituting this into (5.11), expanding the terms using the Binomial Theorem and discarding terms of γ^2 and higher (assuming that γ is moderately small), this gives a good approximation to the steady state

$$\frac{M^2}{\gamma}(1 + 2x_\infty)(1 - x_\infty) = 2x_\infty^3(1 + x_\infty + x_\infty^2).$$

Graphs of x_∞ and η against $\mu = \frac{M^2}{\gamma}$ are shown in Figure (5-3).

Figure (5-4) shows the corresponding values of x_∞, η_∞, the thickness of the viable layer, $\eta_\infty - (\eta_o)_\infty$ and the radius of the necrotic core $(\eta_o)_\infty$.

- *Time period:* An infinite time interval is required to reach the steady state, but the final stage of development is mostly completed when $\tau = O(1/\gamma)$.

- *Discussion:* The development of the tumour in phase III is specified by $\gamma = \lambda/s$, where λ is the rate of loss of cell volume due to necrosis and s is the rate of cell proliferation per unit volume in the growth region. If $M \geq 1$, then this phase starts immediately after phase I, as the nutrient concentration required for quiescence will be lower than that for death.

  Complete histories of model tumour growth are shown in Figure (5-5) and Figure (5-6)

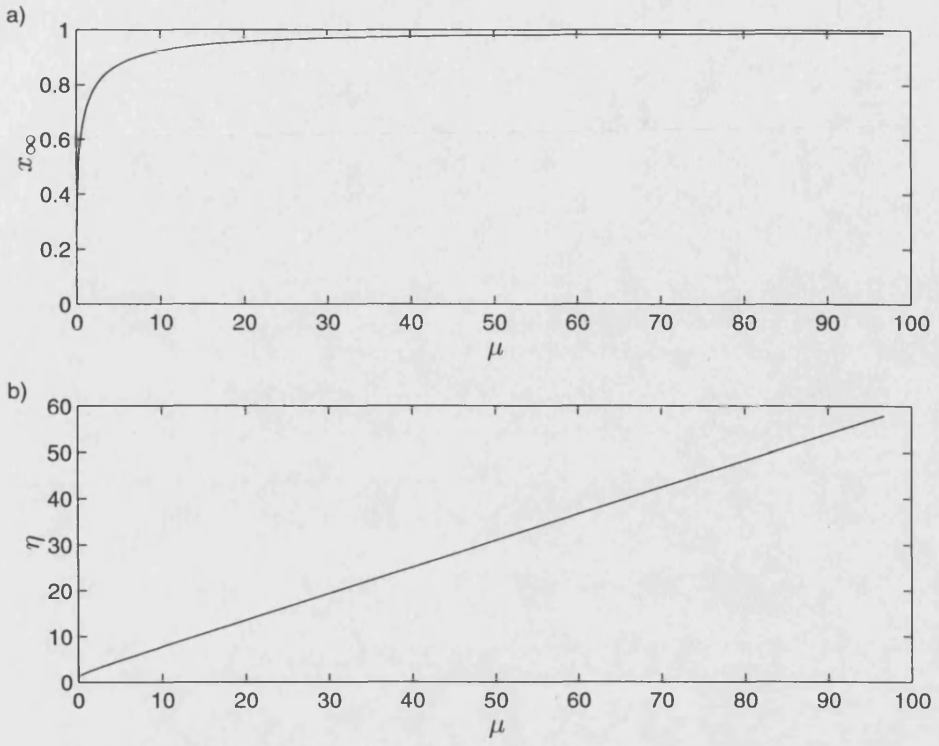

Figure 5-3: Model 1: Graphs showing the steady state values a) x_∞ and b) η versus μ.

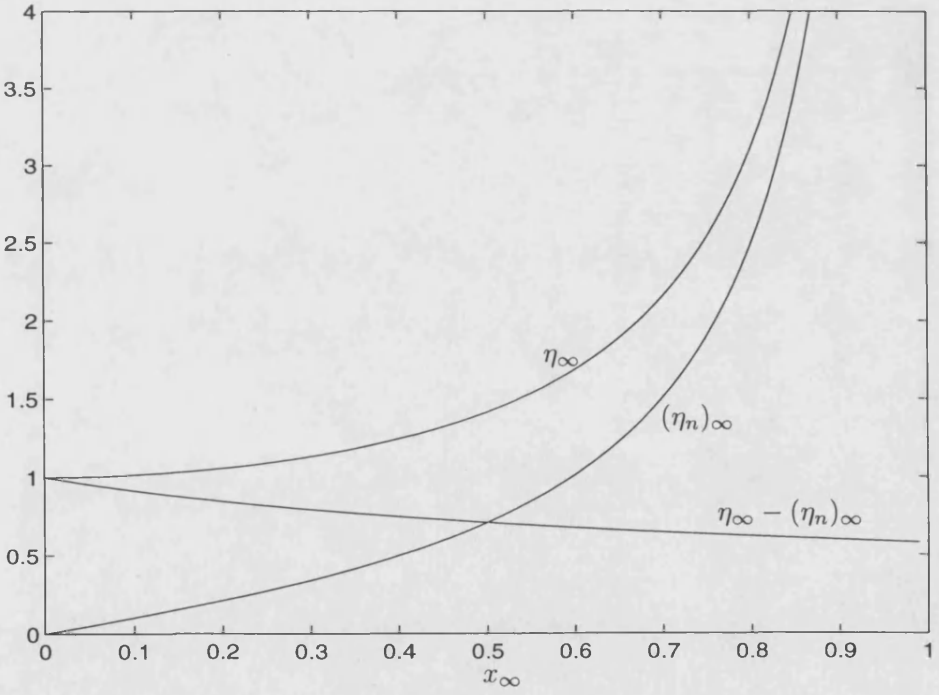

Figure 5-4: Model 1: Steady state values of the dimensionless outer radius of the tumour, η_∞, the dimensionless inner necrotic radius, $(\eta_o)_\infty$, and the thickness of the viable layer $\eta_\infty - (\eta_n)_\infty$ versus x_∞.

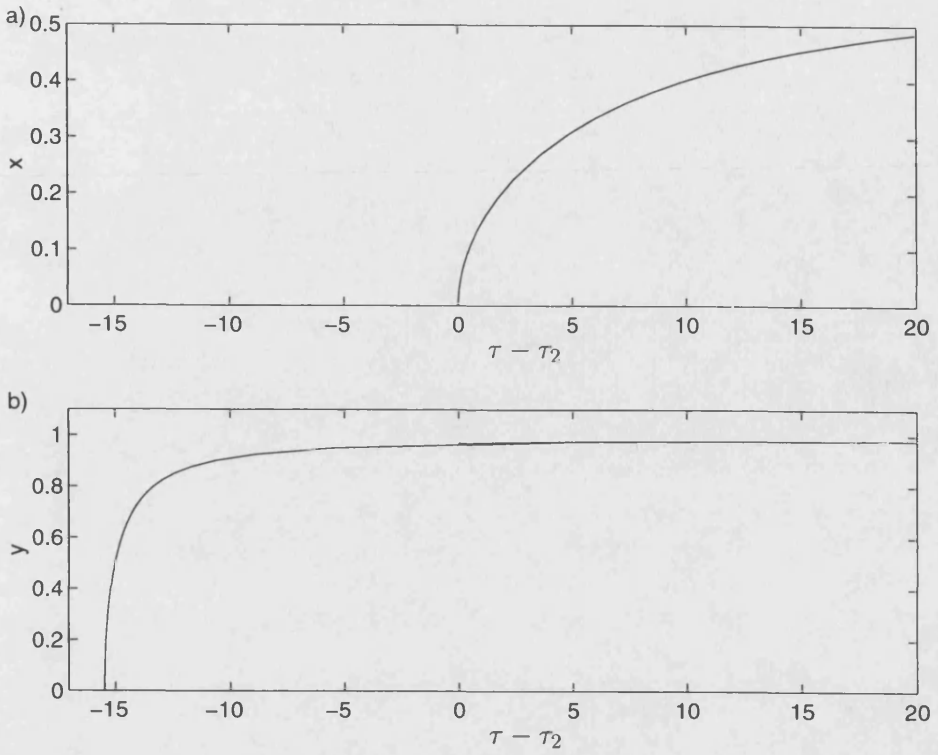

Figure 5-5: Model 1: Graphs to show the change in x and y with time. Again $M = 1/4$.

with experimental settings for γ and the choice of $M = 1/4$. The three growth phases are separated by large dots. Figure (5-7) shows the growth of the 3 radii for one setting of γ. Phase I is not very long, as we chose our initial tumour to be quite large, to fit in with the simulations. In phase III, the necrotic core rapidly increases in size. But, the layer of dividing cells is thin very soon after the start of phase II and remains that way throughout the rest of the development.

5.4 Model 2: Growth of a solid tumour with nutrient dependent proliferation rate.

In the second model, the rate of cell proliferation per unit volume in the growth region is assumed to be linearly proportional to nutrient concentration.

The source term in equation (5.3) means that cell volume is produced homogeneously throughout the layer of proliferating cells. It is known that the rate of mitosis is dependent on nutrient concentration - cells with a high concentration of nutrient will divide faster than those which have a low concentration [22, 30, 34, 81, 84, 107]. Others [114, 124, 212] have shown that the rate of proliferation in tumours decreases with distance from a nutrient source. We want a source function which is zero outside the proliferating layer and increases monotonically with

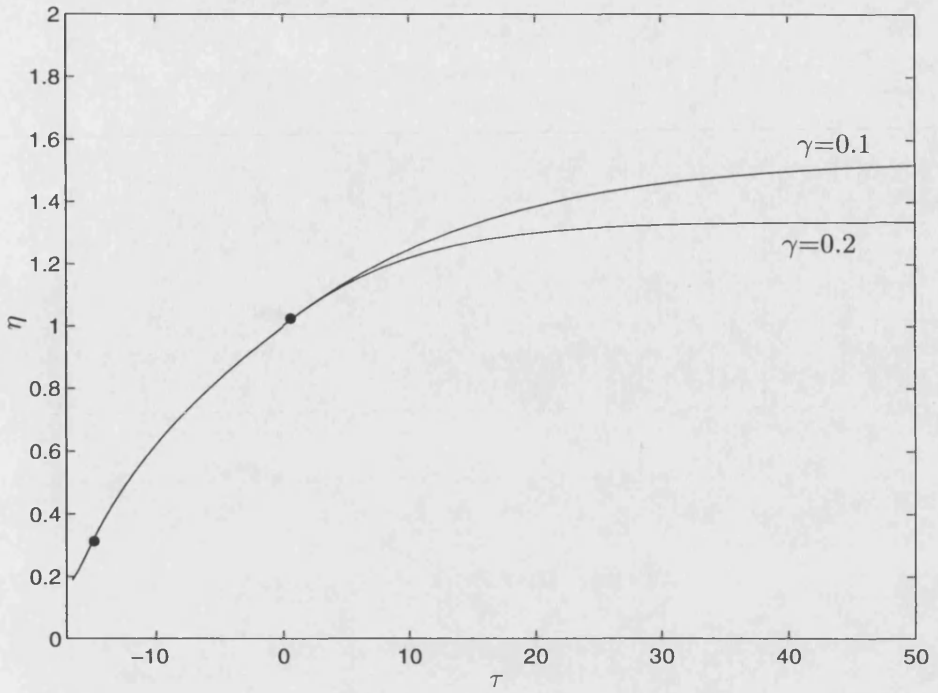

Figure 5-6: Model 1: Graph to show the growth and development of the dimensionless radius of the tumour. M=1/4, γ=0.1 and 0.2. Large dots separate the growth phases.

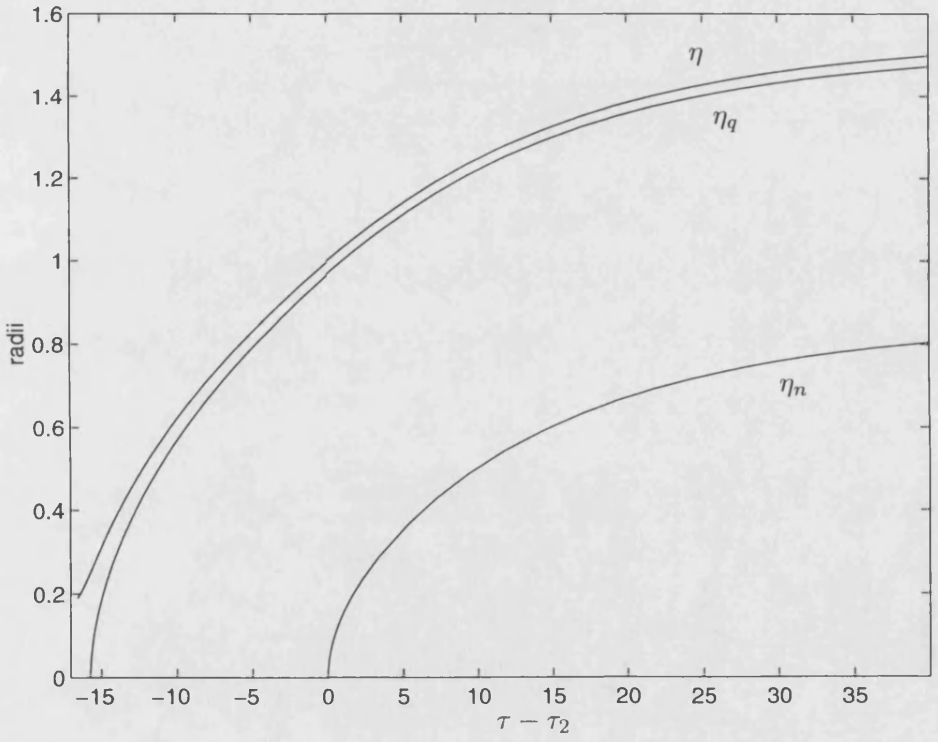

Figure 5-7: Graph to show the growth and development of the dimensionless radii of the tumour. $M = 1/4$, γ=0.1.

5.4. MODEL 2: GROWTH OF A SOLID TUMOUR WITH NUTRIENT DEPENDENT PROLIFERATION RATE.

nutrient concentration within it. For simplicity, let us consider linear dependence on nutrient concentration.

The assumptions are the same as in the last section, except for number (iii), which becomes:

(iii) The rate of cell proliferation per unit volume in the growth region is linearly dependent on the nutrient concentration. High nutrient concentration will lead to high proliferation rates and low concentration will lead to low rates.

Let us take $S(\sigma) = H(\sigma - \sigma_q)F(\sigma)$, where H is the Heaviside function and F is a (continuous) linear function of σ, with $F(\sigma_q) = 0$ and $F(\sigma_\infty) = s$.

i.e.

$$S(\sigma) = sH(\sigma - \sigma_q)\frac{\sigma - \sigma_q}{\sigma_\infty - \sigma_q}. \tag{5.12}$$

From equation (5.6), σ satisfies

$$\sigma(r) = \begin{cases} \sigma_n & \text{if } r \leq R_n \\ \sigma_\infty - \frac{a}{6k}(R_o^2 - r^2) + \frac{aR_n^3}{3k}(\frac{1}{r} - \frac{1}{R_o}) & \text{if } R_n < r \leq R_o. \end{cases}$$

In particular,

$$\sigma_\infty - \sigma_n = \frac{a}{6k}(R_o^2 - R_n^2) - \frac{aR_n^3}{3k}\left(\frac{1}{R_n} - \frac{1}{R_o}\right). \tag{5.13}$$

and

$$\sigma_\infty - \sigma_q = \frac{a}{6k}(R_o^2 - R_q^2) - \frac{aR_n^3}{3k}\left(\frac{1}{R_q} - \frac{1}{R_o}\right). \tag{5.14}$$

So, from (5.12),

$$S(\sigma) = \frac{sH(\sigma - \sigma_q)}{\sigma_\infty - \sigma_q}\left[\sigma_\infty - \sigma_q - \frac{a}{6k}(R_o^2 - r^2) + \frac{aR_n^3}{3k}\left(\frac{1}{r} - \frac{1}{R_o}\right)\right]$$

Putting this into the conservation of mass equation, (5.2), gives

$$R_o^2\frac{dR_o}{dt} = \frac{s}{3}(R_o^3 - R_q^3) + \frac{sa}{6k(\sigma_\infty - \sigma_q)}\left[\frac{R_o^5}{15} - \frac{R_o^2R_q^3}{3} + \frac{R_q^5}{5} - R_n^3\left(\frac{R_o^2}{3} - R_q^2 + \frac{2R_q^3}{3R_o}\right)\right] - \lambda R_n^3. \tag{5.15}$$

Define the dimensionless variables,

$$\alpha = R_o/R_c,\ \alpha_q = R_q/R_c,\ \alpha_n = R_n/R_c \text{ and } \tau = st,$$

where R_c is the value of the outer radius at which central necrosis first occurs, given by equation (5.8).

With the new variables, (5.11) becomes

$$\alpha^2\frac{d\alpha}{d\tau} = \frac{1}{3}(\alpha^3 - \alpha_q^3) - \frac{1}{M^2}\left[\frac{2\alpha^5}{15} - \frac{\alpha^2\alpha_q^3}{3} + \frac{\alpha_q^5}{5} - \alpha_n^3\left(\frac{\alpha^2}{3} - \alpha_q^2 + \frac{2\alpha_q^3}{3\alpha}\right)\right] - \gamma\alpha_n^3, \qquad (5.16)$$

where the dimensionless parameters $M^2 = \frac{\sigma_\infty - \sigma_q}{\sigma_\infty - \sigma_n}$ and $\gamma = \lambda/s$.

The constraint equations, (5.13) and (5.14) become

$$M^2 = \alpha^2 - \alpha_q^2 - 2\alpha_n^3\left(\frac{1}{\alpha_q} - \frac{1}{\alpha}\right), \ \alpha \geq M \text{ only;}$$

$$1 = \alpha^2 - \alpha_n^2 - 2\alpha_n^3\left(\frac{1}{\alpha_n} - \frac{1}{\alpha}\right), \ \alpha \geq 1 \text{ only;}$$

as before.

Phase I: A period of rapid growth of the tumour until the onset of quiescence or the death of a central cell.

- *Range of variables:*

$$\alpha(0) \leq \alpha(\tau) \leq M.$$

- *Constraints:*

$$\alpha_q \equiv 0, \ \alpha_n \equiv 0.$$

- *Growth equation:*

$$\frac{d\alpha}{d\tau} = \frac{\alpha}{3}\left(1 - \frac{2}{5M^2}\alpha^2\right).$$

- *Method:* Explicit integration.

- *Solution:*

$$\alpha(\tau) = e^{\tau/3}\left(\frac{1}{\alpha^2(0)} + \frac{2}{5M^2}(e^{2\tau/3} - 1)\right)^{-1/2}.$$

- *Time period:*

$$0 \leq \tau \leq \tau_1 = \frac{3}{2}\ln\left[\frac{5M^2}{3\alpha^2(0)} - \frac{2}{3}\right].$$

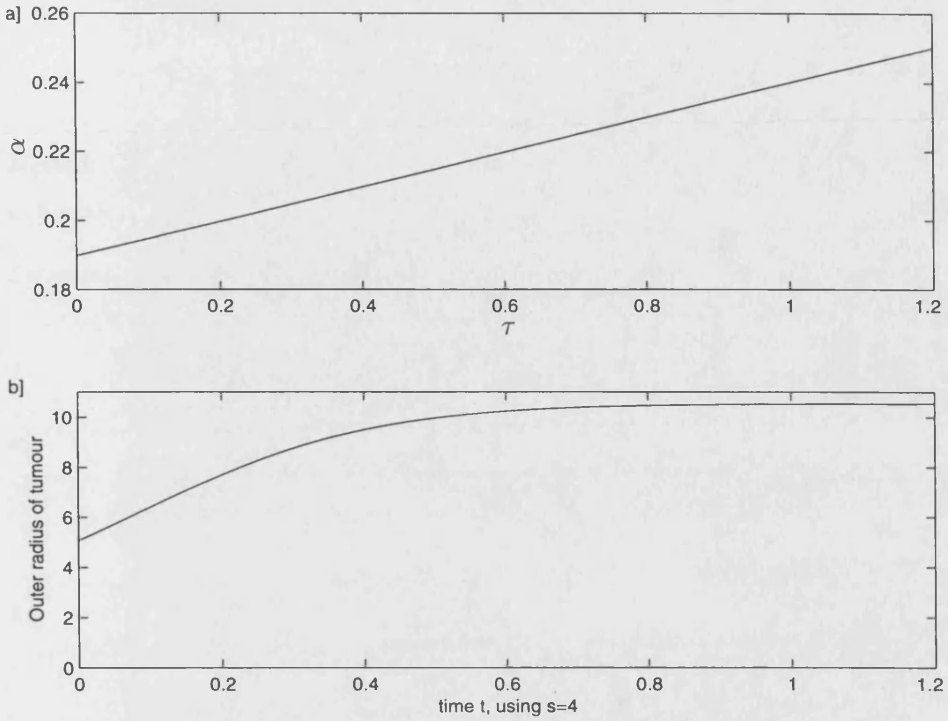

Figure 5-8: Model 2: Graphs showing the first stage of development of a) the dimensionless outer radius; b) the outer radius, with $M = 1/4$.

- *Discussion:* The rate of development of the tumour is shown in Figure (5-8), until growth retardation occurs at the centre of the nodule. If $M < 1$, then this retardation is due to cells becoming quiescent, but if $M \geq 1$, it occurs with the onset of central necrosis. τ_1 is positive only if $\left(\frac{5M^2}{3\alpha^2(0)} - \frac{2}{3}\right) > 1$, so this phase only occurs if $M^2 > 2\alpha^2(0)/5$. This constraint ensures that we choose a suitably small initial spheroid, with ample nutrient diffusing to all of its cells.

Phase II: A period of retarded growth, during which the tumour consists of an outer mantle of dividing cells and an inner viable quiescent core.

- *Range of variables:*

$$M \leq \alpha(\tau) \leq 1, \ 0 \leq y \leq (1 - M^2)^{1/2}.$$

- *Constraints:*

$$\alpha_n \equiv 0, \ M \leq 1, \ M^2 = \alpha^2 - \alpha_q^2.$$

- *Growth equation:*

$$\alpha^2 \frac{d\alpha}{dt} = \frac{1}{3}(\alpha^3 - \alpha_q^3) - \frac{1}{M^2}\left[\frac{2}{15}\alpha^5 - \frac{\alpha^2}{3}\alpha_q^3 + \frac{1}{5}\alpha_q^5\right]. \tag{5.17}$$

- *Method:* Change of variable to $y = \alpha_q/\alpha$ and numerically integrate to obtain all variables as functions of time.

- *Formulation:*

$$y = \frac{(\alpha^2 - M^2)^{1/2}}{\alpha},$$

so,

$$\frac{dy}{d\tau} = \frac{1}{\alpha_q}(1 - y^2)\frac{d\alpha}{d\tau}$$

i.e.

$$\frac{dy}{d\tau} = \frac{1}{3}(1/y - y^2)(1 - y^2) - \frac{1}{15}\left(\frac{2}{y} - 5y^2 + 3y^4\right).$$

- *Solution:* The numerical integration proceeds forwards in time until $\tau = \tau_2$, when $y = (1 - M^2)^{1/2}$.

- *Time period:* This phase ends at time τ_2, when $y = (1 - M^2)^{1/2}$.

- *Discussion:* Tumour growth in the second phase as described in (5.17), is shown in Figure (5-9). The effect of inhibition of mitosis is to change the initial rapid growth to one that is roughly linear in time. This phase begins at $\tau = \tau_1$ and $\alpha = M$ and ends when $\tau = \tau_2$, $\alpha = 1$, with the death of the first cell. Again, the thickness of the mitotic shell (proportional to $1 - y$), decreases very quickly and is relatively "thin" after a short time. $\tau_2 - \tau_1 \to 0$ as $M \to 1$. There is no quiescent shell if $M \geq 1$, as this means that the level of nutrient required for inhibition of mitosis is lower than that required for death. If $M \geq 1$, phase I is immediately followed by phase III and the steady state tumour will consist of a necrotic core surrounded by a dividing mantle.

Phase III: A period of growth retardation, due to death of cells and inhibition of mitosis (if $M < 1$) caused by nutrient deficiency. This phase starts when $\sigma = \sigma_n$ at the centre of the tumour and ends when the steady state is achieved. During this time, the tumour consists of a central necrotic core, consisting of disintegrating debris, surrounded by a shell of quiescent cells, assuming $M < 1$, which is in turn surrounded by a shell of dividing cells.

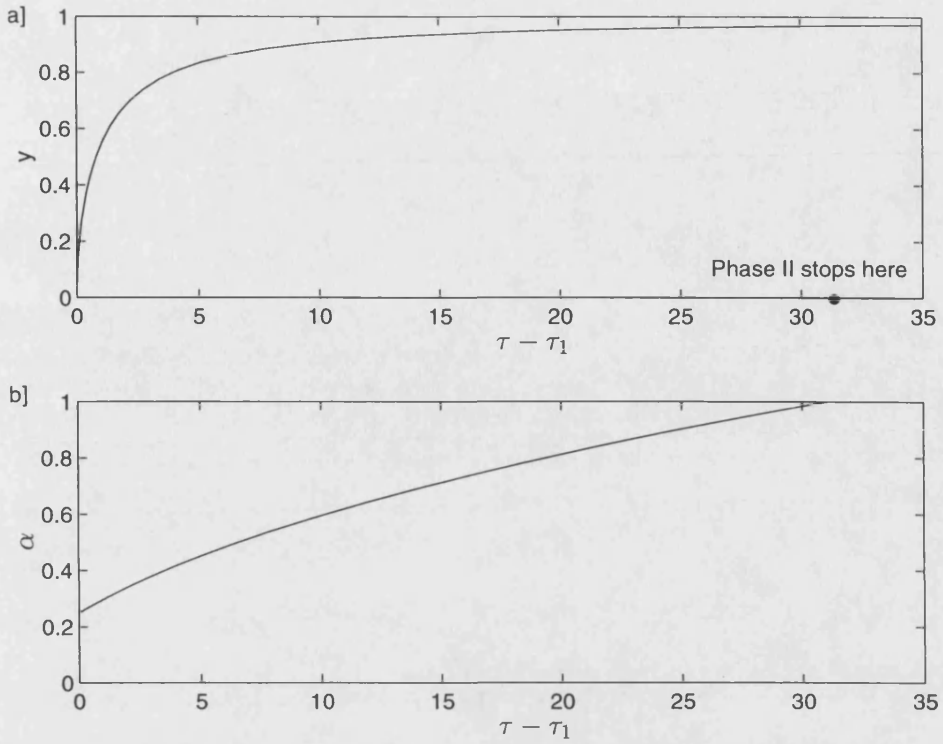

Figure 5-9: Model 2: Graphs showing the second stage of development of a) the ratio of quiescent radius to outer radius; b) the dimensionless outer radius, with $M = 1/4$.

- *Range of variables:*

$$1 \leq \alpha \leq \alpha_\infty,\ (1 - M^2)^{1/2} \leq y \leq y_\infty,\ 0 \leq x \leq x_\infty.$$

- *Constraints:*

$$\alpha \geq \alpha_q \geq \alpha_n \geq 0,\ M < 1,$$

$$M^2 = \alpha^2 - \alpha_q^2 - 2\alpha_n^3 \left(\frac{1}{\alpha_q} - \frac{1}{\alpha} \right),$$

$$1 = \alpha^2 - \alpha_n^2 - 2\alpha_n^3 \left(\frac{1}{\alpha_n} - \frac{1}{\alpha} \right).$$

- *Growth equation*

$$\alpha^2 \frac{d\alpha}{d\tau} = \frac{1}{3}(\alpha^3 - \alpha_q^3) - \frac{1}{M^2} \left[\frac{2\alpha^5}{15} - \frac{\alpha^2 \alpha_q^3}{3} + \frac{\alpha_q^5}{5} - \alpha_n^3 \left(\frac{\alpha^2}{3} - \alpha_q^2 + \frac{2\alpha_q^3}{3\alpha} \right) \right] - \gamma \alpha_n^3.$$

- *Method:* Change variables to $x = \alpha_n/\alpha$ and $y = \alpha_q/\alpha$ and numerically integrate to obtain all variables as functions of time.

- *Formulation:* From the third constraint,

$$3x(2x+1)^{-1/2}\frac{dx}{d\tau} = \frac{1}{\alpha^2}\frac{d\alpha}{d\tau}$$

so

$$3x(1-x)\frac{dx}{d\tau} = \begin{array}{l} \frac{1}{3}(1-x)^2(2x+1)(1-y^3-3\gamma x^3) \\ -\frac{1}{M^2}\left[\frac{2}{15} - \frac{y^3}{3} + \frac{y^5}{5} - x^3\left(\frac{1}{3} - y^2 + \frac{2y^3}{3}\right)\right]. \end{array} \tag{5.18}$$

with

$$M^2(1-x)^2(2x+1) = 1 - y^2 + 2x^3(1-1/y). \tag{5.19}$$

- *Solution:* The numerical integration proceeds forwards in time until the solution curves asymptote to their steady state values x_∞, y_∞, which are solutions of (5.18) and (5.19) with $dx/d\tau = 0$. The growth curves are shown in Figure (5-10).

- *Time period:* It takes an infinite time for the solution to reach the steady state but phase III is mostly completed when $\tau = O(1/\gamma)$.

- *Discussion:* Tumour growth in the final phase, as described in (5.18), is illustrated in Figure (5-10) for a couple of values of $\gamma = \lambda/s$. Again, as in the first model, the value of γ specifies the development of the tumour. If $M \geq 1$, this phase begins when phase I ends. The necrotic radius, R_n, expands quickly towards its asymptote, while the growth rate of the outer and quiescent radii decrease. These effects are shown in Figure (5-11) and Figure (5-12) which are complete histories of model tumour growth at realistic parameter settings. Figure (5-13) shows the complete histories of the growth of the three dimensionless radii. The rate of volume loss per unit volume in the necrotic core (λ) controls the rapidity at which the radii approach their asymptotes, *i.e.* the rate at which the at which the tumour reaches its steady state. Most of the growth is completed in a (dimensional) time of order $1/\lambda$.

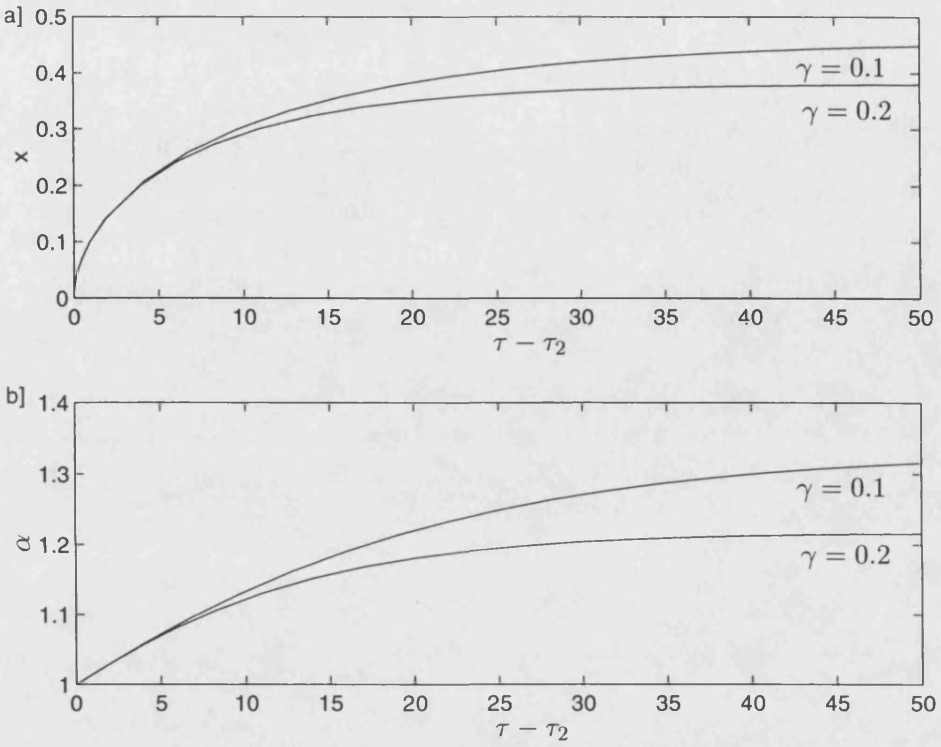

Figure 5-10: Model 2:Graphs showing the last stage of development of a) the ratio of necrotic radius to outer radius; b) the dimensionless outer radius, with $M = 1/4$.

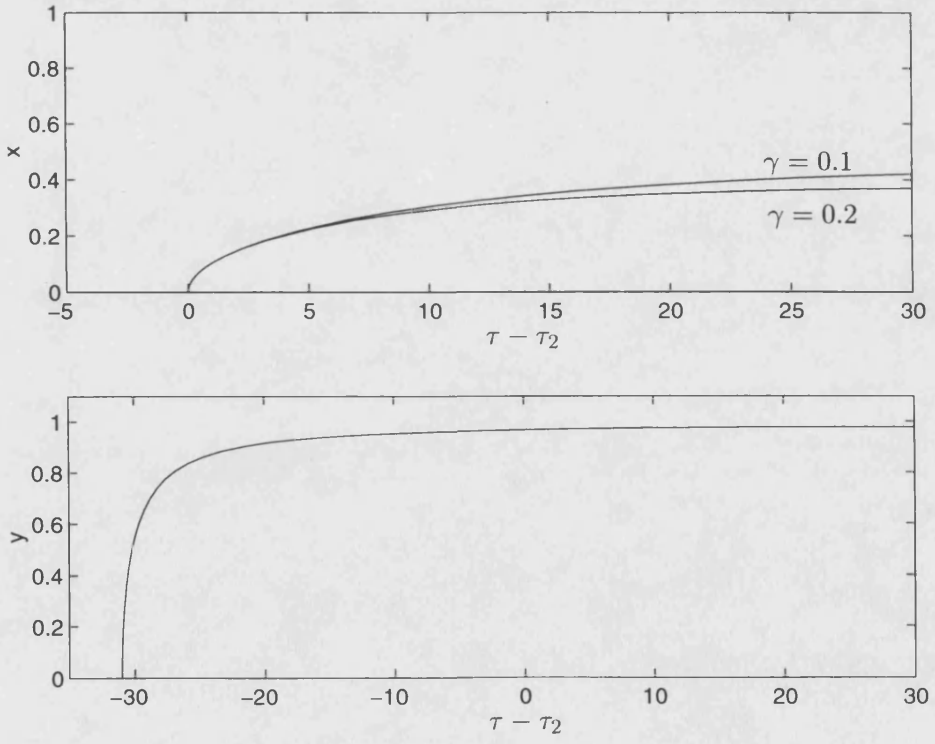

Figure 5-11: Model 2: Graphs showing the development of x and y with time, $M = 1/4$.

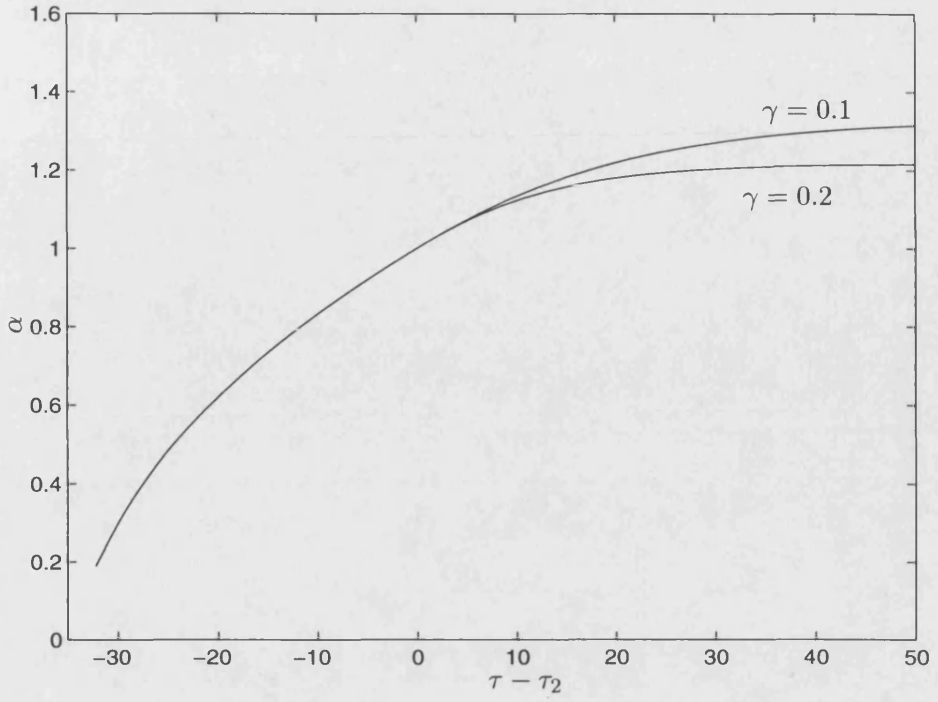

Figure 5-12: Model 2: Graph showing the development of α, the dimensionless outer radius with time, $M = 1/4$.

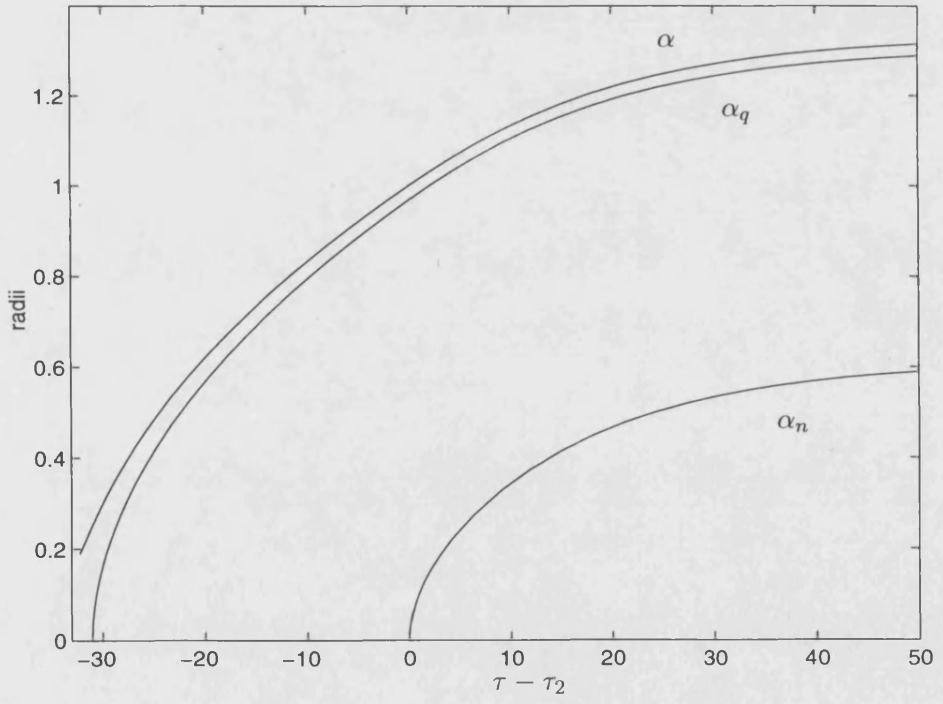

Figure 5-13: Model 2: Graph showing the growth of the dimensionless radii with time, $M = 1/4$, $\gamma = 0.1$.

5.5 Model 3: Growth of a solid tumour with nutrient dependent proliferation rate and non-constant degradation.

In our third model, the rate of cell proliferation per unit volume in the growth region is again taken to be linearly proportional to nutrient concentration, as in section 5.4, but we now assume that degradation of cells (*i.e.* volume loss) in the necrotic core is dependent on the radial distance.

Because of the surface tension in the tumour, there is a pressure which causes cells to flow from the dividing rim into the quiescent shell and eventually into the necrotic core. So, once a cell has died and entered the necrotic core, it will be pushed even closer to the centre by other cells that are dying and flowing in from the quiescent shell. Hence, it can be reasonably assumed that cells nearer the periphery of the necrotic core have died more recently than those near the centre. So, the material at the centre will be made up of compounds which break down into chemicals that permeate out of the core, whereas, near the edge, the cells haven't been dead long enough to start disintegrating. In the shell between these two regions, cells will be degrading gradually into the compounds which break down near the centre.

Moore [162] showed that the rate of cell death increases with distance from the nutrient source. Thus we propose that the volume loss in the necrotic core should be a decreasing function of radial distance.

So, Greenspan's assumption d) in section 5.2 should be replaced by:

d) The necrotic core "loses" cell volume at a rate, which is a decreasing function of radial distance.

Thus,

$$E = \text{Total volume lost from necrotic core in time } t \geq 0 = \int_0^t dt \int_0^{R_n(t)} D(r) r^2 dr.$$

If we choose

$$D(r) = \frac{\chi(R_n - r)}{(r + R_n)},$$

which has the value χ at the centre ($r = 0$) and 0 at the edge of the core ($r = R_n$), then the term E in equation (5.1), is given by

$$E = \frac{4\pi}{3} \int_0^t 3\chi(2\ln 2 - \frac{4}{3}) R_n^3(t) dt.$$

In other words, the volume loss due to disintegration is again proportional to the size of

the necrotic core. So, instead, let us consider

$$D(r) = \frac{\chi(R_n - r)}{R_n(r+1)},$$

which again has the value χ at the origin and zero at the periphery of the core.

Substituting this in the conservation of mass law (5.1) and differentiating with respect to t, this gives

$$R_o^2 \frac{dR_o}{dt} = \int_{R_q}^{R_o} S(\sigma) r^2 dr - \int_0^{R_n} D(r) r^2 dr,$$

where

$$\sigma = \sigma_\infty - \frac{A}{6k}(R_o^2 - r^2) + \frac{AR_n^3}{3k}(\frac{1}{r} - \frac{1}{R_o}) \quad \text{and} \quad S(\sigma) = sH(\sigma - \sigma_q)\frac{\sigma - \sigma_q}{\sigma_\infty - \sigma_q}.$$

Hence,

$$\begin{aligned} R_o^2 \frac{dR_o}{dt} &= \frac{s}{3}(R_o^3 - R_q^3) - \frac{s}{3R_1^2}\left[\frac{2R_o^5}{5} - R_o^2 R_q^3 + \frac{3R_q^5}{5} - R_n^3\left(R_o^2 - 3R_q^2 + \frac{2R_q^3}{R_o}\right)\right] \\ &\quad -\chi\left[\frac{R_n^2}{6} - \frac{R_n}{2} - 1 + \left(1 + \frac{1}{R_n}\right)\ln(R_n + 1)\right]. \end{aligned}$$

Let $u = R_o$, $v = R_q$ and $w = R_n$, for convenience of notation. Then we have

$$\begin{aligned} u^2 \frac{du}{dt} &= \frac{s}{3}(u^3 - v^3) - \frac{s}{3R_1^2}\left[\frac{2u^5}{5} - u^2 v^3 + \frac{3v^5}{5} - w^3\left(u^2 - 3v^2 + \frac{2v^3}{u}\right)\right] \\ &\quad -\chi\left[\frac{w^2}{6} - \frac{w}{2} - 1 + \left(1 + \frac{1}{w}\right)\ln(w + 1)\right] \end{aligned}$$

with the constraints, from the nutrient equation,

$$R_1^2 = u^2 - v^2 - 2w^3\left(\frac{1}{v} - \frac{1}{u}\right) \quad \text{and} \quad R_c^2 = u^2 - 3w^2 + \frac{2w^3}{u}.$$

Phase I: A period of rapid growth of the tumour until the onset of quiescence or the death of a central cell.

- *Range of variables:*

$$u(0) \leq u(t) \leq R_1.$$

- *Constraints:*

$$v \equiv 0, \; w \equiv 0.$$

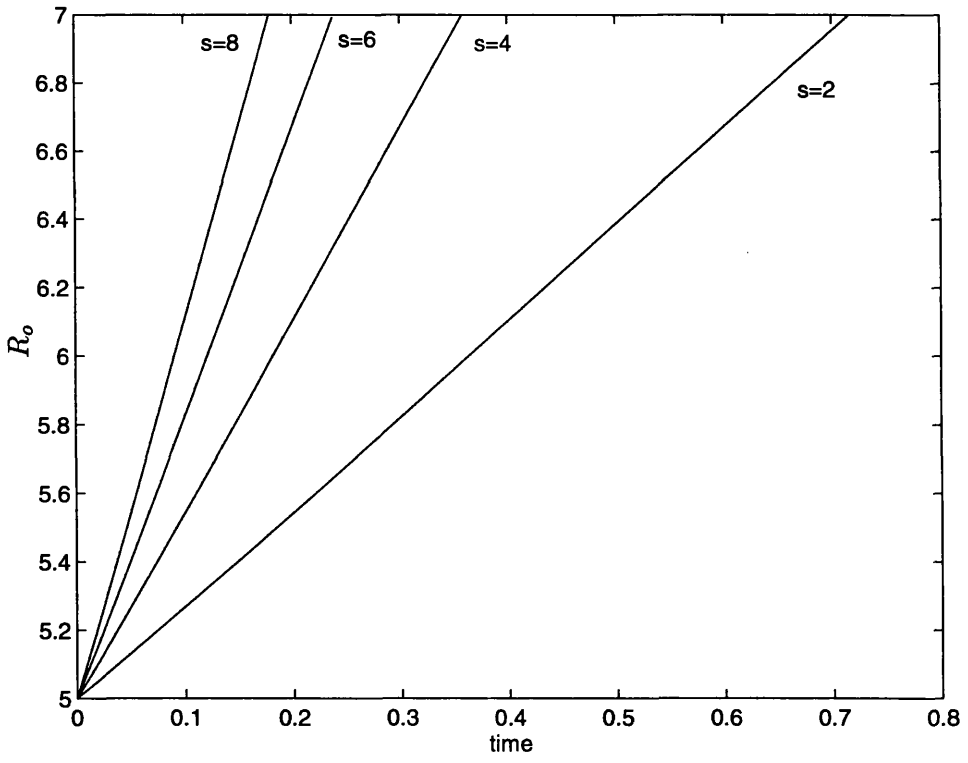

Figure 5-14: Model 3: Graphs showing the first stage of development of the outer radius, with $s = 1, 2, 4, 5$ and $u(0) = 5$, as in simulations.

- *Growth equation:*

$$\frac{du}{dt} = \frac{s}{3}u\left(1 - \frac{2}{5R_1^2}u^2\right).$$

- *Method:* Explicit integration.

- *Solution:*

$$u(t) = \left(\frac{2}{5R_1^2} + \left(\frac{1}{u^2(0)} - \frac{2}{5R_1^2}\right)e^{-2st/3}\right)^{-1/2}; \quad v(t) \equiv 0; \quad w(t) \equiv 0.$$

- *Time period:*

$$0 \leq t \leq t_1 = \frac{3}{2s}\ln\left(\frac{5R_1^2}{3u^2(0)} - \frac{2}{3}\right).$$

- *Discussion:* This first phase is characterised by the rapid growth of the tumour, as shown in Figure (5-14) for several values of the parameter s, which specifies the growth. As long as the level of nutrient at which a cell dies is lower than that at which mitosis ceases, this phase ends when the first cell at the centre of the nodule becomes quiescent.

Phase II: Period of retarded growth, during which the tumour consists of an outer mantle of dividing cells and an inner viable quiescent core.

- *Range of variables:*

$$R_1 \leq u(t) \leq R_c, \quad 0 \leq v(t) \leq (R_c^2 - R_1^2)^{1/2}.$$

- *Constraints:*

$$R_1^2 = u^2 - v^2; \quad w(t) \equiv 0.$$

- *Growth equation:*

$$\frac{du}{dt} = \frac{s}{3}\left(u - \frac{v^3}{u^2}\right) - \frac{s}{3R_1^2}\left[\frac{2u^3}{5} - v^3 + \frac{3v^5}{5u^2}\right].$$

- *Method:* Numerically integrate to obtain all variables as functions of time.
- *Solution:* The numerical integration proceeds forwards in time until $\tau = \tau_2$, when $u = R_c$.
- *Discussion:* The development of the tumour in the second phase is shown in Figure (5-15). Again growth is specified by the parameter s. Because of the inhibition of mitosis, due to nutrient deficiency, the growth of the tumour slows down to be roughly linear. This phase begins when $u = R_1$ and ends when $u = R_c$ with the death of the first cell. As in the two previous models, the thickness of the dividing shell - $u(t) - v(t)$, decreases rapidly and is thin relative to $u(t)$ within a few time steps. $t - t_1 \to 0$ as $\sigma_n \to \sigma_q$. If the nutrient level at which cells die is greater than that at which they cease proliferation, then no quiescent shell forms and phase I is immediately followed by phase III.

PhaseIII : A period of retarded growth due to inhibition of mitosis and the death of cells which begins when $\sigma = \sigma_n$ at the centre of the the tumour and lasts until the steady state is achieved.

- *Range of variables:*

$$R_c \leq u(t); \quad (R_c^2 - R_1^2)^{1/2} \leq v(t); \quad 0 \leq w(t).$$

- *Constraints:*

$$R_1^2 = u^2 - v^2 - 2w^3\left(\frac{1}{v} - \frac{1}{u}\right) \quad \text{and} \quad R_c^2 = u^2 - 3w^2 + \frac{2w^3}{u}. \tag{5.20}$$

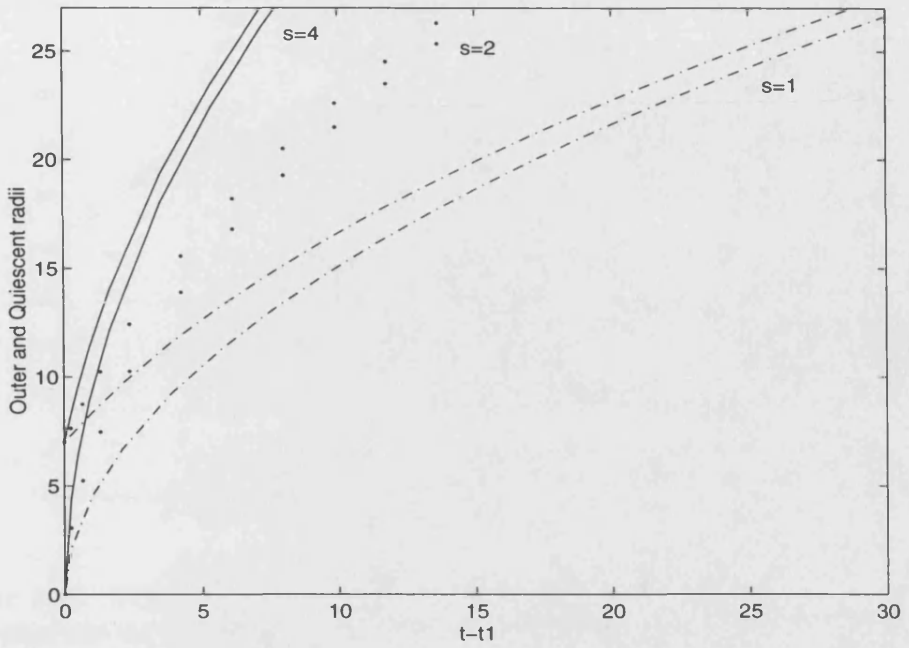

Figure 5-15: Model 3: Graphs showing the second stage of development of the outer radius and quiescent radius, with $s = 1$ (dash-dotted line), $s = 2$ (dotted line) and $s = 4$ (solid line).

- *Growth equation:*

$$u^2\frac{du}{dt} = \frac{s}{3}(u^3 - v^3) - \frac{s}{3R_1^2}\left[\frac{2u^5}{5} - u^2v^3 + \frac{3v^5}{5} + w^3\left(u^2 - 3v^2 + \frac{2v^3}{u}\right)\right] - \chi\left[\frac{w^2}{6} - \frac{w}{2} - 1 + \left(1 + \frac{1}{w}\right)\ln(w+1)\right] \quad (5.21)$$

- *Method:* Numerically integrate to obtain all variables as functions of time.
- *Solution:*The numerical integration proceeds forwards in time until the solution curves asymptote to their steady state values u_∞, v_∞, w_∞, which are solutions of (5.20) and (5.21) with $du/dt = 0$.
- *Discussion:* The growth rate of the tumour in phase III is specified by the value of χ and the corresponding growth curves are shown in Figure (5-16) for two values of χ. When χ is increased, the rate at which volume is lost in the necrotic core due to disintegration is also increased. This leads to a smaller necrotic core, and hence a smaller overall size of the steady state tumour. The decrease in the rate of growth is also faster and the rapidity of the approach to the asymptote curves is greater. In dimensional units, $t = O(1/\chi)$ characterises the main period of activity in the last phase of growth. Figure (5-17) and Figure (5-18) are complete histories of model tumour growth for different values of the parameters s and χ.

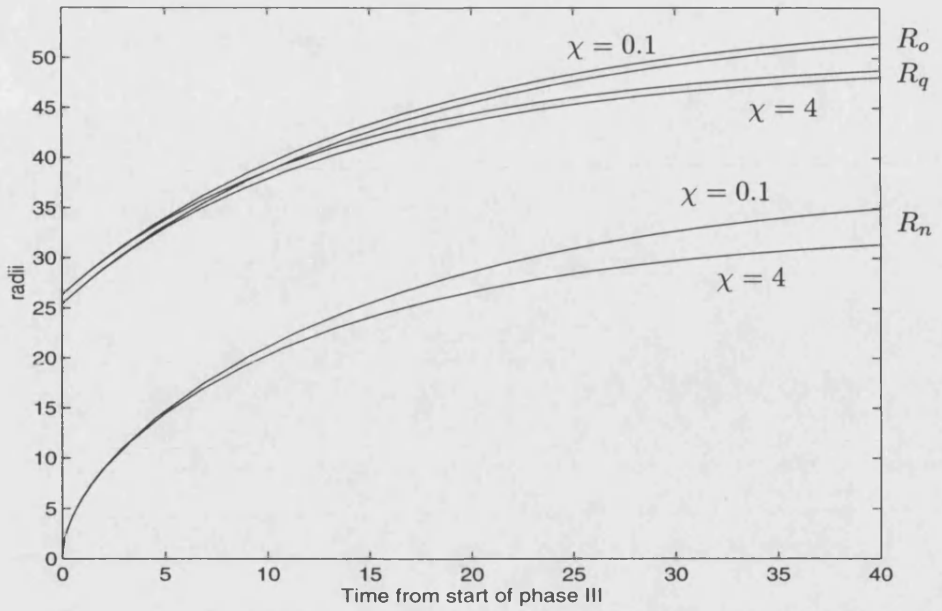

Figure 5-16: Model 3: Graphs showing the final stage of development of the outer, quiescent and necrotic radii, with $s = 4$ and for two values of χ.

Figure (5-19) and Figure (5-20) show the development of the three radii for the three models looked at so far, with Figure (5-20) just showing the first two phases of growth and only part of the third phase. The parameters chosen were $M = 1/4$ for all three models, $\gamma = 0.1$ for the first and $\gamma = 0.2$ for the second. For model three, $\chi = 2.18$. This value of χ was calculated so that the average value of $D(r)$ on $[0, R_n] = 3\lambda$. The growth of the tumour in Phases I and II is the same for both models 2 and 3, as changing the rate of degradation of cells in the necrotic core will not affect anything until a necrotic core forms.

The parameter M is the ratio of size the outer radius at which quiescence first occurs to the size of the outer radius when necrosis first occurs. As can be seen from Figure (5-20), adding nutrient dependent proliferation to the growth assumptions, results in a less steep rate of growth of the initial tumour for a fixed value of M. Hence tumour grows more slowly, which leads to the time period of Phase I in models 2 and 3 being slightly longer than that of model 1. Growth in Phase II of models 2 and 3 is also slower than that in model 1. This again leads to the time period of Phase II being a lot longer for these models than model 1.

5.6 Model 4: Growth of a solid tumour with non-constant nutrient consumption.

Now, let us consider the growth of an MCS with non-constant nutrient consumption by living cells.

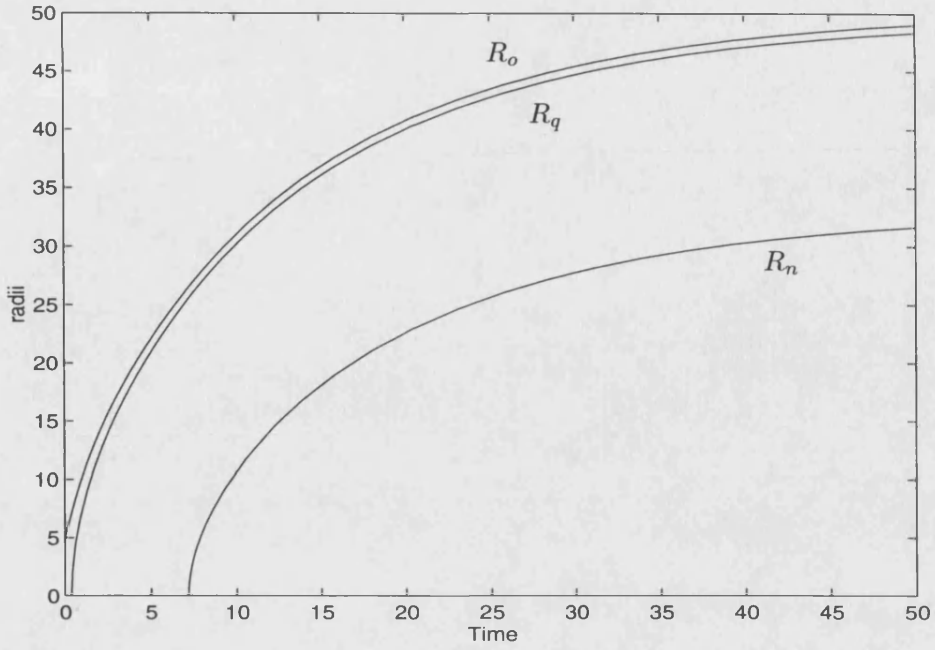

Figure 5-17: Model 3: Graph showing the total growth history of the three radii of the tumour with $s = 4$ and $\chi = 4$.

In the three previous models, we assumed that the nutrient was consumed at a constant rate, a, by all living cells. It has been shown that oxygen and glucose consumption, per unit volume of spheroid, decreases as the MCS grows [31, 34, 82]. Freyer *et al.* [84] have shown that the consumption of oxygen per unit volume of an MCS is four times less at the equilibrium size than the consumption of a tiny initial spheroid. Thus it is reasonable to assume from this that quiescent cells consume less nutrients than proliferating cells. Assumption (ii) of Section (5.3) now becomes:

(ii) The nutrient is consumed at a constant rate, Q, by quiescent cells and a constant rate, $P > Q$, by proliferating cells.

The assumption of diffusive equilibrium of nutrient implies that the equation for the concentration, σ is:

$$\frac{1}{r^2}\frac{d}{dr}\left(r^2\frac{d\sigma}{dr}(r)\right) = \frac{P}{k}H(r - R_q(t))H(R_o(t) - r) + \frac{Q}{k}H(r - R_n(t))H(R_q(t) - r)$$

[k = diffusivity of the nutrient (same for all living cells)]. The requirements for this equation are that σ and $\frac{d\sigma}{dr}$ are continuous across every interface, $\sigma = \sigma_\infty$ at $r = R_o(t)$ and that σ is bounded at the origin.

The general solution to this equation is:

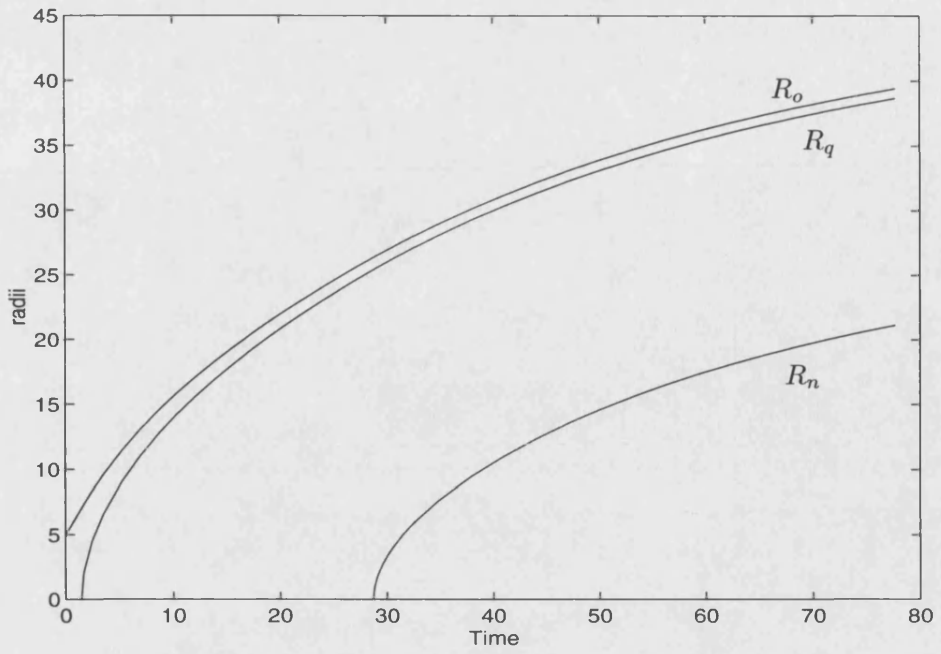

Figure 5-18: Model 3: Graph showing the total growth history of the three radii of the tumour with $s = 1$ and $\chi = 2$.

$$\sigma(r) = \begin{cases} -\frac{a}{r} + b & \text{if } r \leq R_n \\ \frac{Q}{6k}r^2 - \frac{c}{r} + d & \text{if } R_n < r \leq R_q \\ \frac{P}{6k}r^2 - \frac{e}{r} + f & \text{if } R_q < r \leq R_o, \end{cases}$$

where a, b, c, d, e and f are arbitrary constants.

Using the facts that $\frac{d\sigma}{dr}$ is continuous across $r = R_n(t)$ and $r = R_q(t)$, σ is bounded at $r = 0$, $\sigma(R_n(t)) = \sigma_n$, $\sigma(R_q(t)) = \sigma_q$ and $\sigma(R_o(t)) = \sigma_\infty$ gives

$$\sigma(r) = \begin{cases} \sigma_n & \text{if } r \leq R_n \\ \sigma_q - \frac{Q}{6k}(R_q^2 - r^2) + \frac{QR_n^3}{3k}\left(\frac{1}{r} - \frac{1}{R_q}\right) & \text{if } R_n < r \leq R_q \\ \sigma_\infty - \frac{P}{6k}(R_o^2 - r^2) + \left(\frac{1}{r} - \frac{1}{R_o}\right)\left(\frac{R_q^3}{3k}(P - Q) + \frac{QR_n^3}{3k}\right) & \text{if } R_q < r \leq R_o \end{cases} \tag{5.22}$$

Continuity of σ at $r = R_n$ gives the relationship:

$$\sigma_q - \sigma_n = \frac{Q}{6k}\left(R_q^2 - 3R_n^2 + 2\frac{R_n^3}{R_q}\right). \tag{5.23}$$

5.6. MODEL 4: GROWTH OF A SOLID TUMOUR WITH NON-CONSTANT NUTRIENT CONSUMPTION.

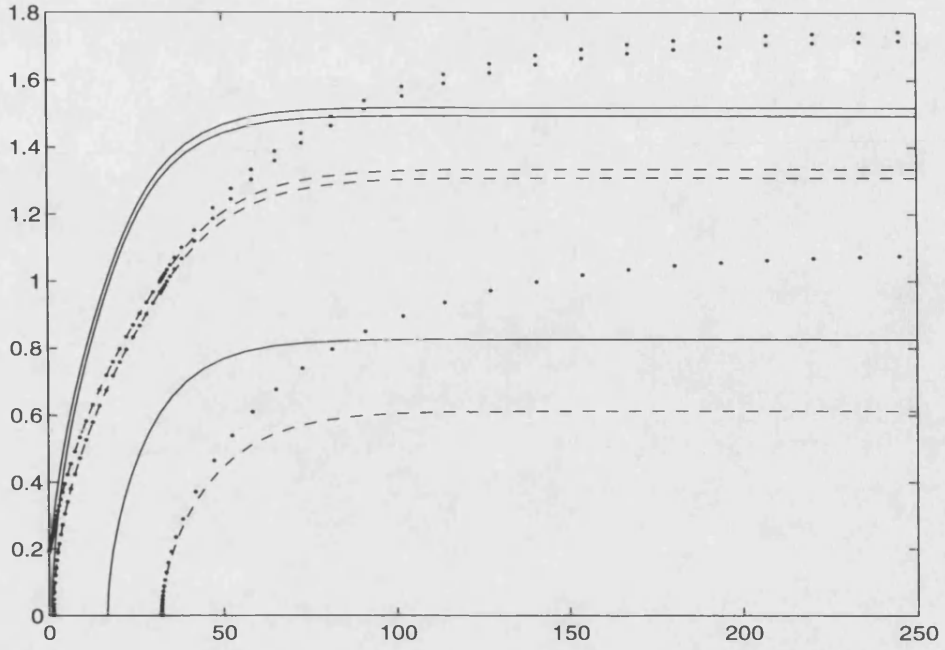

Figure 5-19: Graph showing the development of the three dimensionless radii for models 1 to 3. Model 1 is shown by a solid line, Model 2 by a dashed line and model 3 by a dotted line. The parameters chosen were $M = 1/4$, $\gamma = 0.1$ for model 1, $\gamma = 0.2$ for model 2 and for model 3, $\chi/s = 2.18$.

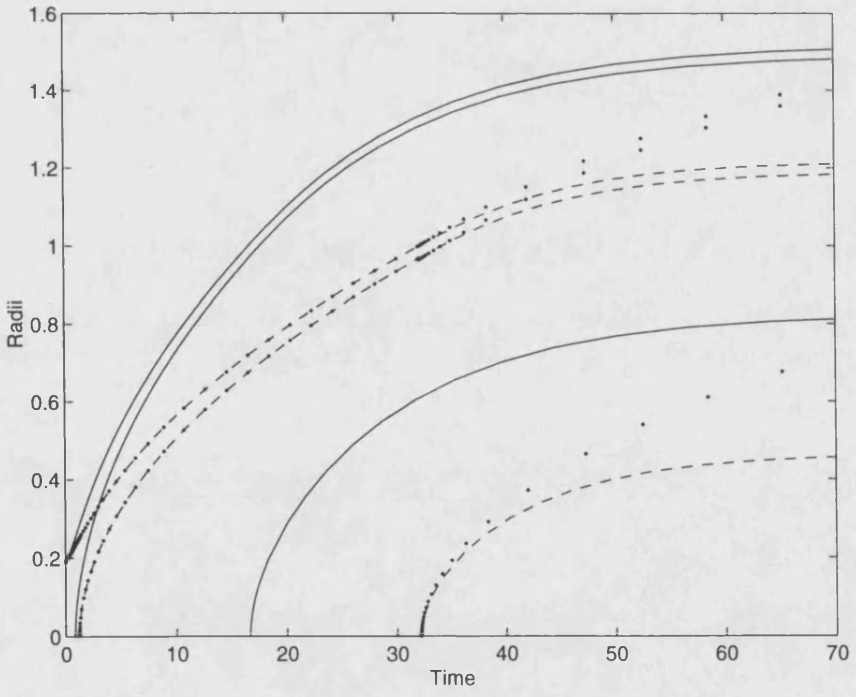

Figure 5-20: Graph showing the first two stages of development of the three dimensionless radii for models 1 to 3. Parameters are the same as in Figure (5-19).

5.6. MODEL 4: GROWTH OF A SOLID TUMOUR WITH NON-CONSTANT NUTRIENT CONSUMPTION.

Continuity of σ at $r = R_q$ gives the relationship:

$$\sigma_\infty - \sigma_q = \frac{P}{6k}(R_o^2 - R_q^2) - \frac{[R_q^3(P-Q) + QR_n^3]}{3k}\left(\frac{1}{R_q} - \frac{1}{R_o}\right) \tag{5.24}$$

The value of the outer radius at which quiescence first occurs is

$$R_{qc} = \left[\frac{6k}{P}(\sigma_\infty - \sigma_q)\right]^{1/2}$$

and the value of the quiescent radius at which necrosis first occurs is

$$R_{nq} = \left[\frac{6k}{Q}(\sigma_q - \sigma_n)\right]^{1/2}.$$

This means that the value of the outer radius at which necrosis first occurs is

$$R_c = \frac{R1^{1/3}}{3P} + R2,$$

where

$$\begin{aligned} R1 = \; & -27P^2(P-Q)R_{nq}^3 + \\ & 9P\left[PQ^2(\frac{8}{3}Q - 3P)R_{nq}^6 + SP(12PQ - 9P^2 - 4Q^2)R_{nq}^4 + PS^2(2Q-3P)R_{nq}^2 + \frac{PS^3}{3}\right]^{1/2} \end{aligned}$$

and

$$R2 = \frac{(3P-2Q)R_{nq}^2 + S}{R1^{1/3}}, \quad S = 6k(\sigma_\infty - \sigma_q).$$

From (5.4)

$$R_o^2\frac{dR_o}{dt} = \frac{s}{3}[R_o^3 - R_q^3] - \lambda R_n^3.$$

Define the dimensionless variables:

$$\phi = R_o/R_c, \quad \phi_q = R_q/R_c, \quad \phi_n = R_n/R_c \text{ and } \tau = st.$$

With these new variables (5.6) becomes:

$$\phi^2\frac{d\phi}{d\tau} = \frac{1}{3}[\phi^3 - \phi_q^3] - \frac{\lambda}{s}\phi_n^3.$$

Now, $Q = qP$ for some real number $q < 1$. In experiments on the growth and related oxygen consumption of V-79 MCS, Freyer *et al.* [84] discovered that equilibrium or plateau phase cells had a fivefold lower rate of oxygen consumption than exponential phase cells. Thus it

5.6. MODEL 4: GROWTH OF A SOLID TUMOUR WITH NON-CONSTANT NUTRIENT CONSUMPTION.

is reasonable to assume that proliferating cells consume five times as much nutrient as quiescent cells. So, from now on, let us take $q = 1/5$. Then the dimensionless versions of (5.23) and (5.24) are :

$$\frac{R_{nq}^2}{R_c^2} = \phi^2 - 3\phi_n^2 + \frac{2\phi_n^3}{\phi_q}$$

and

$$\frac{R_{qc}^2}{R_c^2} = \phi^2 - \frac{13}{5}\phi_q^2 + \frac{8\phi_q^3}{5\phi} - \frac{2}{5}\phi_n^3\left(\frac{1}{\phi_q} - \frac{1}{\phi}\right).$$

Let the dimensionless parameters $M = R_{qc}/R_c$, $N = R_{nq}/R_c$ and $\gamma = \lambda/s$. Then

$$\phi^2\frac{d\phi}{d\tau} = \frac{1}{3}[\phi^3 - \phi_q^3] - \gamma\phi_n^3;$$

$$N^2 = \phi_q^2 - 3\phi_n^2 + \frac{2\phi_n^3}{\phi_q};$$

and

$$5M^2 = 5\phi_q^2 - 13\phi_q^2 + \frac{8\phi_q^3}{\phi} - 2\phi_n^3\left(\frac{1}{\phi_q} - \frac{1}{\phi}\right).$$

Phase I: A period of exponential growth of the tumour until the onset of quiescence or death.

- *Range of variables:*

$$\phi(0) \leq \phi(\tau) \leq M.$$

- *Constraints:*

$$\phi_q \equiv 0 \equiv \phi_n.$$

- *Growth equation:*

$$\frac{d\phi}{d\tau} = \frac{1}{3}\phi.$$

- *Method:* Explicit integration.

- *Solution:*

$$\phi(\tau) = \phi(0)e^{\tau/3}$$

- *Time periodj:*

$$0 \leq \tau \leq \tau_1 = 3\ln\left(\frac{M}{\phi(0)}\right).$$

- *Discussion:* The tumour grows exponentially, until growth retardation occurs at the centre of the MCS. If $M < 1$, then this retardation is due to the onset of quiescence, but if $M \geq 1$, it is due to cells dying.

Phase II: A period of retarded growth in which the tumour consists of an inner core of quiescent cells surrounded by a shell of dividing cells.

- *Range of variables:*

$$M \leq \phi(\tau) \leq 1.$$

- *Constraints:*

$$\phi_n \equiv 0, \quad M \leq 1, \quad 5M^2 = 5\phi^2 - 13\phi_q^2 + \frac{8\phi_q^3}{\phi}.$$

- *Growth equation:*

$$\phi^2 \frac{d\phi}{d\tau} = \frac{1}{3}(\phi^3 - \phi_q^3).$$

- *Method:* Change of variable to $y = \phi_q/\phi$ and numerically integrate to obtain all variables as functions of time.

- *Formulation:*

$$\frac{M^2}{\phi^2} = 1 - \frac{13}{5}y^2 + \frac{8}{5}y^3.$$

So,

$$\frac{M^2}{\phi^3}\frac{d\phi}{d\tau} = \frac{y}{5}[13 - 12y]\frac{dy}{d\tau}.$$

i.e.

$$\frac{y}{5}(13 - 12y)\frac{dy}{d\tau} = \frac{1}{3}(1 - y^3)[1 - \frac{13}{5}y^2 + \frac{8}{5}y^3]$$

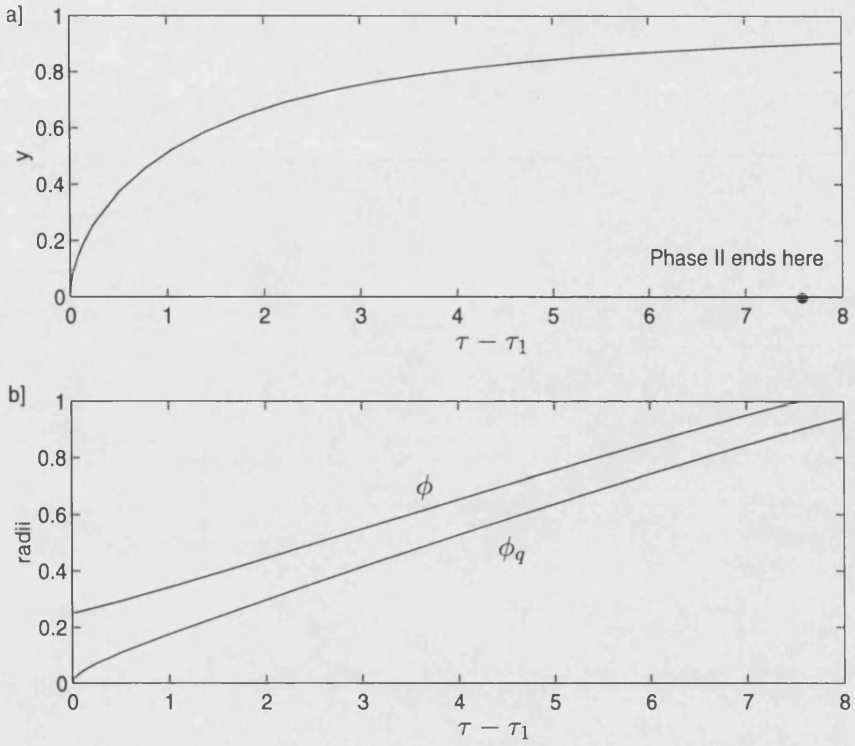

Figure 5-21: Model 4: Graphs showing the second stage of development of a) the ratio of the quiescent radius to the outer radius; and b) the dimensionless outer radius, with $M = 1/4$.

- *Solution:* The numerical integration proceeds forwards in time until $\tau = \tau_2$, when $\phi = 1$ (y is the solution of $M^2 = 1 - \frac{13}{5}y^2 + \frac{8}{5}y^3$).
- *Discussion:* Figure (5-21) shows the development of the tumour in Phase II. Inhibition of proliferation has the effect of changing the initial rapid growth to roughly linear growth. If $M < 1$, this phase begins at $\tau = \tau_1$, $\phi = M$ and ends when $\phi = 1$ and $\tau = \tau_2$.

Phase III: A second period of retarded growth due to the death of cells and, if $M < 1$, the inhibition of mitosis. The phase begins when $\sigma = \sigma_n$ at the centre of the MCS and lasts indefinitely.

- *Range of variables:*

$$1 \leq \phi \leq \phi_\infty, \quad 0 \leq x \leq x_\infty.$$

- *Constraints:*

$$\frac{N^2}{\phi^2} = y^2 - 3x^2 + \frac{2x^3}{y},$$

$$\frac{5M^2}{\phi^2} = 5 - 13y^2 + 8y^3 - 2x^3\left(\frac{1}{y} - 1\right).$$

- *Growth equation:*

$$\phi^2\frac{d\phi}{d\tau} = \frac{1}{3}(\phi^3 - \phi_q^3) - \gamma\phi_n^3.$$

- *Method:* Change of variables to $x = \phi_n/\phi$ and $y = \phi_q/\phi$ and numerically integrate to obtain all variables as functions of time.

- *Formulation:*

$$\frac{N^2}{\phi^3}\frac{d\phi}{d\tau} = 3x\left(1 - \frac{x}{y}\right)\frac{dx}{d\tau} - y\left(1 - \frac{x^3}{y^3}\right)\frac{dy}{d\tau}$$

i.e.

$$N^2y\left[13y - 12y^2 - 12x + 11xy + \frac{x^3}{y^2}(x-1)\right]\frac{dy}{d\tau} =$$

$$\frac{1}{3}(1 - y^3 - 3\gamma x^3)\left(y^2 - 3x^2 + \frac{2x^3}{y}\right)[5M^2(y-x) - N^2x(1-y)]. \qquad (5.25)$$

and

$$N^2\left(5 - 13y^2 + 8y^3 - 2x^3\left(\frac{1}{y} - 1\right)\right) = 5M^2\left(y^2 - 3x^2 + \frac{2x^3}{y}\right) \qquad (5.26)$$

- *Solution* The numerical integration proceeds forwards in time until the solution curves asymptote to their steady states, which are solutions of (5.25)(5.26) with $dy/d\tau = 0$.

- *Discussion* The parameter γ specifies the growth in the last phase of tumour development. If $\gamma = \lambda/s$ is small then this means that either the rate of volume loss from the necrotic core, λ is small, or s, the rate of cell proliferation per unit volume in the growth region is large. In the first instance, the necrotic core will develop quickly and asymptote towards a relatively large equilibrium size, while P, Q and s(or γ) will decide the size of the proliferating and quiescent shells. In the second, the proliferating rim will be relatively large at equilibrium, while P, Q and λ will decide the size of the necrotic core and quiescent shell. Both of these cases lead to the tumour having a relatively large overall size at its equilibrium. Alternatively, if γ is large, this means that either there is a lot of necrotic disintegration in the core or not much proliferation in the growing rim. This will lead to a smaller tumour at equilibrium.

  The development of x and y during phase III is shown in Figure (5-22).

5.6. MODEL 4: GROWTH OF A SOLID TUMOUR WITH NON-CONSTANT NUTRIENT CONSUMPTION.

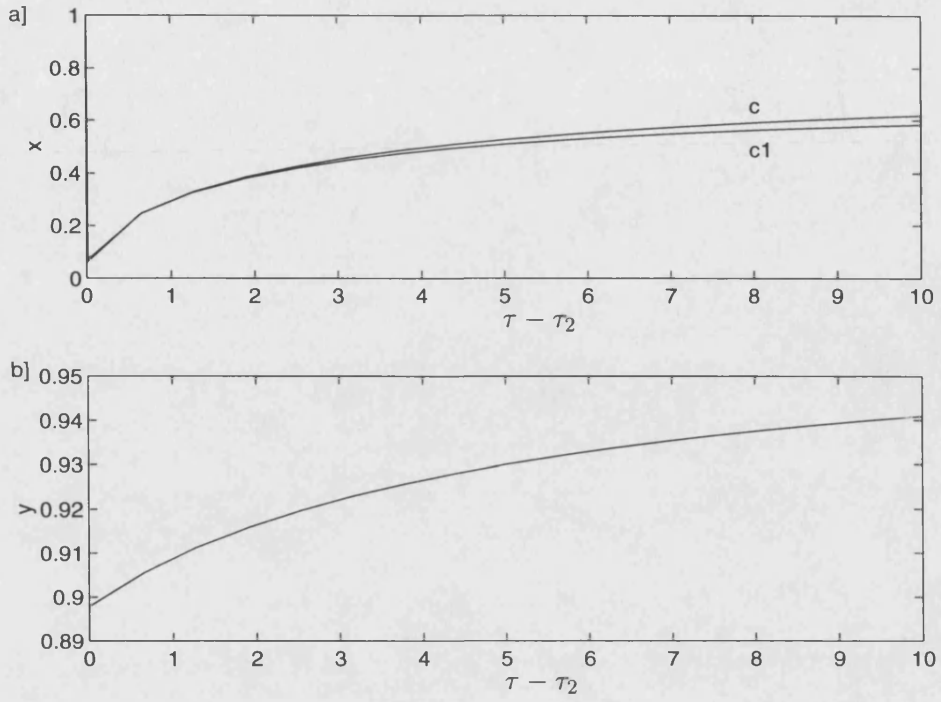

Figure 5-22: Model 4: Graphs showing the last stage of development of a) the ratio of the quiescent radius to the outer radius; and b) the ratio of the necrotic radius to the outer radius; M=1/4.

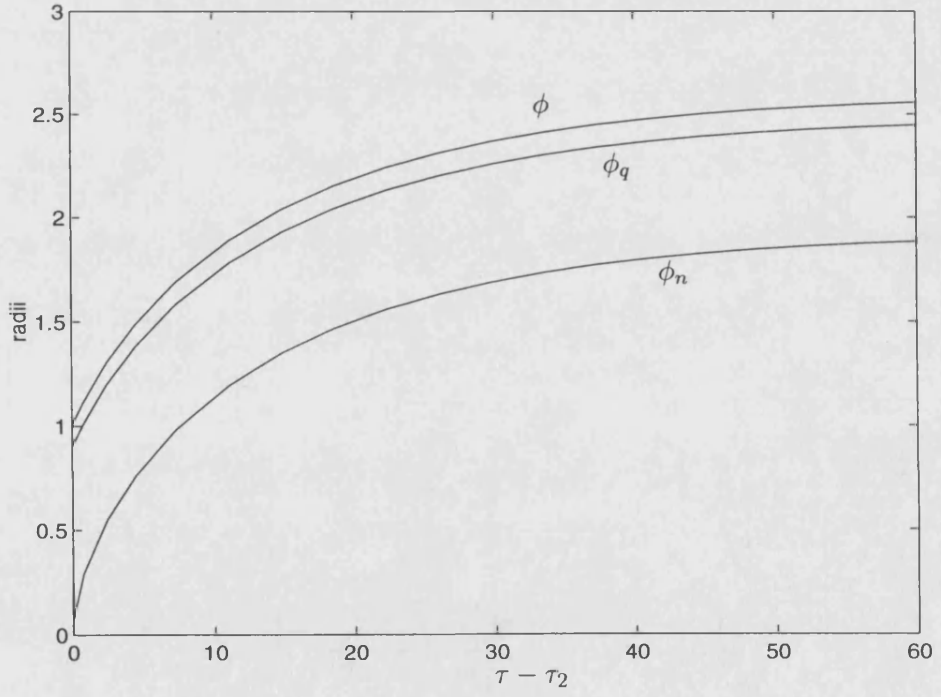

Figure 5-23: Model 4: Graph showing the last stage of development of the radii, M=1/4, $\gamma = 0.1$.

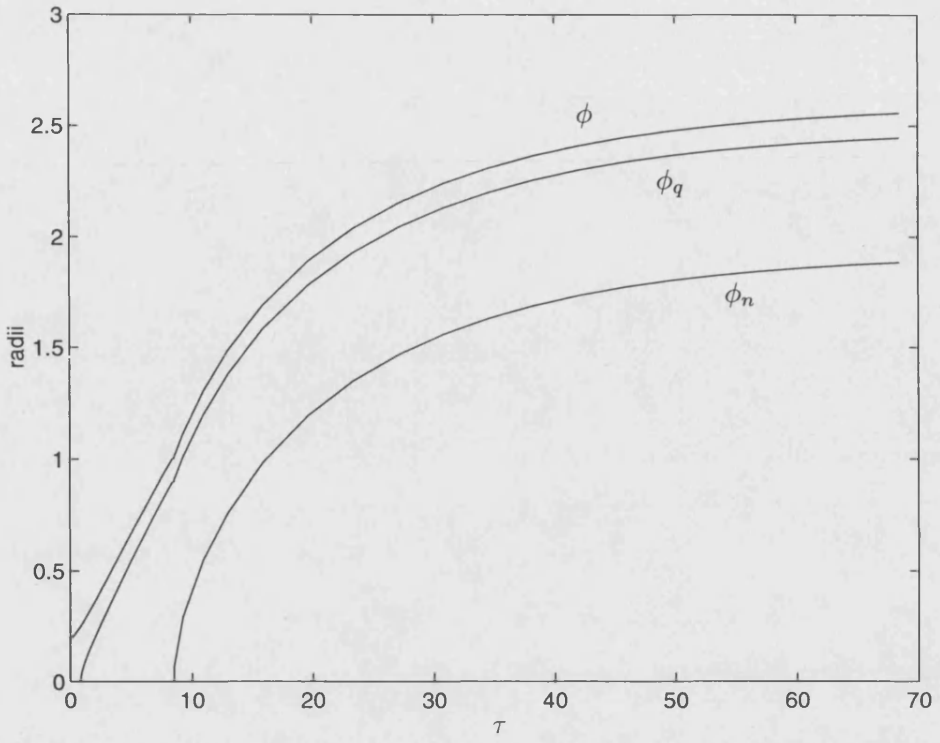

Figure 5-24: Model 4: Graph showing the development of the necrotic, quiescent and outer radii, M=1/4, $\gamma = 0.1$.

5.7 Conclusion

In this chapter, we have reviewed Greenspan's simple model of solid tumour growth and extended it gradually, by replacing the original terms by ones which are more biologically realistic. The aim of this was to find out if these changes, which made the model mathematically intractable, did enhance the resulting growth curves or if they were features which could justifiably be ignored. In Greenspan's model, cells became quiescent if the concentration of a mitotic inhibitor was high enough. There is no experimental evidence to prove the existence of mitotic inhibitors, and so in all of our models presented in this chapter, we ignore this feature and replace it with nutrient deficiency being the cause of quiescence.

Figure (5.7) and Figure (5-26) show the comparison between the growth curves of the tumour's outer radius from:

a) Greenspan's original model;

b) The simulation in Chapter 3;

c) Folkman and Hochberg's experimental results for V-79 MCS.

d) Model 1, in which cell proliferation was constant throughout the outer rim;

e) Model 2, in which cell proliferation was linearly dependent on nutrient concentration within the tumour;

f) Model 3, for which we added non-constant necrotic core degradation to model 2 and

g) Model 4 for which we added non-constant nutrient consumption to model 3.

As can be seen, the simulation growth curve is the best fit to the experimental curve, with Model 4 being the next best. Making note of the different lengths of time that the model's graphs are plotted for, it appears that each time the model is made more complex or realistic, the growth curve becomes a better fit to the experimental one.

Thus, we conclude, adding more realistic terms does lead to the resulting growth curves being better fits to the experimental growth curves of V-79 MCS. A very simple model that can be mathematically analysed can be very useful in estimating parameters and highlighting the salient features for similar models, but often, as in this case, the results gained do not match experimental data very well at all.

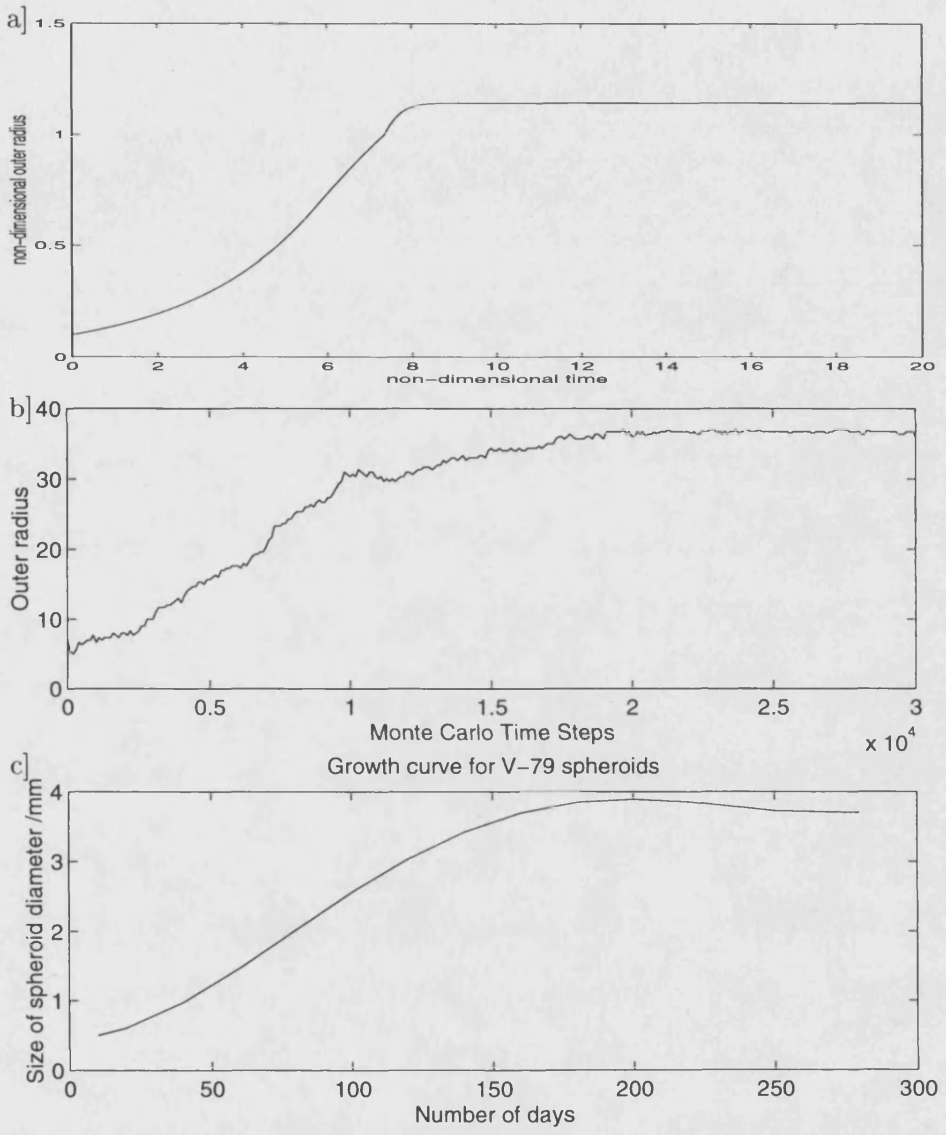

Figure 5-25: Graphs showing the development of the outer radii of Greenspan's model (parameters $Q^2 = 0.4,\ \gamma = 0.2$), Chapter 3's simulation and Folkman and Hochberg's experimental results for V-79 spheroids.

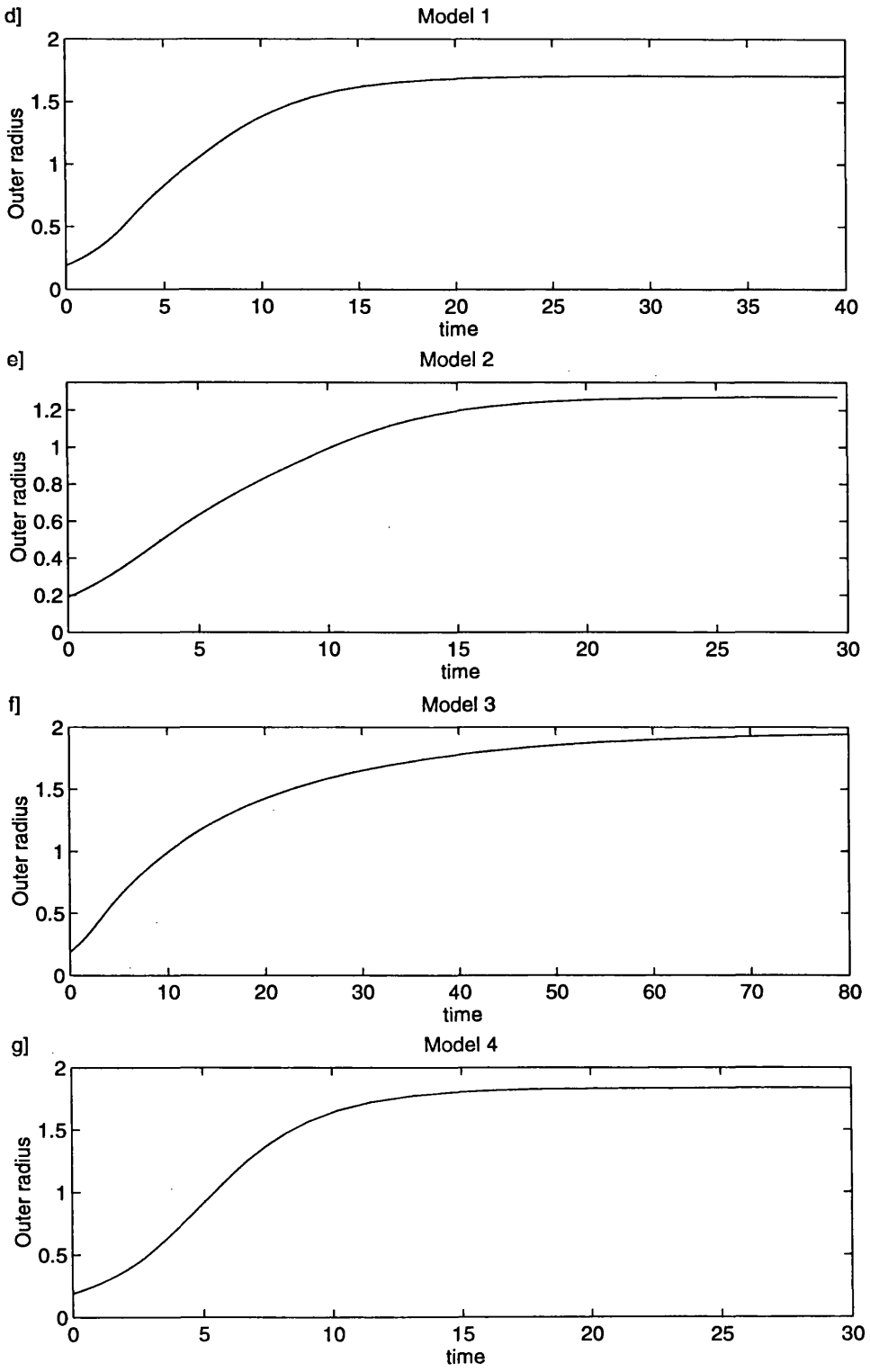

Figure 5-26: Graphs showing the development of the outer radii for all four models with M=1/2, $\gamma = 0.5$ and $\chi/s = 3.08$.

Chapter 6

Acid Mediation Hypothesis of Tumour Invasion

6.1 Introduction.

Clinical tests have shown that tumours *in situ* use approximately ten times as much glucose as normal cells [112, 120, 233]. Even in the presence of high O_2 concentration, tumour cells tend to break glucose down into lactic acid via the path of aerobic glycolysis, instead of into CO_2 and H_2O [225]. This is very inefficient and produces 19 times less energy. Studies [112, 120, 233] have shown that malignant tumours take up more glucose than benign tumours and that among malignant tumours, increased uptake of glucose strongly correlates with poorer patient prognosis.

The production of lactic acid and the poor organisation of vasculature in tumour tissues, which results in the acid being inadequately removed, leads to the reduction of extracellular pH within the tumour. Tumour interstitial pH is typically 0.5 units lower than in normal tissue [12, 90, 105, 113, 126, 165]. Even in the absence of glycolysis, tumour interstitial pH may be lower than normal pH, presumably due to CO_2 production [146]. Normal cells have an optimal extracellular pH (pH_e) of 7.4 with a sharp decline in viability below pH_e of 7.1, whereas tumour cells typically proliferate optimally at a pH_e of 6.8 [33, 48, 87, 189, 200, 208]. Despite the difference in extracellular pH, intracellular pH in tumours is roughly the same as normal intracellular pH [165].

Martin and Jain [146] have shown that there is a pH gradient extending from a tumour edge into surrounding normal tissue with the pH at the interface being significantly less than 7.1. Chronic exposure to low pH destroys the gap junctions between normal cells, and hence limits the ability of individual cells to cooperatively maintain viability. The death of normal cells at the tumour's edge leaves an interstitial gap for the tumour to grow into.

Gatenby and Gawlinski [86] hypothesise that transformation-induced reversion of tumour tissue to primitive glycolytic metabolic pathways, with resultant increased acid production and the diffusion of that acid into surrounding healthy tissue, creates a peritumoural microenvironment in which tumour cells survive and proliferate, whereas normal cells are unable to remain viable. They propose that the following temporal sequence would ensue:

a) high H^+ ion concentrations in tumours will extend, by chemical diffusion, as a gradient into adjacent normal tissue, exposing these normal cells to tumour-like interstitial pH;

b) normal cells immediately adjacent to the tumour edge are unable to survive in this chronically acid environment; and

c) the progressive loss of layers of normal cells at the tumour-host interface facilitates tumour invasion.

They then present a mathematical model of the tumour-host interface based on this acid mediation hypothesis of tumour invasion.

The behaviour of the normal tissue is determined by a) the logistic growth of the cells and b) the interaction of the cells with excess H^+ ions leading to a death rate proportional to excess acid concentration. The cancerous tissue growth is determined by a) the logistic growth of the cells and b) cellular diffusion with a coefficient dependent on normal cell density. It is assumed that excess acid is produced at a rate proportional to cancer cell density and diffuses chemically. They include an uptake term to take account of the mechanisms for increasing local pH.

The non-dimensional equations governing their system are:

$$\begin{aligned} \frac{\partial \eta_1}{\partial \tau} &= \eta_1(1-\eta_1) - \delta_1 \Lambda \eta_1 \\ \frac{\partial \eta_2}{\partial \tau} &= \rho_2 \eta_2(1-\eta_2) + \Delta_2 \frac{\partial}{\partial \xi}\left[(1-\eta_1)\frac{\partial \eta_2}{\partial \xi}\right] \\ \frac{\partial \Lambda}{\partial \tau} &= \delta_3(\eta_2 - \Lambda) + \frac{\partial^2 \Lambda}{\partial \xi^2} \end{aligned} \tag{6.1}$$

where η_1 is non-dimensional normal cell density, η_2 is non-dimensional cancer cell density, Λ is non-dimensional acid concentration, τ time and ξ space.

The fixed points of this system are:

FP 1 :	$\eta_1^* = 0,$	$\eta_2^* = 0,$	$\Lambda^* = 0;$
FP 2 :	$\eta_1^* = 1,$	$\eta_2^* = 0,$	$\Lambda^* = 0;$
FP 3 :	$\eta_1^* = 1 - \delta_1,$	$\eta_2^* = 1,$	$\Lambda^* = 1;$
FP 4 :	$\eta_1^* = 0,$	$\eta_2^* = 1,$	$\Lambda^* = 1.$

A linear stability analysis shows that FP1 and FP2 are unconditionally unstable. FP4 is stable and FP3 is unstable when $\delta_1 > 1$ and *vice versa* when $\delta_1 < 1$.

They claim that this crossover at $\delta_1 = 1$ can be identified with the transformation of non-invasive tumours ($\delta_1 < 1$) into invasive malignant tumours ($\delta_1 > 1$). However, this is incorrect, as if FP2 is replaced by FP3 via a travelling wave, then this is still invasion, just not so aggressive as that when $\delta_1 > 1$. It would not make sense to have a model, which is primarily set up as one of tumour invasion, exhibiting non-invasiveness.

For highly invasive tumours, the mathematical model predicts a previously unrecognised hypocellular interstitial gap in some malignancies, which is supported by clinical observations and *in vitro* experiments [39]. A strong correlation between the interfacial structure and the tumour growth velocity is also predicted. This growth velocity can be correlated to the speed of a travelling wave, if it exists, from FP2 to FP4 ($\delta_1 > 1$) or that of one from FP2 to FP3 ($\delta_1 < 1$). Gatenby and Gawlinski show that these waves exist numerically, but do not address the problem of analytical existence.

6.2 Travelling wave analysis.

The purpose of this section is to prove analytically the existence of travelling waves in a slight simplification of Gatenby and Gawlinski's model.

The non-dimensional equations of their model are:

$$\begin{aligned}
\frac{\partial \eta_1}{\partial \tau} &= \eta_1(1-\eta_1) - \delta_1 \Lambda \eta_1; \\
\frac{\partial \eta_2}{\partial \tau} &= \rho_2 \eta_2 (1-\eta_2) + \Delta_2 \frac{\partial}{\partial \xi}\left[(1-\eta_1)\frac{\partial \eta_2}{\partial \xi}\right] \\
\frac{\partial \Lambda}{\partial \tau} &= \delta_3(\eta_2 - \Lambda) + \frac{\partial^2 \Lambda}{\partial \xi^2}.
\end{aligned}$$

As mentioned above, this system has four spatially uniform steady states in (η_1, η_2, Λ) space: $(0,0,0)$, $(1,0,0)$, $(1-\delta_1,1,1)$ and $(0,1,1)$. $(0,0,0)$ and $(1,0,0)$ are unconditionally unstable and $(1-\delta_1,1,1)$ is stable and $(0,1,1)$ unstable when $\delta_1 < 1$ and *vice-versa* when $\delta_1 > 1$.

Our aim in this section is to prove the existence of travelling waves of this system from a) $(1,0,0)$ to $(1-\delta_1,1,1)$ if $\delta_1 < 1$; and b) $(1,0,0)$ to $(0,1,1)$ if $\delta_1 > 1$.

Firstly, we will show that any solution of this system must be bounded using the comparison theorem [23, 64, 223]. Then we prove that when the term involving diffusion of cancer cells is discarded, waves exist for all wave speeds, $c > 0$. These results are then applied to the full system to show that waves also exist for all c.

6.2.1 Boundedness of solutions.

We claim that

1) If $\eta_2(\xi,0) \in [0,1]\ \forall\xi$, then $\eta_2(\xi,\tau) \in [0,1]\ \forall\tau \geq 0,\ \xi$.

2) If $\Lambda(\xi,0) \in [0,1]\ \forall\xi$, then $\Lambda(\xi,\tau) \in [0,1]\ \forall\tau \geq 0,\ \xi$.

3) If $\delta_1 > 1$ and $0 \leq \eta_1(\xi,0) \leq 1\ \ \forall\xi$ then $0 \leq \eta_1(\xi,\tau) \leq 1\ \forall\tau \geq 0,\ \xi$. If $\delta_1 < 1$ and $1-\delta_1 \leq \eta_1(\xi,0) \leq 1\ \ \forall\xi$ then $1-\delta_1 \leq \eta_1(\xi,\tau) \leq 1\ \forall\tau \geq 0,\ \xi$.

The following theorem is a simplification of Theorem 5.1, page 125 [64], so as to be easily applied to system (6.1) (See also Theorem 5.5, p.244 [223] and Theorem 5.10, p.75 [23]):

Theorem 6.1: Comparison Theorem for a System of Equations.

a) Let E_i, $i = 1,\ldots,n$, be uniformly elliptic linear second order partial differential operators in m spatial dimensions,

$$E_i\theta = \sum_{j,k=1}^{m} a_{jki}(x,t)\frac{\partial^2\theta}{\partial x_j \partial x_k} + \sum_{j=1}^{m} b_{ji}(x,t)\frac{\partial\theta}{\partial x_j},$$

with uniformly bounded coefficients, defined in a closed space-time domain $\overline{Q}$, where $Q = \Omega \times (0,T)$ for some $T > 0$, and for some unbounded domain $\Omega \in \mathbb{R}^m$.

b) Let $F(x,t,\phi)$, defined for $(x,t) \in \overline{Q}$, $\phi \in \mathbb{R}^n$, be Lipschitz continuous in ϕ, uniformly for $(x,t) \in \overline{Q}$. Let F be quasi-monotone non-decreasing, *i.e.* $\dfrac{\partial F_i}{\partial \phi_j} \geq 0,\ i \neq j$.

c) Let ϕ and $\underline{\phi}$ be continuous functions from $\overline{Q}$ into $\mathbb{R}^n$, C^2 in Q, bounded, and satisfying (for each $i = 1,\ldots,n$)

$$\frac{\partial\phi_i}{\partial t} - E_i\phi_i \geq F_i(x,t,\phi), \qquad \frac{\partial\underline{\phi_i}}{\partial t} - E_i\underline{\phi_i} \leq F_i(x,t,\underline{\phi}),$$
$$\phi \geq \underline{\phi} \text{ for } t = 0, \qquad \phi,\ \underline{\phi} \text{ bounded as } x \to \pm\infty.$$

Then $\phi \geq \underline{\phi}$ in $\overline{Q}$.

Corollary 6.2 (p.244 [223]): If $F(x,t,u_0) \equiv 0$ and $u(x,0) \geq u_0$ $(u(x,0) \leq u_0)$ then $u(x,t) \geq u_0$ $(u(x,t) \leq u_0)$.

An *invariant set* $\Sigma \subset \mathbb{R}^m$ is a set such that if $\mathbf{u}$ is a solution of

$$\mathbf{u}_t = \mathbf{f}(u) + D\nabla^2\mathbf{u} \text{ in } \Omega \times (0,T] \text{ with } \mathbf{u} \text{ bounded as } x \to \pm\infty$$
$$\text{and } \mathbf{u}(x,0) \in \Sigma \text{ for each point } (x,0) \in \Omega \times \{0\} \tag{6.2}$$

then $\mathbf{u}(x,t) \in \Sigma$ for each point $(x,t) \in \Omega \times [0,T]$.

Theorem 6.3 (Theorem 5.17 [23]): Let $\mathbf{f}$ be Lipschitz continuous and let $-\infty < \mathbf{a} < \mathbf{b} < \infty$ be two constant vectors in $\mathbb{R}^m$ such that

$$f_i(\mathbf{v}) \geq 0 \quad \text{for} \quad v_i = a_i, \quad \mathbf{a} \leq \mathbf{v} \leq \mathbf{b},$$
$$f_i(\mathbf{v}) \leq 0 \quad \text{for} \quad v_i = b_i, \quad \mathbf{a} \leq \mathbf{v} \leq \mathbf{b}.$$

Then $\Sigma = \{\mathbf{v} \mid \mathbf{a} \leq \mathbf{v} \leq \mathbf{b}\} \subset \mathbb{R}^m$ is an invariant set for the problem (6.2).

Put $z_1 = \eta_1$, $z_2 = -\eta_2$, $z_3 = -\Lambda$; then we have

$$\begin{aligned}
\frac{\partial z_1}{\partial \tau} &= z_1(1-z_1) + \delta_1 z_1 z_3 = f_1(z_1,z_2,z_3) \\
\frac{\partial z_2}{\partial \tau} &= p_2 z_2(1+z_2) + \Delta_2 \frac{\partial}{\partial \xi}\left[(1-z_1)\frac{\partial z_2}{\partial \xi}\right] = f_2(z_1,z_2,z_3) + \Delta_2 \frac{\partial}{\partial \xi}\left[(1-z_1)\frac{\partial z_2}{\partial \xi}\right] \\
\frac{\partial z_3}{\partial \tau} &= \delta_3(z_2 - z_3) + \frac{\partial^2 z_3}{\partial \xi^2} = f_3(z_1,z_2,z_3) + \frac{\partial^2 z_3}{\partial \xi^2}
\end{aligned} \tag{6.3}$$

Then

$$\frac{\partial f_1}{\partial z_2} = 0, \quad \frac{\partial f_1}{\partial z_3} = \delta_1 z_1, \quad \frac{\partial f_2}{\partial z_1} = 0, \quad \frac{\partial f_2}{\partial z_3} = 0, \quad \frac{\partial f_3}{\partial z_1} = 0, \quad \frac{\partial f_3}{\partial z_2} = \delta_3 > 0.$$

In order to be able to use Theorem 6.1, we need this to be a quasi-monotone non-decreasing system, *i.e.* we require that $z_1 \geq 0$. But this is what we are trying to prove and so we need to use Theorem 6.3 first.

Let $\mathbf{a} = (0,-1,-1)$ and $\mathbf{b} = (1,0,0)$. Then

$$f_1(z_1,z_2,z_3) = z_1(1 - z_1 + \delta_1 z_3) \quad f_1(a_1,z_2,z_3) = 0 \quad f_1(b_1,z_2,z_3) = \delta_1 z_3 \geq 0 \text{ for } \mathbf{a} \leq \mathbf{z} \leq \mathbf{b}$$

$$f_2(z_1,z_2,z_3) = z_2(1-z_2) \quad f_2(a_2,z_2,z_3) = 0 \quad f_2(b_2,z_2,z_3) = 0$$

$$f_3(z_1,z_2,z_3) = \delta_3(z_2 - z_3) \quad f_3(a_1,z_2,z_3) = \delta_3(z_2+1) \quad f_3(b_1,z_2,z_3) = \delta_3 z_2 \leq 0 \text{ for } \mathbf{a} \leq \mathbf{z} \leq \mathbf{b}$$

So, by Theorem 6.3, $\Sigma = \{\mathbf{v} \mid \mathbf{a} \leq \mathbf{v} \leq \mathbf{b}\}$ is an invariant set for our problem and hence if $z_1(x,0) \geq 0$ then $z_1(x,t) \geq 0$ for all t. Thus (6.3) is a quasi-monotone non-decreasing system and we can apply Theorem 6.1 to it.

Since, for $\delta_1 < 1$, $\mathbf{z}_1^* = (1-\delta_1, -1, -1)$ and $\mathbf{z}_2^* = (1,0,0)$ are solutions of the problem, $\mathbf{z}_1^*$ may be considered as a sub-solution and $\mathbf{z}_2^*$ a super-solution. So if $\mathbf{z}_1^* \leq \mathbf{z}(\xi,0) \leq \mathbf{z}_2^*$ then $\mathbf{z}_1^* \leq \mathbf{z}(\xi,\tau) \leq \mathbf{z}_2^* \ \ \forall \tau \geq 0$. In other words $1-\delta_1 \leq z_1 = \eta_1 \leq 1$, $0 \leq -z_2 = \eta_2 \leq 1$ and $0 \leq -z_3 = \Lambda \leq 1$.

Similarly for $\delta_1 > 1$, $\mathbf{z}_3^* = (0,-1,-1)$ is a sub-solution and $\mathbf{z}_2^*$ is a super-solution and hence $0 \leq \eta_1 \leq 1$, $0 \leq \eta_2 \leq 1$ and $0 \leq \Lambda \leq 1$.

6.2.2 Ignoring diffusion of cancer cells.

From Gatenby-Gawlinski, $\Delta_2 = 4 \times 10^{-5} \ll \rho_2 = 1$ and so system (6.1) can be approximated by:

$$\begin{aligned} \frac{\partial \eta_1}{\partial \tau} &= \eta_1(1-\eta_1) - \delta_1 \Lambda \eta_1 \\ \frac{\partial \eta_2}{\partial \tau} &= \rho_2 \eta_2 (1-\eta_2) \\ \frac{\partial \Lambda}{\partial \tau} &= \delta_3(\eta_2 - \Lambda) + \frac{\partial^2 \Lambda}{\partial \xi^2}. \end{aligned} \tag{6.4}$$

Travelling waves are the solutions of this system, having the special form $u(s) = \eta_1(\xi,\tau)$, $v(s) = \eta_2(\xi,\tau)$, $w(s) = \Lambda(\xi,\tau)$, where $s = \xi + c\tau$, *i.e.* each field has some wavefront, propagating with velocity $c > 0$. Substituting these forms into the above system gives a new system of ordinary differential equations:

$$cu' = u(1-u-\delta_1 w); \tag{6.5}$$

$$cv' = \rho_2 v(1-v); \tag{6.6}$$

$$cw' = \delta_3(v-w) + w''. \tag{6.7}$$

For waves to exist, with the properties claimed, we require solutions of this system which satisfy

a) $u(-\infty) = 1$, $u(\infty) = 1-\delta_1$, $v(-\infty) = 0$, $v(\infty) = 1$,
$w(-\infty) = 0$, $w(\infty) = 1$, for $\delta_1 < 1$ and

b) $u(-\infty) = 1$, $u(\infty) = 0$, $v(-\infty) = 0$, $v(\infty) = 1$,
$w(-\infty) = 0$, $w(\infty) = 1$, for $\delta_1 > 1$.

Equation (6.6) can be solved analytically to give the solution:

$$v(s) = \frac{1}{1 + k\exp(-\rho_2 s/c)}.$$

where k is an arbitrary constant. We choose $k = 1$, without loss of generality by fixing the

origin appropriately and so that $v \in [0,1]$, $v \not\equiv 1$. It can be seen that this solution has the right limits as $s \to \pm\infty$ and does not oscillate. As $0 < v < 1$ for $-\infty < s < \infty$, $\frac{dv}{ds} > 0$ for all s, and so v is a monotonically increasing function.

This solution for v can be substituted into (6.7) and then this equation solved, using the variation of parameters technique [37] to find w.

We define

$$w(s) = \frac{\alpha\beta}{\alpha+\beta}[I_1(s) + I_2(s)] \tag{6.8}$$

where $\alpha = \frac{1}{2}(c + \sqrt{c^2 + 4\delta_3}\,) > 0$, $\beta = \frac{1}{2}(-c + \sqrt{c^2 + 4\delta_3}\,) > 0$,

$$I_1 = \int_s^\infty \frac{e^{\alpha s}e^{-\alpha t}}{1+e^{-\gamma t}}\,dt, \quad I_2 = \int_{-\infty}^s \frac{e^{-\beta s}e^{\beta t}}{1+e^{-\gamma t}}\,dt, \quad \text{and } \gamma = \rho_2/c > 0,$$

which satisfies the differential equation (6.7).
As $(1+e^{-\gamma t})^{-1} \in [0,1]$,

$$w(s) \le \frac{\alpha\beta}{\alpha+\beta}\left[\int_s^\infty e^{-\alpha t}e^{\alpha s}\,dt + \int_{-\infty}^s e^{\beta t}e^{-\beta s}\,dt\right] = \frac{\alpha\beta}{\alpha+\beta}\left[\frac{1}{\alpha}+\frac{1}{\beta}\right] = 1.$$

Also the integrands of I_1 and I_2 are both positive, so we must have $w(s) \in [0,1]\ \forall s$.

I_1 is well defined as $s \to \infty$, as the integrand is exponentially decaying. Similarly, I_2 is well defined for $s \to -\infty$. We want that $w \to 0$ as $s \to -\infty$, so we need to show that $I_1(s)$, $I_2(s) \to 0$ as $s \to -\infty$ for any α, β, γ. Let $s < 0$ without loss of generality. Then

$$\begin{aligned}
I_1(s) &= \int_s^\infty \frac{e^{\alpha s}e^{-\alpha t}}{1+e^{-\gamma t}}\,dt = \int_s^{s/2} \frac{e^{\alpha s}e^{-\alpha t}}{1+e^{-\gamma t}}\,dt + \int_{s/2}^\infty \frac{e^{\alpha s}e^{-\alpha t}}{1+e^{-\gamma t}}\,dt \\
&\le \int_s^{s/2} \frac{e^{\alpha s}e^{-\alpha t}}{1+e^{-\frac{1}{2}\gamma s}}\,dt + \int_{s/2}^\infty e^{\alpha s}e^{-\alpha t}\,dt \\
&= \frac{e^{\alpha s}}{\alpha(1+e^{-\frac{1}{2}\gamma s})}(e^{-\frac{1}{2}\alpha s} - e^{-\alpha s}) + \frac{e^{\alpha s}}{\alpha}e^{-\frac{1}{2}\alpha s} \\
&= \frac{1}{\alpha(1+e^{-\frac{1}{2}\gamma s})}(e^{\frac{1}{2}\alpha s} - 1) + \frac{1}{\alpha}e^{\frac{1}{2}\alpha s} \\
&\to 0 \text{ as } s \to -\infty \\
I_2(s) &= \int_{-\infty}^s \frac{e^{-\beta s}e^{\beta t}}{1+e^{-\gamma t}}\,dt \le \int_{-\infty}^s e^{-\beta s}e^{(\beta+\gamma)t}\,dt \\
&= \frac{e^{\gamma s}}{\beta+\gamma} \to 0 \text{ as } s \to -\infty
\end{aligned}$$

Thus I_1, $I_2 \to 0$ and hence $w \to 0$ as $s \to -\infty$.

Now, we are required to show that $w \to 1$ as $s \to \infty$

$$\left|\int_{-\infty}^{s} \frac{e^{\beta t}e^{-\beta s}}{1+e^{-\gamma t}}\,dt - \frac{1}{\beta}\right| = \left|\int_{-\infty}^{s} \frac{e^{\beta t}e^{-\beta s}}{1+e^{-\gamma t}}\,dt - \int_{-\infty}^{s} e^{\beta t}e^{-\beta s}\,dt\right| = \left|e^{-\beta s}\int_{-\infty}^{s} \frac{e^{\beta t}e^{-\gamma t}}{1+e^{-\gamma t}}\,dt\right|$$

$$\leq e^{-\beta s}\int_{-\infty}^{s} e^{(\beta-\gamma)t}\,dt = e^{-\beta s}\frac{e^{(\beta-\gamma)s}}{\beta-\gamma} = \frac{e^{-\gamma s}}{\beta-\gamma} \to 0 \text{ as } s \to \infty$$

$$\Rightarrow \int_{-\infty}^{s} \frac{e^{\beta t}e^{-\beta s}}{1+e^{-\gamma t}}\,dt \to \frac{1}{\beta} \text{ as } s \to \infty.$$

Also

$$\left|\int_{s}^{\infty} \frac{e^{-\alpha t}e^{\alpha s}}{1+e^{-\gamma t}}\,dt - \frac{1}{\alpha}\right| = \left|\int_{s}^{\infty} \frac{e^{-\alpha t}e^{\alpha s}}{1+e^{-\gamma t}}\,dt - \int_{s}^{\infty} e^{-\alpha t}e^{\alpha s}\,dt\right| = \left|e^{\alpha s}\int_{s}^{\infty} \frac{e^{-(\alpha+\gamma)t}}{1+e^{-\gamma t}}\,dt\right|$$

$$\leq e^{\alpha s}\int_{s}^{\infty} e^{-(\alpha+\gamma)t}\,dt = \frac{e^{-\gamma s}}{\alpha+\gamma} \to 0 \text{ as } s \to \infty$$

$$\Rightarrow \int_{s}^{\infty} \frac{e^{-\alpha t}e^{\alpha s}}{1+e^{-\gamma t}}\,dt \to \frac{1}{\alpha} \text{ as } s \to \infty.$$

Thus

$$w(s) = \frac{\alpha\beta}{\alpha+\beta}\left[\int_{s}^{\infty} \frac{e^{-\alpha t}e^{\alpha s}}{1+e^{-\gamma t}}\,dt + \int_{-\infty}^{s} \frac{e^{\beta t}e^{-\beta s}}{1+e^{-\gamma t}}\,dt\right] \to \frac{\alpha\beta}{\alpha+\beta}\left[\frac{1}{\alpha}+\frac{1}{\beta}\right] = 1 \text{ as } s \to \infty.$$

$$w(s) = \frac{\alpha\beta}{\alpha+\beta}[I_1(s)+I_2(s)] \qquad \frac{dw}{ds} = \frac{\alpha\beta}{\alpha+\beta}[\alpha I_1 - \beta I_2]$$

$$\frac{d^2w}{ds^2} = \frac{\alpha\beta}{\alpha+\beta}\left[\frac{\alpha-\beta}{1+e^{-\gamma s}} + \alpha^2 I_1 + \beta^2 I_2\right] = \frac{\alpha\beta}{\alpha+\beta}\left[\frac{c}{1+e^{-\gamma s}} + \alpha^2 I_1 + \beta^2 I_2\right] > 0$$

(by definition of α and β) $\Rightarrow \frac{dw}{ds}$ is increasing,

$$\text{i.e. } \frac{dw}{ds} > \left.\frac{dw}{ds}\right|_{s=-\infty} = \lim_{s\to-\infty}\frac{\alpha\beta}{\alpha+\beta}[\alpha I_1(s) - \beta I_2(s)] = 0 \text{ as } \lim_{s\to-\infty} I_1, I_2 = 0$$

$$\Rightarrow \frac{dw}{ds} > 0 \Rightarrow w \text{ is monotonically increasing.}$$

Hence we have a monotonically increasing solution of (6.7) that satisfies $w(s) \in [0,1]\ \forall s$, $w \to 0$ as $s \to -\infty$ and $w \to 1$ as $s \to \infty$.

From (6.5), the equation for u is $u' = \frac{u}{c}(1-u-\delta_1 w)$. Using the Bernoulli substitution, $U = 1/u$, we can reduce this equation to a linear first order ODE:

$$\frac{dU}{ds} = \frac{1}{c}[1 - U(1-\delta_1 w(s))].$$

Define $P(s) = \frac{s}{c} - \frac{\delta_1}{c}W(s)$, where $W(s) = \int_{-\infty}^{s} w(t)\,dt$. Note that since w is exponentially small as $s \to -\infty$, then so is $W(s)$.

Now

$$\frac{d}{ds}[U(s)e^{P(s)}] = \left[U'(s) + \left(\frac{1}{c} - \frac{\delta_1}{c}w(s)\right)U(s)\right]e^{P(s)} = \frac{1}{c}e^{P(s)}$$

so

$$U(s) = e^{-P(s)}\int_{-\infty}^{s}\frac{1}{c}e^{P(t)}\,dt \quad \text{satisfies the differential equation.}$$

$U(s) \geq 0 \Rightarrow u(s) = 1/U(s) \geq 0.$

$$\begin{aligned} U(s) - 1 &= e^{-P(s)}\int_{-\infty}^{s}\frac{1}{c}e^{P(t)}\,dt - e^{-s/c}\int_{-\infty}^{s}\frac{1}{c}e^{t/c}\,dt \\ &= \frac{1}{c}e^{-P(s)}\left[\int_{-\infty}^{s}\left\{e^{P(t)} - e^{-\delta_1 W(s)/c}e^{t/c}\right\}\,dt\right] \quad \left(\text{as } P(s) = \frac{s}{c} - \frac{\delta_1 W(s)}{c}\right) \\ &= \frac{1}{c}e^{-P(s)}\left[\int_{-\infty}^{s}e^{P(t)}[1 - e^{\delta_1[W(t)-W(s)]/c}]\,dt.\right] \end{aligned}$$

Now, $\frac{dW}{ds} = w(s) \geq 0$ so W is an increasing function of s.
Therefore $W(t) \leq W(s)$, as $t \leq s$. $\Rightarrow e^{\delta_1[W(t)-W(s)]/c} \leq 1 \Rightarrow U(s) - 1 \geq 0$. *i.e.* $u(s) \leq 1$.
Thus $u(s) \in [0, 1]$.

We need to show that $U = 1/u$ has the correct behaviour at $s = \pm\infty$.
Firstly, consider w.

$$w(s) = \frac{\alpha\beta}{\alpha+\beta}\left[\int_{s}^{\infty}e^{\alpha s}e^{-\alpha t}v(t)\,dt + \int_{-\infty}^{s}e^{-\beta s}e^{\beta t}v(t)\,dt\right] \quad \text{where} \quad v(t) = \frac{1}{1+e^{-\gamma t}}$$

Now,

$$v(t) = \frac{1}{1+e^{-\gamma t}} = \frac{e^{\gamma t}}{1+e^{\gamma t}} = \begin{cases} \sum_{n=0}^{\infty}(-1)^n e^{-n\gamma t} & \text{for } t > 0 \\ \sum_{n=0}^{\infty}(-1)^n e^{(n+1)\gamma t} & \text{for } t < 0 \end{cases} \quad \text{Binomial Theorem}$$

So, for $s > 0$:

$$\begin{aligned} w(s) &= \frac{\alpha\beta}{\alpha+\beta}\left[\int_{s}^{\infty}e^{\alpha s}e^{-\alpha t}\left(\sum_{n=0}^{\infty}(-1)^n e^{-n\gamma t}\right)\,dt + \int_{0}^{s}e^{-\beta s}e^{\beta t}\left(\sum_{n=0}^{\infty}(-1)^n e^{-n\gamma t}\right)\,dt\right. \\ &\quad \left. + \int_{-\infty}^{0}e^{-\beta s}e^{\beta t}\left(\sum_{n=0}^{\infty}(-1)^n e^{(n+1)\gamma t}\right)\,dt\right] \end{aligned}$$

and for $s < 0$:

$$w(s) = \frac{\alpha\beta}{\alpha+\beta}\left[\int_0^\infty e^{\alpha s}e^{-\alpha t}\left(\sum_{n=0}^{\infty}(-1)^n e^{-n\gamma t}\right)\,dt + \int_s^0 e^{\alpha s}e^{-\alpha t}\left(\sum_{n=0}^{\infty}(-1)^n e^{(1+n)\gamma t}\right)\,dt + \int_{-\infty}^{s} e^{-\beta s}e^{\beta t}\left(\sum_{n=0}^{\infty}(-1)^n e^{(n+1)\gamma t}\right)\,dt\right]$$

All series are absolutely convergent and we know from before that the integrals are well behaved. Therefore we can swap the order of summation and integration.

Thus, for $s > 0$:

$$w(s) = \begin{cases} \dfrac{\alpha\beta}{\alpha+\beta}\left[\displaystyle\sum_{n=0}^{\infty}(a_n e^{-n\gamma s} - b_n e^{-\beta s})\right] & \text{if } \dfrac{\beta}{\gamma} \notin \mathbb{Z}^+ \\ \dfrac{\alpha\beta}{\alpha+\beta}\left[\displaystyle\sum_{\substack{n=0\\ n\neq N_1}}^{\infty}(a_n e^{-n\gamma s} - b_n e^{-\beta s}) + (-1)^{N_1}\left(s + \dfrac{1}{\alpha+\beta} + \dfrac{1}{2\beta+\gamma}\right)e^{-\beta s}\right] & \text{if } \dfrac{\beta}{\gamma} = N_1 \in \mathbb{Z}^+ \end{cases} \tag{6.9}$$

$$\text{where } a_n = \frac{(-1)^n(\alpha+\beta)}{(\alpha+n\gamma)(\beta-n\gamma)} \quad \text{and} \quad b_n = \frac{(-1)^n(2n+1)\gamma}{(\beta+(n+1)\gamma)(\beta-n\gamma)}.$$

and for $s < 0$:

$$w(s) = \begin{cases} \dfrac{\alpha\beta}{\alpha+\beta}\left[\displaystyle\sum_{n=0}^{\infty}(c_n e^{(1+n)\gamma s} - d_n e^{\alpha s})\right] & \text{if } \dfrac{\alpha}{\gamma} \notin \mathbb{Z}^+ \\ \dfrac{\alpha\beta}{\alpha+\beta}\left[\displaystyle\sum_{\substack{n=0\\ n\neq N_2}}^{\infty}(c_n e^{(1+n)\gamma s} - d_n e^{\alpha s}) + (-1)^{N_2}\left(\dfrac{1}{2\alpha-\gamma} + \dfrac{1}{\alpha+\beta} - s\right)e^{\alpha s}\right] & \text{if } \dfrac{\alpha}{\gamma} = 1 + N_2 \in \mathbb{Z}^+ \end{cases} \tag{6.10}$$

(Note $2\alpha - \gamma = 2(N_2+1)\gamma - \gamma = (2N_2+1)\gamma > 0$)

$$\text{where } c_n = \frac{(-1)^n(\alpha+\beta)}{(\alpha-(1+n)\gamma)(\beta+(1+n)\gamma)} \quad \text{and} \quad d_n = \frac{(-1)^n(2n+1)\gamma}{(\alpha+n\gamma)(\alpha-(n+1)\gamma)}.$$

Note that these expressions for w tend to the correct limits as $s \to \pm\infty$.

We require the function w to be continuous and so we require that $\lim_{s\to 0_+} w(s) = \lim_{s\to 0_-} w(s)$.

$$\text{Now for } \frac{\beta}{\gamma}, \frac{\alpha}{\gamma} \notin \mathbb{Z}^+, \qquad \lim_{s\to 0_+} w(s) = \frac{\alpha\beta}{\alpha+\beta}\left[\sum_{n=0}^{\infty}(a_n - b_n)\right]$$

$$\text{and} \quad \lim_{s\to 0_-} w(s) = \frac{\alpha\beta}{\alpha+\beta}\left[\sum_{n=0}^{\infty}(c_n - d_n)\right]$$

$$\text{So, } \frac{\alpha+\beta}{\alpha\beta}\left[\lim_{s\to 0_+} w(s) - \lim_{s\to 0_-} w(s)\right] = \sum_{n=0}^{\infty}(a_n - c_n + d_n - b_n).$$

$$\begin{aligned} a_n - c_n - (b_n - d_n) &= (-1)^n\left[\frac{\alpha+\beta}{(\alpha+n\gamma)(\beta-n\gamma)} - \frac{\alpha+\beta}{(\alpha-(n+1)\gamma)(\beta+(n+1)\gamma)}\right] \\ &\quad -(-1)^n\left[\frac{(2n+1)\gamma}{(\beta+(n+1)\gamma)(\beta-n\gamma)} - \frac{(2n+1)\gamma}{(\alpha-(n+1)\gamma)(\alpha+n\gamma)}\right] \\ &= (-1)^n\left[\frac{(\alpha+\beta)(2n+1)\gamma(\alpha-\beta-\gamma)}{(\alpha+n\gamma)(\beta-n\gamma)(\alpha-(n+1)\gamma)(\beta+(n+1)\gamma)}\right] \\ &\quad -(-1)^n\left[\frac{(\alpha+\beta)(2n+1)\gamma(\alpha-\beta-\gamma)}{(\alpha+n\gamma)(\beta-n\gamma)(\alpha-(n+1)\gamma)(\beta+(n+1)\gamma)}\right] \\ &= 0 \end{aligned}$$

$$\text{For } \frac{\beta}{\gamma} = N_1 \in \mathbb{Z}^+, \frac{\alpha}{\gamma} \notin \mathbb{Z}^+, \lim_{s\to 0_-} w(s) = \frac{\alpha\beta}{\alpha+\beta}\left[\sum_{n=0}^{\infty}(c_n - d_n)\right] \text{ and}$$

$$\lim_{s\to 0_+} w(s) = \frac{\alpha\beta}{\alpha+\beta}\left[\sum_{\substack{n=0\\ n\neq N_1}}^{\infty}(a_n - b_n) + (-1)^{N_1}\left(\frac{1}{\alpha+\beta} + \frac{1}{2\beta+\gamma}\right)\right]$$

So

$$\begin{aligned} \frac{\alpha+\beta}{\alpha\beta}\left[\lim_{s\to 0_+} w(s) - \lim_{s\to 0_-} w(s)\right] &= \sum_{\substack{n=0\\ n\neq N_1}}^{\infty}(a_n - c_n + d_n - b_n) \quad - c_{N_1} + d_{N_1} \\ &\quad +(-1)^{N_1}\left(\frac{1}{\alpha+\beta} + \frac{1}{2\beta+\gamma}\right) \\ &= (-1)^{N_1}\left(\frac{1}{\alpha+\beta} - \frac{(\alpha+\beta)}{(\alpha-(1+N_1)\gamma)(\beta+(1+N_1)\gamma)}\right) \\ &\quad +(-1)^{N_1}\left(\frac{1}{2\beta+\gamma} + \frac{(2N_1+1)\gamma}{(\alpha+N_1\gamma)(\alpha-(M_1+1)\gamma)}\right) \end{aligned}$$

Now $N_1\gamma = \beta$. So, rearranging, we have

$$\frac{\alpha+\beta}{\alpha\beta}\left[\lim_{s\to 0_+} w(s) - \lim_{s\to 0_-} w(s)\right] = (-1)^{N_1}\left[\frac{1}{\alpha-\beta-\gamma} - \frac{1}{\alpha-\beta-\gamma}\right] = 0$$

Similarly, the limits are equal, for $\frac{\beta}{\gamma} \notin \mathbb{Z}^+$, $\frac{\alpha}{\gamma} = 1 + N_2 \in \mathbb{Z}^+$ and $\frac{\beta}{\gamma}, \frac{\alpha}{\gamma} \in \mathbb{Z}^+$.

$\Rightarrow \lim_{s \to 0_+} w(s) - \lim_{s \to 0_-} w(s) = 0$ for any α, β, $\gamma \Rightarrow w$ is continuous at $s = 0$.

By definition

$$W(s) = \int_{-\infty}^{s} w(t)\, dt$$

By substituting for w with the expressions given in (6.9) and (6.10), and noting again that the series are absolutely convergent, and hence the order of integration and summation can be swapped, we obtain the following series representation of W:

For $s > 0$:

$$W(s) = \begin{cases} s + k_1 - \dfrac{\alpha\beta}{\alpha+\beta}\left[\displaystyle\sum_{n=1}^{\infty} \frac{a_n}{n\gamma} e^{-n\gamma s} + \sum_{n=0}^{\infty} \frac{b_n}{\beta} e^{-\beta s}\right] & \text{if } \dfrac{\alpha}{\gamma}, \dfrac{\beta}{\gamma} \notin \mathbb{Z}^+ \\ s + k_2 + \dfrac{\alpha\beta}{\alpha+\beta}\left[\displaystyle\sum_{n=0}^{\infty} \frac{b_n}{\beta} e^{-\beta s} - \sum_{n=1}^{\infty} \frac{a_n}{n\gamma} e^{-n\gamma s}\right] & \text{if } \dfrac{\beta}{\gamma} = N_1 \in \mathbb{Z}^+, \dfrac{\alpha}{\gamma} \notin \mathbb{Z}^+ \\ s + k_3 + \dfrac{\alpha\beta}{\alpha+\beta}\left[\displaystyle\sum_{\substack{n=0 \\ n \neq N_1}}^{\infty} \frac{b_n}{\beta} e^{-\beta s} - \sum_{\substack{n=1 \\ n \neq N_1}}^{\infty} \frac{a_n}{n\gamma} e^{-n\gamma s}\right] & \text{if } \dfrac{\beta}{\gamma} \notin \mathbb{Z}^+, \\ \quad - \dfrac{\alpha}{\alpha+\beta}(-1)^{N_1}\left[\dfrac{1}{\alpha+\beta} + \dfrac{1}{2\beta+\gamma} + s + \dfrac{1}{\beta}\right] e^{-\beta s} & \dfrac{\alpha}{\gamma} = 1 + N_2 \in \mathbb{Z}^+ \\ s + k_4 + \dfrac{\alpha\beta}{\alpha+\beta}\left[\displaystyle\sum_{\substack{n=0 \\ n \neq N_1}}^{\infty} \frac{b_n}{\beta} e^{-\beta s} - \sum_{\substack{n=1 \\ n \neq N_1}}^{\infty} \frac{a_n}{n\gamma} e^{-n\gamma s}\right] & \text{if } \dfrac{\beta}{\gamma} = N_1 \in \mathbb{Z}^+, \\ \quad - \dfrac{\alpha}{\alpha+\beta}(-1)^{N_1}\left[\dfrac{1}{\alpha+\beta} + \dfrac{1}{2\beta+\gamma} + s + \dfrac{1}{\beta}\right] e^{z-\beta s} & \dfrac{\alpha}{\gamma} = 1 + N_2 \in \mathbb{Z}^+ \end{cases}$$

and for $s < 0$:

$$W(s) = \begin{cases} \dfrac{\alpha\beta}{\alpha+\beta} \displaystyle\sum_{n=0}^{\infty} \left(\frac{c_n}{(n+1)\gamma} e^{(1+n)\gamma s} - \frac{d_n}{\alpha} e^{\alpha s}\right) & \text{if } \dfrac{\alpha}{\gamma} \notin \mathbb{Z}^+ \\ \displaystyle\sum_{\substack{n=0 \\ n \neq N_2}}^{\infty} \left(\frac{c_n e^{(1+n)\gamma s}}{(1+n)\gamma} - \frac{d_n}{\alpha} e^{\alpha s}\right) + \frac{(-1)^{N_2}}{\alpha}\left[\frac{1}{\alpha+\beta} + \frac{1}{2\alpha-\gamma} - s + \frac{1}{\alpha}\right] e^{\alpha s} & \\ & \text{if } \dfrac{\alpha}{\gamma} = 1 + N_2 \in \mathbb{Z}^+ \end{cases}$$

where the constants

$$k_1 = \frac{\alpha\beta}{\alpha+\beta}\left[\sum_{n=0}^{\infty}\left(\frac{c_n}{(n+1)\gamma}-\frac{d_n}{\alpha}-\frac{b_n}{\beta}\right)+\sum_{n=1}^{\infty}\frac{a_n}{n\gamma}\right];$$

$$k_2 = \frac{\alpha\beta}{\alpha+\beta}\left[\sum_{\substack{n=0\\ n\neq N_2}}^{\infty}\left(\frac{c_n}{(1+n)\gamma}-\frac{d_n}{\alpha}\right)+\sum_{n=1}^{\infty}\frac{a_n}{n\gamma}-\sum_{n=0}^{\infty}\frac{b_n}{\beta}\right.;$$

$$\left.+\frac{(-1)^{N_2}}{\alpha}\left(\frac{1}{2\alpha-\gamma}+\frac{1}{\alpha+\beta}-\frac{1}{\alpha}\right)\right];$$

$$k_3 = \sum_{n=0}^{\infty}\left(\frac{c_n}{(1+n)\gamma}-\frac{d_n}{\alpha}\right)+\sum_{\substack{n=1\\ n\neq N_1}}^{\infty}\frac{a_n}{n\gamma}-\sum_{\substack{n=0\\ n\neq N_1}}^{\infty}\frac{b_n}{\beta}+\frac{(-1)^{N_1}}{\beta}\left(\frac{1}{2\beta+\gamma}+\frac{1}{\alpha+\beta}+\frac{1}{\beta}\right);$$

and

$$k_4 = \frac{\alpha\beta}{\alpha+\beta}\left[\sum_{\substack{n=0\\ n\neq N_2}}^{\infty}\left(\frac{c_n}{(1+n)\gamma}-\frac{d_n}{\alpha}\right)+\frac{(-1)^{N_2}}{\alpha}\left(\frac{1}{\alpha+\beta}+\frac{1}{2\alpha-\gamma}-\frac{1}{\alpha}\right)\right]$$

$$+\frac{\alpha\beta}{\alpha+\beta}\left[\sum_{\substack{n=1\\ n\neq N_1}}^{\infty}\left(\frac{a_n}{n\gamma}-\frac{b_n}{\beta}\right)+\frac{b_0}{\beta}+\frac{(-1)^{N_1}}{\beta}\left(\frac{1}{\alpha+\beta}+\frac{1}{2\beta+\gamma.}+\frac{1}{\beta}\right)\right].$$

Thus $W(s)\to 0$ as $s\to-\infty$ and $W(s)\to s+k_0(\frac{\alpha}{\gamma},\frac{\beta}{\gamma})$ as $s\to\infty$, where

$$k_0(\frac{\alpha}{\gamma},\frac{\beta}{\gamma}) = \begin{cases} k_1 & \text{if } \frac{\alpha}{\gamma},\ \frac{\beta}{\gamma}\notin\mathbb{Z}^+ \\ k_2 & \text{if } \frac{\alpha}{\gamma}=1+N_2\in\mathbb{Z}^+,\ \frac{\beta}{\gamma}=N_1\in\mathbb{Z}^+ \\ k_3 & \text{if } \frac{\alpha}{\gamma}\notin\mathbb{Z}^+,\ \frac{\beta}{\gamma}\notin\mathbb{Z}^+ \\ k_4 & \text{if } \frac{\alpha}{\gamma}=1+N_2\in\mathbb{Z}^+,\ \frac{\beta}{\gamma}=N_1\in\mathbb{Z}^+ \end{cases}$$

Now $P(s)=\frac{1}{c}(s-\delta_1 W(s))$ and so $P(s)\to s/c$ as $s\to-\infty$ and $P(s)\to\frac{1}{c}[(1-\delta_1)s-\delta_1 k_0]$ as $s\to\infty$.

Let

$$U_0(s) = e^{-P(s)}\int_{-\infty}^{s}\frac{1}{c}e^{\frac{t}{c}}\,dt = e^{(-\frac{s}{c}+\frac{\delta_1}{c}W(s))}e^{\frac{s}{c}}$$
$$= e^{\delta_1 W(s)/c}\to 1 \text{ as } s\to-\infty.$$

Moreover

$$U_0(s)-U(s) = e^{-P(s)}\int_{-\infty}^{s}\frac{1}{c}e^{\frac{t}{c}}(1-e^{-\frac{\delta_1}{c}W(t)})\,dt$$
$$\leq e^{-P(s)}\int_{-\infty}^{s}\frac{1}{c}e^{\frac{t}{c}}\frac{\delta_1}{c}W(t)\,dt\to 0 \text{ as } s\to-\infty$$

because W is exponentially small.

Therefore $U(s)\to 1$ as $s\to-\infty$.

Now we want to show that $U(s) \to \infty$ if $\delta_1 > 1$ and $U(s) \to \frac{1}{1-\delta_1}$ if $\delta_1 < 1$.

Fix $\delta_1 > 1$.

$$P(s) = \frac{1}{c}[s - \delta_1 W(s)] \Rightarrow P'(s) = \frac{1}{c}[1 - \delta_1 w(s)].$$

We know that w is an increasing function of s, $w \to 0$ as $s \to -\infty$ and $w \to 1$ as $s \to \infty$. Therefore, by the Intermediate Value Theorem, there exists $s_1 \in \mathbb{R}$ such that $w(s_1) = 1/\delta_1$. For $s < s_1$, P is a strictly increasing function and strictly decreasing if $s > s_1$. Therefore, there exists an s_2, $-\infty < s_2 < s_1$, and a $\delta > 0$ such that $e^{P(s)} > \delta > 0$ for $s_2 < s < s_1$.

$$\text{For } s > s_1 \int_{-\infty}^{s} \frac{1}{c} e^{P(t)}\, dt > \int_{-\infty}^{s_2} \frac{1}{c} e^{P(t)}\, dt + \int_{s_1}^{s} \frac{1}{c} e^{P(t)}\, dt + \frac{\delta}{c}(s_1 - s_2) > \frac{\delta}{c}(s_1 - s_2).$$

Hence for $s > s_1$,

$$\begin{aligned} U(s) &= e^{-P(s)} \int_{-\infty}^{s} \frac{1}{c} e^{P(t)}\, dt > e^{-P(s)} \frac{\delta}{c}(s_1 - s_2) \\ &\to \frac{\delta}{c}(s_1 - s_2) e^{[(\delta_1 - 1)s - \delta_1 k_0]} \to \infty \text{ as } s \to \infty. \end{aligned}$$

Now fix $\delta_1 < 1$.
Define

$$U_1(s) = e^{-\delta_1 k_0/c} e^{-P(s)} \int_{-\infty}^{s} \frac{1}{c} e^{(1-\delta_1)t/c}\, dt,$$

where k_0 is the constant such that $W(s) \to s + k_0$ as $s \to \infty$.

In order to show that for $\delta_1 < 1$, $U(s) \to \frac{1}{1-\delta_1}$ as $s \to \infty$, we will firstly show that $U_1(s) \to \frac{1}{1-\delta_1}$ as $s \to \infty$, and then $U(s) - U_1(s) \to 0$ as $s \to \infty$.

$$\begin{aligned} \left| U_1(s) - \frac{1}{1-\delta_1} \right| &= \frac{1}{1-\delta_1} \left| e^{-P(s)} e^{[(1-\delta_1)s - \delta_1 k_0]/c} - 1 \right| \\ &= \frac{1}{1-\delta_1} \left| e^{\delta_1 (W(s) - s - k_0)/c} - 1 \right| \\ &\to 0 \text{ as } s \to \infty. \\ \text{Therefore } U_1(s) &\to \frac{1}{1-\delta_1} \text{ as } s \to \infty. \end{aligned}$$

$P(s) \to \frac{1}{c}[(1 - \delta_1)s - \delta_1 k_0]$ as $s \to \infty$. Therefore, given $\epsilon > 0$, there exists an S such that whenever $s > S$, $(1 - \delta_1 - \epsilon)s - \delta_1 k_0 < cP(s) < (1 - \delta_1 + \epsilon)s - \delta_1 k_0$.

So

$$\begin{aligned}
|U_1(s)-U(s)| &\leq \left|\frac{1}{c}e^{-P(s)}\int_{-\infty}^{S}\left[e^{[(1-\delta_1)t-\delta_1 k_0]/c}-e^{P(t)}\right]\,dt\right| \\
&\quad +\left|\frac{1}{c}e^{-P(s)}\int_{S}^{s}\left[e^{[(1-\delta_1)t-\delta_1 k_0]/c}-e^{P(t)}\right]\,dt\right| \\
&< Ae^{-P(s)}+\left|\frac{1}{c}e^{-P(s)}e^{-\delta_1 k_0/c}\int_{S}^{s}\left[e^{(1-\delta_1)t/c}-e^{[(1-\delta_1)t-\delta_1\epsilon t]/c}\right]\,dt\right| \\
\text{where } A &= \left|\frac{1}{c}\int_{-\infty}^{S}\left[e^{[(1-\delta_1)t-\delta_1 k_0]/c}-e^{P(t)}\right]\,dt\right| \text{ - constant} \\
|U_1(s)-U(s)| &< (A+B)e^{-P(s)}+\frac{e^{-[P(s)+\delta_1 k_0/c]}}{1-\delta_1}\left|e^{(1-\delta_1)s/c}-e^{[(1-\delta_1)s-\delta_1\epsilon s]/c}\right| \\
\text{where } B &= e^{-\delta_1 k_0/c}\left[\frac{e^{(1-\delta_1)S/c}}{1-\delta_1}-\frac{e^{[(1-\delta_1)S-\delta_1\epsilon S]/c}}{1-\delta_1-\delta_1\epsilon}\right] \text{ - constant} \\
\text{So } |U_1(s)-U(s)| &< (A+B)e^{-P(s)}+\frac{e^{[-(1-\delta_1)s-\delta_1\epsilon s]/c}}{1-\delta_1}\left|e^{(1-\delta_1)s/c}-e^{[(1-\delta_1)s-\delta_1\epsilon s]/c}\right| \\
&= (A+B)e^{-P(s)}+\frac{e^{-\delta_1\epsilon s/c}}{1-\delta_1}\left|1-e^{-\delta_1\epsilon s/c}\right|. \\
\text{Now } P(s) &\to \infty \text{ as } s\to\infty \text{ so } e^{-P(s)}\to 0. \\
\text{Thus } |U(s)-U_1(s)| &\to 0 \text{ as } s\to\infty
\end{aligned}$$

Hence for $\delta_1 < 1$, $U(s) \to \frac{1}{1-\delta_1}$ as $s \to \infty$.

Now, $U(s) = 1/u(s)$, so $u(s) \to 1$ as $s \to -\infty$, $u(s) \to 0$ if $\delta_1 > 1$ and $u(s) \to 1-\delta_1$ if $\delta_1 < 1$ as $s \to \infty$.

We have shown that the three equations, (6.5), (6.6) and (6.7), have solutions which satisfy $u, v, w \in [0,1]$ and tend to the required limits as $s \to \pm\infty$ for all positive values of c. This implies that system (6.4) has travelling wave solutions for all positive values of c.

We propose that, as $\Delta_2 \ll \rho_2$, (6.4) is a close approximation to (6.1), and hence it can be reasonably assumed that there also exist travelling wave solutions to the latter system, for all $c > 0$.

6.3 Marginal Stability.

6.3.1 Introduction.

One of the simplest equations that exhibits simple travelling waves is the Fisher-Kolmogorov equation [65, 133]:

$$\frac{\partial\phi}{\partial t} = \frac{\partial^2\phi}{\partial x^2} + \phi - \phi^2.$$

The situation of interest here is the one in which a front is moving to the right, replacing the unstable state $\phi = 0$ by the stable state $\phi = 1$. The velocity γ of a front growing out of a sufficiently localised region where $\phi \neq 0$ initially cannot be determined by steady state considerations. It can be shown [220] that the equation $\frac{d^2\phi}{dx^2} = -\gamma\frac{d\phi}{dx} - \phi + \phi^2$ for uniformly translating fronts $\phi(s) = \phi(x - \gamma t)$ admits solutions for any velocity γ. Nevertheless, there is a naturally selected velocity, γ^*. Aronson and Weinberger [11] rigorously proved that the speed of the physically most relevant fronts that are initially sufficiently localised [such that $\phi(x, t = 0)$ drops off faster than e^{-x}], approaches the value $\gamma^* = 2$ for long times.

Dee and colleagues [17, 49, 50] showed that the velocity $\gamma^* = 2$ of the Fisher-Kolmogorov equation is just the one at which the front appears to be "marginally stable", in that front solutions that move slower than γ^* are unstable to perturbations (in the co-moving frame) while those that move faster are stable *i.e.* the wave profile is stable to perturbations in the co-moving frame only if the speed is greater than γ^*.

γ^* is referred to as the marginal stability point.

Marginal Stability Hypothesis:

The natural speed for propagation of initially localised fronts into an unstable state is in general the one corresponding to the marginal stability point [220].

This hypothesis was tested numerically by Dee *et al.* [17, 49, 50] for several equations in which fronts give rise to dynamical pattern selection.

6.3.2 Determining the marginal stability point.

In the following section, we outline the method in [220] for finding the marginal stability point, and then use this on the system (6.1).

Consider propagation into an unstable state $\phi = 0$ described by an equation $\phi_t = F(\phi, \phi_x, \dots)$. It is convenient [197] to transform to the variable p by writing $\phi = e^{-p}$. In the leading edge where $p \to \infty$ for $x \to \infty$, the dynamical equation for p then becomes of the form

$$p_t = -f(q, q_x, \dots) \text{ where } q \equiv p_x. \tag{6.11}$$

(This is true since $F(\phi, \phi_x, \phi_{xx}, \dots) < \infty$ when $\phi = 0$, and can be proved by using Taylor's Theorem).

Note that when $q = k$, independent of x, we have $f(q = k, 0, 0, \dots) = \omega(k)$, where $\omega(k)$ is given by the dispersion relation [106] for perturbations of the form $\phi \sim e^{-kx+\omega(k)t}$.

In a frame moving with a constant velocity, *i.e.* $p(x,t) = p(x-ct,t)$, we have

$$p_t = cq - f(q, q_x, \dots). \tag{6.12}$$

Firstly consider steady state front solutions, *i.e.* a solution $q = k$, constant, whose profile propagates with a speed c. For such a solution, $p_t = 0$ in the moving frame, and thus we obtain

$$ck - f(k, 0, \dots) = 0 \ \ i.e. \ \ c = \frac{\omega(k)}{k}, \ \text{ by definition of } \omega. \tag{6.13}$$

To study the stability of these steady state front solutions, consider a bounded perturbation $\delta \sim e^{-\mu x}$ in ϕ, with $\mu > 0$ and $\mu \ll 1$. Substituting $\overline{u} = u + \mu x$ into (6.12), we obtain

$$\begin{aligned}
\overline{u}_t &= u_t = cu_x - f(u_x, u_{xx}, \dots) = c(\overline{u} - \mu) - f(\overline{u}_x - \mu, \overline{u}_{xx}, \dots) \\
&= c(q - \mu) - f(q - \mu, q_x, q_{xx}, \dots) \\
&= c(q - \mu) - f(q, q_x, \dots) + \mu f_q(q, q_x, \dots) + o(\mu^2) \ \text{ using Taylor's Theorem} \\
&= cq - f(q, q_x, \dots) - \mu(c - f_q(q, q_x, \dots)) + o(\mu^2)
\end{aligned}$$

Now,we are considering front solutions, *i.e.* $q = k$, and thus

$$\overline{u}_t = ck - w(k) - \mu(c - f_q(k, 0, 0, \dots) + o(\mu^2) = -\mu(c - f_q(k, 0, 0, \dots) + o(\mu^2)$$

from (6.13).

$\mu \ll 1$ and so we can ignore terms of $o(\mu^2)$ and above. Thus, perturbations with small μ are stable if

$$\mu(c - f_q(k, 0, 0, \dots)) > 0 \ \Rightarrow \ c > f_q(k, 0, \dots) \ \text{ since } \mu > 0. \tag{6.14}$$

Now, $f(q = k, 0, \dots) = \omega(k)$, and so (6.14) is equivalent to

$$c > \frac{d\omega}{dk}.$$

The marginal stability point, $k = k^*$, $c = c^*$ is defined to be the one at which the profile of the wave ceases to be unstable/becomes stable to small perturbations and is thus given by:

$$c^* = \left.\frac{d\omega}{dk}\right|_{k=k^*}$$

with c^* given by (6.13).

From (6.1), the equation for η_2 is

$$\frac{\partial \eta_2}{\partial \tau} = \rho_2 \eta_2 (1 - \eta_2) + \Delta_2 \frac{\partial}{\partial \xi} \left[(1 - \eta_1) \frac{\partial \eta_2}{\partial \xi} \right]$$

Let $\phi = \eta_2$, $\tau = t$ and $x = \xi$. Then

$$\phi_t = F(\phi, \phi_x, \phi_{xx}) = \rho_2 \phi (1 - \phi) + \Delta_2 \left[(1 - \eta_1) \phi_{xx} - \frac{\partial \eta_1}{\partial x} \phi_x \right].$$

We transform to the variable p by writing $\phi = e^{-p}$. Then

$$p_t = -\rho_2 (1 - e^{-p}) - \Delta_2 \left[(1 - \eta_1)((p_x)^2 - p_{xx}) + \frac{\partial \eta_1}{\partial x} p_x \right].$$

In the leading edge where $p \to \infty$ for $x \to \infty$, the dynamical equation for p then becomes of the form

$$p_t = -f(q, q_x) = -\rho_2 - \Delta_2 \left[(1 - \eta_1)(q^2 - q_x) + \frac{\partial \eta_1}{\partial x} q \right] \quad \text{where } q = p_x. \tag{6.15}$$

In a frame moving with constant velocity c (*i.e.* $s = x - ct = 0$), (6.15) becomes

$$p_t = cq - f(q, q_x) = cq - \rho_2 - \Delta_2 [(1 - u(s = 0; c))(q^2 - q_x) + u'(s = 0; c) q]$$

where $u(s) = u(x - ct) = \eta_1(x, t)$ and $u' = \dfrac{du}{ds}$.

$$w(k) = f(k, 0) = \rho_2 + \Delta_2 k [(1 - u(s = 0; c)k + u'(s = 0; c)]$$

Now $c^*(k^*) = \dfrac{w(k^*)}{k^*} = \dfrac{dw}{dk}\Big|_{k=k^*} \Rightarrow k^* = \sqrt{\dfrac{\rho_2}{\Delta_2(1 - \eta_1)}}$

$$\Rightarrow c^* = \Delta_2 u(s = 0; c) + 2\sqrt{\rho_2 \Delta_2 (1 - u(s = 0; c))}. \tag{6.16}$$

6.3.3 Solving for the marginally stable point.

We use the analytical solution of system (6.4) to approximate $u(s, c)$ in equation (6.16) *i.e.*

$$u(s) = \frac{e^{P(s)}}{\int_{-\infty}^{s} \frac{1}{c} e^{P(t)} dt} \quad \text{where } P(s) = \frac{s}{c} - \frac{\delta_1}{c} \int_{-\infty}^{s} w(t) dt \text{ and } w(t) \text{ is given in (6.8)}$$

Let

$$g(c) \equiv \Delta_2 \eta_1'(0; c) + 2\sqrt{\rho_2 \Delta_2 (1 - \eta_1(0; c))} - c$$

The secant method (Section 18.2 [135]) is a two-point method of iteration to find the roots of

$g(c) = 0$. The general iteration formula is:

$$c_{n+1} = c_n - \frac{g(c_n)(c_n - c_{n-1})}{g(c_n) - g(c_{n-1})} \quad n \geq 1, \qquad c_1 = c_0 + g(c_0)$$

Using this method, we obtained a value of 0.01 for c^*. This value of the speed of invasion of the tumour can be equated to the rate of growth of the radius of a radially symmetric tumour. Thus, in dimensional terms, the rate of growth of the tumour radius is 0.019 mm/day. The rate of growth of an MCS in the linear phase is approximately 0.006-0.016 mm/day [71], which is slightly lower, so our value of c^* is a good estimate of the speed of invasion of a malignant tumour.

Gatenby and Gawlinski display equation (6.16), without showing the derivation of it. They then use an incorrect solution for u, which doesn't even solve the simplified equation, to solve the transcendental equation (6.16) and obtain a value of $c^* = 0.0126 \equiv 0.03$mm/day for $\delta_1 = 12.5$. This is almost twice the speed recorded for a fast growing MCS *in vitro* [71] and seems rather high to be biologically realistic.

6.4 Simulation of Acid Mediated Invasion.

This simulation, based on the Extended Potts model, discussed in Chapter 3, includes cells which grow and divide and cells which maintain relatively constant volume. We consider healthy and dead normal cells as different cell types, in addition to cancer cells, with different volume constraints for each type. Target volumes for healthy and dead normal cells remain constant in time. Target volumes increase for cancer cells, to simulate growth. The volume constraints for cancer, healthy and dead cells are successively weaker. Accordingly, cancer cells can grow at the expense of dead normal cells.

The effects of nutrient on cancer cell growth are ignored, as in Gatenby and Gawlinski's continuum model. So, there are no necrotic or quiescent cells to consider, unlike the simulation presented in Chapter 3.

Despite having different volume constraints, healthy and dead normal cells have the same binding properties. Healthy cells have the strongest adhesive bonds with healthy cells and tumour-tumour bonds are the weakest, with tumour-healthy bonds in between. The resulting surface tension keeps the tumour compact. This hierarchy of binding strengths is consistent with biological evidence [167, 232].

Tumour cells grow in response to the demands of an increasing target volume with mitosis occurring whenever the ratio of surface area to volume for a cell drops below a threshold (see Chapter 3 for details of this). The cell splits in a plane through the centre of mass corresponding to a minimal cross section with all the array elements on one side of the cell assigned a previously

unused index. After a split, each daughter cell starts with half the target volume of the parent cell so as not to be unduly stressed by a large deviation from the mandated size of the progenitor. Since, experimentally, mean tumour cell size is comparable to mean normal cell size, we apply mitosis at twice the typical cell volume, which corresponds to an area/volume ratio of 0.6.

Again, we do not include the growth of normal cells.

As well as having a lattice which stores the spin number of a cell at its lattice sites, there is a second lattice which stores the value of acid concentration at each lattice site. This chemical lattice is then super-imposed on the cell lattice for calculations.

As we are assuming that all the cancer cells in the aggregate are supplied with a homogeneous source of nutrient and therefore proliferating at the same rate, we assume that they are also producing the same amount of acid each. This acid is then allowed to diffuse across the chemical lattice. Healthy cells die in response to the acid gradient extending from the edge of the tumour. We also assume that the healthy cells "absorb" some of this acid. This is to take into account the mechanisms for increasing local pH e.g. buffering and large scale vascular evacuation.

At every time step, the acid lattice is updated. We model the diffusion of the acid by using the following simple discretisation of the diffusion equation:

For a lattice site (x, y, z):

$$\text{updated acid}(x,y,z) = \frac{1}{12}\left[6 \times \text{old acid}(x,y,z) + \sum_{n'bours,\ (x',y',z')} \text{old acid}(x',y',z')\right]$$

where (x', y', z') is one of the six nearest neighbours of (x, y, z).

Then the acid concentration that a cell i is subjected to is just the sum of acid concentration over all array sites, (x, y, z), making up cell i.

If we fix the rate of removal of acid, A_r by healthy cells and also the concentration of acid required to kill a healthy cell, then the rate of acid production, A_p determines the dynamics of the system. This corresponds to the parameter δ_1 in Gatenby and Gawlinski's continuum model.

If $A_p < A_r$ ($\delta_1 < 1$), then there is no hypocellular interstitial gap of dead cells and the tumour is confined in its growth. To simulate co-existence of tumour tissue and cancer tissue, we would have to change the order of binding strengths to:

$$\text{strength of healthy-healthy bonds} > \text{cancer-cancer bonds} > \text{healthy-cancer bonds},$$

which is not so consistent with biological evidence [167, 232]. Also this is a model of tumour invasion via acid production and so this case, where the acid removal by normal cells is greater than the production by tumour cells, is not really of any interest.

If $A_p > A_r$ ($\delta_1 > 1$), then a gap does form and the tumour is able to invade the surrounding healthy tissue. This scenario is shown in Figure (6-1).

We recorded the total volume of the tumour as it developed and from this, we calculated the average radius, using the formula:

$$\text{average radius} = \left(\frac{3}{4\pi}\text{volume of tumour}\right)^{1/3}$$

Figure (6-2)[a] shows the development of the average radius of the tumour with time. The speed of invasion of the tumour edge can be calculated, by fitting a straight line to the curve and finding its gradient. This was found to be 0.0244 pixels/MCTS. This speed can be increased (decreased) by increasing (decreasing) A_p and the increase in cancer cells' target volume per time step.

The continuum model is in only one spatial dimension, but we can compare it to the simulation by assuming that the continuum tumour is radially symmetric and that the distance of the wavefront from the left hand boundary in the numerical simulation ($x+1$) then represents the radius of the tumour. The graph of this is shown in Figure (6-2)[b].

The two graphs shown in Figure (6-2) are quite comparable in shape, as both are linear and so it would be reasonable to say that 0.024pixels/MCTS$\approx$ 0.02 mm/day.

6.5 Conclusions.

In this chapter, we have proved analytically the existence of travelling waves, for all speeds $c > 0$, in a slightly simplified version of Gatenby and Gawlinski's [86] model of acid-mediated invasion. To obtain the simplified model, a term of $O(10^{-4})$ from an equation of $O(1)$, was ignored, and it was thus assumed that this was similar enough to the original system to be able to say that Gatenby and Gawlinski's full model also exhibits travelling waves, from $(1,0,0)$ to $(0,1,1)$ if $\delta_1 > 1$ and from $(1,0,0)$ to $(1-\delta_1,1,1)$ if $\delta_1 < 1$.

It was then proved, using marginal stability theory [49, 220], that the minimum speed at which these waves are stable if $\delta_1 = 12.5$, is $c^* = 0.01$. In physical terms, this speed of the wavefront corresponds to the rate of growth of the radius of a spherically symmetric tumour or MCS. For this model, $c^* = 0.019$ mm/day in dimensional terms, which is consistent with experimental evidence [71].

A simulation of acid-mediated invasion, based on the Extended Potts Model, was then presented and compared with Gatenby and Gawlinski's continuum model. It was found that the ratio of acid production to acid removal, $\frac{A_p}{A_r}$, correlated with the parameter δ_1, in that if $\frac{A_p}{A_r} < 1$, the tumour was non-invasive and slow growing, while if $\frac{A_p}{A_r} > 1$, an interstitial gap formed between the tumour and healthy tissue, into which the tumour invaded.

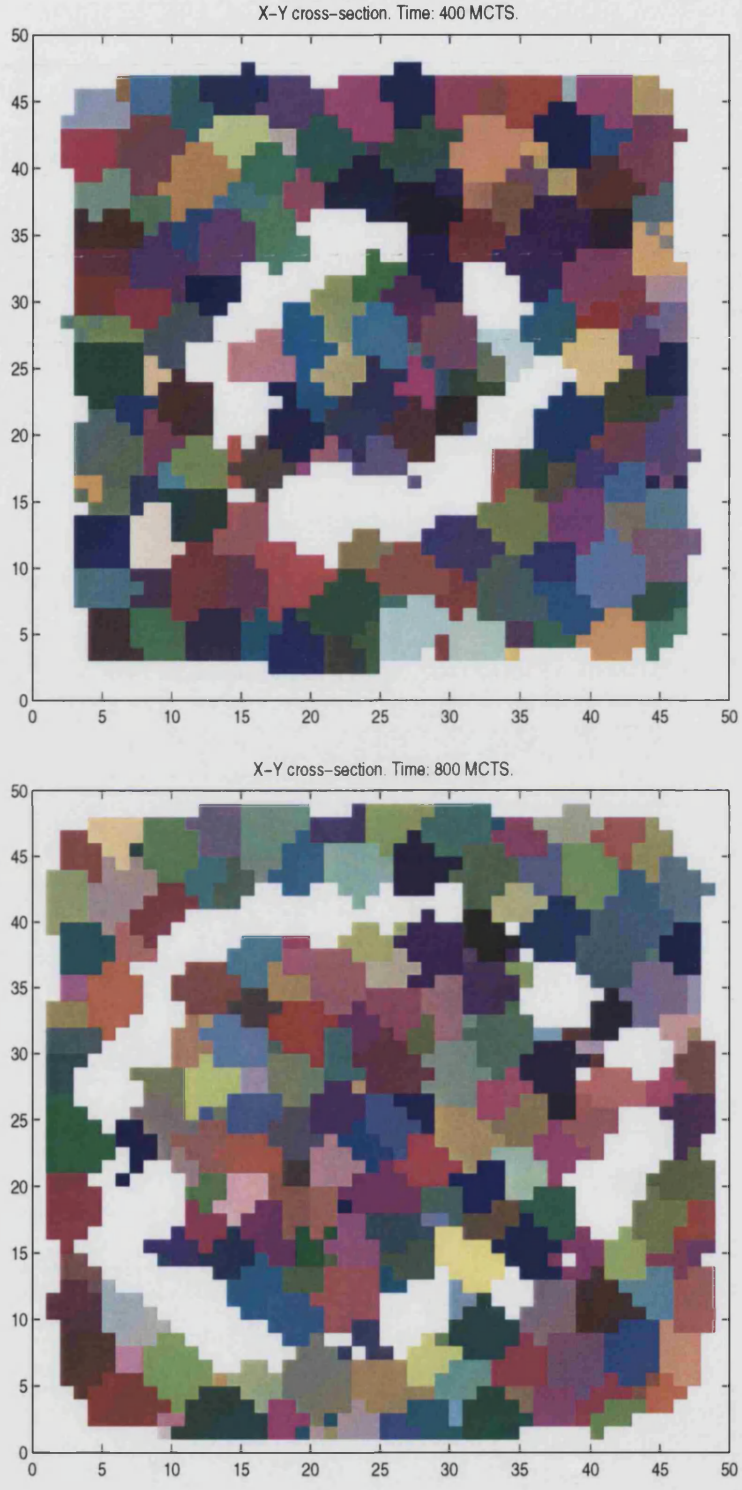

Figure 6-1: Acid-mediated invasion. Tumour and live cells are shown individually, while the dead normal cells are shown as a solid white ring.

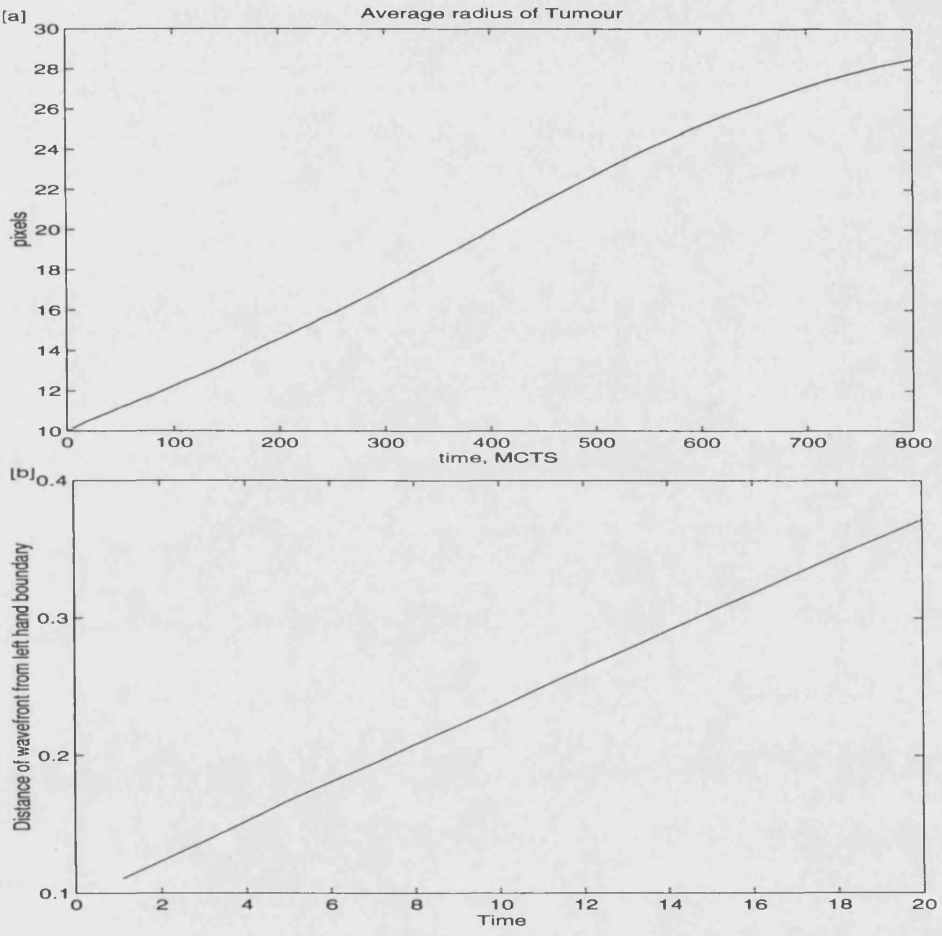

Figure 6-2: Comparison between simulation [a] and Gatenby's model [b].

The growth graph of the average radius of the simulated tumour was roughly linear and by measuring the gradient of this graph, the rate of growth of the radius was calculated to be 0.024 pixels/MCTS. As can be seen from Figure 6-2, the growth graph from the simulation and that from Gatenby's model are comparable and so we can equate the growth rates. Thus 0.024 pixels/day$\approx$ 0.019 mm/day.

In the next chapter, we extend Gatenby's simple model of tumour invasion, to include the effects of nutrient on tumour growth.

Chapter 7

Extension of Gatenby and Gawlinski's model with Comparison to Simulation

Tumours have been shown to produce lactic acid via the pathway of aerobic glycolysis [225]. This leads to the reduction of extracellular pH within the tumour. Normal cells can only function at a pH of 0.3 more alkaline than the typical pH within tumours [33]. Hence, when the tumour-produced acid diffuses into the surrounding healthy tissue, the nearest cells die, forming a gap into which the tumour can grow. This forms the basis for Gatenby and Gawlinski's acid mediation hypothesis [86], discussed in Chapter 6.

In this chapter, we present a mathematical model and also a simulation, which are based on the acid-mediation model developed by Gatenby and Gawlinski [86], as discussed in Chapter 6. We extend their model to include the effects of an essential nutrient, e.g. glucose, oxygen, on cancer cell growth and also include the death of cancer cells due to lack of that nutrient.

7.1 Description of the model.

The model is a system of five coupled reaction diffusion equations which determine the spatial distribution and temporal evolution of five fields: $N_1(r,\theta,\phi,t)$, the density of normal tissue; $N_2(r,\theta,\phi,t)$, the density of living tumour tissue; $N_3(r,\theta,\phi,t)$, the density of dead tumour tissue; $L(r,\theta,\phi,t)$, the excess concentration of H^+ ions; and $G(r,\theta,\phi,t)$, the concentration of essential nutrient. The units of N_1, N_2 and N_3 are cells/cm^3 and excess H^+ ions and nutrient concentration are expressed as a molarity (M). r, θ, ϕ and t are the position in space (in cm and radians) and time (s) respectively.

We assume that all growth is spherical and that spherical symmetry prevails at all times. Thus time t and radial distance r are the only independent variables.

The behaviour of normal tissue is determined by

a) the logistic growth of N_1, with growth rate p_1 and carrying capacity K;

b) the interaction of N_1 with excess H^+ ions leading to a death rate proportional to L and

c) the interaction of N_1 with the toxic waste produced by the dead cancer cell's disintegration, leading to a death rate proportional to N_3.

When cells die, their membranes rupture and their contents spill out uncontrollably. Some of the cell's chemicals have damaging effects on the surroundign tissue [54]. We assume that these chemicals cause nearby live cells to die at a rate proportional to N_3.

We assume that healthy tissue is well regulated and participating normally in an organ and will, therefore, not be diffusing in space. The equation governing N_1 development is therefore:

$$\frac{\partial N_1}{\partial t} = p_1 N_1 \left(1 - \frac{N_1}{K}\right) - d_1 L N_1 - D_1 N_3 N_1 \tag{7.1}$$

$d_1 L$ is the excess acid concentration dependent death rate in accordance with Gatenby and Gawlinski. The logistic growth term means that the healthy tissue occupies all available space, unless there is sufficient acid or toxic waste present to cause degradation.

The behaviour of the tumour tissue is determined by

a) proliferation of cells at a rate proportional to a function of nutrient concentration, $\tilde{g}(G)$;

b) death of cells at a rate proportional to another function of nutrient concentration, $\tilde{d}(G)$ and

c) cellular diffusion with an N_1-dependent diffusion coefficient, $D_{N_2}[N_1]$.

As dead cells will only be present when there is little nutrient, the death of tumour cells due to toxic waste products and nutrient deficiency have been combined to one term which only features nutrient deficiency.

Following Gatenby, we choose $D_{N_2}[N_1] = D_2(1 - N_1/K)$. D_2 is the diffusion coefficient for cancerous tissue in the absence of healthy tissue and when healthy tissue is at its carrying capacity, the diffusion coefficient for tumour tissue is zero and the tumour is confined. This means that the tumour is unable to spread without the healthy tissue being first diminished from its carrying capacity. Therefore, the equation governing tumour development is:

$$\frac{\partial N_2}{\partial t} = p_2 \tilde{g}(G) N_2 - d_2 \tilde{d}(G) N_2 + \frac{D_2}{K}\left[(K - N_1)\frac{1}{r^2}\frac{\partial}{\partial r}\left(r^2 \frac{\partial N_2}{\partial r}\right) - \frac{\partial N_1}{\partial r}\frac{\partial N_2}{\partial r}\right].$$

It is known that the proliferation of a cell is dependent on nutrient concentration - cells with a high concentration of nutrient will divide faster, up to some saturation level, than those

which have a low concentration [22, 30, 34, 81, 84, 107]. So, we require the function $\tilde{g}$ to be 0 when G is 0, 1 when G is greater than or equal to some critical value G_0, and monotonically increasing between these values. The simplest function that satisfies these criteria is

$$f(G) = \begin{cases} 1 & \text{if } G \geq G_0 \\ \frac{G}{G_0} & \text{if } G \leq G_0. \end{cases}$$

But, this is a slightly unrealistic function from a biological point of view because it is not continuously differentiable at G_0, that is $\lim_{G \to G_0^-} f'(G) \neq \lim_{G \to G_0^+} f'(G)$.

Thus we choose the simplest continuously differentiable function that satisfies the criteria

$$\tilde{g}(G) = \begin{cases} 1 & \text{if } G \geq G_0 \\ 1 - \left(1 - \frac{G}{G_0}\right)^2 & \text{if } G \leq G_0. \end{cases}$$

Note that here we are allowing G to take negative values. However, it is physically unrealistic for a concentration of a chemical to take negative values. From equation (7.1), it can be seen that if N_1 is initially non-negative, then it will remain non-negative. Thus, from equation (7.2), if G is initially non-negative then it remains so for all time.

Similarly, cells die with a rate proportional to some function of "lack" of nutrient if concentration is less than a critical value. So, we take $\tilde{d}$ to be the continuously differentiable function given by:

$$\tilde{d}(G) = \begin{cases} 0 & \text{if } G \geq G_0 \\ \left(1 - \frac{G}{G_0}\right)^2 & \text{if } G \leq G_0. \end{cases}$$

Dead cancer tissue is produced when cancer cells die, so the equation governing the development of the necrotic core is:

$$\frac{\partial N_3}{\partial t} = d_2 \tilde{d}(G) N_2.$$

We assume that the acid is produced at a rate proportional to the cancer cell density and diffuses chemically. An uptake term is also included c.f. [86]. Thus, the equation governing acid concentration is:

$$\frac{\partial L}{\partial t} = p_4 N_2 - d_4 L + \frac{D_4}{r^2}\left(r^2 \frac{\partial L}{\partial r}\right).$$

The amount of nutrient produced is proportional to the density of blood vessels in an area. Since we are assuming that the tumour is avascular, this means that nutrient can only be produced in regions of normal tissue. Thus blood vessel density is proportional to normal cell density. Hence we take the production rate of nutrient to be proportional to normal tissue

density. For simplicity, we assume that the same amount of nutrient is consumed by all living cells at all times and so it is just degraded at a rate proportional to G. Nutrient also diffuses chemically. The equation governing nutrient concentration is:

$$\frac{\partial G}{\partial t} = p_5 N_1 - d_5 G + \frac{D_5}{r^2}\left(r^2 \frac{\partial G}{\partial r}\right). \tag{7.2}$$

The following transformation of variables renders the above equations dimensionless:

$$N_1' = \frac{N_1}{K},\ N_2' = \frac{N_2}{K},\ N_3' = \frac{N_3}{K},\ L' = \frac{L}{L_0},\ G' = \frac{G}{G_0},\ t' = p_1 t,\ r' = \sqrt{\frac{p_1}{D_4}}r$$

where $L_0 = p_4 K/d_4$. Using these transformations, and dropping the primes for convenience, the dimensionless form of the equations become:

$$\begin{aligned}
\frac{\partial N_1}{\partial t} &= N_1(1 - N_1 - \delta_1 L - \rho_1 N_3); \\
\frac{\partial N_2}{\partial t} &= \rho_2 g(G) N_2 - \delta_2 d(G) N_2 + \Delta_2 \left[(1 - N_1)\frac{\partial}{\partial r}\left(r^2 \frac{\partial N_2}{\partial r}\right) - \frac{\partial N_1}{\partial r}\frac{\partial N_2}{\partial r}\right]; \\
\frac{\partial N_3}{\partial t} &= \delta_2 d(G) N_2; \\
\frac{\partial L}{\partial t} &= \delta_4(N_2 - L) + \frac{\partial^2 L}{\partial x^2}; \\
\frac{\partial G}{\partial t} &= \rho_5 N_1 - \delta_5 G + \Delta_5 \frac{\partial^2 G}{\partial x^2}.
\end{aligned} \tag{7.3}$$

where

$$\begin{aligned}
&\delta_1 = \frac{d_1 p_4}{d_4 p_1} K,\ \rho_1 = \frac{D_1}{p_1} K,\ \rho_2 = \frac{p_2}{p_1},\ \delta_2 = \frac{d_2}{p_1},\ \Delta_2 = \frac{D_2}{D_4}, \\
&\delta_4 = \frac{d_4}{p_1},\ \rho_5 = \frac{p_5 K}{p_1 G_0},\ \delta_5 = \frac{d_5}{p_1},\ \Delta_5 = \frac{D_5}{D_4}
\end{aligned}$$

and

$$d(G) = \begin{cases} 0 & \text{if } G \geq 1 \\ (1-G)^2 & \text{if } G \leq 1 \end{cases}, \qquad g(G) = 1 - d(G).$$

Parameter	Estimate	References	Non-dim'l Parameter	Estimate
p_1, p_2	1×10^{-6}/s	[219]	δ_1	$10 \times d_1$
K	5×10^{7}/cm^3	[219]	ρ_1	$5 \times 10^{13} D_1$
d_1	$0 \rightarrow 10$/M.s	[86]	ρ_2	1
D_1	$0 \rightarrow 2 \times 10^{-14}$ s/cm^3		δ_2	0.6
d_2	6×10^{-5}/s	[198]	Δ_2	4×10^{-5}
D_2	2×10^{-10}cm^2/s	[45]	δ_4	110
p_4	2.2×10^{-17} Mcm^3/s	[86]	ρ_5	3.6×10^{2}
d_4	1.1×10^{-4}/s	[86]	δ_5	3.6×10^{2}
D_4	5×10^{-6}cm^2/s	[86]	Δ_5	0.078
p_5	5.7×10^{-4} Mcm^3/s	[22]		
d_5	3.6×10^{-4}/s	[22]		
D_5	3.9×10^{-7}cm^2/s	[31, 198]		
G_0	7.9×10^{7} M	[22]		

Table 7.1: Parameter values of dimensional and non-dimensional systems.

7.1.1 Fixed Points.

The fixed points (spatial homogeneity and temporal invariance) of the system are found by setting the spatial and temporal derivatives in (7.3) to zero and solving for the fields. The following two fixed points are thus obtained:

$$\begin{array}{lllll} \text{FP 1:} & N_1^* = 0 & N_2^* = 0 & N_3^* = d^* & L^* = 0 \quad G^* = 0 \\ \text{FP 2:} & N_1^* = 1 & N_2^* = 0 & N_3^* = 0 & L^* = 0 \quad G^* = \frac{\rho_5}{\delta_5}. \end{array}$$

These correspond to three physical states: FP 1, the trivial absence of all living tissue, acid and nutrient, with necrotic tissue at a constant level d^*, determined by the initial conditions; and FP 2, the healthy tissue existing at its carrying capacity, in the absence of tumour tissue and acid.

The eigenvalues of the linearisation of (7.3) at $(0, 0, d^*, 0, 0)$ are:

$$\mu = 1, \ -\delta_2, \ 0, \ -\delta_4, \ -\delta_5;$$

and at $(1, 0, 0, 0, \frac{\rho_5}{\delta_5})$, the eigenvalues are:

$$\mu = 0, \ -1, \ \rho_2, \ -\delta_4, \ -\delta_5.$$

So the linear stability analysis shows that $(0, 0, d^*, 0, 0)$ and $(1, 0, 0, 0, \frac{\rho_5}{\delta_5})$ are both unstable fixed points.

7.2 Solutions of the Model.

We have performed computer simulations of the full system (7.3), using the DYLAN differential algebraic equation solver, owned by QuantiSci Ltd.[51], and suitable boundary and initial conditions. Biological parameter values are shown in Table 7.1. We take the value of δ_1 to be 1 in these simulations. The dimensionless system size was taken to be 2, *i.e.* $0 \leq r \leq 2$. The results are shown in Figure (7.2).

The peak of tumour cells produce acid, which diffuses into the nearby normal tissue, killing the nearest cells and providing a gap into which the tumour can grow. As the normal tissue to the right of the peak retreats, the cancer peak moves from left to right, leaving a core of dead cancer cells behind it, formed by cells dying due to lack of nutrient.

For the chosen values of parameters, we recorded the size of the tumour radius *i.e.* the largest value of r for which N_2 was non-zero. The results are shown in Figure (7-2). From this, we obtained an approximate speed of invasion, $c = 0.00967 \approx 0.00934$ mm/day, for the tumour. This speed is very comparable to those obtained from *in vitro* experiments on MCS

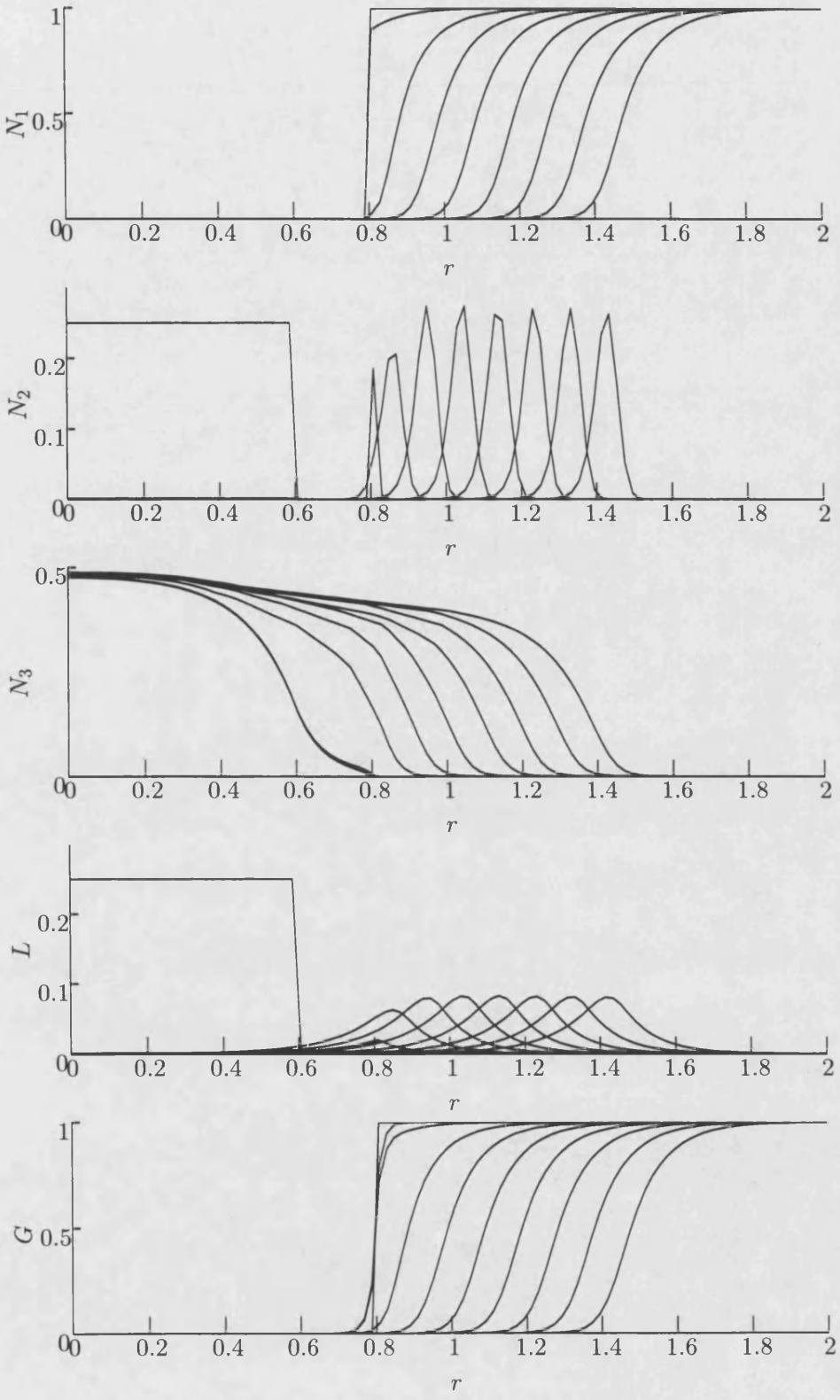

Figure 7-1: Graphs showing the development of the normal cell density, cancer cells density, dead cell density, acid concentration and nutrient concentration.

(0.006-0.016 mm/day [71]), but it could be decreased (or increased) by decreasing (increasing) one or more of Δ_2, δ_1, ρ_2 or ρ_5 or increasing (decreasing) either of δ_2 or δ_5.

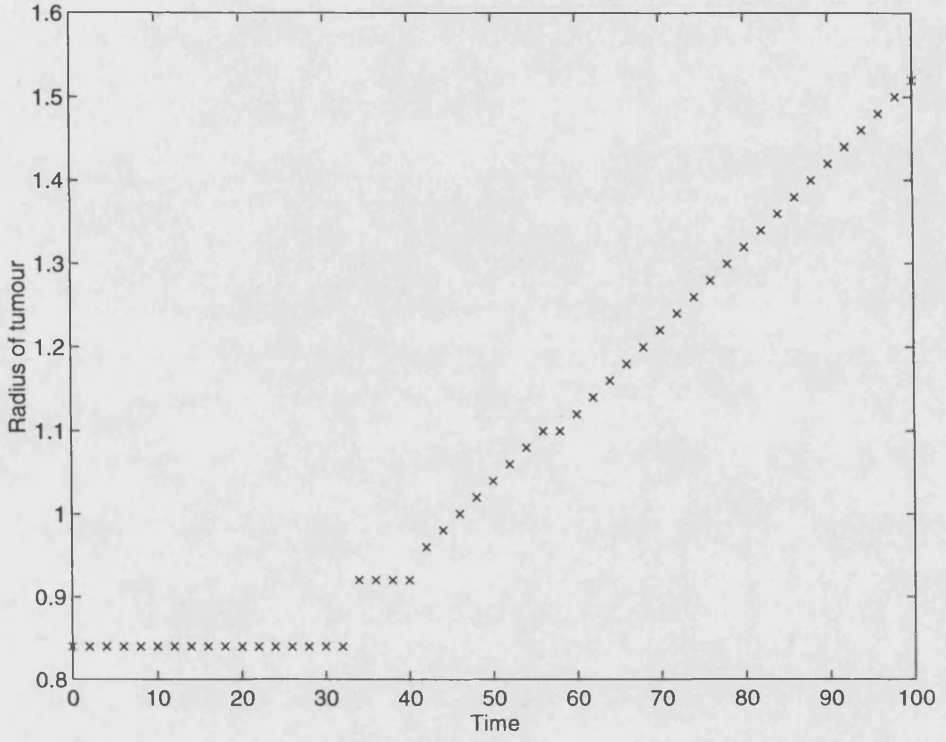

Figure 7-2: Graph of tumour radius vs. time.

7.3 Discussion.

This model includes the effects of nutrient on three-dimensional tumour growth and also includes acid-mediated invasion [86]. Unlike the model presented in Chapter 4, these are models of tumour invasion and hence the tumour does not stop growing. It is reasonable to assume that the model has travelling waves associated with it, although proving this would be beyond the scope of this thesis.

The model presented in this chapter is more biologically realistic than that of Gatenby and Gawlinski [86], as it incorporates variables which not only describe the interaction between a growing tumour and surrounding normal tissue, but also models large-scale tumour morphological structures such as central necrosis. Also, growth takes place in three dimensions, instead of just one.

We have replaced the unrealistic logistic growth term for cancer cells, which forces the tumour to occupy all available space, no matter what, with nutrient-dependent growth and death terms. This ensures that there is no co-existence between tumour and healthy tissue,

which seems more realistic for such a model of invasion.

As can be seen from Figure (7.2), the "travelling wave" of live cancer cells is a homotypic one, *i.e.* the density of live cancer cells drops back to zero behind the wave front. The dead cells readily fill the space that is left behind the rim of live cancer cells as it advances. As the variable r is describing the radius of a spherically symmetric tumour, our model gives rise to a tumour which has a rim of live, potentially proliferating cells, and a central necrotic core. The width of the live rim quickly tends to a constant, while its cells grow into the interstitial gap created by the acid production. The radius of the growing necrotic core shadows the growth of the tumour's outer radius.

In biological terms, to have a system which has travelling waves associated with it, is rather unrealistic, as all tumours are confined in their growth by the size of the host in which they reside, and its ability to remain alive while carrying a tumour burden. As we are considering an avascular tumour, the model should incorporate variables which restrain the growth of the tumour so that it saturates, as in experiments [71]. In order to obtain saturating growth in these models, quiescent cells, disintegration of dead cells (*i.e.* volume loss from the necrotic core) and the effects of metabolic wastes or a mitotic inhibitor would have to be included:

- If a percentage of the live tumour cells were no longer participating in mitosis and therefore in volume production, then this would lead to an overall decrease in the rate of increase in tumour volume. When cells die, they eventually disintegrate into chemical compounds which are freely permeable through cell membranes. The cell volume lost this way is replaced by cells pushed inwards by the forces of adhesion and surface tension. Thus, this would also cause a reduction in the increase of tumour volume.

- Metabolic wastes are produced by all living cells and are usually removed by nearby blood or lymph vessels. However, in an avascular tumour, where the only means of removal is diffusion, there will be a critical size (as with nutrient) where the wastes would not be sufficiently removed and nearby cells would be poisoned. These dead cells would then disintegrate, reducing the rate of increase in tumour volume. Some of the chemicals that spill out of the dead cells, when they die, may have damaging effects on the surrounding tissue [54] and perhaps cause the death of other cells, thus also leading to volume reduction.

- There is evidence that control of mitosis in some mammalian tissue is partially determined via negative feedback from the tissue itself [24, 175, 228]. The agents of negative feedback, chalones, are tissue specific, mitotic inhibitors produced by the tissues. It has been suggested that a breakdown in the normal functioning of the chalone mechanism may be responsible for limitless tissue growth in some types of cancer growth [24], but the addition of a mitotic inhibitor to our model would aid to decrease the total tumour

volume.

If the volume gained by the tumour, by growing into space formed by the disintegration of healthy cells killed by excess acid, can be balanced by the volume lost by all the above mentioned processes, then growth rate would eventually saturate. But, this would be a complicated system, and although it would perhaps be able to simulate initial exponential growth, the results would be very similar to the simple model presented in Chapter 4.

7.4 Simulation.

This simulation, based on the Extended Potts Model, discussed in Chapter 3, includes cells which grow and divide, cells which shrink and decay and cells which maintain relatively constant volume. We consider necrotic, quiescent and proliferating tumour cells as distinct types, in addition to live healthy cells and dead healthy cells, which are also considered as distinct types. Each type of cell has a different growth rate and volume constraint. Target volumes for live healthy, dead healthy and quiescent tumour cells remain constant in time. Target volumes increase for proliferating cells, to simulate growth and decrease for necrotic cells to simulate decay.

The volume constraints for proliferating, quiescent and necrotic cells are successively weaker. Accordingly, proliferating cells can grow at the expense of quiescent cells, which in turn, recoup their losses from decaying necrotic cells. As well as this hierarchy of volume constraints for the tumour cells, the volume constraints of proliferating tumour cells, live healthy cells and dead healthy cells are successively weaker. Proliferating tumour cells and healthy cells can grow at the expense of dead healthy cells, but tumour cells are more aggressive than healthy cells about keeping the volume that they have gained.

Again, as in all the other simulations, normal cells have the strongest adhesive bonds with normal cells and tumour-tumour bonds are the weakest, with tumour-normal bonds in between. Although growth and decay rates differ for proliferating, necrotic and quiescent cells, all tumour cells have the same binding properties. Similarly, live and dead healthy cells have the same binding properties.

Proliferating tumour cells grow in response to the demands of an increasing target volume with mitosis occurring whenever the ratio of surface area to volume for a cell drops below a threshold. This criterion for cell division reflects the fact that cell volume determines the demand for nutrients while cell surface area limits the rate of nutrient absorption. Since tumour cells grow and divide continuously without observing regulatory signals, the simplest assumption is that their growth rate is directly proportional to the supply of nutrients up to some saturating rate. The cell splits in a plane through the centre of mass corresponding to a minimal cross section with all the array elements on one side of the cell assigned a previously unused

index. After a split, each daughter cell starts with half the target volume of the parent cell so as not to be unduly stressed by a large deviation from the mandated size of the progenitor. Since, experimentally, mean tumour cell size is comparable to mean normal cell size, we apply mitosis at twice the typical cell size, which corresponds to a area/volume ratio of 0.6.

We do not include the growth of normal cells, since cell division in normal tissue does not affect the tissue volume. Inhibition of cell division in normal tissue keeps the rate of cell division in homeostasis with the rate of cell death. The much slower mitosis of normal cells should not affect the tumour's growth.

In addition to the lattice that stores the spin numbers of the cells, there are two further lattices which store the concentration of nutrient and the concentration of acid. These chemical lattices are then super-imposed on the cell lattice for calculations.

We assume that the healthy tissue (live and dead cells) is a homogeneous source of nutrient, and this nutrient is then allowed to diffuse into the tumour. The amount of nutrient consumed by tumour cells is taken to be proportional to their metabolic rates. Proliferating tumour cells consume the most amount of nutrient, whilst quiescent cells consume a quarter of this value [84] and dead cells consume none.

Tumour cells change type in response to the ensuing nutrient gradient within the tumour. In addition to type changes caused by shifting boundaries between regions within the tumour, individual cells can change type by relocating, as long as they are alive. Since cells are free to move by gradually shifting their boundaries at random, they occasionally migrate to an adjacent region of the tumour. When this migration happens, proliferating and quiescent cells change type according to nutrient availability. Though necrotic cells may undergo passive relocation, they are no longer viable and never revert to quiescence or proliferation.

Tumour cells' acid production is also proportional to their metabolic rate. Thus proliferating cells produce 4 times as much acid as quiescent cells (as they are absorbing 4 times as much glucose, which they then covert into lactic acid), whilst necrotic cells produce none. This acid diffuses from the tumour edge into the healthy tissue and healthy cells die when the acid concentration at a point becomes higher than a critical level. It is also assumed that the healthy cells "absorb" some of the acid. This is to take into account the mechanisms for increasing local pH e.g. buffering and large scale vascular evacuation.

The acid and nutrient concentrations are updated at every time step. We model the diffusion of the chemicals by using the following simple discretisation of the diffusion equation:

For a lattice site (x, y, z):

$$\text{updated chemical}(x,y,z) = \frac{1}{12}\left[6 \times \text{old chem'l}(x,y,z) + \sum_{n'bours,\ (x',y',z')} \text{old chem'l}(x',y',z')\right]$$

where (x', y', z') is one of the six nearest neighbours of (x, y, z).

Then the acid concentration (or nutrient concentration) that a cell, i, is subjected to is just the sum of acid (nutrient) concentration over all array sites (x, y, z) making up cell i.

The simulation of decay of necrotic cells by reduction of target volume depends upon depth within the tumour. It is assumed that cells nearer the centre of the tumour will have been dead longer than those near the necrotic/quiescent boundary and therefore will be more likely to have broken down into diffusible compounds and hence will lose volume more readily than those that have just died. So we take the rate of reduction of volume to be proportional to the individual cell's distance from the edge of the necrotic core, up to some saturating rate. Necrotic cells in the outer layer of the core maintain constant volume while cells in the fourth layer from the edge and beyond lose two units of volume at each time step with a linear increase in the decay rate for intervening layers.

The depth of a cell within the tumour is measured as the minimum distance from the centre of mass of the cell to the outer edge of the tumour along each of the three orientations of the array (*i.e.* in the x, y and z directions).

7.5 Results.

We start off with a small homogeneous aggregate of tumour cells surrounded by live healthy tissue. As in Chapter 3, most cells are initially set to be cuboids, to avoid packing problems, but the dynamics of the model soon cause them to round to a more natural shape. After a short while, an interstitial gap forms, consisting of dead healthy cells, which separates the tumour from the healthy tissue. The tumour then readily grows into this gap and eventually gets to the size where the nutrient can no longer diffuse sufficiently to the centre and a quiescent core forms - Figure (7-3). Further growth leads to the formation of a necrotic core. This can be seen in Figure (7-4).

By recording the total volume of the tumour at every time step, we can estimate the average radius, using the following formula:

$$\text{Average tumour radius } = \left(\frac{3}{4\pi}\text{Total volume of tumour}\right)^{1/3}.$$

Figure (7-5) shows the graph of tumour radius versus time. By calculating the gradient of the linear part of this graph, we can calculate the speed of invasion of the tumour to be 0.8 pixels/1000 MCTS.

For easier comparison, the two growth graphs, from the continuum model and the simulation, are shown in Figure (7-6). As can be seen, they are quite similar in shape and so we can say that 0.8 pixels/1000 MCTS $\approx$ 0.00934 mm/day.

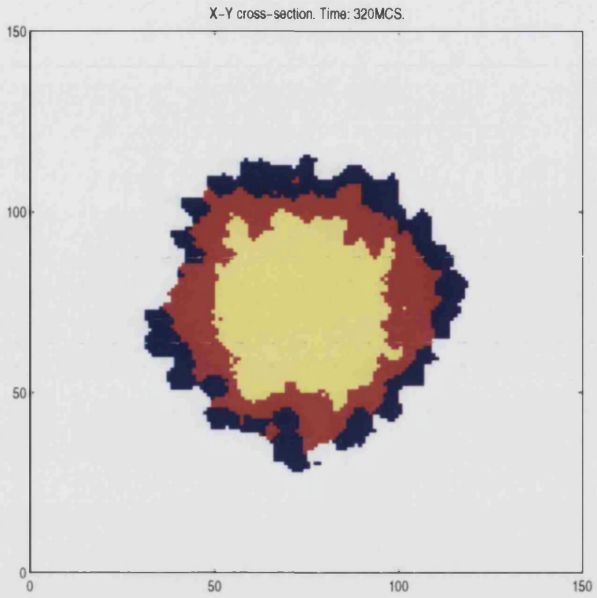

Figure 7-3: Simulation results. Key: white= healthy cells, light grey = quiescent, darker grey = dead healthy cells, dark grey = cancer cells.

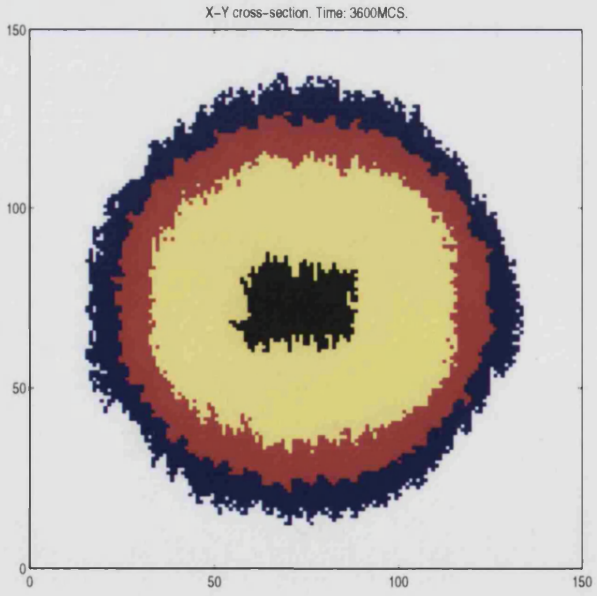

Figure 7-4: Simulation results. Key: white= healthy cells, light grey = quiescent, darker grey = dead healthy cells, dark grey = cancer cells, black = necrotic core.

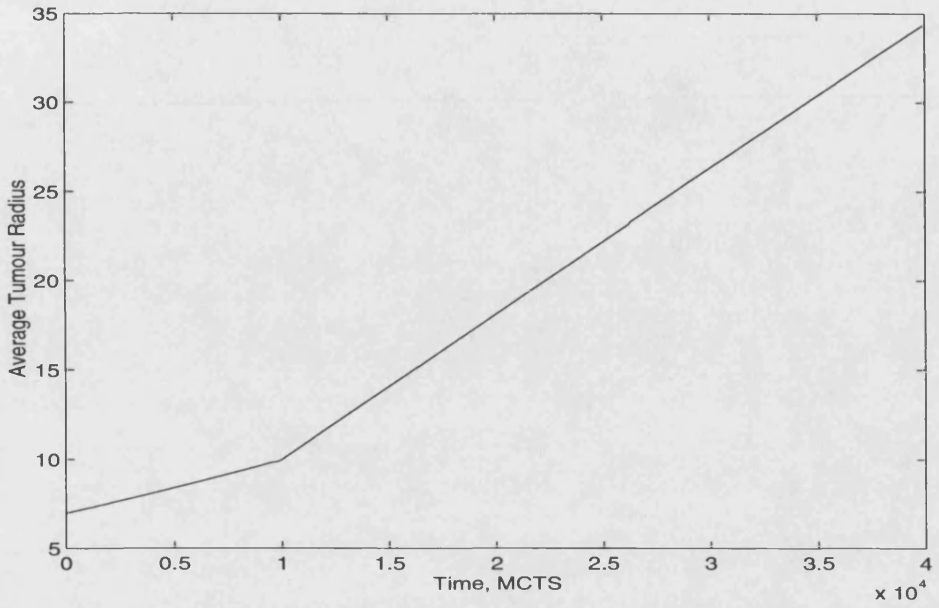

Figure 7-5: Graph of average tumour radius versus time.

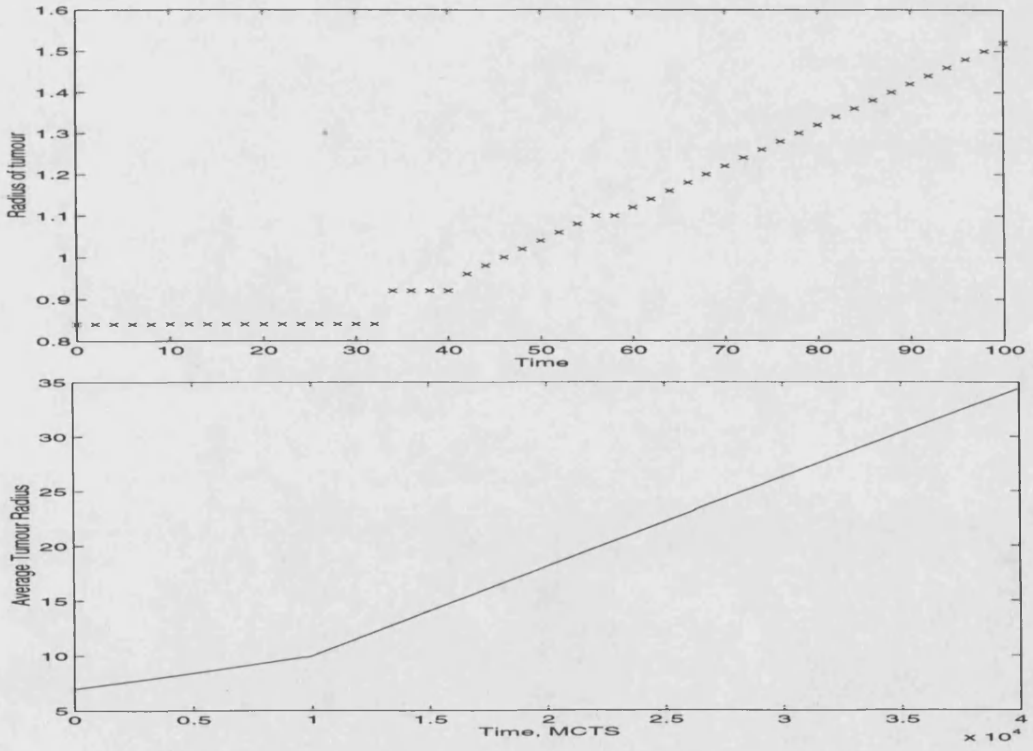

Figure 7-6: Comparison of radius graphs of continuum model (top) and simulation (bottom).

7.6 Conclusion.

In this chapter, we have extended Gatenby and Gawlinski's [86] one-dimensional model of acid-mediated tumour invasion. The present three-dimensional model is more biologically realistic, as we not only incorporate variables which describe the interaction between a growing tumour and surrounding normal tissue, but also model large-scale tumour morphological structures such as central necrosis. The tumour has an outer rim of live, potentially proliferating cells, which grow into the interstitial gap created by tumour-produced acid. A growing necrotic core closely follows behind the rim of live tumour cells.

We have replaced the unrealistic logistic growth term for cancer cells, which forces the tumour to occupy all available space, no matter what, with nutrient dependent growth and death terms. This ensures that there is no co-existence between tumour and healthy tissue, which seems more realistic for such a model of invasion.

We then presented a simulation which included acid-mediated invasion of an avascular tumour into healthy tissue, the diffusion of an essential nutrient into the tumour and the growth and death of tumour cells, dependent on this nutrient. The growth graph of the average tumour radius was then compared to the graph of development of the tumour radius in the continuum model. The two graphs were visually very similar in shape and so we are able to say that 0.8 pixels/1000MCTS $\approx$ 0.00934 mm/day.

Chapter 8

Angiogenesis and Metastasis

8.1 Angiogenesis.

Neovascularisation is the formation of new vessels in tissues in which the previously existing vessels do not function at all or are not sufficient any longer. Angiogenesis is generally considered as the formation of blood vessels during embryonic development, in several other developmental processes, under pathologic conditions, and in tumours [180].

All living tissues require nutrients and oxygen and must get rid of the waste products. In tissues larger than a critical size, diffusion of these substances is an inadequate supply method and a circulatory system, e.g. lymph or blood, is needed [172]. Since malignant tissues often have increased requirements [183], they also need vascularization. Tumours cannot grow beyond a few million cells (1-3mm in diameter) without a dedicated blood supply [232]. Research carried out by Folkman *et al.* [66, 74] shows that cancer cells produce distinct chemicals, collectively known as Tumour Angiogenesis Factor (TAF), which stimulate the rapid formation of capillaries. It is not known what triggers this activity [180].

There are two types of angiogenic factors, those that act directly on the vascular endothelial cells and those that induce other cells into producing factors which act on the endothelial cells [69, 72]. Several angiogenic factors have been identified in recent years. [72] contains a summary of these factors. It appears that for angiogenesis to occur, several angiogenic factors need to act together, either directly or indirectly.

As the tumour, *in vivo* approaches its diffusion limited size, the local TAF concentration increases and induces neighbouring blood vessels to grow towards and into the colony. The new capillary growth induced by TAF is even more rigorous and continuous than a similar outgrowth of capillary sprouts observed in fresh wounds or an inflammation [66].

TAF is not found in any normal tissue in the body, except the placenta. It does not produce a permanent change in capillary endothelial cells, since withdrawal of TAF is followed by the

disappearance of newly formed capillaries [66].

Once the capillaries reach the tumour, the malignancy becomes vascularized and perfusion supplants simple diffusion as the dominant mechanism for the supply of nutrients and the removal of wastes. As soon as the tumour connects with the circulatory system, all constraints imposed on it by diffusion are eliminated and subsequent growth is explosive [102]. This burst seems to be governed by an equilibrium between the rate of proliferation and the absolute distance from a vessel [124]. The initial necrotic core disappears after neovascularisation of the tumour [15]. However, necrosis reappears in spite of the dense vasculature. This seems to be due to the enormous increase in tumour volume and physical obstruction of the capillaries via compression by the expanding tumour mass.

The exponential growth is also not maintained indefinitely. When the diameter of the tumour reaches 1-3 cm [67], the growth rate slows down and the growth curve is more Gompertzian (see Section (1.3)) rather than an exponential curve [4]. Several ideas have been proposed to explain the overall deceleration in growth of the vascular stage. Tannock [212] observed that in a mouse mammary tumour, the capillary endothelial cells' turnover time was longer than that of the tumour cells. This means that the distance between capillaries increases as the tumour grows and the proliferation rate far from the capillaries then decreases, giving rise to an overall decrease in the growth rate of the tumour as a whole. Another observation is that when a tumour is 1-3cm diameter, vascular obstruction occurs [97]. This confines flow to the outer periphery of the tumour and may give rise to the formation of large regions of necrosis [67]. Folkman also put forward the idea that there may be a critical depth within most tumours beyond which there is no blood flow due to external pressures.

As well as the rapid increase in tumour growth, the vascularization of a tumour can have other serious consequences. It has been suggested that angiogenesis is a precursor to a more malignant phase of growth [20, 75, 91, 180] in that the vascularization of a tumour promotes the propagation of the more aggressively growing tumour cells [190]. These malignant tumour cells actively invade and destroy the adjacent host tissue. At this stage, the malignant carcinoma loses its quasi-spherical shape and the periphery of the tumour is covered with finger-like protrusions, resulting from the local invasion of the host tissue [47, 232]. The irregular shape of such a tumour can cause complications during surgical excision of a cancer, since the tumour may only be partially visible and the surgeon is required to remove tissue beyond the observed tumour boundary in order to prevent regrowth.

Finally, the most important and frequently devastating consequence of tumour vascularization is the increase in the risk of metastasis [60, 150, 169]. The immature vasculature is easily invaded by the actively mobile tumour cells, and hence the disease can be spread around the body via the blood system. There is a direct correlation between the intensity of tumour vasculature and the metastatic potential of the tumour [60, 150, 169]. Indeed, the density of

the tumour vasculature can now be used as a prognostic factor [77].

Cancer cells often occupy less than half the volume of a tumour. One to ten percent of the volume is contributed by blood vessels weaving through the tumour mass. The remaining space is filled primarily by an abundant collagen-rich matrix - the interstitium - that surrounds cancer cells and can separate them from the vasculature. (Healthy tissue contains an extracellular matrix as well, but the interstitium in tumours is usually more extensive) [122].

All studies on tumour-related angiogenesis so far have shown that the growth of tumours (primary and metastases) is dependent on vascularization, and therefore on angiogenesis [75]. The blood supply of an organ, once established, is very stable, but that of a tumour is much more transient. Experimental results indicate that a tumour must continually recruit new blood vessels to keep from withering away [147]. When blood flow into the tumour is prevented, tumour growth stops and regression to complete extinction may occur [13, 73].

8.1.1 The Process of Angiogenesis.

Many techniques have been formulated in order to examine the sequence of events leading up to neovascularisation. For example, the cloning of capillary endothelial cells in culture is a method used for studying angiogenesis *in vitro* [69, 70, 121]. It would be too complex and complicated to study angiogenesis in a whole organism, but *in vitro* studies give quite general results, so various model systems have been formulated *in vivo*. Some examples of the models using implants of tumour fragments to induce angiogenesis are the rabbit ear chamber [117], the transparent chamber in mouse skin [6], the mouse corneal micropocket [164], the hamster cheek pouch chamber [98, 226], the rabbit corneal micropocket [91], the chick chorio-allantoic membrane [5] and the dorsal air sack in rats [74]. Some of these models are reviewed in [75].

The main function of endothelial cells is the lining of the different types of vessels: venules and veins, arterioles and arteries and small lymphatic vessels [136, 180]. These cells lie in a monolayer upon a continuous basal lamina which serves as a scaffold and intercellular contacts between the endothelial cells are very close. Folkman [69] showed that endothelial cells can construct a capillary tube, make branches and assemble an entire capillary network *in vitro*, unaided by other cell types. This is a large factor in their important rôle in angiogenesis.

The initial reaction of the endothelial cells in neighbouring blood vessels, which are nearest the source of TAF, is to start altering their structure. The cells thicken and finger-like protrusions can be observed on the abluminal surface [14, 180]. They then start to produce proteases and collagenases. These chemicals begin to make the basal lamina beneath the activated endothelial cells thinner and weaker. Intercellular gaps between endothelial cells form due to the weakening of intercellular contacts and those cells which have loosened their contacts with their neighbours are free to migrate towards the chemotactic stimulus [234]. Neighbouring cells then

migrate to fill the gap that the others have left. The migrating endothelial cells accumulate in the region where TAF concentration first reached a threshold level and the congregation of endothelial cells in one place causes the wall of the vessel to bulge which leads to the formation of a sprout.

Only very small cells or molecules can normally pass through the gaps in the basal lamina and so the endothelial cells continue to secrete enzymes which degrade a hole in the basal lamina, degrade the intercellular matrix through which they must migrate [147] and also degrade the stroma in the extra cellular matrix surrounding this hole.

The first steps of angiogenesis are performed by migrating endothelial cells only and no proliferation occurs [180]. The capillary sprouts can only grow in length by recruiting endothelial cells from the parent vessel. Sprouting can occur without proliferation, although the growth of these sprouts ceases after a few days if proliferation is prevented. If the sprouts did continue to grow, gaps, resulting in abnormal permeability would develop in the parent vessel. Thus, proliferation of endothelial cells is necessary for a successful completion of angiogenesis [196]. Migration and proliferation are independent events and separate angiogenic factors may be required to stimulate these activities of endothelial cells [14].

In the initial stages of neovascularisation, the outgrowing sprouts are solid strands of endothelial cells. The first sign of tube formation is the appearance of vacuoles within the cytoplasm of capillary endothelial cells. Neighbouring cells develop subsequent similar vacuoles which later fuse to form a tube-like structure. The establishment of these lumina is independent of any known stimulus [180].

Branching of tubes occurs in a similar way. The intracellular vacuoles become Y or T-shaped, and branching is realised off the principal tube by the fusion of neighbouring vacuoles [69].

In the second stage of neovascularisation, cells immediately behind those at the tip proliferate, pushing the lumen forward [147].

Circulation cannot be observed at first in the tubes, as most of the sprouts are dead ends. The process of fusion of neighbouring sprouts or tubes is called anastomosis, and is one of the most important events during angiogenesis.

Initially, sprouts from one parent vessel grow roughly parallel to each other [108, 109, 154]. After a specific distance away from the parent vessel, they incline toward each other. Neighbouring sprouts come near to each other at their leading tips. The endothelial cells at the very top of each tip form finger-like protrusions which meet and make first contacts with each other. These primary contacts tighten and develop into contact structures. Intercellular gaps in both tips enlarge and unite to form a continuous lumen.

A new basal lamina is not formed immediately during migration and proliferation within a sprout. During the maturation of newly formed vessels, endothelial cells lay down a basal layer

all over the new vessel to reinforce the vessel and change its permeability. This seems to occur in cooperation with pericytes or advential cells [36], which during this stage migrate toward the vessel wall and make close contacts with endothelial cells.

Even after the formation of the basal lamina and the immigration of pericytes, permanent repair and remodelling of the new vessel's wall takes place. Migration of endothelial cells does not cease completely and the cells move up and down the new tube. New sprouts can also form from the new vessel.

Blood circulation commences as soon as loops (anastomoses) and a network of connected tubes have formed, since the new lumina are connected directly to the parental vessel. Angiogenesis still proceeds until the whole tumour is penetrated. Even then, the process does not stop since new tumour masses are continually being produced, which need to be vascularized and within solid tumours, newly formed blood vessels frequently collapse and regress.

8.1.2 Angiogenesis Simulation.

This simulation, based on the Extended Potts model, discussed in Chapter 3, includes tumour cells, healthy cells and a blood vessel. We simulate on a three dimensional lattice which contains a tumour, surrounded by healthy cells and a blood vessel running along one side.

We consider the tumour to be in a diffusion limited steady state, where the increase in total volume of the tumour, due to proliferation, is balanced by the volume lost due to necrotic disintegration. Thus, although some tumour cells are still proliferating, the total volume remains constant.

For simplicity, the effects of nutrient on cancer cell growth are ignored, as this has no effect on the overall size of the tumour. Hence it is assumed that the tumour is homogeneous and consists only of cells who neither grow nor die, *i.e.* cancer cells whose target volumes remain constant in time. The target volumes of healthy cells also remain constant as we are again ignoring growth of normal tissue. The volume constraints for cancer and healthy cells are the same.

Healthy cells have the strongest adhesive bonds with healthy cells and tumour-tumour bonds are the weakest, with tumour-healthy bonds in between. The resulting surface tension keeps the tumour compact. This hierarchy of binding strengths is consistent with biological evidence [167, 232].

As well as having a lattice which stores the spin number of a cell at its lattice sites, there is a second lattice which stores the value of TAF concentration at each lattice site. This chemical lattice is then super-imposed on the cell lattice for calculations.

The tumour cells produce TAF which then diffuses through the normal tissue towards the blood vessel. The TAF lattice is updated at every time step. We model the diffusion of TAF by using the following simple discretisation of the diffusion equation:

For a lattice site (x, y, z):

$$\text{updated TAF}(x,y,z) = \frac{1}{12}\left[6 \times \text{old TAF}(x,y,z) + \sum_{n'bours,\ (x',y',z')} \text{old TAF}(x',y',z')\right]$$

where (x', y', z') is one of the six nearest neighbours of (x, y, z).

Then the TAF concentration of a cell i is just the sum of TAF concentration over all array sites, (x, y, z), making up cell i.

If the concentration of TAF at a point on the blood vessel is high enough, then a sprout is formed. These sprouts are the beginning of the formation of a capillary. To keep things simple, individual endothelial cells are not considered, and the initial sprouts are just blocks of cells. The endothelial cells in the sprouts and capillaries grow towards the tumour up the gradient of TAF extending from it. We model this growth by allowing a pixel belonging to a capillary to grow into one belonging to a healthy cell with probability given by:

$$P(\text{capillary grows into healthy cell}) = \begin{cases} 0 & \text{if } \Delta C \leq 0 \\ 1 - \exp(-\Delta C/3) & \text{if } \Delta C \geq 0 \end{cases} \quad \text{where}$$

ΔC = TAF concentration at healthy cell pixel − TAF at capillary pixel.

8.1.3 Results.

We start off with a tumour at its diffusion limited steady state, embedded in healthy tissue. A blood vessel runs down the side of the lattice - Figure (8-1). For clarity, all pictures show a cross-section though the tissues and individual cells are not shown.

As in the other simulations, all cells are initially set to be cubes to avoid packing problems but again the dynamics of the model quickly allows them to round to a more natural shape.

After a while, the concentration of TAF, at the nearest point of the blood vessel to the tumour, builds up until eventually it reaches the threshold level where it initiates the formation of a sprout - Figure (8-2). At a later time again, more sprouts have formed along the length of the blood vessel and the older sprouts have started to grow towards the tumour - Figure (8-3). Note that this growth takes place in three dimensions.

Eventually some of the capillaries join up to form anastomoses - Figure (8-4) and carrying on growing until the tumour is finally penetrated - Figure (8-5).

8.1.4 Discussion.

This is a very simple simulation of angiogenesis and only the essential features have been concentrated on. The effects of nutrient on the tumour and the dynamics of the tumour cells have been ignored and also the blood vessels thought of as a single entity, instead of consisting

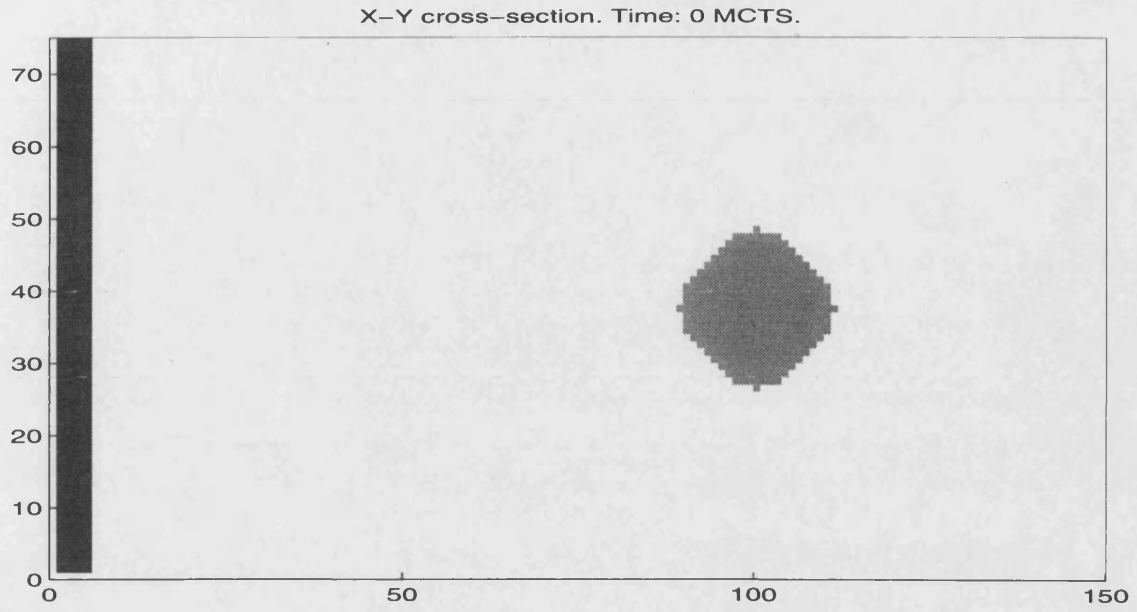

Figure 8-1: Initial configuration of the tumour (light grey) embedded in healthy tissue (white), with a blood vessel (dark grey) running down the side of the lattice.

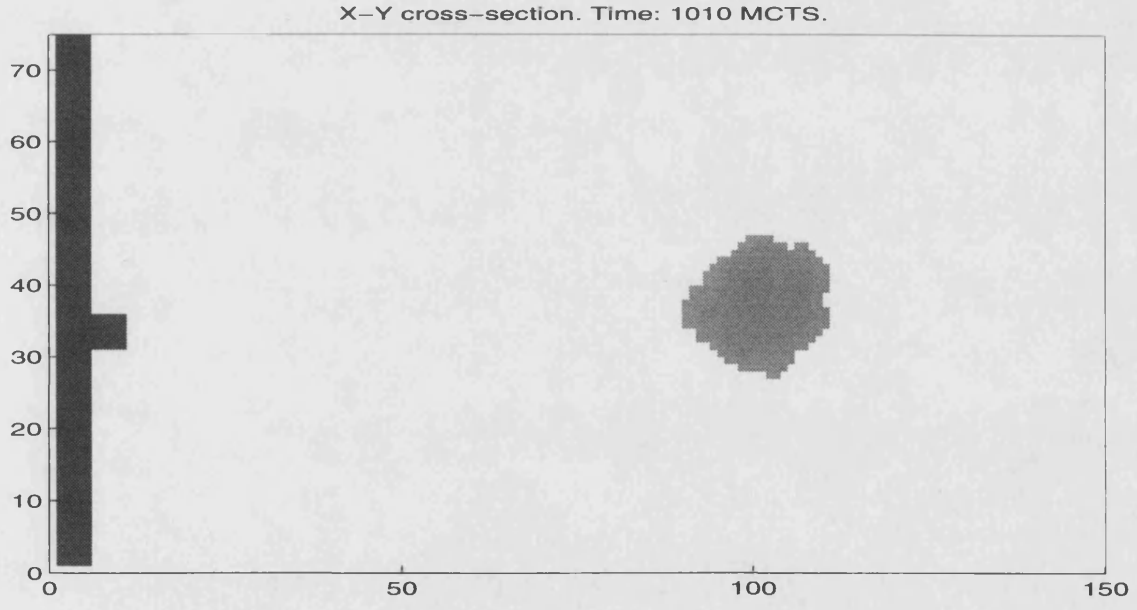

Figure 8-2: Formation of a sprout. Key: light grey=tumour, white=healthy cells, dark grey=blood vessels.

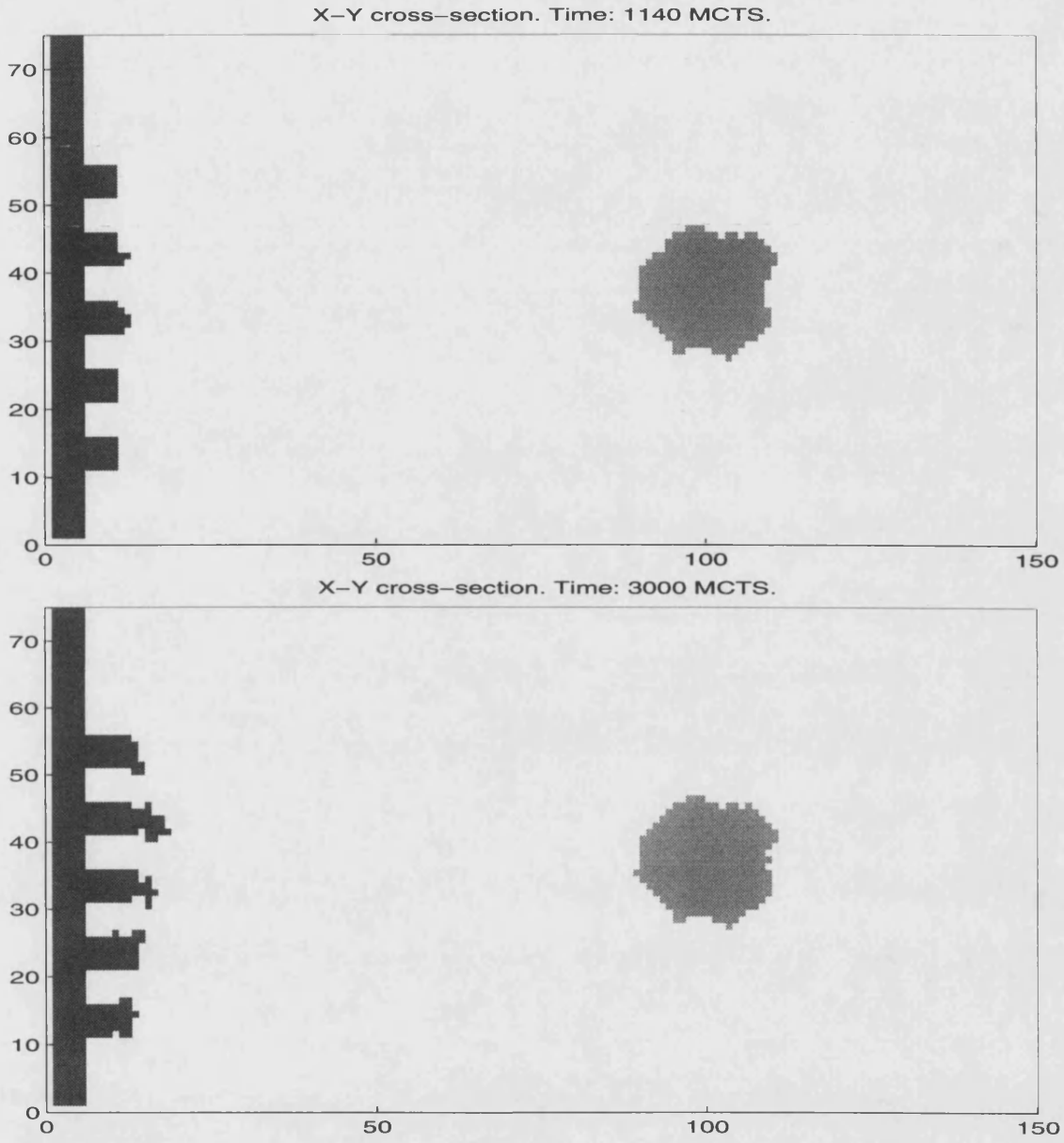

Figure 8-3: Growth of capillaries towards tumour. Key: light grey=tumour, white=healthy cells, dark grey=blood vessels.

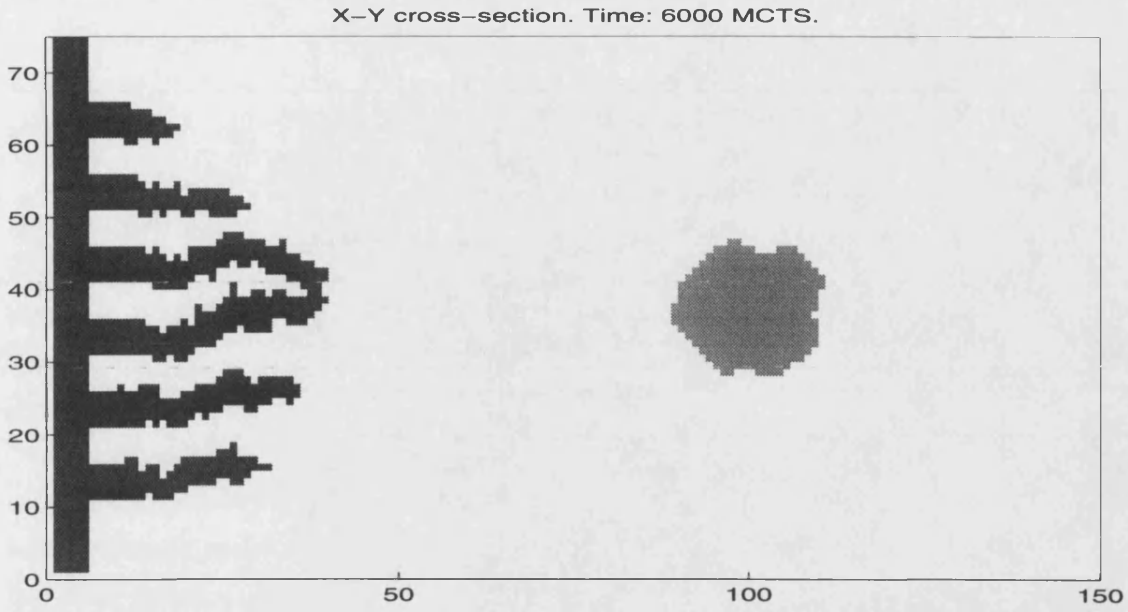

Figure 8-4: Formation of an anastomose. Key: light grey=tumour, white=healthy cells, dark grey=blood vessels.

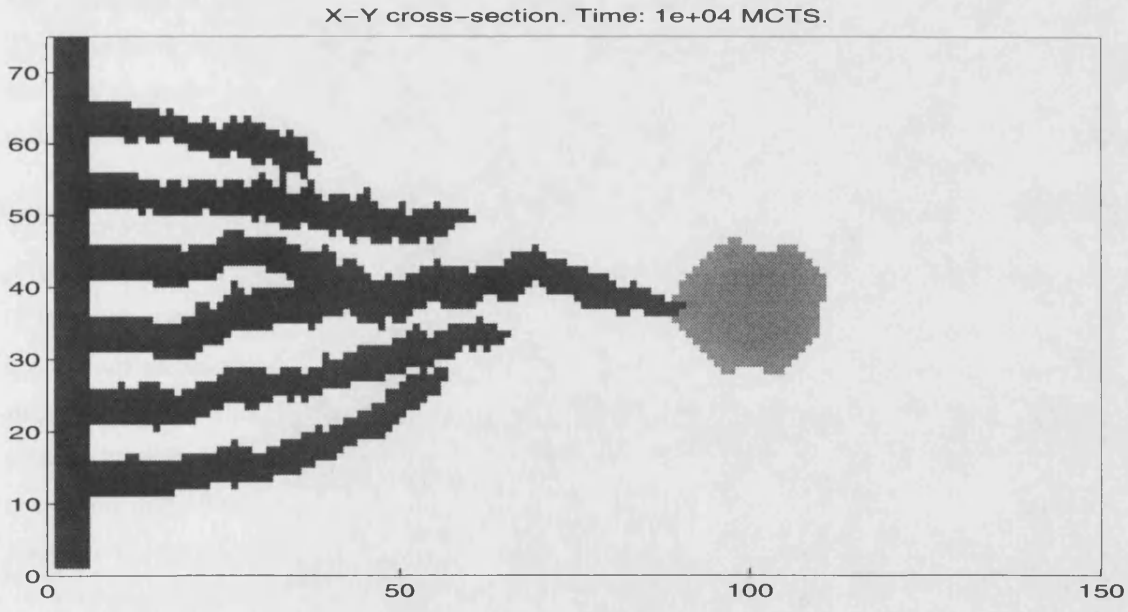

Figure 8-5: Penetration of tumour by capillaries. Key: light grey=tumour, white=healthy cells, dark grey=blood vessels.

of individual cells. However, as Figures 8.1-8.5 show, the global details of angiogenesis have been captured well.

In order to make the simulation more realistic, we would have to include the dynamics of individual endothelial cells that constitute the walls of the blood vessels and also the effects of nutrient on the tumour.

The migration of endothelial cells towards the initial chemotactic stimulus could be modelled by adding TAF governed movement for EC in the cell sorting part of the code. Also, TAF-dependent proliferation of EC should be added to model the proliferation of EC behind the tip of the sprout. The formation of lumen within the capillaries could be achieved by changing the coupling strengths of the endothelial cells - see [95] for details of vacancy nucleation in simulations using the Potts model.

The diffusion of nutrient from the blood vessel to the tumour should be added and tumour cells should become quiescent or die, according to the level of nutrient that they are receiving. This would mean that the growth of the tumour was in dynamic equilibrium, instead of just being switched off, and would lead to an explosion in growth once the tumour had been penetrated by the capillaries.

8.2 Metastasis.

Malignant tumours may spread to distant sites, with cells detaching from the primary tumour and migrating to remote sites via the blood stream, in the lymphatics or across tissue spaces. This process is known as metastasis and the secondary tumours formed are metastases. The majority of deaths from cancer are due to the formation of metastases at sites remote from the primary tumour.

The most common type of malignant tumours are carcinomas (cancer of the epithelia), which are solid tumours of the external and internal surfaces of tissues and organs. Lung cancer, prostate cancer, breast cancer and colorectal cancer account for over 50 % of all reported cancer in England and Wales [173]. In the majority of patients suffering from carcinomas, the disease has already metastasised before detection, resulting in multiple metastases which may occur in sites far removed from the primary cancer. Hence, the disease cannot be cured by treating the primary tumour alone. Metastases can be difficult to treat, can cause a number of unpleasant symptoms and often prove to be fatal. The estimated annual death rate is 1 in 341 for men and 1 in 387 for women [174].

Vascularization of the tumour increases the risk of metastasis [60, 150, 169], as the immature vasculature is easily invaded by the actively mobile tumour cells, and hence the disease can spread around the body via the blood stream.

It is thought that tumour metastasis is a highly selective competition favouring the survival

of a subpopulation of metastatic cells pre-existent within the heterogeneous population of the primary tumour [63]. This metastatic subpopulation dominates the primary tumour mass early in its growth. The cells in the subpopulation grow faster than the other tumour cells, adhere less to each other and become more metastatic the more they divide. They seem to have the ability to divide many more times than other tumour or normal cells.

Tumour cells are thought to be more easily separated from a solid tumour mass than their counterpart normal cells from surrounding tissues [167, 221]. Also, adhesion between highly metastatic cells and other tumour cells is noticeably lower than that demonstrated by normal cells or benign tumour cells [207]. This implies that the organisation of tumour cells within the tumour itself may influence metastatic behaviour - if the subpopulation of metastatic cells is initially in the centre of the tumour, then the cells are less likely to be able to escape from the mass than those near the periphery, or they may even die due to lack of nutrient or poisoning by toxic waste products.

The arrest and metastasis formation of lymph-borne tumour cells at the regional lymph nodes and the arrest of malignant cells that enter the blood stream and form distant organ metastases are thought to be determined by anatomical and mechanical considerations [167]. It has been known for a long time that different types of cancer tend to form secondary tumours in certain organs and not in others [47]. The important tumour cell properties in the mechanical lodgement of circulating tumour cell clumps are their release into the lymph and blood systems and their abilities to undergo heterotypic and homotypic adhesion during their transport to distant sites. The most frequent distant organ site of blood-borne metastatic involvement is lung.

To explain metastatic colonisation that cannot be due to mechanical lodgement and anatomical considerations, Paget [178, 179] proposed the 'seed and soil' hypothesis. This proposes that the micro-environment of each organ (the 'soil') influences the implantation, invasion and survival of particular tumour cells ('seed'). Tumour cells that form metastases are not invincible, and cannot grow just anywhere. It follows from Paget's hypothesis that both seed and soil must have unique properties. For example, the cancer cell must be able to survive the journey through the blood stream, have the capacity for implantation on the 'chosen' organ and be able to survive and multiply to form a new colony once implantation has occurred. Also, the organ must be susceptible to implantation of the cells and be a suitable site for proliferation and vascularization to occur.

8.2.1 Metastasis Simulation.

We extend the simulation presented in Chapter 3 to include cancer cells that vary in their growth rate and adhesivity. All details of the simulation are the same, except for this. We model solely the first stage of metastasis, *i.e.* the separation of single or clumps of cells breaking away from

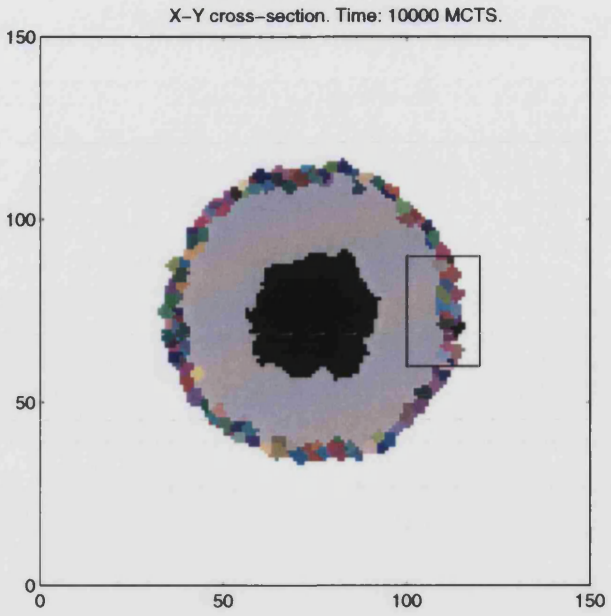

Figure 8-6: Formation of necrotic core and loosening of some cell bonds. Healthy cells, quiescent tumour and dead cells are not shown individually, but represented by solid blocks of white, grey and black, respectively.

the tumour mass, and do not consider invasion of cells into blood or lymphatic vessels or their subsequent implantation and growth in a suitable organ.

When a tumour cell divides, its daughters do not always have the same properties as the parent [167, 232]. For example, daughter cells may be more aggressive in their growth and also adhere less to other cancer cells, thus being more likely to break away from the tumour mass into the normal tissue. The model presented in Chapter 3 is developed to include the first stage of metastasis by allowing the daughter cells to have randomly fluctuating growth rates and adhesivities with respect to the values of their parent cell, according to a probability matrix.

8.2.2 Results.

We start off with the same initial conditions as in Chapter 3, with cuboid cells Figure (3-2). Later, when a quiescent shell and a necrotic core have formed, there is evidence of cells in the proliferating rim which are weakening their bonds with their neighbours. The development of one of these cells is shown in Figure (8-7), where the pictures are close-ups of the region of the tumour outlined in Figure (8-6). (This box moves with the periphery of the tumour as it grows). Once the cell has separated itself from the tumour, it is free to move through the healthy tissue towards a blood or lymphatic vessel. Although only a single cell is shown to have broken away from the tumour mass, this simulation has the capacity to model small aggregates of tumour cells breaking away from the tumour mass.

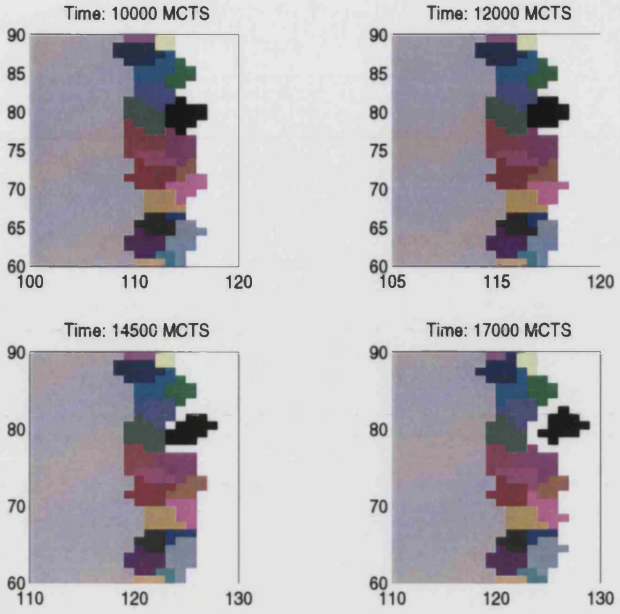

Figure 8-7: Detail of cancer cell (black) loosening its bonds with its neighbours. Cancer cells are shown individually and quiescent cells are shown as a solid block of grey.

8.2.3 Discussion.

The simplest simulation of avascular tumour growth, presented in Chapter 3, was developed to model the separation of cancer cells from a tumour mass. The growth rates and adhesivities of daughter cells were allowed to fluctuate from that of their progenitor and this led to the separation of a cell on the periphery from the tumour mass. The more realistic simulation of Chapter 7 could be developed in the same way to produce similar results.

8.3 Conclusions.

In this chapter, we have discussed the biological background of angiogenesis and tumour metastasis. We then presented simulations of these important processes.

The approach to simulating angiogenesis was a very simple one. Individual endothelial cells were not considered and the effects of nutrient on the tumour and the dynamics of the tumour were ignored. However, the results captured the global details very well. Using the ideas of the previously presented simulations, this model could be extended to a very realistic simulation of angiogenesis.

The simulation of tumour metastasis was also very simple in the approach taken to modelling it, but again, combined with other ideas presented in this thesis, a more realistic model could be generated.

Conclusions

The aim of the work in this thesis has been to explore the two main avenues of mathematically modelling tumour growth - continuum models and computer simulations. From very simple simulation models of cell movement and proliferation, we gradually built up a realistic simulation of avascular tumour growth. Every step of progress in the simulation was mirrored by a continuum model describing similar processes.

The simulations produced results which agreed closely with experimental results, but the parameters in the continuum models were much easier to verify in accuracy, as they could be varied more widely, while still maintaining fairly realistic tumour growth.

The parts of this thesis which are most relevant, and perhaps most useful, from a biological point of view, are the simulations presented in Chapter 8 on tumour metastasis and angiogenesis. From the work done here, a simulation could be produced that modelled a tiny tumour, provided with nutrient that has diffused from a nearby blood vessel, growing until it reached its diffusion-limited steady state. The cells within the tumour would be genetically unstable and when dividing, would produce daughter cells that had the potential to separate from the tumour mass. At the same time, the tumour would be producing TAF which would diffuse towards the nearby blood vessel and eventually cause sprouts to form on it. The process of angiogenesis would then proceed, as in Chapter 8, or maybe in a less simple manner, until the capillaries penetrated the tumour. At this point, the growth of the tumour would be explosive, and the blood vessels would be close enough to the tumour for the metastatic cells to enter the blood stream and be taken to places where they could implant and form another colony.

Having a simulation that models the growth of a tumour from the initial stages, to the point where the tumour presents a threat to the health of its host, could be a very useful tool for clinicians who wish to investigate specific aspects of growth, or new methods of angiogenesis prevention.

Bibliography

[1] J.A. Adam. A simplified mathematical model of tumour growth. *Mathematical Biosciences*, **81**:229–244, (1986).

[2] J.A. Adam. A mathematical model of tumour growth II Effects of geometry and spatial non-uniformity. *Mathematical Biosciences*, **86**:183–211, (1987).

[3] J.A. Adam. A mathematical model of tumour growth III Comparison with experiment. *Mathematical Biosciences*, **86**:213–227, (1987).

[4] J.A. Adam and N. Bellomo, editors. *A Survey of Models for Tumor-Immune System Dynamics.* Birkhäuser, Boston, U.S.A., (1997).

[5] O.S. Alfthan. Comparative study of the growth of skin and human skin tumours on the chorio-allantoic membrane of the embryonated chicken eggs. *Annals Med. Exp. Biol. Fenn.*, **34**:36, (1956).

[6] G.H. Algire. The adaption of the transparent chamber technique to the mouse. *Journal of the National Cancer Institute*, **4**:1, (1943).

[7] E.L. Alpen and M.S. Mendonca. Nutritionally induced quiescence of 9L cells: correlations with increased survival after X-irradiation. *Proceedings: 34th Annual Radiation Research Society Meeting*, (1986).

[8] M.P. Anderson, D.J. Srolovitz, G.S. Grest, and P.S. Sahni. Computer simulation of grain growth - I. kinetics. *Acta Metallica*, **32**:783–791, (1984).

[9] P. Antonelli, D.I. MacClaren, T.D. Rogers, M. Lathrop, and M.A. Willard. Pattern-reversal, engulfment and duality in exchange-type cell aggregation kinetics. *Journal of Theoretical Biology*, **49**:385–400, (1975).

[10] P. Armstrong. Cell sorting out: The self-assembly of tissues in vitro. *Critical Reviews in Biochemistry and molecular Biology*, **24**:119–149, (1989).

[11] D.G. Aronson and H.F. Weinberger. Multidimensional nonlinear diffusion arising in population genetics. *Advances in Math.*, **30**:33, (1978).

[12] B.S. Ashby. pH studies in human malignant tumours. *Lancet*, **2**:312–315, (1966).

[13] D.H. Ausprunck, K. Falterman, and J. Folkman. The sequence of events in the regression of corneal capillaries. *Laboratory Investigations*, **38**:284–294, (1978).

[14] D.H. Ausprunk and J. Folkman. Migration and proliferation of endothelial cells in preformed and newly formed blood vessels during tumor angiogenesis. *Microvascular Research*, **14**:53–65, (1977).

[15] D.H. Ausprunk, D.R. Knighton, and J. Folkman. Vascularization of normal and neoplastic tissues grafted to the chick chorioallantois. *American Journal of pathology*, **79**:597, (1975).

[16] R. Baserga. Resting cells and the G1 phase of the cell cycle. *Journal of Cellular Physiology*, **95**:377–382, (1978).

[17] E. Ben-Jacob, H. Brand, G. Dee, L. Kramer, and J.S. Langer. Pattern propagation in nonlinear dissipative systems. *Physica D (Amsterdam)*, **14D**:348–364, (1985).

[18] J.J. Berman and G.W. Moore. Spontaneous regression of residual tumor burden: prediction by Monte Carlo simulation. *Analytical Cellular Pathology*, **4**:359–368, (1992).

[19] J.J. Berman and G.W. Moore. The role of cell death in the growth of preneoplastic lesions: a Monte Carlo simulation model. *Cell Proliferation*, **25**:549–557, (1992).

[20] C.H. Blood and B.R. Zetter. Tumor interactions with the vasculature - angiogenesis and tumor-metastasis. *Biochemica et Biophysica Acta*, **1032**:89–118, (1990).

[21] Y. Boucher, M. Leunig, and R.K. Jain. Tumor angiogenesis and interstitial hypertension. *Cancer Research*, **56**:4264–4266, (1996).

[22] A. Bredel-Geissler, U. Karback, S. Walenta, L. Vollrath, and W. Mueller-Klieser. Proliferation-associated oxygen consumption and morphology of tumor cells in monolayer and spheroid culture. *Journal of Cellular Physiology*, **153**:44–52, (1992).

[23] N.F. Britton. *Reaction-Diffusion Equations and Their Applications to Biology.* Academic Press, (1986).

[24] W.S. Bullough. Mitotic and functional homeostasis: A speculative review. *Cancer Research*, **25**:1683–1727, (1965).

[25] W.S. Bullough and J.U.R. Deol. The pattern of tumour growth. *Symp. Soc. Exp. Biol.*, **25**:255–275, (1971).

[26] W.S. Bullough and E.B. Laurence. Mitotic control by internal secretion: The role of the chalone-adrenaline complex. *Experimental Cell Research*, **33**:176, (1964).

[27] W.S. Bullough and E.B Laurence. Control of cancer in mouse and hamster melanomata by means of the melanocyte chalone. *European Journal of Cancer*, **4**:607, (1968).

[28] A.C. Burton. Rate of growth of solid tumors as a problem of diffusion. *Growth*, **30**:157–176, (1966).

[29] C.P. Calderón and T.A. Kwembe. Modelling tumor growth. *Mathematical Biosciences*, **103**:97–114, (1991).

[30] J. Carlsson. A proliferation gradient in three-dimensional colonies of cultured human glioma cells. *International Journal of Cancer*, **20**:129–136, (1977).

[31] J. Carlsson and H. Acker. Relations between pH, oxygen partial pressure and growth in cultured spheroids. *International Journal of Cancer*, **42**:715–720, (1988).

[32] J.J. Casciari, S.V. Sortichos, and R.M. Sutherland. Mathematical-modelling of microenvironment and growth in EMT6/R0 multicellular tumor spheroids. *Cell Proliferation*, **25**:1–22, (1992).

[33] J.J. Casciari, S.V. Sortichos, and R.M. Sutherland. Variations in tumour growth rates and metabolism with oxygen concentration, glucose concentration, and extracellular pH. *Journal of Cellular physiology*, **151**:386–394, (1992).

[34] J.J. Casciari, S.V. Sotirchos, and Sutherland.R.M. Glucose diffusivity in multicellular spheroids. *Cancer Research*, **48**:3905–3909, (1988).

[35] M.A.J. Chaplain and N.F. Britton. On the concentration profile of a growth inhibitory factor in multicell spheroids. *Mathematical Biosciences*, **115**:233–243, (1993).

[36] W.J. Cliff. Observations on healing tissue: a combined light and electron microscopic investigation. *Philosophical Transactions of the Royal Society of London B*, **246**:305, (1963).

[37] E.A. Coddington and R. Carlson. *Linear Ordinary Differential Equations.* SIAM, Philadelphia, (1997).

[38] A.D. Conger and M.C. Ziskin. Growth of mammalian multicellular tumour spheroids. *Cancer Research*, **43**:556–60, (1983).

[39] R.S. Cotran, V. Kumar, and S.L. Robbins. *Pathologic Basis of Disease, 4th edition.* W.B. Saunders, Philadelphia, (1989).

[40] F.W. Cummings. On surface geometry coupled to morphogen. *Journal of Theoretical Biology*, **137**:215–219, (1989).

[41] F.W. Cummings. A model of morphogenetic pattern formation. *Journal of Theoretical Biology*, **144**:547–566, (1990).

[42] F.W. Cummings. Aspects of growth and form. *Physica D*, **79**:146–163, (1994).

[43] F.W. Cummings. A model of growth and form based on adhesion molecules. *Journal of Theoretical Biology*, **178**:229–238, (1996).

[44] F.W. Cummings. Geometrical concepts in epithelial sheets. *Journal of Theoretical Biology*, **179**:41–49, (1996).

[45] P.A. Dale, J.A. Sherratt, and P.K. Maini. The speed of corneal epithelial wound healing. *Applied Mathematics Letters*, **7**:11–14, (1994).

[46] M. Dan-Sohkawa, H. Yamanaka, and K. Watanabe. Reconstruction of Bipinnaria larvae from dissociated embryonic cells of the starfish, Asterina-Pectinifera. *Journal of Embryology and Experimental Morphology*, **94**:47–60, (1986).

[47] D. Darling and D. Tarin. The spread of cancer in the human body. *New Scientist*, **127**:50–53, (1990).

[48] A. De Hemptinne, R. Marrannes, and V. Vanheel. Surface ph and the control of intracellular in cardiac and skeletal muscle. *Can. J. Physiol. Pharmacol.*, **65**:970–977, (1986).

[49] G. Dee. Propagation into an unstable state. *J. Stat. Phys.*, **39**:705–717, (1985).

[50] G. Dee and J.S. Langer. Propagating pattern selection. *Phys. Rev. Lett.*, **50**:383–386, (1983).

[51] DYLAN differential algebraic equation solver. QuantiSci Ltd. Chiltern House, 45 Station Road, Henley-on-Thames, RG9 1AT. UK.

[52] M.J. Dorie, R.F. Kallman, and M.A. Coyne. Effect of Cytochalasin B, Nocodazale and irradiation on migration and internalization of cells and microspheres in tumour cell spheroids. *Experimental Cell Research*, **166**:370–378, (1986).

[53] M.J. Dorie, R.F. Kallman, D.F. Rapacchietta, D. van Antwerp, and Y.R. Huang. Migration and internalization of cells and polystyrene microspheres in tumour cell spheroids. *Experimental Cell Research*, **141**:201–209, (1982).

[54] K. Douglas. Making friends with death-wish genes. *New Scientist*, 30 July:31–34, (1994).

[55] D. Drasdo. Growing tissue cell populations: a stochastic model based on the Monte Carlo method. Technical report, Max-Planck-Institut für Kolloid-und Grenzflächenforschung, Kantstr. 55, D-14513 Teltow, Berlin, Germany. e-mail = Drasdo@mpikg-teltow.mpg.de, (1995).

[56] D. Drasdo and R. Kree. Simulated tissue: a condensed matter approach to growing cell assemblies and histological processes. Technical report, Max-Planck-Institut, Teltow and Inst.f. Theoretic. Physik, Georg-August Universität, address same as above, (1995).

[57] D. Drasdo, R. Kree, and J.S. McCaskill. Monte Carlo approach to tissue-cell populations. *Physical review E*, **52**:6635–6657, (1995).

[58] R.E. Durand. Multicell spheroids as a model for cell kinetic studies. *Cell Tissue Kinetics*, **23**:141–159, (1990).

[59] L. Edelstein-Keshet. *Mathematical models in biology.* Random House, (1988).

[60] L.M. Ellis and I.J. Fidler. Angiogenesis and breast cancer metastasis. *Lancet*, **346**:388–390, (1995).

[61] G.B. Ermentrout and L. Edelstein-Keshet. Cellular automata approaches to biological modelling. *Journal of Theoretical Biology*, **160**:97–133, (1993).

[62] P.J. Fialkow. Clonal origin of human tumors. *Annual Review of Medicine*, **30**:135–143, (1979).

[63] I.J. Fidler. Tumor heterogeneity and the biology of cancer invasion and metastasis. *Cancer Research*, **38**:2651–2660, (1978).

[64] P.C. Fife. *Mathematical Aspects of Reacting and Diffusing Systems*, volume **28** of *Lecture Notes in Biomathematics.* Springer-Verlag, (1979).

[65] R.A. Fisher. The wave of advance of advantageous genes. *Ann. of Eugenics*, **7**:355–369, (1937).

[66] J. Folkman. Tumor angiogenesis: therapeutic implications. *New England Journal of Medicine*, **285**:1182–1186, (1971).

[67] J. Folkman. Tumour angiogenesis. *Advances in Cancer Research*, **19**:331–358, (1974).

[68] J. Folkman. Angiogenesis in cancer, vascular, rheumatoid and other diseases. *Nature Medicine*, **1**:21–31, (1995).

[69] J. Folkman and C. Haudenschild. Angiogenesis in vitro. *Nature*, **288**:551–556, (1980).

[70] J. Folkman, C. Haudenschild, and B. Zetter. Long-term culture of capillary endothelial cells. *Proc. Natl. Acad. Sci. USA*, **76**:5217, (1979).

[71] J. Folkman and M. Hochberg. Self-regulation of growth in three dimensions. *Journal of Experimental Medicine*, **138**:745–753, (1973).

[72] J. Folkman and M. Klagsbrun. Angiogenic factors. *Science*, **235**:442–447, (1987).

[73] J. Folkman, R. Langer, R.J. Linhardt, C. Haudenschild, and S. Taylor. Angiogenesis inhibition and tumor regression caused by heparin or a heparin fragment in the presence of cortisone. *Science*, **221**, (1983).

[74] J. Folkman, E. Merler, C. Abernathy, and *et al.* Isolation of a tumour factor responsible for angiogenesis. *Journal of Experimental Medicine*, **133**:275–288, (1971).

[75] J. Folkmann. Tumor angiogenesis. *Advances in Cancer Research*, **43**:175–203, (1985).

[76] R.A. Foty, G. Forgacs, C.M. Pfleger, and M.S. Steinberg. Liquid properties of embryonic tissues - measurement of interfacial tensions. *Physical Review Letters*, **72**:2298–2301, (1994).

[77] R.E. Frank, T.J. Saclarides, S. Leurgans, N.J. Speziale, E.A. Drab, and D.B. Rubin. Tumor angiogenesis as a predictor of recurrence and survival in patients with node-negative colon-cancer. *Annals of Surgery*, **222**:695–699, (1995).

[78] S.E. Fraser, C.R. Green, H.R. Bode, and N.B. Gilula. Selective disruption of gap junctional communication interferes with a patterning precess in hydra. *Science*, **237**:49–55, (1987).

[79] J.P. Freyer. Role of necrosis in regulating the growth saturation of multicell spheroids. *Cancer Research*, **48**:2432–9, (1988).

[80] J.P. Freyer and P.L. Schor. Regrowth of cells from multicell tumour spheroids. *Cell Tissue Kinetics*, **20**:249, (1987).

[81] J.P. Freyer and R.M. Sutherland. Proliferative and clonogenic heterogeneity of cells from EMT6/Ro multicellular spheroids induced by the glucose and oxygen supply. *Cancer Research*, **46**:3513–3520, (1986).

[82] J.P. Freyer and R.M. Sutherland. Proliferative and clonogenic heterogeneity of cells from EMT6/Ro multicellular spheroids induced by the glucose and oxygen supply. *Cancer Research*, **46**:3513–3520, (1986).

[83] J.P. Freyer and R.M. Sutherland. Regulation of growth saturation and development of necrosis in EMT6/Ro multicellular spheroids by the glucose and oxygen supply. *Cancer Research*, **46**:3513–3520, (1986).

[84] J.P. Freyer, E. Tustanoff, A.J. Franko, and R.M. Sutherland. In situ oxygen consumption rates of cells in V-79 multicellular spheroids during growth. *Journal of Cellular Physiology*, **118**:53–61, (1984).

[85] D.R. Garrod and M.S. Steinberg. Tissue-specific sorting out in two dimensions in relation to contact inhibition of cell movement. *Nature*, **244**:568–9, (1973).

[86] R.A. Gatenby and E.T. Gawlinski. A reaction-diffusion model of cancer invasion. *Cancer Research*, **56**:5745–5753, (1996).

[87] L.E. Gerweck and M.P. Fellenz. The simultaneous determination of intracellular pH and cell energy status. *Radiation Research*, **125**:257–261, (1991).

[88] A. Gierer, S. Berking, H. Bode, C.N. David, K. Flok, G. Hansmann, H. Schaller, and E. Trenkner. Regeneration of hydra from reaggregated cells. *Nature*, **239**:98–101, (1972).

[89] E.N. Gilbert. Random subdivisions of space into crystals. *The Annals of Mathematical Statistics*, **33**:958–972, (1962).

[90] R.J. Gillies, A. Liu, and A. Bhujwalla. ^{3}1P-MRS measurements of extracellular pH of tumours using 3-aminopropyl phosphate. *American Journal of Physiology*, **36**:C195–C203, (1994).

[91] M.A. Gimbrone, R.S. Cotran, S. Leapman, and J. Folkman. Tumour growth and neovascularization: an experimental model using the rabbit cornea. *J. Natl. Cancer Inst.*, **52**:413–427, (1974).

[92] L. Glass. Instability and mitotic patterns in tissue growth. *Journal of Dynamical Systems Measurement and Control*, **95**:324–327, (1973).

[93] J.A. Glazier. The thermodynamics of cell sorting. *Bussei Kenkyu*, **65**:691–700, (1995).

[94] J.A. Glazier, M.P. Anderson, and G.S. Grest. Coarsening in the 2-dimensional soap froth and the large Q-Potts-model - a detailed comparison. *Philosophical Magazine B-Physics of Condensed Matter Structural Electronic Optical and Magnetic Properties*, **62**:615–645, (1990).

[95] J.A. Glazier and F. Graner. Simulation of the differential adhesion driven rearrangement of biological cells. *Physical Review E*, **47**:2128–2154, (1993).

[96] J.A. Glazier, R.C. Raphael, F Graner, and Y Sawada. The Energetics of Cell Sorting in Three Dimensions. In D. Beysens, M.A. Felix, G. Forgacs, and F. Gaill, editors, *Interplay of Genetic and Physical Processes in the Development of Biological Form*, pages 54–61. Springer, (1995).

[97] R.J. Goldacre and B Sylven. On the access of blood-borne dyes to various tumour regions. *British Journal of Cancer*, **16**:306–322, (1962).

[98] C.M. Goodall, A.G. Anders, and P. Shubik. Studies of vascular patterns in living tumours with a transparent chamber inserted in hamster cheek pouch. *Journal of the National Cancer Institute*, **35**:497–505, (1965).

[99] F. Graner. Can surface adhesion drive cell rearrangement? Part I: biological cell-sorting. *Journal of Theoretical Biology*, **164**:455–476, (1993).

[100] F. Graner and J.A. Glazier. Simulation of biological cell sorting using a two-dimensional extended Potts model. *Physical Review Letters*, **69**:2013–2016, (1992).

[101] F. Graner and Y. Sawada. Can surface adhesion drive cell rearrangement? Part II: geometrical model. *Journal of Theoretical Biology*, **164**:477–506, (1993).

[102] H.P. Greenspan. Models for the growth of a solid tumor by diffusion. *Studies in Applied Mathematics*, **51**:317–340, (1972).

[103] H.P. Greenspan. On the self-inhibited growth of cell cultures. *Growth*, **38**:81–95, (1974).

[104] H.P. Greenspan. On the growth and stability of cell cultures and solid tumors. *Journal of Theoretical Biology*, **51**:229–242, (1976).

[105] J.R. Griffiths. Are cancer cells acidic? *British Journal of Cancer*, **64**:425–427, (1991).

[106] P. Grindrod. *Patterns and Waves: The Theory and Applications of Reaction-Diffusion Equations.* Oxford Applied Mathematics and Computing Science Series. Clarendon Press, Oxford, (1991).

[107] K. Groebe and W. Mueller-Klieser. Distributions of oxygen, nutrient and metabolic waste concentrations in multicellular spheroids and their dependence on spheroid parameters. *European Biophysics Journal*, **19**:169–181, (1991).

[108] T.W. Grunt, A. Lametschwandter, and K. Karrer. The characteristic structural features of the blood vessels of the Lewis lung carcinoma (a light microscopy and scanning electron microscopy study). *Scanning Electron Microscopy*, **2**:575–589, (1986).

[109] T.W. Grunt, A. Lametschwandter, K. Karrer, and O. Staindl. The angioarchitecture of the Lewis lung carcinoma in laboratory mice (a light and scanning electron microscope study). *Scanning Electron Microscopy*, **2**:557–574, (1986).

[110] F. Haessner. *Recrystalization of metallic materials*, page 3. Riederer Verlag, Stuttgart, (1978).

[111] M. Haji-Karim and J. Carlsson. Proliferation and viability in cellular spheroids of human origin. *Cancer Research*, **38**:1457–64, (1978).

[112] R.A. Hawkins, C. Hoh, J. Glaspy, Y. Cho, M. Dahlbom, S. Rege, and C. Messa. The role of positron emission tomography in oncology and other whole-body applications. *Seminars in Nuclear Medicine*, **22**:268–284, (1992).

[113] A. Heinz, G. Sachs, and J.A. Schafe. Evidence for activations of an active electrogenic pump in Ehrlich ascites tumor cells during glycolysis. *Journal of Membrane Biology*, **61**:143–153, (1981).

[114] D.g. Hirst and J. Denekamp. Tumour cell proliferation in relation to the vasculature. *Cell Tissue Kinetics*, **12**:31–42, (1979).

[115] J. Holtfreter. . *Arch. Exptl. Zellforsch. Gewebezuecht*, **23**:169, (1900).

[116] J. Holtfreter. . *Review of Cancer Biology*, **3**:220, (1944).

[117] A.G. Ide, N.H. Baker, and S.L. Warren. Vascularization of the brown-pearce rabbit epithelioma transplant as seen in the transparent ear chamber. *Am. J. Roentgenol. Radium Therapy*, **42**:891, (1939).

[118] W.R. Inch, J.A. McCredie, and R.M. Sutherland. Growth of nodular carcinomas in rodents compared with multicell spheroids in tissue culture. *Growth*, **34**:271–282, (1970).

[119] C.G. Ioannides and T.L. Whiteside. T-Cell recognition of human tumors: implications for molecular immunotherapy of cancer. *Clinical Immunology and Immunopathology*, **66**:91–106, (1993).

[120] B.A. Jabour, Y. Choi, C.K. Ooh, S.D. Rege, J.L. Soong, R.B. Lufkin, W.M. Hanafee, J. Maddhi, and L. Chaiken. Extracranial head and neck tumours: PET imaging with 2-[F-18]fluoro-2-deoxy-D-glucose. *Radiology*, **186**:27–35, (1993).

[121] E.A. Jaffe, R.L. Nachman, C.G. Becker, and C.R. Minick. Culture of human endothelial cells derived from umbilical veins. *Journal of Clinical Investigation*, **52**:2745, (1973).

[122] R.K. Jain. Barriers to drug delivery in solid tumors. *Scientific American*, **271**:58–65, (1994).

[123] Y. Jiang, H. Levine, and J.A.G. Glazier. Possible collaboration of differential adhesion and chemotaxis cooperate in mound formation of *dictyostelium*. *Biophys. Journal*, In press, (1998).

[124] B. Jones and R.S. Camplejohn. Strathmokinetic measurement of tumour cell proliferation in relation to vascular proximity. *Cell Tissue Kinetics*, **16**:351–355, (1983).

[125] D.S. Jones and B.D. Sleeman. *Differential equations and mathematical biology.* George Allen and Unwin, London, (1983).

[126] F. Kallinowski, P. Vaupel, S. Runkel, G. Berg, H.P. Fortmeyer, K.H. Baessler, K. Wagner, W. Mueller-Klieser, and S. Walenta. Glucose uptake, lactate release, ketone body turnover, metabolic micromillieu, and pH distributions in human breast cancer xenografts in nude rats. *Cancer Research*, **48**:7264–7272, (1988).

[127] S.H. Kauffman, editor. *Apoptosis: Pharmacological Implications and Therapeutic Opportunities, Advances in Pharmacology, volume 41.* Academic Press, London, (1997).

[128] Y. Kawakami, M.I. Nishimura, N.P. Restifo, S.L. Topalian, B.H. O'Neil, J. Shilyansky, J.R. Yannelli, and S.A. Rosenberg. T-Cell recognition of human melanoma antigens. *Journal of Immunotherapy*, **14**:88–93, (1993).

[129] J.F.R. Kerr. Shrinkage necrosis; a distinct mode of cellular death. *Journal of Pathology*, **105**:13–20, (1971).

[130] J.F.R. Kerr, Wyllie, and A.R. Currie. Apoptosis: A basic biological phenomenon with wide-ranging implications in tissue kinetics. *British Journal of Cancer*, **26**:239–257, (1972).

[131] G. Klein. Immune and non-immune control of neoplastic development. *Cancer*, **45**(10):2486–2499, (1980).

[132] D.I. Kleinerman, P. Tronsco, S-H Lin, L.L Pisters, E.R. Sherwood, T. Brooks, A.C. von Eschenbach, and J-T Hsieh. Consistent expression of an epithelial cell adhesion molecule (C-CAM) during human prostate cancer development and loss of expression in prostrate cancer: implication as a tumour suppressor. *Cancer Research*, **55**:1215–1220, (1995).

[133] A.N. Kolmogorov, I.G. Petrovskiĭ, and N.S. Piskunov. A study of the equation of diffusion with increase in the quantity of matter, and its application to a biological problem. *Bull. Univ. Moskou Ser. Int. Sec.*, **A 1**, Number 6:1–72, (1937).

[134] S.E. Koonin and D.C. Meredith. *Computational Physics: FORTRAN version*, chapter 8 - Monte Carlo Methods, pages 197–220. Addison-Wesley, (1990).

[135] E. Kreyszig. *Advanced Engineering Mathematics.* John Wiley & Sons, 6th edition, (1988).

[136] J.M. Lackie and J.A.T. Dow, editors. *The Dictionary of Cell Biology.* Academic Press, 2nd edition, (1995).

[137] A.K. Laird. Dynamics of tumour growth. *British Journal of Cancer*, **18**:490–502, (1964).

[138] A.K. Laird. Dynamics of relative growth. *Growth*, **21**:249–264, (1965).

[139] A.K. Laird. Dynamics of tumour growth: Comparison of growth rates and extrapolation of growth curve to one cell. *British Journal of Cancer*, **19**:278–291, (1965).

[140] A.K. Laird, S.A. Tyler, and A.D. Barton. Dynamics of normal growth. *Growth*, **21**:233–248, (1965).

[141] J. Landry, J.P. Freyer, and R.M. Sutherland. Shedding of mitotic cells from the surface of multicell spheroids during growth. *Journal of Cell Physiology*, **106**:23–32, (1981).

[142] J. Landry, J.P. Freyer, and R.M. Sutherland. A model for the growth of multicellular spheroids. *Cell Tissue Kinetics*, **15**:585–594, (1982).

[143] R. Langer, H. Brem, K. Falterman, M. Klein, and J. Folkman. Isolation of a cartilage factor that inhibits tumor neovascularisation and growth. *Science*, **193**:70–72, (1976).

[144] M. M. LaBarbera and S. Vogel. The design of fluid transport systems in organisms. *American Scientist*, **70**:54–60, (1982).

[145] P. Marrack and J. Kappler. The T-cell and its receptor. *Scientific American*, **254**:28–37, (1986).

[146] G.R. Martin and R.K. Jain. Non-invasive measurement of interstitial pH profiles in normal and neoplastic tissue using fluorescent ration imaging microscopy. *Cancer Research*, **54**:5670–5674, (1994).

[147] T.H. Maugh. Angiogenesis: Inhibitors link many diseases. *Science*, **212**:1374–1375, (1981).

[148] D. McClay and C. Ettensohn. Cell adhesion in morphogenesis. *Annual Review of Cell Biology*, **3**:319–345, (1987).

[149] J.A. McCredie, W.R. Inch, J. Kruuv, and T.A. Watson. The rate of tumour growth in animals. *Growth*, **29**:331–347, (1965).

[150] P. McCulloch, A. Choy, and L. Martin. Association between tumor angiogenesis and tumor-cell shedding into effluent venous-blood during breast-cancer surgery. *Lancet*, **346**:1334–1335, (1995).

[151] D.L.S McElwain and G.J. Pettet. Cell migration in multicell spheroids: swimming against the tide. *Bulletin of Mathematical Biology*, **55**:655–674, (1993).

[152] N. Metropolis, A.W. Rosenbluth, M.N. Rosenbluth, A.H. Teller, and E. Teller. Equation of state calculations by fast computing machines. *Journal of Chemical Physics*, **21**:1087, (1953).

[153] S. Michelson. A system for Monte Carlo simulation of heterogeneous tumor cell populations. *Computers and Mathematics with Applications*, **20**:139–148, (1990).

[154] A. Miodonski, J. Kus, E. Olsewski, and R. Tyrankiewicz. Scanning electron microscopic studies on blood vessels. *Arch. Otolaryngol.*, **106**:321, (1980).

[155] Masayuki Miyasaka. Cancer metastasis and adhesion molecules. *Clinical orthopaedics and related research*, **312**:10–18, (1995).

[156] J.C.M. Mombach, R.M.C. Dealmeida, and J.R. Iglesias. 2-cell correlations in biological tissues. *Physics Review*, **47**:3712–3716, (1993).

[157] J.C.M. Mombach, R.M.C. Dealmeida, and J.R. Iglesias. Mitosis and growth in biological tissues. *Physics Review E*, **48**:598–602, (1993).

[158] J.C.M. Mombach and J.A. Glazier. Single cell motion in random aggregates of embryonic cells. *Physical Review Letters*, **76**:3032–3035, (1995).

[159] J.C.M. Mombach and J.A. Glazier. Single cell motion in aggregates of embryonic cells. *Physical Review Letters*, **76**:3032–3035, (1996).

[160] J.C.M. Mombach, J.A. Glazier, R.C. Raphael, and M. Zajac. Quantitative comparison between differential adhesion models and cell sorting in the presence and absence of fluctuations. *Physical Review Letters*, **75**:2244–2247, (1995).

[161] G.W. Moore and J.J. Berman. Cell growth simulations predicting polyclonal origins for 'monoclonal' tumors. *Cancer Letters*, **60**:113–119, (1991).

[162] J.V. Moore, P.S. Haselton, and C.M. Buckley. tumour cords in 52 human bronchial and cervical squamous cell carcinomas: Inferences for their cellular kinetics and radiobiology. *British Journal of Cancer*, **51**:407–413, (1985).

[163] A. Moscona. Development of heterotypic combinations of dissociated embryonic chick cells. *Proceedings of the Society for Experimental Biology and Medicine*, **92**:410–416, (1956).

[164] V.R. Muthukkaruppan, L. Kubai, and R. Auerbach. Tumor-induced neovascularization in the mouse eye. *Journal of the National Cancer Institute*, **69**(3):699–708, (1982).

[165] K. Newell, A. Franchi, J. Pouyssegur, and I. Tannock. Studies with glycolysis-deficient cells suggest that production of lactic acid is not the only cause of tumor acidity. *Proceedings of the National Academy of Sciences of the USA*, **90**:1127–1131, (1993).

[166] S. Newman and W. Comper. Generic physical-mechanisms of morphogenesis and pattern formation. *Development*, **110**:1–18, (1990).

[167] G.L. Nicholson. Cancer metastasis: tumor cell and host organ properties important in metastasis to specific secondary sites. *Biochimica et Biophysica Acta*, **948**:175–224, (1988).

[168] K. Noda. . *Zool. Mag.*, **80**:99, (1971).

[169] J.A. Norton. Tumor angiogenesis - the future is now. *Annals of Surgery*, **222**:693–694, (1995).

[170] L. Norton. A Gompertzian model of human breast cancer growth. *Cancer Research*, **48**:7067–7071, (1988).

[171] K. Nubler-Jung and B. Mardini. Insect epidermis - polarity patterns after grafting result from divergent cell adhesions between host and graft tissue. *Development*, **110**:1071–1079, (1990).

[172] L. Olsen, J.A. Sherratt, P.K. Maini, and F. Arnold. A mathematical model for the capillary endothelial cell-extracellular matrix interactions in wound-healing and angiogenesis. *IMA Journal of Mathematics Applied in Medicine and Biology*, **14**:261–281, (1997).

[173] *Cancer Statistics, Registrations*, England and Wales, (1989). Series MB1, No. 22.

[174] *Mortality Statistics, Cause*, England and Wales, (1993). Series DH2, No. 20.

[175] E.E. Osgood. A unifying concept of the etiology of the leukemias, lymphomas and cancers. *Journal of the National Cancer Institute*, **18**:155–162, (1957).

[176] M.R. Owen and J.A. Sherratt. Pattern formation and spatio-temporal irregularity in a model for macrophage-tumour interactions. *Journal of Theoretical Biology*, **189**:63–80, (1997).

[177] M.R. Owen and J.A. Sherratt. Modelling that macrophage invasion of tumours: Effects on growth and composition. *IMA Journal of Mathematics Applied in medicine and Biology*, **15**:165–185, (1998).

[178] S. Paget. The distribution of secondary growths in cancer of the breast. *Lancet*, i:571–573, (1889).

[179] S. Paget. Stephen Paget paper reproduced from the Lancet, 1889. *Cancer and Metastasis Reviews*, **8**:98–101, (1989).

[180] N. Paweletz and M. Knierim. Tumor-related angiogenesis. *Critical reviews in Oncology/Hematology*, **9**:197–242, (1989).

[181] A.J. Perumpanani, J.A. Sherratt, and J. Norbury. Mathematical modelling of capsule formation and multinodularity in benign tumour growth. *Nonlinearity*, **10**:1599–1614, (1997).

[182] A.J. Perumpanani, J.A. Sherratt, J. Norbury, and H.M. Byrne. Biological inferences from a mathematical model for malignant invasion. *Invasion and Metastasis*, **16**:209–221, (1996).

[183] H.C. Pitot, editor. *Fundamentals of Oncology.* Marcel Deckker, New York, (1986).

[184] R.T. Prehn. Stimulatory effects of immune reactions upon growth of untransplanted tumors. *Cancer Research*, **54**:908–914, February 15 (1994).

[185] A.S. Qi, X. Zheng, C.Y. Du, and B.S. An. A cellular automaton model of cancerous growth. *Journal of Theoretical Biology*, **161**:1–12, (1993).

[186] S. Ratner and G.H. Heppner. Mechanisms of lymphocyte traffic in neoplasia. *Anticancer Research*, **5**:475–482, (1986).

[187] M. Robertson, J. Armstrong, and P. Armstrong. Adhesive and non-adhesive membrane domains of amphibian embryo cells. *Journal of Cell Science*, **44**:19–31, (1980).

[188] M. Rosenstein, T.J. Eberlein, and S.A. Rosenberg. Adoptive immunotherapy of established syngeneic solid tumors: role of T lymphoid subpopulations. *The Journal of Immunology*, **132**:2117–2122, (1984).

[189] H. Rubin. pH and population density in the regulation of animal cell multiplication. *The Journal of Cell Biology*, **51**:686–702, (1971).

[190] R.W. Ruddon. *Cancer Biology.* Oxford University Press, second edition, (1987).

[191] J.H. Russell, L. Musil, and D.E. McCulley. A novel and distinct effect of the cytotoxic T lymphocyte-target interaction. *The Journal of Immunology*, **140**:427–432, (1988).

[192] T. Rytomaa and K. Kiviniemi. Control of DNA replication in rat chloroleukaemia by means of the granulocytic chalone. *European Journal of Cancer*, **4**:595, (1968).

[193] M.P. Sarras, Z. Xiaoming, J.K. Huff, M.A. Accaviti, P.L. St John, and D.R. Abrahamson. Extracellular-matrix (mesoglea) of hydra-vulgaris .3. formation and functions during morphogenesis of hydra cell aggregates. *Developmental Biology*, **157**:383–398, (1993).

[194] N.J. Savill and P. Hogeweg. Modelling morphogenesis: From single cells to crawling slugs. *Journal of Theoretical Biology*, **184**:229–235, (1997).

[195] J.A. Sherratt and M.A. Nowak. Oncogenes, antioncogenes and the immune-response to cancer - a mathematical model. *Proceedings of the Royal Society of London Series B - Biological Sciences*, **248**:261–271, (1992).

[196] M.M Sholley, G.P. Ferguson, H.R. Seibel, J.L. Montour, and J.D. Wilson. Mechanisms of neovascularization. vascular sprouting can occur without proliferation of endothelial cells. *Laboratory Investigations*, **51**:624–634, (1984).

[197] B. Shraiman and D. Ben Simon. On the dynamical mechanism for velocity selection. *Physica Scripta*, **T9**:123–125, (1985).

[198] R.M. Shymko and L. Glass. Cellular and geometric control of tissue growth and mitotic instability. *Journal of Theoretical Biology*, **63**:355–374, (1976).

[199] J.M.W. Slack. Embryology - we have a morphogen. *Nature*, **327**:553–554, (1987).

[200] L.L. Spriet. Phosphofructokinase activity and acidosis during short term tetanic contractions. *Canadian Journal of Physiological Pharmacology*, **69**:298–304, (1991).

[201] G.G. Steel. *Growth Kinetics of Tumors*. Oxford: Clarendon Press, (1977).

[202] M.S. Steinberg. Mechanism of tissue reconstruction by dissociated cells, II: Time course of events. *Science*, **137**:762–3, (1962).

[203] M.S. Steinberg. On the mechanism of tissue reconstruction by dissociated cells, I. Population kinetics, differential adhesiveness, and the absence of directed migrations. *Proceedings of the National Academy of Sciences U.S.A.*, **48**:1577, (1962).

[204] M.S. Steinberg. On the mechanism of tissue reconstruction by dissociated cells, III. Free energy relations and the reorganization of fused, heteronomic tissue fragments. *Proceedings of the National Academy of Sciences U.S.A.*, **48**:1769, (1962).

[205] M.S. Steinberg. Reconstruction of tissues by dissociated cells. *Science*, **141**:401–408, (1963).

[206] M.S. Steinberg. Does differential adhesion govern self-assembly processes in histogenesis? Equilibrium configurations and the emergence of a hierarchy among populations of embryonic cells. *Journal of Experimental Zoology*, **173**:395, (1970).

[207] W.G. Stetler-Stevenson, S. Aznavoorian, and L.A. Liotta. Tumor cell interactions with the extracellular matrix during invasion and metastasis. *Annual Review of Cell Biology*, **9**:541–573, (1993).

[208] M. Stubbs, L. Rodrigues, F.A. Howe, J. Wang, K.S. Joong, R. Veech, and J.R. Griffin. Metabolic consequences of a reversed pH gradient in rat tumours. *Cancer Research*, **54**:4011–4016, (1994).

[209] D. Sulsky, S. Childress, and J.K. Percus. A model of cell sorting. *Journal of Theoretical Biology*, **106**:275–301, (1984).

[210] R.M. Sutherland, W.R. Inch, and J.A. McCredie. Growth of multicell spheroids in tissue culture as a model of nodular carcinomas. *Journal of the National Cancer Institute*, **46**:113–120, (1971).

[211] M. Takeichi. Cadherin cell-adhesion receptors as a morphogenetic regulator. *Science*, **251**:1451–1455, (1991).

[212] I.F. Tannock. The relation between cell proliferation and the vascular system in a transplanted mouse mammary tumour. *British Journal of Cancer*, **22**:258–273, (1968).

[213] U. Technau and T.W. Holstein. Cell sorting during the regeneration of hydra from reaggregated cells. *Developmental Biology*, **151**:117–127, (1992).

[214] M. Thain and M. Hickman, editors. *The Penguin Dictionary of Biology.* Penguin Group, ninth edition, (1994).

[215] R.H. Thomlinson and L.H. Gray. The histological structure of some human lung cancers and the possible implications for radio therapy. *British Journal of Cancer*, **9**:539–549, (1955).

[216] S.L. Topalian. MHC class II restricted tumor antigens and the role of CD4+ cells in cancer immunotherapy. *Current Opinion in Immunology*, **6**:741–745, (1994).

[217] S.L. Topalian, D. Solomon, and S.A. Rosenberg. Tumor-specific cytolysis by lymphocytes infiltrating human melanomas. *The Journal of Immunology*, **142**:3714–3725, (1989).

[218] P. Townes and J. Holtfreter. . *Journal of Experimental Zoology*, **128**:53, (1955).

[219] P. Tracqui, G.C. Cruywagen, D.E. Woodward, G.T. Bartor, J.D. Murray, and E.C.A. Alvord. A mathematical model of glioma growth: the effect of chemotherapy on spatio-temporal growth. *Cell Proliferation*, **25**:17–31, (1995).

[220] W. van Saarloos. Dynamical velocity selection: marginal stability. *Physical Review Letters*, **58**:2571–2574, (1987).

[221] C. Van Waes, D.M. Surh, Z. Chen, M. Kirby, J.S. Rhim, R. Brager, R.B. Sessions, J. Poore, G.T. Wolf, and T.E. Carey. Increase in suprabasilar integrin adhesion molecule expression in human epidermal neoplasms accompanies increased proliferation occurring with immortalization and tumor progression . *Cancer Research*, **55**:5434–5444, (1995).

[222] P.W. Vaupel, S. Frinak, and H.I. Bicher. Heterogeneous oxygen partial pressure and pH distribution in c3H mouse mammary adenocarcinoma. *Cancer Research*, **41**:2008–13, (1981).

[223] A.I. Volpert, V.A. Volpert, and V.A. Volpert. *Translations of Mathematical Monographs: Travelling Wave Solutions of Parabolic Equations*, volume 140, chapter 5. American Mathematical Society, (1991).

[224] J.S. Wainscoat and M.F. Fey. Assessment of clonality in human tumours: A review. *Cancer Research*, **50**:1355–1360, (1990).

[225] O. Warburg. *The Metabolism of Tumors (English translation by F.Dickens.* Constable Press, London, 1930.

[226] B.A. Warren and P. Shubik. The growth of the blood supply to melanoma transplants in the hamster cheek pouch. *Laboratory Investigations*, **15**:464, (1966).

[227] D. Weaire, B. Bolton, P. Molho, and J.A. Glazier. Investigation of an elementary model for magnetic froth. *Journal of Physics: Condensed Matter*, **3**:2101–2114, (1991).

[228] P. Weiss. Specificity in growth control. In E.G. Butler, editor, *Geological Specificity and Growth*, page **195**. Princeton U.P., (1955).

[229] T. Williams and R. Bjerknes. Stochastic model for abnormal clone spread through epithelial basal layer. *Nature*, **236**:19–21, (1972).

[230] H.V. Wilson. . *Journal of Experimental Zoology*, **5**:245, (1907).

[231] L. Wolpert. *The Triumph of the Embryo*, chapter 11 - Cell multiplication and cancer. Oxford University Press, (1993).

[232] A.D. Wyllie. Growth and neoplasia. In R.N.M.Macsween and K.Whaley, editors, *Muir's Textbook of Pathology*, chapter 10. Edward Anderson, (1992).

[233] Y. Yonekura, R.S. Benua, and A.B. Brill. Increased accumulation of 2-deoxy-2[^{18}F]fluoro-D-glucose in liver metastasis from colon cancer. *Journal of Nuclear Medicine*, **23**:1133–1137, (1982).

[234] B. Zetter. Migration of capillary endothelial cells is stimulated by tumour-derived factors. *Nature*, **285**:41–43, (1980).